TU TECHNISCHE
UNIVERSITÄT
WIEN

DISSERTATION

Influence of atmospheric aging on the stability of binding media in paintings:
Study of their degradation behaviour when exposed to UV-light, corrosive gases, and humidity

ausgeführt zum Zwecke der Erlangung des akademischen Grades eines Doktors der Naturwissenschaften unter der Anleitung von

Em. O. Univ. Prof. Univ. Doz. Dipl.-Ing. Dr. Manfred Schreiner

am Institut für Chemische Technologien und Analytik (E164)

eingereicht an der Technischen Universität Wien (TU Wien)

Fakultät für Technische Chemie

von

Laura Pagnin, MSc.

Matrikelnummer e11830144

Wien, 2021

"Seasons flow in a cycle.
Life too, passes through difficult winters.
But after any winter, spring will follow".

~Toshikazu Kawaguchi~

CONTENTS

ABSTRACT

The aim of this PhD thesis primarily focused on the characterization and chemical stability of polymeric synthetic paints recently used in the artistic and industrial field, i.e. acrylic emulsions, alkyd, and styrene-acrylic resins. The need for scientific knowledge derives from the fact that some research topics have yet to be understood, such as the influence of various pigments (e.g. synthetic ultramarine, cobalt blue, titanium white, etc.) in the paint degradation processes, the interaction between paint and atmospheric agent, and the effect that the combination of pollutants has on the overall stability of the paints. These topics were studied applying several complementary analytical techniques available at the Institute of Natural Sciences and Technology in the Arts (ISTA) at the Academy of Fine Arts Vienna, such as Attenuated Total Infrared Spectroscopy (ATR-FTIR) and μ-Raman Spectroscopy, and at the Technical University of Vienna (TU Wien), such as Atomic Force Microscopy (AFM) and Laser-Induced Breakdown Spectroscopy (LIBS). The chosen experimental methods are useful for the investigation of molecular-chemical reactions and also semiquantitative aspects occurring during artificial aging. The various results obtained from the different analytical techniques chosen are implemented through multivariate statistical methods (i.e. PCA, and Random Forest Discrimination) in order to fully exploit the chemical information on these materials, combine the results with each other, and obtain complete information on the interaction of the pollutants agents and paints.

The PhD thesis was divided into two parts in order to individually evaluate the deteriorating action of the two main atmospheric pollutants, UV-light and pollutant gases. In the first part, the degradation behavior of paints subjected to accelerated aging by UV-light was studied. The UV-light radiation chosen provides radiation with wavelengths between 295 and 3000 nm, simulating outdoor sunlight conditions. This study demonstrated that the type of inorganic pigment in the mixture and the Pigment/Binder (P/BM) ratio used has a significant impact on the stability of the

binding media. Moreover, chemometric methods and advanced techniques showed that the degradation effect of UV-light varied also according to the binder, pigment granulometry, showing different trends comparing the top and inner paint layers. The second part of the thesis focused on studying the degradation reactions caused by pollutant gases and relative humidity (RH). The paint samples were exposed to different corrosive gases, such as SO_2, O_3, H_2S, and NO_x. Synthetic air was mixed with different amounts of RH (50 and 80 %) and gases in the ppb and/or ppm range to represent the atmospheric environment. In general, the results showed that binders present a different degradation behavior when exposed to pollutant gases. Specifically, RH has more influence on acrylic paints, different gases on alkyd paints, and the gas×RH combination on styrene-acrylic paints. However, the type of pigment in the mixture and the RH content applied in the accelerated weathering chamber also influence the deteriorating phenomena. In addition to this experimental evaluation, a preliminary study on cleaning methods for painted materials was carried out. This last part represents the connection between chemical investigations on cultural heritage and conservation practices useful for preserving modern artworks.

The knowledge gained from the results obtained might support conservators and restorers for the development of appropriate conservation strategies, as well as to artists for a better selection of art materials. Finally, the research carried out can be applied to further research projects that study different classes of pigments, synthetic binders, and degradation processes of artistic objects and industrial products.

ZUSAMMENFASSUNG

Das Ziel dieser Dissertation konzentrierte sich hauptsächlich auf die Charakterisierung und chemische Stabilität von polymeren synthetischen Farben, die neuerdings im künstlerischen und industriellen Bereich verwendet wurden, d. h. Acrylemulsionen, Alkyd und Styrol-Acryl-Harze. Der Bedarf an wissenschaftlichen Erkenntnissen ergibt sich aus der Tatsache, dass einige Forschungsthemen noch nicht verstanden sind, wie zum Beispiel der Einfluss verschiedener Pigmente (z.B. synthetisches Ultramarin, Kobaltblau, Titanweiß, etc.) auf Lackabbauprozesse, die Wechselwirkung zwischen Lack und Witterungseinflüssen sowie die Wirkung der Schadstoffkombination auf die Gesamtstabilität der Lacke. Diese Themen wurden unter Anwendung von mehrerer komplementärer analytischer Methoden, die am Institut für Naturwissenschaften und Technologie der Künste (INTK) der Akademie der bildenden Künste Wien verfügbar sind, untersucht, wie zum Beispiel Abgeschwächte Total-Infrarot-Spektroskopie (ATR-FTIR) und µ-Raman-Spektroskopie, und an der Technischen Universität Wien (TU Wien), wie zum Beispiel Rasterkraftmikroskopie (AFM) und Laserinduzierte Durchbruchspektroskopie (LIBS) werden durchgeführt. Die gewählten experimentellen Methoden eignen sich zur Untersuchung molekular-chemischer Reaktionen sowie semiquantitativer Aspekte, die während der künstlichen Alterung auftreten. Die Ergebnisse der verschiedenen gewählten Analysetechniken wurden durch multivariate statistische Methoden (d.h. PCA und Random Forest Discrimination) umgesetzt, um die chemischen Informationen über diese Materialien vollständig auszuschöpfen, die Ergebnisse miteinander zu kombinieren und vollständige Informationen über die Wechselwirkung der Schadstoffe und Lacke zu erhalten.

Die Dissertation wurde in zwei Teile gegliedert, um die schädliche Wirkung der beiden Hauptschadstoffe UV-Licht und Schadgase einzeln zu bewerten. Im ersten Teil wurde das Abbauverhalten von Lacken untersucht, die einer beschleunigten Alterung durch

UV-Licht ausgesetzt sind. Die gewählte UV-Lichtstrahlung liefert Strahlung mit Wellenlängen zwischen 295 und 3000 nm und simuliert so die Bedingungen des Sonnenlichts im Freien. Diese Studie zeigte, dass die Art des anorganischen Pigments in der Mischung und das verwendete Verhältnis Pigment/Bindemittel (P/BM) einen signifikanten Einfluss auf die Stabilität des Bindemittels haben. Darüber hinaus wurde durch die Umsetzung der Ergebnisbewertung mit chemometrischen Methoden und fortschrittlichen Techniken gezeigt, dass die Abbauwirkung von UV-Licht auch je nach Bindemittel und Pigment Granulometrie variiert und unterschiedliche Trends beim Vergleich der oberen und inneren Lackschichten zeigt. Der zweite Teil der Arbeit konzentriert sich auf die Untersuchung der Abbaureaktionen durch Schadgase und relative Luftfeuchtigkeit (RH). Die Lackproben wurden verschiedenen korrosiven Gasen wie SO_2, O_3, H_2S und NO_x ausgesetzt. Synthetische Luft wurde mit unterschiedlichen Mengen an RH (50 und 80 %) und Gasen im ppb- und/oder ppm-Bereich gemischt, um die atmosphärische Umgebung darzustellen. Generell zeigten die Ergebnisse, dass Bindemittel ein unterschiedliches Abbauverhalten zeigen, wenn sie Schadgasen ausgesetzt sind. Konkret hat RH mehr Einfluss auf Acrylfarben, verschiedene Gase auf Alkydfarben und das Gas×RH-Kombination auf Styrol-Acrylfarben. Aber auch die Art des Pigments in der Mischung und der RH-Gehalt, der in der beschleunigten Bewitterungskammer aufgetragen wird, beeinflussen die Verschlechterungsphänomene. Zu dieser experimentellen Bewertung wurde eine Vorstudie zu Reinigungsverfahren für lackierte Materialien durchgeführt. Dieser letzte Teil stellt die Verbindung zwischen chemischen Untersuchungen des kulturellen Erbes und Konservierungspraktiken dar, die für die Erhaltung moderner Kunstwerke nützlich sind. Die aus den Ergebnissen gewonnenen Erkenntnisse könnten Konservatoren und Restauratoren bei der Entwicklung geeigneter Konservierungsstrategien unterstützen und Künstlern eine bessere Auswahl von Kunstmaterialien ermöglichen. Schließlich können die durchgeführten Untersuchungen in weitere Forschungsprojekte einfließen, um die verschiedenen Abbauprozesse von Pigmentklassen, synthetische Bindemittel in Kunstobjekten und Industrieprodukten durch zu leuchten.

LIST OF ABBREVIATIONS

AFM	Atomic Force Microscopy
ANOVA	Analysis of Variance
ASCA	Analysis-of-Variance-Simultaneous Component Analysis
ATR-FTIR	Attenuated Total Reflection Fourier-Transform Infrared Spectroscopy
BA	Butyl Methacrylate
CCD	Charge Coupled Device
C.I.	Color Index
CMC	Critical Micelle Concentration
dp	Penetration Depth
EA	Ethyl Acrylate
IRE	Internal Reflection Element
LIBS	Laser-Induced Breakdown Spectroscopy
MCT	Mercury Cadmium Telluride
n	Refractive Index
OVA	One-Vs-All Scheme
P/BM	Pigment/Binder Ratio
PCA	Principal Component Analysis
PEO	Polyethylene Oxide
ppm	Parts Per Million
PVA	Polyvinyl Acetate
RDF	Random Decision Forest
RH	Relative Humidity
SEM	Scanning Electron Microscopy
Tg	Glass Transition Temperature
UV-light	Ultraviolet Light

ACKNOWLEDGMENTS

This thesis would not have been possible without the supervision, support, and encouragement of Prof. Dr. Manfred Schreiner throughout this academic achievement. Thanks to the numerous opportunities he offered me, such as attending international conferences, writing papers in leading scientific journals, employing new analytical techniques, and developing innovative investigative approaches, my academic background would not have been the same.

I am grateful to Prof. Dr. Rita Wiesinger, who has always been able to give me a lot of advices from the scientific point of view and reassurances about all insecurities throughout my doctorate. I will not forget the long chats we had together, always trying to find the positive side in the face of problems or failures.

I would like to thank Prof. Dr. Katja Sterflinger, who allowed me to finish my academic qualification by always giving me advice and never making me lack of help or support. I also thank her for the opportunity to collaborate with external institutions allowing me to develop my scientific profile in the field of diagnostics for cultural heritage.

I would like to thank Prof. Dr. Andreas Limbeck and his research group for the collaboration and help shown during the acquisition and processing of LIBS data and the writing of papers necessary for the doctorate achievement. Furthermore, I would like to be grateful to Prof. Dr. Hinrich Grothe, and in particular to Dr. Georg Ramer and Dr. Ayse Koyun, for the great help showed during the AFM training, for the interesting conversations and the constant availability.

I would like to thank Dr. Rosalba Calvini and Prof. Francesca Caterina Izzo for the opportunity to collaborate and share scientific ideas with them that have allowed me to develop research topics still ongoing. I can never be grateful enough for their patience, encouragement, and support that they still demonstrate to me. I hope to be able to keep these great collaborations in the future as well.

Furthermore, I would like to thank Prof. Dr. Johannes Weber for the help and availability given during the SEM measurements. I thank him for the funny coffee breaks and for all sweets he has always offered me. I also thank Dr. Marta Anghelone, who, in addition to the numerous advice given to me during the doctorate, always has been a trusted friend to confide in during difficult times.

Special thanks to the whole INTK group. I thank Dr. Federica Cappa for the fun lunchtime conversations and the "desperate" moments in organizing the lectures. Dr. Dubravka Jembrih-Simbürger for the support and advice had given when I needed it. Dr. Wilfried Vetter and Karin Wallner for numerous conversations, especially about food. Dr. Guadalupe Pinar for the laughs spent during coffee breaks. Dr. Valentina Pintus who encouraged and helped me during my doctorate and who supported me in continuing my university career with determination. A heartfelt thanks to all of you.

I especially thank my colleague but above all friend Laura Rabbachin who endured me during every crisis and who has always managed to find the time to cheer me up. Thanks for all the laughs, all the noodle dinners, and the great adventures we have had together.

A big thanks to (almost Dr.) Cecilia Pesce. Despite the distance, the moments of existential panic, and the difficulties, she always managed to find the right words and the encouragement I needed. I have grown a lot with her in many ways, and I understand what the word friendship really means.

A special thanks to Christian. In a few lines, it is impossible to explain all the gratitude I feel towards him. I thank him for always being there, for supporting me, putting up with me, spending hours on the phone with me in difficult moments, for motivating me every day, but above all, for continuing to love me. Now we are at a crossroads, and it is up to us to choose the way.

Ultima, ma assolutamente non meno importante, vorrei ringraziare la mia famiglia, la mia famiglia "allargata", gli amici "Trevigiani nel mondo", gli amici Viennesi, tutte le persone che ho potuto conoscere durante questi anni per tutto il supporto, l'amicizia, e l'affetto che mi hanno dimostrato e per essermi sempre stati vicini. Con la vostra presenza, avete reso possibile questo grande risultato della mia vita, e spero possiate essermi accanto anche per i prossimi traguardi futuri.

This PhD thesis was a collaboration between the Institute of Natural Sciences and Technology in Art of the Academy of Fine Arts (Vienna) and the Technical University TU Wien (Vienna).

1

INTRODUCTION

Modern and contemporary art had an outstanding development from the 1950s on and subsequently a deep impact on the market and production of innovative artistic materials, involving more and more professionals in the fields such as conservation-restoration, art history, and conservation science. Despite the use of the latest generation polymeric materials, the artworks require adequate conservation plans, as the complex chemical composition of the materials used made the prevention assessment and the knowledge of their chemical-physical stability difficult. For this reason, since the beginning of the early 2000s, these materials have been investigated and studied by various research groups and organizations through morphological, mechanical, chemical, and physical analyzes in order to understand their state-of-art, their chemical composition, and to support conservators and restorers in evaluating the prevention of the degradation of these materials when exposed to different atmospheric conditions.

Specifically, the knowledge concerning material degradation processes, linked to the change of chemical properties of the altered surfaces due to the chemical species constituting the atmospheric environment, is still of current interest. The atmospheric degradation that influences the stability of materials is mainly due to the interaction between the atmospheric constituents and the humidity; in this way, the water settles in a thin layer on the materials and, acting as a solvent, attracts the pollutants present in the air, both gaseous and particulate matter. Therefore, having a general overview of the chemical-physical reactions that occur during the surface degradation of

materials, it is essential to develop and apply new strategies to monitor, analyze, and understand the different phases that occur during these deterioration processes. Nowadays, from the commercial point of view, routine analysis is carried out only to improve protective materials that prevent these effects. However, a more detailed and microanalytical investigation of the materials would allow to better comprehend the chemical-structural changes of the materials for industrial employment, applications in different fields of research (coating studies, corrosion science, cosmetics), and above all for the prevention of cultural heritage that over time risks to be completely destroyed.

In this thesis, an analytical procedure was developed in order to carry out a qualitative/semi-quantitative and statistical evaluation for the molecular stability of modern art materials. Results will explain the chemical interactions that occur between the atmospheric environment, modern paints, and the stability or degradation processes that are developed in contact with UV-light and air pollutant agents.

The innovative aspects of this work are based on scientific concepts which are still under investigation:

1)   The study and the molecular-chemical identification of new synthetic paint materials recently used in the artistic field;

2)   The analysis of the interaction between various pigments/binder's mixture used and the different degradation effects under UV-light exposure;

3)   The study of accelerated aging by using controlled atmospheres with relative humidity and polluting gases; the mechanisms occurring between corrosive gases and modern paint materials;

4)   The evaluation of a correct and effective method for cleaning these paint materials in order to properly remove the degradation deposits and maintain the aesthetic and physical mechanical integrity of the original materials.

The discussed investigations were performed by applying several analytical techniques, such as Attenuated Total Reflection infrared spectroscopy (ATR-FTIR),

μ-Raman spectroscopy, Atomic Force Microscopy (AFM), and Laser-Induced Breakdown Spectroscopy (LIBS). These methods led to a comprehensive and systematic investigation of the chemical reactions occurring during artificial aging of synthetic art materials. Using ATR-FTIR and Raman spectroscopy, it was possible to identify new degradation products on the surfaces. In addition to these chemical investigations, AFM was used to investigate the morphological changes observed according to the different pollutant agent, and finally, by LIBS it was possible to increase the elemental qualitative knowledge of modern art materials. The correlation of these results was studied by multivariate analysis to understand if the degradation impact on paints is favoured from the interaction and combination of the pollutants or the different components constituting the art materials. This information is important for the cultural heritage field, the prevention, the conservation practises, and the research of new restoration methods. Moreover, the scientific topic can be of interest to study the degradation of photo-electrochemical devices, the prevention of plastic industrial products, and the development of innovative solutions for air purification.

2

MATERIALS

2.1 Acrylic and Styrene-acrylic emulsions

In the twentieth century, artistic paint materials underwent a significant evolution from the stability and chemical-physical properties perspective. In previous centuries, the most used binder was petroleum, but the development and innovation of new technologies in the field of artistic materials allowed the creation of new binding media such as the polyvinyl acetate (PVA) emulsions, the vinyl-acrylic emulsions, the alkyd resins, water-miscible oils, etc. [1]. Among them, acrylic emulsion paints have been the most successful. Chemically, the two main monomers used for the formation of the acrylic polymer are the esters of acrylate and methacrylate acids, respectively. Although acrylic resins were used as early as the late 1930s, waterborne acrylic emulsions were only widely applied as artist's paints since the 1960s. Their success is mainly due to their rapid drying and the presence of water in the paint mixture instead of organic solvents. For this reason, acrylic emulsions have been revolutionary in the paint and coatings industry [2]. There are many categories of acrylic emulsions, but the two main ones are thermoplastics and thermosettings. The first represents the acrylic product most used by artists. Thermoplastic acrylic emulsions have long polymer chains, so film formation occurs without any additional chemical action (except the evaporation of the solvent or water). On the other hand, thermosetting acrylics have a slightly shorter chain length and are usually used for industrial applications [3]. Still considering thermoplastic acrylics, they can be divided into two forms: acrylic solution and acrylic emulsion. In the first case, the acrylic polymer is

dissolved in an organic solvent. In contrast, in the acrylic emulsions, the insoluble acrylic polymer is dispersed in an aqueous phase and stabilized with a surfactant (biphasic system), able to lower the interfacial tension. The surfactants used in this step are generally added in low concentrations. They can be anionic (sodium lauryl sulfate or dodecylbenzene sulphonate), cationic (quaternary ammonium compounds), or non-ionic (alkylphenol ethoxylates) [4,5].

Over the years, there were technological developments to improve the chemical and physical properties of acrylic emulsions, such as the addition of additives. They can improve the chemical performance of the acrylic binder by e.g. increasing its resistance to light degradation and thermal resistance [6]. In addition, they can be added to the acrylic matrix both during the manufacturing of the polymer emulsion and in the formulation of the paint itself (Fig. 1). Some of them are:

- Coalescing agent: It makes paints more resistant to dirt pickup when dried by forming coherent films.

- Defoamers: They reduce the tendency of surfactants to foam.

- Freeze-thaw agents: They increase the resistance to freezing.

- pH buffer: Monitoring the pH value of acrylic paints is important as it affects the physical properties and performance of the polymer system. For example, acrylic paint is more stable if slightly acid.

- Preservatives: They prevent the growth of microorganisms during the drying phase and storage.

- Protective colloids and sequestering agents: They allow for steric stabilization and the removal of metal ions that risk precipitating.

- Surfactants: As previously described, they allow for electrostatic stabilization and steric hindrance mechanisms.

- Thickeners and dispersing agents: They avoid the formation of pigment agglomerates and their steric and electrostatic stabilization.

Acrylic emulsions became particularly useful due to their physical properties, specifically, the glass transition temperature (Tg), above which a polymer can be flexible and rubbery. In the case of waterborne acrylic emulsions, copolymers with a Tg just below ambient temperature (around 10-15 °C) are selected. The polymeric film obtained will be flexible enough to avoid cracking [7].
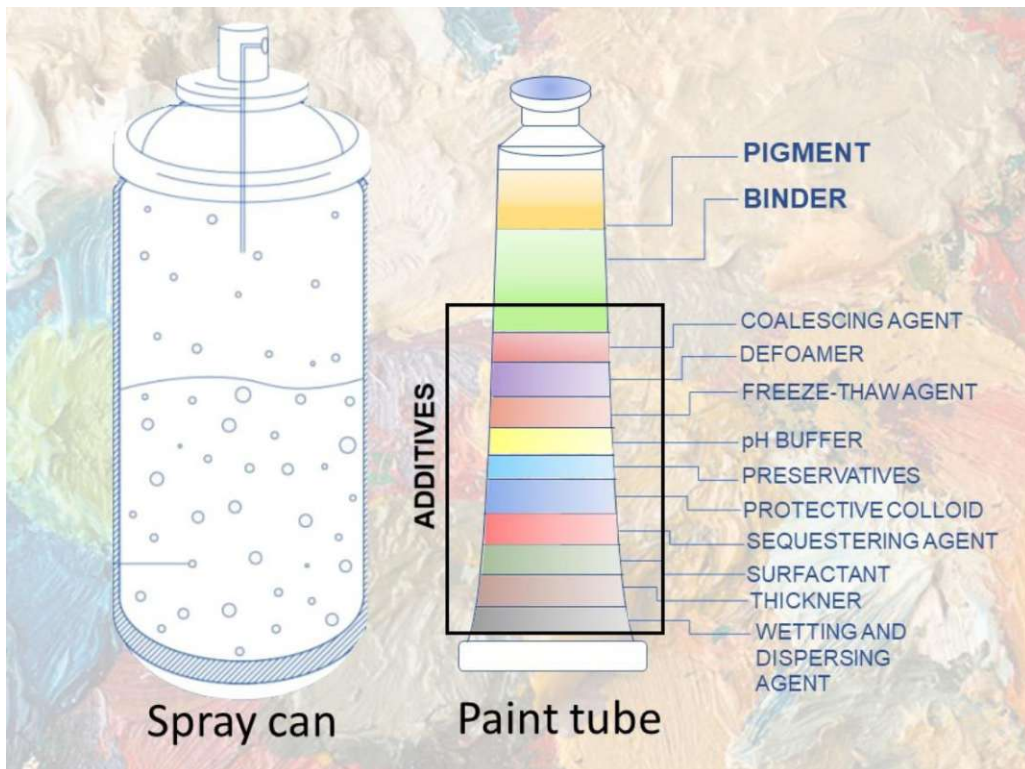
Fig. 1: Representation of all chemical components present
in acrylic paint tube and spray can.

Furthermore, another characteristic of acrylic paints is the drying speed. However, there are differences between the solution and the emulsion forms. The emulsions are dispersed and diluted in water (reducing its toxicity), while a solution dries by evaporating the solvent [8]. However, a feature that can compromise the chemical and physical stability of acrylic emulsions is the presence of additives. E.g., surfactants (the main one is polyethylene oxide, PEO) tend to migrate into the paint-air interface both during the film formation and long-term aging.

This phenomenon causes mechanical stress which leads to surface morphological changes such as increase of roughness and gloss. Once the surface is physically compromised, it will be more subject to other degradation factors making the whole paint more unstable.

In the research study presented here, a large part of the results was evaluated considering previous studies carried out [9–13] and subsequent assessments were considered trying to investigate this chemical phenomenon. As previously mentioned, during the last years of technological development, various monomers have been added to acrylic emulsions to lower production costs and improve their chemical-physical performance, creating new synthetic binders such as styrene-acrylic emulsions. In recent years, this synthetic polymer has found wide application in the coatings industry as well as in the artistic field, especially for spray paints and contemporary murals [14]. The stability of styrene-acrylic emulsions in artworks is still poorly understood [15,16]. However, due to the photochemical reactions involving styrene monomers, it would be more prone to yellowing and less chemically resistant.

2.1.1 Polymerization and film formation

At the industrial formulation level, these emulsions are made by means of the so-called *emulsion polymerization*. Although this reaction is extremely complicated and, in some ways still not fully understood, four main components are involved:

- The monomers (generally acrylic acid, methacrylic acid, ethyl acrylate (EA), and n-butyl methacrylate (nBA));
- Water (able to disperse the heat derived from the generated exothermic reaction);
- The surfactant, and an initiator.
- In addition, protective colloids can be added, such as polyacrylic acids or polyvinyl alcohol, for stabilizing the emulsion and avoiding the formation of agglomerates [4].

The first step of the emulsion polymerization is the mixture of water and surfactant, so that the surfactant micelles are present at a certain concentration, the so-called critical micelle concentration (CMC). In this way, the micelles present in the aqueous phase will be displayed with their hydrophobic part (apolar) inside and the hydrophilic one (polar) outside the micelle. The surfactants used can be divided between anionic and cationic. The first ones, such as alkyl sulphates and carboxylic acid phosphates, can be added in small quantities, however with the risk of causing foaming. On the other hand, the latter, generally phenols with alkyl chains or ethoxylated alkyl alcohols, exhibit less surface activity but may not form appropriate micelles. Depending on the type of product to be obtained, the most suitable surfactants will be selected and used in the polymerization process [17]. Subsequently, the monomers are added and mixed with the water-surfactant mixture. In this way, some monomers break down into droplets and some dissolve in the surfactant micelles. The third phase consists in the addition of the initiator, which is dissolved in the water. For acrylic emulsions, the commonly used initiators are persulphates of potassium, sodium, and ammonium. These sulphate anions initiate the polymerization in the aqueous phase by reacting with the monomers and forming new ion radicals. These propagating species allow the growth of the polymer chain by adding more monomer molecules to the radicals [18].
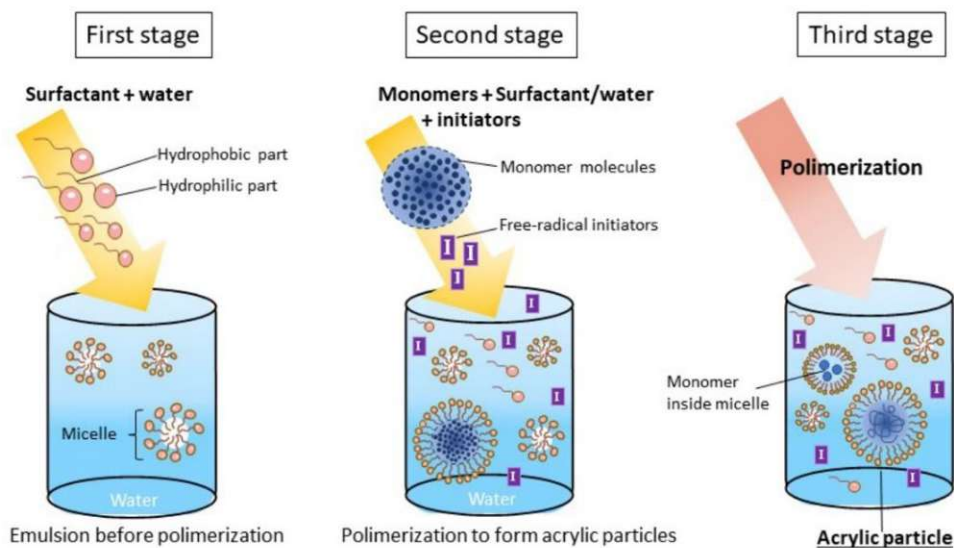

Fig. 2: Chemical formation of acrylic particles by polymerization.

The polymer particles also grow inside the surfactant micelles until they reach the stabilization phase. In Fig. 2, a schematic representation of the polymerization emulsion in aqueous phase is shown.

Once the paint has been applied to a surface, the drying process begins. It will be different for polymers in solution or in emulsion. In the latter case, the polymeric units will be of larger size and will have the form of polymeric spheres dispersed in aqueous solution. The film formation process is based on two steps [19]. The first is the evaporation of water, controlled by the diffusion of the vapor pressure of the water itself. Subsequently, the polymer molecules in the dispersed phase will gather each other, also incorporating the pigment particles and additives present. This phenomenon is called coalescence. Finally, the last remaining amount of water evaporates, forming the final dried polymer layer. Once the adhesion process of the polymer spheres is completed, it will be irreversible [3]. Fig. 3 shows the stages of film formation.
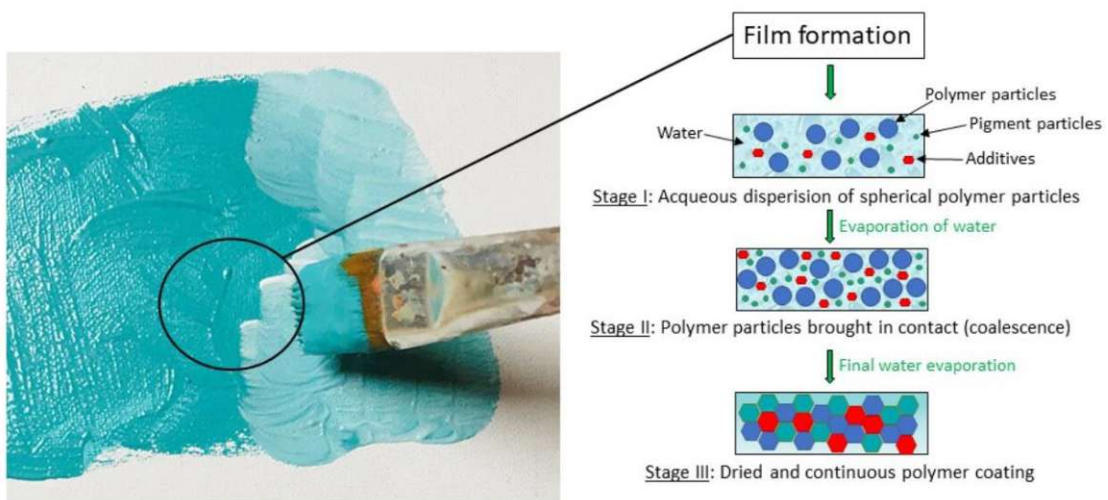

Fig. 3: Chemical mechanisms for film formation in an emulsion system.

However, some factors can influence the film formation stages. First of all, the complete evaporation of the water must take place, to avoid that some water molecules remain trapped in the dried film. The time required to complete this phase depends on several factors, especially from the so-called "open time" of the mixture. It indicates the time within which a layer of wet paint can be "overcoated", avoiding aesthetic

defects such as layering [20]. Monitoring the glass transition temperature (Tg) of the polymers used to create the film is also important. If higher than the drying temperature, the film will not be thick enough due to the non-plasticity of the emulsions, subsequently compromising the coalescence phase. If, on the other hand, the Tg value is low, the resulting film will be soft and flexible but with poor physical-chemical characteristics unlike polymers with high Tg. For this reason, the so-called "coalescing agents" are added to industrial formulations, which lower the Tg of the binder without altering its technical properties. In fact, it allows the solvation of the polymer particles, favouring their aggregation [21].

2.2 Alkyd resins

Alkyd resins are a binding medium widely used as a product in the coating industry and in the artistic field. They were introduced in the late '30s, even if their success was only in the late '50s, as artists began to replace it with the traditional binder used since ancient times, namely oil [1]. Alkyds are oil-modified polyester resins; the latter is fundamental in the chemical formulation of the alkyd product as it allows to obtain a flexible film. The term "alkyd" derives from the two main components of which it is composed: a polyhydric alcohol (or polyol) and a polybasic carboxylic acid. Industrially, the alkyd resin is prepared by heating the oil component with phthalic acid anhydride and glycerol to obtain a polyester containing fatty acids. In general, the polyester obtained is a hard, crosslinked thermosetting resin which, by adding a monobasic fatty acid, is able to reduce its degree of crosslinking [22]. Below and in Fig. 4, the different components of an alkyd resin are described:
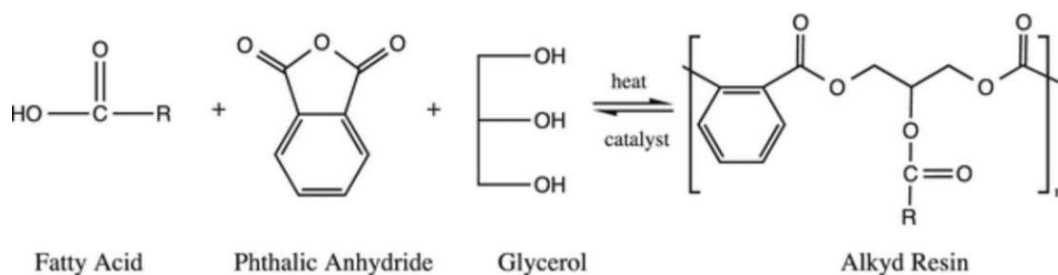

Fig. 4: Principal reaction for the formation of an alkyd polymer [23].

- Polyol: Generally, the two most used are glycerol and pentaerythritol. The first was used before 1960, to obtain alkyds with short and medium oil chains, whereas pentaerythritol was applied for long oil alkyds. The latter dry more quickly and the film produced is more flexible and durable (greater water resistance).

- Polybasic acid: The common polybasic acid is the phthalic anhydride of the dibasic acid of which all alkyd paints are generally composed. Alternative products are dibasic acids such as: isophthalic, terephthalic, and maleic acid [24].

- Drying oil: The oily component, i.e. monobasic fatty acids, allows alkyds to differentiate themselves from other polymeric products obtained from the condensation of polybasic acids with polyvalent alcohols. Depending on the different fatty acid used, the alkyd resin will have certain drying characteristics. As reported in the literature [25], the best drying properties are obtained by adding an unsaturated fatty acid. The three main ones are: linseed, soybean, and safflower oil. Linseed oil is the most common but tends to yellow easily. For this reason, it is mainly used in paint mixture with dark color pigments.

An important classification of the alkyd resins is by the proportion of oil to resin, or "oil length". Three are the main categories, i.e. short-oil resins (< 40% oil content); medium-oil resins (40 to 60% oil content); and long-oil resins (> 60-70% oil content), the latter the most stable. According to this percentage in the resins, it determines certain physical and solubility properties of the paints. Some of these are hardness, durability, flexibility, viscosity, chemical resistance, and stability. Because of its aesthetical appearance similar to the traditional drying oil but the shorter drying time, alkyd resins became very popular, widening the range of possibilities of artists, including Pablo Picasso and Jackson Pollock [4].

2.2.1 Drying process and film formation

The drying mechanism of the alkyd resin is similar to that of oil and can be divided into two different phases. The first process takes place through the physical drying of the resin where, after the evaporation of the solvent, a uniform film is formed. The second process occurs chemically and is called lipid autoxidation [22]. This phenomenon is more complex than the previous one and occurs by involving the free radical chain. It can be divided into three steps: initiation, propagation, and termination (Fig. 5). The first phase can take place by the action of some initiating species in the substrate, by thermal decomposition of the hydroperoxide, or by the presence of a metal dryer. Subsequently, the formation of hydroperoxide (propagation reaction) takes place by means of a faster reaction involving high partial pressures of oxygen. Finally, with the termination step, radical recombination leads to the formation of peroxy, ether, and C-C crosslinks, obtaining a final dried alkyd film. Lipid autoxidation involves the fatty acid group of the alkyd resin. In fact, the drying power varies according to the type of oil and the chemical reactivity of the double bonds of unsaturated acids. They favor the reaction with oxygen in the air to form a polymeric film [26]. Specifically, with the first step of autoxidation, a bis-allyl hydrogen atom from the unsaturated fatty acid is extracted (Fig. 6). It causes the formation of a radical species, which is stabilized by its delocalization due to the pentadienyl structure. The reaction of molecular oxygen with this pentadienyl species is very rapid, leading to the formation of a peroxidic radical with conjugated double bonds. The main reaction involved is the extraction of a hydrogen atom from another resin molecule to form a hydroperoxide and propagate the radical chain [27]. Subsequently, the hydroperoxide decomposes leading to the formation of non-volatile crosslinked species or species such as alcohols, ketones, aldehydes, and carboxylic acids [28].
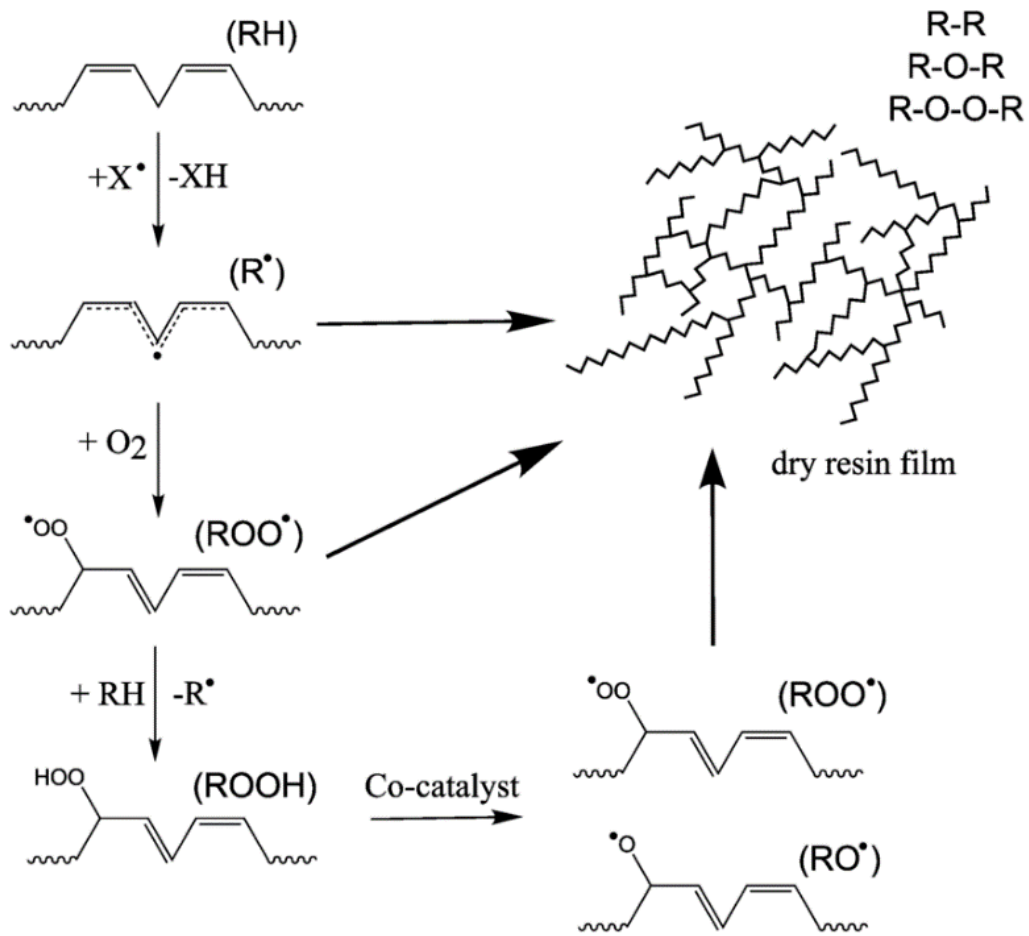
Fig. 5: Chemical drying process of alkyd resins [29].

However, alkyd paints dry faster than oils, and this is due to the presence of dryers, the degree of unsaturation of its fatty acid chains or the presence of phthalic groups which lead to less oxidation reactions. It is precisely through this innovative crosslinking process that alkyd resins represented a revolution in paint technology, both in the industrial and artistic field [30].
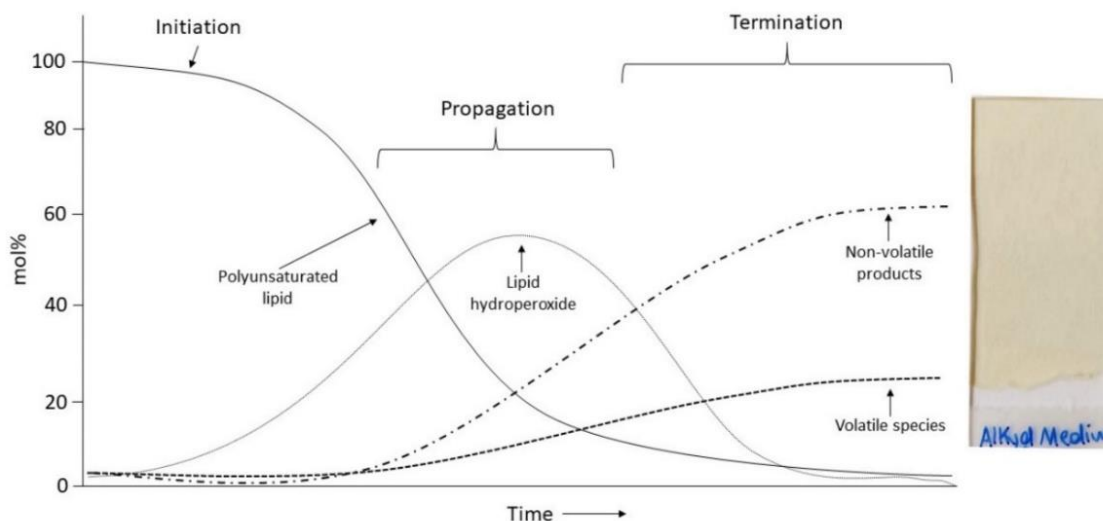
Fig. 6: Representation of fatty acid chain autoxidation of an alkyd resin.

2.3 Sample preparation

For this study, samples were prepared with different mixtures of pure acrylic emulsion (Plextol® D498, Kremer Pigmente, Germany), alkyd resin (Alkyd Medium 4, Lukas, Germany), and styrene-acrylic emulsion (Acronal S790, BASF, Germany) in combination with nine inorganic pigments. All pigments are products of Kremer (Kremer Pigmente, Germany). The chosen materials (Tab. 1) are not only used in the artistic field but also in industry and daily life. These inorganic pigments, for example, are employed for buildings, production of industrial objects and even cosmetics, while organic binders, modified in their chemical-physical properties during recent years, are increasingly employed in various sectors such as transportation, construction or art [31]. After having weighed the pure materials, they were put on a mortar and mixed with a muller for a few minutes. The pigment/binder (P/BM) ratio chosen is 1:3. The paints were spread on glass slides using the so-called Doctor Blade technique (Fig. 7) [32]. Once the correct paint consistency was achieved, a small amount was placed on a glass slide with a spatula. Between the slide in question, two other slides were placed under which an aluminum foil with a thickness of 150 μm was placed.

14

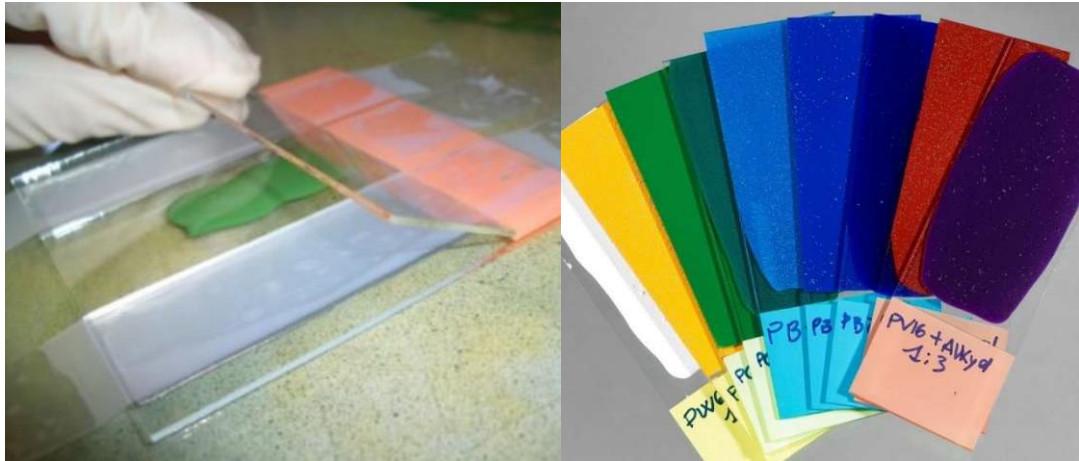In this way, using another slide, the spreading paint will have an ideal wet film thickness of 150 μm.

Fig. 7: Sample preparation by the so-called Doctor-Blade technique and representation of the final mock-ups.

In total 288 samples were prepared, considering every combination between pigments and binders and the experiment number carried out. The samples were dried under room conditions (ca. 22 °C and 30% relative humidity) for three weeks before starting the artificial aging (Fig. 7).

Tab. 1: Inorganic and organic materials used for the sample preparation.

Pigment	Chemical composition	C.I. Name
Titanium white	TiO_2	PW6
Cadmium yellow	CdS	PY37
Cobalt green	Co_2TiO_4	PG50
Hydrated chromium oxide green	$Cr_2O_3 \cdot H_2O$	PG18
Cerulean blue	$CoSnO_3$	PB35
Cobalt blue	$CoO \cdot Al_2O_3$	PB28
Artificial ultramarine blue	$Na_{8-10}Al_6Si_6O_{29}S_{2-4}$	PB29
Iron oxide red	Fe_2O_3	PR101
Manganese violet	$NH_4MnP_2O_7$	PV16

Binder	Chemical composition	Commercial Name
Acrylic emulsion	p(nBA/MMA)	Plextol® D498
Alkyd resin	Polymer oil-modified polyester-resin based on orthophthalic acid and pentaerythritol	Alkyd Medium 4
Styrene-acrylic emulsion	P(nBMA-2EHA-Styrene) terpolymer	Acronal S790

3

ACCELERATED AGING

3.1 Atmospheric pollution

When a material gets in contact with the surrounding environment, the interaction between its surface and the components present in the ambient atmosphere is inevitable. This interconnection causes the formation of degradation products and in many cases to the loss of appearance over time, especially in the case of art objects, and functionality for industrial materials. Additionally, in the ambient atmosphere, it is also necessary to consider the relative humidity (RH), the influence of the light radiation, the temperature, and oxidizing reactions due to pollutant gases. These factors, especially in the case of cultural heritage, cause significant degradation processes: i.e., different physical and chemical surface changes [33].

Prevention and restoration actions will have to evolve reducing the impact of damage due to air pollution, different biological and physical processes, and the combination with UV-radiation, which gives rise to new forms of damage. Many studies were developed for the characterization and prevention of art objects exposed in indoor environments [34], in which the parameters such as relative humidity, temperature, and pollutant agents are more easily controlled. The problem occurs when artworks such as sculptures, murals, coated, and painted objects are exhibited outdoor, and they are challenging to monitor and protect.

3.1.1 Polymer photodegradation

Photo-oxidation occurs when a polymeric surface is periodically subjected to light irradiation and oxygen to the point of causing its degradation. The damages caused by photo-oxidative degradation are mainly alterations in the chemical and physical properties of the polymer. UV-light is generally classified into three specific regions according to the different wavelengths in which they operate (Fig. 8). They can be divided in: UV-A (400 to 315 nm, near UV), UV-B (315 to 280 nm, middle UV) which can cause chain splitting and/or crosslinking of the polymer chemical structure, and finally UV-C (280 to 100 nm, far UV), which is completely absorbed by the atmosphere [35].
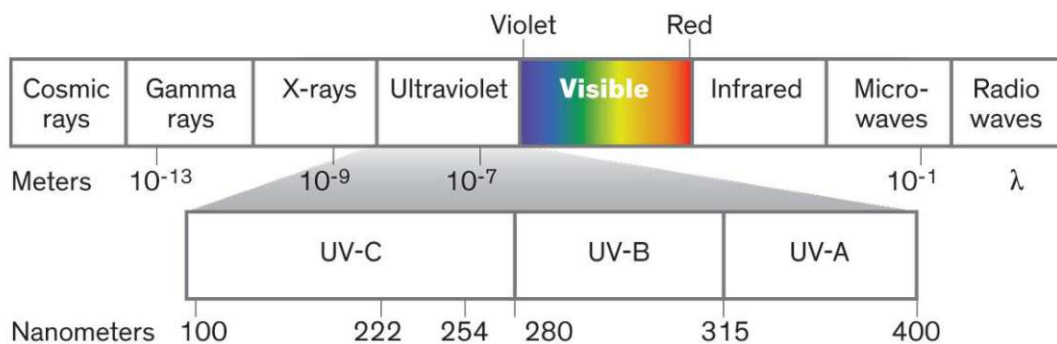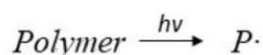

Fig. 8: UV-light range in the electromagnetic spectrum [36].

Photo-oxidation (Fig. 9) comprises several steps in which various photochemical reactions act on the surface of the exposed polymers [37]. The first stage is called *initiation*. When the UV-radiation hits the polymeric matrix, it absorbs part of the photons and some molecules inside the polymeric structure are activated, forming an alkyl radical polymer (P → P· + P·). The absorbed energy can be released in different ways, such as by breaking chemical bonds (photolysis) or by transferring the energy to another atom or molecule [38]. Subsequently, with the *chain propagation* phase, the formation of peroxy radicals (POO·) takes place through the reaction of the polymeric alkyl radicals (P·) with oxygen (O_2); finally, hydroperoxides (POOH) and a new polymeric alkyl radical (P·) are formed. The third phase involves chain scission

reactions, or even *chain branching*, which leads to the formation of alkoxy polymeric radicals (PO·) and hydroxyl radicals (OH). An effect of the alkoxy polymeric radicals (PO·) is the possible formation of in-chain ketones by β-scission reactions; it leads to a decrease in the molecular weight, a loss of their chemical/physical properties, and an increase in the solubility of the polymer. The last phase is called the *termination* reaction which, through crosslinking reactions of free radicals, lead to non-radical products resulting in less solubility and flexibility. The resulting products of photochemical reactions are mainly chemical compounds such as aldehydes, ketones, and carboxylic acids at the end of a polymer chain [39].
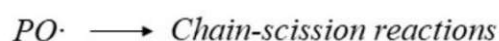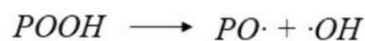
INITIATION

$$Polymer \xrightarrow{h\nu} P\cdot$$

CHAIN PROPAGATION

$$P\cdot + O_2 \longrightarrow PO_2\cdot$$
$$PO_2\cdot + PH \longrightarrow PO_2H + P\cdot$$

CHAIN BRANCHING

$$POOH \longrightarrow PO\cdot + \cdot OH$$
$$PO\cdot \longrightarrow Chain\text{-}scission \ reactions$$

TERMINATION

$$PO_2\cdot + PO_2\cdot \longrightarrow PO_4P \ (\longrightarrow PO_2P + O_2)$$
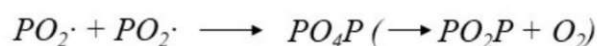
Fig. 9: Free-radical oxidation reactions.

3.1.1.1 Photo-oxidation of acrylic and styrene-acrylic emulsions

As previously mentioned, UV-radiation can compromise in long-term the chemical/physical stability of modern and contemporary artworks based on acrylic and styrene-acrylic emulsions, especially when they are exposed outdoors. This research topic has been extensively studied in the last 30 years [40–42], especially considering the photo-oxidation reactions in the wavelength range between 315 and 400 nm (UV-

A), on poly (n-butyl acrylate/methyl methacrylate) and poly (ethyl acrylate/methyl methacrylate) emulsions.

Chiantore et al. [43] classify two main photo-oxidative reactions that most damage acrylic polymers: crosslinking and β-scission reactions that compromise the film's mechanical properties. At the molecular level, tertiary hydrogens are the first elements that undergo photolysis or photochemical processes. In fact, acrylic polymers, having tertiary hydrogen attached in the alpha position to the ester group, are more reactive to photodegradation than methacrylic polymers. Whether photolysis or photochemical processes, macroradicals are generated and will be further subject to β-scission or crosslinking reactions. With β-scission reactions, volatile products and low molecular weight monomers are formed which, evaporating from the film, reduce the mass of binder in the material exposed to photo-oxidation [44]. Depending on the length of the polymer side chains, one of the two reactions will be favoured. In the case of short side chains (< 4C) a β-scission reaction will develop, while with a longer side group, the polymer will be subject to crosslinking by photo-oxidation of the side group itself.

After the abstraction of tertiary hydrogen and the reaction of the alkyl radical with oxygen, ketones are formed. They subsequently undergo scission which leads to the formation of carboxylic acids. The ketones formed can also be unsaturated which, undergoing further oxidation, form hydroperoxides and alcoholic groups, or γ-lactones for intramolecular reactions. The final products deriving from the chain-scission reactions and macroradical disproportion are vinyl groups and terminal double bonds. These groups can be attacked by photochemical reactions and form conjugated double bond systems that cause further degradation [45]. The damages caused by photo-oxidative degradation affect the mechanical, physical, and chemical properties of polymers leading to a more brittle, rigid and fragile film. Monitoring and studying these effects on acrylic and styrene-acrylic works of art are very important for conservators and restorers, who, on the basis of the results obtained, will have to develop an adequate conservation and preventive plan [9,11].

3.1.1.2 Photo-oxidation of alkyd resins

As extensively studied [30,46], alkyd resins undergo polymerization and photodegradation processes similar to those of drying oils, due to their fatty acid content. The auto-oxidation process already takes place during the drying phase of the resin and continues even after hardening. The C-O-O-C peroxide bond formed with the self-oxidation of unsaturated bonds during drying is particularly weak therefore, when subjected to the action of UV-radiation, it tends to form peroxide and hydroperoxide radicals [47]. They react with the alkyd chain leading to further crosslinking and/or β-scission reactions (which produce aldehydes, alcohols, and carboxylic acids) and possible tertiary hydrogen extraction. The first and main phase of the photodegradation of aromatic polyesters is called Norrish type I, which leads to the formation of free phthalic acid. Subsequently, secondary reactions will lead to the extraction of hydrogen and the formation of ketones, aldehydes, alkene, and carboxylic acids. They, once further excited to a single photochemical state, allow the rearrangement in the molecule. Subsequent hydrogen abstraction leads to Norrish type II reactions forming alcohols, cyclic structures, carboxylic acids, and accumulation of vinyl groups. The formation of conjugated double bonds and cyclic structures is the main cause of yellowing of the paint film [25,48–50]. In summary, the formation of short chains and volatile products, mainly due to the Norrish type I and chain-scission reactions, cause the shrinking of the film. Therefore, the photo-oxidative degradation of the alkyd resin is given by an excessive molecular crosslinking which makes the paint layer rigid and brittle, up to the loss of the mechanical properties of the film.

3.1.1 Pollutant gas aging

When a material gets in contact with the surrounding environment, the interaction between its surface and the components present in the ambient atmosphere is inevitable. This interconnection causes the formation of degradation products and in many cases to the loss of appearance over time, especially in the case of art objects,

and functionality for industrial materials. In the ambient atmosphere, additionally to the relative humidity (RH), the influence of the UV-light, and the temperature, it is necessary to consider also the oxidizing agents due to pollutant gases. These factors, especially in the case of cultural heritage, cause significant degradation processes: i.e., different physical and chemical surface reactions (Fig. 10).

In many research projects, the UV-light initiated degradation processes are explained [51,52], but there are still ongoing studies concerning the influence that temperature, relative humidity (RH) and pollutant gases have on outdoor paint materials. The most relevant inorganic polluting gases present in urban atmospheres are SO_2, H_2S, NO_x, and O_3. They have different characteristics [53]:

- SO_2 is produced during the combustion of fossil fuels and the metal refining process, making it one of the most important polluting gases presents in the atmosphere [54]. The study of its interaction with paint mixtures will be interesting to understand the reactions occurred on old artworks exposed to outdoor conditions during the last century.

- H_2S is emitted from natural and anthropological sources, interacting with materials such as pigments and organic polymers, and leading to the formation of substitution reactions. It contributes to metal corrosion by being dissolved in the aqueous surface film forming HS^- ions as an active corrosion agent. Pigments chosen are mainly inorganic, so the formation of degradation products is expected.

- NO_x is generally emitted from fossil fuel combustion processes and it contributes to the formation of other air pollutants, such as ozone, particulate matter, and acid rain.

- O_3 is a product of atmospheric photochemistry, is sensitive to UV-light, and is reacting with water molecules to form energetic oxygen atoms and hydroxyl radicals.
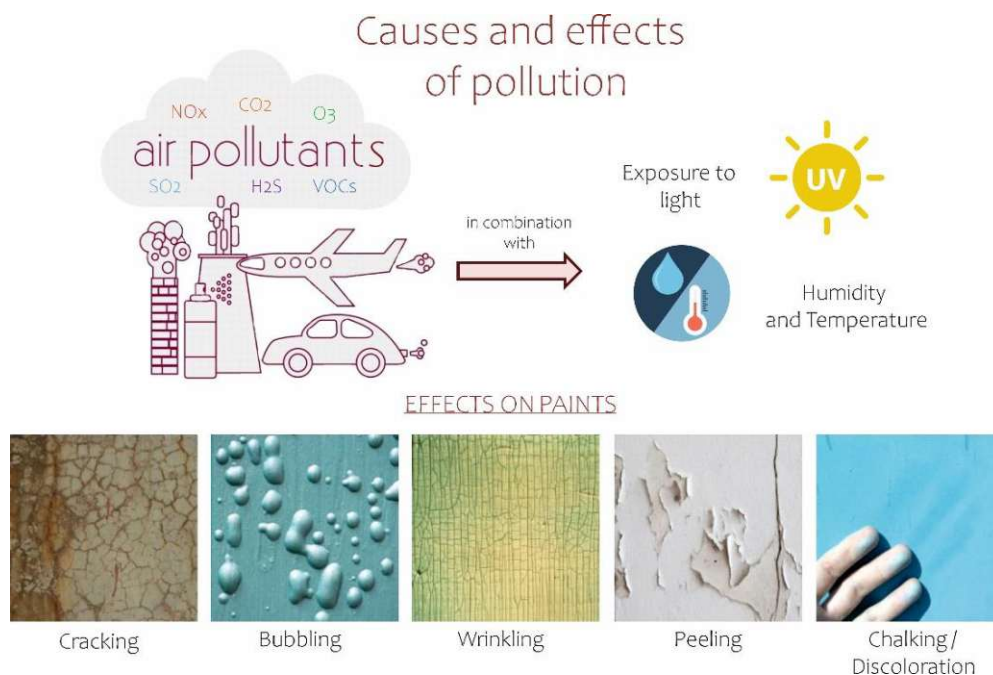
Fig. 10: Example of possible atmospheric degradation effects on paints.

Although recently the concentration of these gases in the air has reduced (except for ozone), the study of their interaction with artistic materials remains important; both for the study of modern artworks (20th century) and for those latest [55]. As previously mentioned these polluting gases can interact with the atmospheric humidity present and, forming ionic compounds and free hydrogen ions, can interact more with the surface of the materials and form new corrosive species. Compared to the research carried out on the corrosion of other artistic materials, the interaction with inorganic pigments mixed with organic binders and the surrounding environment is still under investigation [56]. Generally, paints and coatings are used not only for aesthetic purposes but also to prevent deterioration of the underlying substrate when exposed to ambient atmosphere. However, for this objective, the paint or coating must maintain its mechanical and physical properties such as adhering adequately to the surface on which it has been applied. Although some of these materials maintain these characteristics over time, most of them suffer morphological and chemical damage due to the degradation process. Some reasons may be: incorrect formulation of the commercial product, paint materials not suitable for the environment in which it was

exhibited, problems in applying the product to the substrate, drying phase not completed, particularly hostile environmental conditions, especially for the artworks [57]. The latter in particular is aggravated by the cross effect given by the interaction between polluting gases and atmospheric humidity. Even when water occurs in the form of water vapor, it is capable of dissolving and dissociating most chemical compounds into their acidic or basic constituents. At the molecular level, when this dissociation occurs and the acid or base comes into contact with a material (such as paints in this case) a chemical attack can occur. The polluting gases, with different reactivity, react with the atmospheric water forming hygroscopic compounds.

In the study carried out here, the polluting gases chosen (SO_2, H_2S, and NO_x) are part of the so-called acid gases [58,59], which react with air humidity forming either precipitations or condensation giving acids, such as sulfuric and/or nitric acids. The chemical attack resulting from condensation on a paint is more aggressive than that deposited by precipitation (acid rain), because the humidity condensed on a surface in the form of tiny droplets tends to evaporate over time. Subsequently, the acid components inside begin to be concentrated and the corrosive action leads to attack the substrate on which the condensate resides are. In contrast, acid rain is a more diluted form of the gaseous acid components. However, even in this case, the chemical compounds deposited split the chemical bonds of the paint materials most susceptible to deterioration. The chemical groups particularly vulnerable to attack and split of acidic substances are the ether and ester bonds, where the splitting occurs by reaction of the hydrogen ion [60] (Fig. 11).
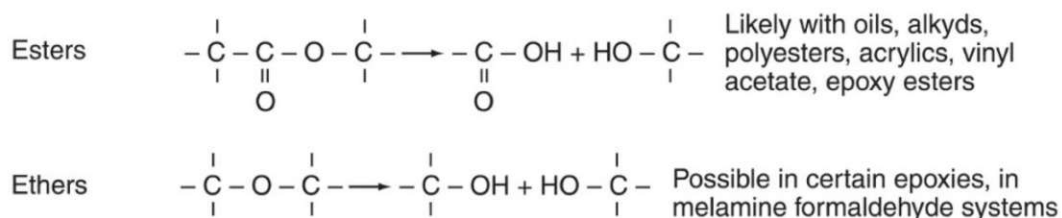

Fig. 11: Chemical groups vulnerable to acidic gas action [61].

3.2 UV-light and artificial weathering conditions

In order to simulate the natural sunlight action on the paint surfaces, the light aging was carried out in a UVACUBE SOL2/400 FUV chamber (Dr. Hönle GmbH UV-Technology, Germany). The emitting radiation was supplied by a Xenon Arc lamp using a H2 filter, with the possibility to provide radiations between 295 and ca. 3000 nm, similar to outdoor solar conditions (Fig. 12). The irradiance of the Xenon lamp was monitored with a UV-Meter Basic sensor (Dr. Hönle, Germany) and reached an approximate value of 170 W/m^2. Temperature and RH were separately measured in the chamber using the AQL S500 sensor (Aeroqual Limited, New Zealand). During accelerated aging, the chamber temperature was around 38°C and the RH varied between 10 and 20%. According to the data typical for Central Europe, it is possible to assume that the radiation value obtained is similar to natural aging caused by solar radiation [62].

As previously explained, light aging is part of a research study carried out several years ago and the study presented here represents the final stage. Therefore, only selected paints were aged by UV-light, in this case the alkyd paints (Tab. 2). Accelerated light exposure of the samples was performed for a total of 1008 h. In one year, natural exposure to external sunlight is around 1000 h. Therefore, it is possible to approximate that the actual artificial aging of 1008 h is equivalent to about one year of natural light exposure [63]. The slide, on which the paint was spread, was divided into six regions (Fig. 12) to obtain different aging periods (from 168 to 1008 h) on each paint sample. Regions that were not exposed to artificial light were covered without contact with a filter made of a 100% silver-aluminum reflective material. The reflective cover was moved weekly to get the full set of 1008 hours aged samples.

Fig. 12: UV-light aging chamber used and representative set of samples aged.

Tab. 2: List of the mock-ups aged with UV-light and aging conditions used.

Samples			UV-light exposure time
Binder	**Pigment**	**P/BM ratio**	
Alkyd resin	PB29	1:2, 1:3, 1:6	from 168 to 1008 h
	PG18		
	PY37		

Total number of samples: 18, aged regions: 162

On the other hand, for the aging tests using pollutant gases a greater number of mock-ups were prepared as the study presented here focuses on this type of accelerated aging (Tab. 3). The gas mixing unit consists of various units such as corrosion resistant stainless-steel pipes, high precision pressure, gas mixing valves, gas flow meters (flowmeter with floating ball, BURDE&CO), and gas sensors. As shown in Fig. 13, the flow of dry synthetic air (Messer Griesheim Austria, O_2 20.5%, rest N_2) is divided into two separate streams. One is humidified in a bottle filled with double-distilled water (100% humidified air stream) and then combined with the untreated airflow to an air stream with different desired levels of relative humidity (RH %). To this humidified air stream, the desired concentration of acidifying/corrosive gases can be

batched via the flowmeters. All gases pass the pressure reducing valves before passing through the flowmeters. All gas streams are combined by gas mixing valves to enter the "weathering chamber". The latter is made of a co-polyester material (Bel-Art™ SP Scienceware™), including gas inlets and outlets able to reach a total volume of 30 cm^3. In the chamber, the gas mixture was continuously circulated with a gas flow rate of 100 L/h. The relative humidity content (RH %) chosen is 50 and 80% for a total exposure time of 168 h. The gas concentration values were selected on the basis of the annual report published by the European Environment Agency for Air Quality Monitoring (Tab. 3) in order to reproduce a long-term aging of the gas [64]. The gas concentration was monitored daily during the accelerated aging using a specific gas sensor (Aeroqual Limited, New Zealand, model AQL S200). During the ageing experiments, the value could vary by ± 1–0.5 ppm. The samples were aged with gaseous pollutants which represent the main and most harmful corrosive gases at the atmospheric level, namely hydrogen sulphide (H$_2$S), sulfur dioxide (SO$_2$), nitrogen oxide (NO$_x$), and ozone (O$_3$).
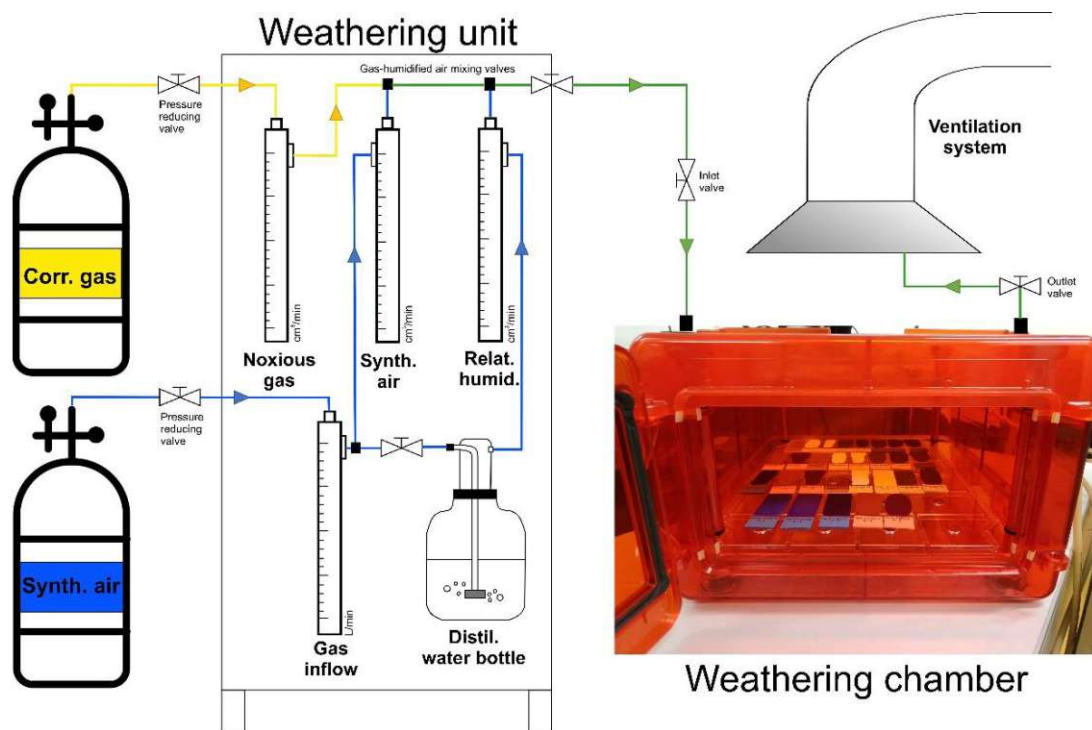

Fig. 13: Pollutant gas mixing and aging chamber used.

Tab. 3: List of the mock-ups aged with pollutant gases and aging conditions used.

Samples			Gas concentration (ppm)	Relative humidity (RH %)
Binder	**Pigment**	**P/BM ratio**		
Acrylic emulsion, Alkyd resin, Styrene-acrylic emulsion	Pure	1:3	H_2S: 0.25 SO_2: 15 NO_x: 15 O_3: 2500	50 and 80 %
	PW6			
	PY37			
	PG50			
	PG18			
	PB35			
	PB28			
	PB29			
	PR101			
	PV16			

Total number of samples: 270

4

ANALYTICAL METHODS
AND EVALUATION

The analytical techniques employed were selected to adequately investigate the three main objectives of this study, namely the identification of the main compounds in synthetic paint materials, the analysis of the influence of different inorganic pigments, and their chemical stability to UV-light and pollutant gases.

For an appropriate evaluation of unaged and aged synthetic paint materials both analytical methods commonly employed in the field of cultural heritage and more advanced and innovative techniques were selected. Initially, the morphological changes on the sample surface due to the different impact of polluting atmospheric agents were studied by *3D Optical Microscopy*. Depending on the results obtained, a more advanced microscopic technique was employed, namely *Atomic Force Microscopy (AFM)*. For the chemical evaluation of the degradation phenomena, spectroscopic methods based on the interaction of electromagnetic radiation with the materials under examination were applied. *Fourier Transform Infrared spectroscopy (FTIR-ATR)* and *Raman spectroscopy* are two complementary techniques widely used for the analysis of artistic materials that give information both of the organic components (through the evaluation of the functional groups of the ligand molecules) and of those inorganic belonging to the pigments in the mixture. These analyzes were carried out to obtain qualitative and semi-quantitative information, focusing on the degradation reactions and evaluation of the surface mapping. Finally, the use of *Laser-Induced Breakdown spectroscopy (LIBS)* made it possible to investigate the elemental

surface distribution of paints using low lateral resolutions making this technique very promising for the application of imaging on modern art materials. Finally, several *multivariate and statistical methods* were applied to the obtained results, allowing to verify the main spectral differences between the unaged and aged samples, and to understand the influence of UV-light, type of corrosive gas, relative humidity, and type of inorganic pigment on the deterioration process of binders (acrylic emulsion, alkyd resin, and styrene-acrylic emulsion).

The basic theory of these analytical and multivariate methods and their applicability for degradation studies is discussed in the next chapters.

4.1 Infrared spectroscopy

In the field of cultural heritage, infrared spectroscopy (IR) is one of the most common and widely used spectroscopic techniques. It is able to determine different molecular structures by absorbing the IR radiation of the different functional groups and is often used for the identification of inorganic and organic compounds [65]. Generally, the infrared portion in the electromagnetic spectrum is divided into three regions; the near, middle, and far infrared. The near IR works with high energy ranges (about 14.000-4.000 cm^{-1}, i.e. a wavelength of 0.7-2.5 μm) and is able to excite harmonic or combined modes of molecular vibrations. The mid-infrared (about 4.000-400 cm^{-1}, a wavelength of 2.5-25 μm) is used to study the fundamental vibrations of molecules and the associated rotational-vibrational structure. Finally, far infrared (about 400-10 cm^{-1}, a wavelength of 25-1.000 μm) is used to detect low-frequency vibrations. To monitor intermolecular vibrations, the terahertz region (2-130 cm^{-1}), bordering the microwave region, can be used [66]. A molecule is able to absorb infrared radiation in three different ways (Fig. 14), resulting in an increase in energy proportional to the absorbed light:

- The *translational* energy reflects the energy required to move a molecule in space;
- The *rotational* energy is responsible to rotation of the molecule around its

center of mass; generally, it occurs at lower energies (longer wavelengths);

- The *vibrational* energy (near infrared) induces the vibrational movement of the single atoms of the molecule [67]. The latter involves electrons of molecules being raised to a higher electron energy, which is the *electronic transition* (ultraviolet region of the electromagnetic spectrum).
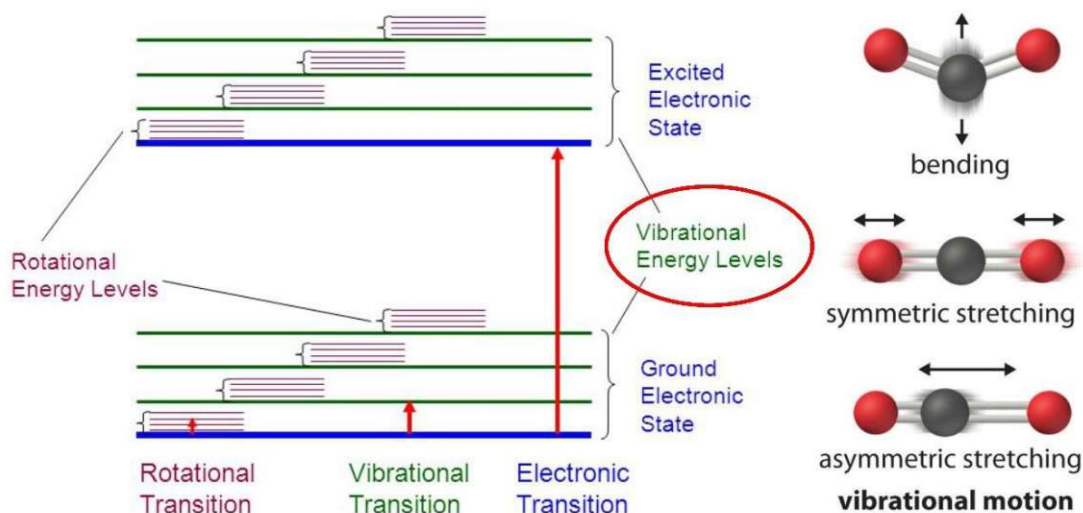

Fig. 14: Absorption of IR radiation at high energy level and corresponding molecule movement with vibrational motion.

The movement of a molecule formed by molecular bonds follows the orientation along the three Cartesian axes (x, y, z) and is determined by the number of atoms present in the molecule. It corresponds to 3N, defined as degrees of freedom, i.e. the maximum number of potential transitions. For a non-linear molecule these modes are 3N-6 (3N degrees of freedom minus 3 translation and 3 rotation), while for a linear molecule they are 3N-5 (3N degrees of freedom minus 3 translation and 2 rotation). The infrared radiation to take place in a vibrational transition when a change in the molecular electric dipole occur as a result of the change in position of the atoms. For example, homoatomic molecules (such as N_2 or O_2) are not active in the infrared, while molecules, such as CO_2, exhibiting asymmetrical vibrations in their structure can resonate with the radiation and produce an instant dipole. Furthermore, the so-called overtone bands (higher harmonics) can also be observed due to the anharmonicity of

the chemical bond [68]. Theoretically, the absorption of IR radiation by a molecule can be compared to two atoms attached to each other by a mass-less spring. Thus, considering a simple diatomic molecule, only one vibration is possible. This phenomenon is explained by Hooke's law which relates the mass of atoms in a molecule, the bond energy, and the absorption frequency, as shown in the equation (1):

$$\nu = \frac{1}{2\pi C} \sqrt{\frac{\kappa}{\mu}}$$

(1)

where κ is the Hooke's constant, which depends on the energy and length of the bond, and μ, (defined as reduced mass), which depends on the masses involved. From equation (1) it can be assumed that the resulting vibration is proportional to the frequency of the photon. Consequently, atoms of low atomic number (e.g. H, O, C) and strong bonds lead to higher absorbance frequencies.

Another important feature of IR absorption is its intensity, described as (2):

$$I_{IR} \propto \left(\frac{d\mu}{dQ}\right)^2$$

(2)

where μ is the dipole moment, and Q the normal coordinates (which describe the position of the atoms from their equilibrium positions). The greater the difference in electronegativity, the stronger the absorption will be [69]. Intensity also refers to the number of specific vibrating groups in the molecule. There are mainly two types of vibrational motions: the stretching of the chemical bond and the bond angle deformation (also called bending). Stretching (partially represented in Fig. 14) is the periodic variation of the interatomic distance and differs between symmetrical (if the two atoms approach or move away simultaneously) or asymmetrical - in the opposite case. Bending can also be symmetrical or asymmetrical but involves either the plane on which it is present or outside of that plane. In the first case, it is called scissoring, while the asymmetrical one is called rocking; the symmetrical out-of-plane deformation is called twisting, while the asymmetrical out-of-plane deformation is

called wagging. Although IR spectroscopy is one of the most reliable methods for the identification of functional groups constituting organic and inorganic compounds, it is also widely applied in the field of quantitative analysis. The main theory of IR quantification is based on Lambert Beer's law; it describes the relationship between the absorbed light (on which the intensity of the IR signal depends) and the concentration of the species present in the sample. In fact, as shown in the equation (3):

$$\log_{10}\left(\frac{I_0}{I_1}\right) = A = \varepsilon l C$$

(3)

where I_0 is the intensity of the incident light and I_1 the intensity of the transmitted light. They result in A, i.e. the absorbance of the sample, which is equal to ε, the molar attenuation coefficient or absorbency of the attenuating species; l, the optical path length; and C, the concentration of the substance.

4.1.1 Attenuated Total Reflection Infrared spectroscopy (ATR-FTIR)

In the industrial field for the production of polymers, aqueous dispersions, resin coatings, but also for aging studies and surface degradation effects, the most used IR spectroscopic analysis method is ATR (Attenuated Total Reflection). This method has many advantages, such as providing surface information and being non-destructive to the sample [70]. The analyzes consist in placing the sample in close contact with the surface of a transparent material (to allow the passage of IR radiation) having a significantly higher refractive index (n) than the sample itself; it is called IRE (Internal Reflection Element) [71]. The materials commonly used for IRE are ZnSe ($n = 2.4$), Ge ($n = 4$), and diamond ($n = 2.4$). As IR radiation passes through this material, it undergoes complete internal reflection at the boundary with a low refractive index (n_2) material. This occurs only when the incident angle is higher than the critical angle (θ_c) defined as:

$$\theta_c = \sin^{-1}\left(\frac{n_2}{n_1}\right)$$

(4)

This phenomenon is known as *total reflection*, which results in an evanescent wave that extends into the sample (Fig. 15). Part of the energy of the evanescent wave is absorbed by the sample and the reflected radiation (a part absorbed by the sample) is returned to the detector. The penetration depth (*dp*) of the evanescent wave depends on the wavelength used, the angle of incidence, and the refractive indices of the ATR crystal and the sample to be studied. It is defined as the distance from the point where the evanescent wave decays exponentially to *1/e* (37%) of its surface amplitude and can be described according to the Harrick´s approximation (5), considering the refractive index of the IRE (n_1) and of the sample (n_2), and the angle of incidence at the surface (θ) [72].

$$dp = \frac{\lambda}{2\pi n_1 \sqrt{\sin^2\theta - (n_2/n_1)^2}}$$

(5)

The reflection number can be varied by varying the angle of incidence. The reflected radiation leaving the IRE material is then collected by the detector, generally a Fourier transform spectrometer.
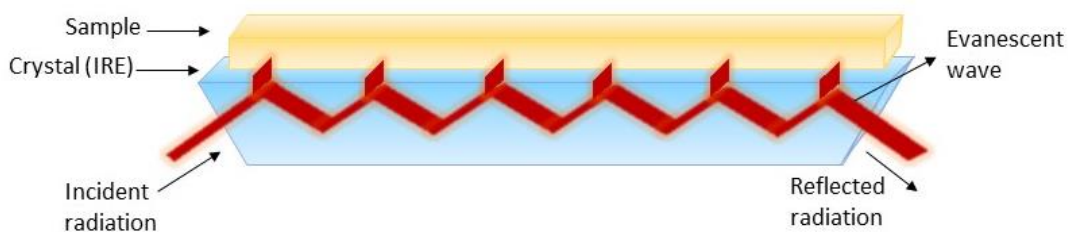

Fig. 15: Scheme of multiple internal reflections in a high refractive index crystal.

34

4.1.2 ATR-FTIR spectroscopy: Instrument and parameters

For the ATR-FTIR investigations, a LUMOS Microscope (Bruker Optics®, Germany) with a germanium crystal was employed. The instrument is equipped with a photoconductive cooled MCT detector. On each sample, five measuring spots were acquired in the spectral range between 4000 and 480 cm^{-1} performing 64 scans at a resolution of 4 cm^{-1}. The resulting spectra were collected and evaluated by the software OPUS® 8.0 (Bruker Optics®, Germany). The chemical depth information obtained by the ATR-FTIR measurements, considering the R.I. of the germanium crystal (n_1 = 4.01) and the angle of incidence of the IR beam (θ = 45°), in a spectral region between 4000 and 480 cm^{-1}, is around 0.65 µm. For the qualitative and semi-quantitative analysis, the spectra were averaged, baseline corrected, and vector normalized. Subsequently, the main absorbance bands of selected materials were integrated. As shown in a previous study [73], selecting specific bands for the semi-quantitative evaluation will allow more reliable data to be obtained for a better investigation of chemical changes after aging. For the chemical mapping, the total mapped area had a dimension of 1.0 x 1.5 mm^2; six measuring spots along the x-axis (optical aperture approx. 0.2 mm) and six spots along the y-axis (optical aperture approx. 0.1 mm) were collected for a total of 36 spots. Each chemical mapping experiment was carried out in three different areas of the samples.

4.2 Raman spectroscopy

In the past, by this technique, the radiation was scattered with a different frequency from the incident light using a system of optical filters. Nowadays, the principle has evolved and when a material interacts with monochromatic light most of the incident radiation interacts with the sample molecules which in turn can be absorbed, dispersed, or transmitted [74]. The diffuse interaction between material and source is represented as a collision between a vibrating molecule and an incident proton. The effects of the latter after the interaction with the material under examination can be divided into:

- *Elastic scattering* of the proton, also called Rayleigh scattering, where the released energy of the molecule and the proton remains the same.
- *Inelastic scattering* of the proton, also called the Raman effect, where the energy released by the proton changes upon interaction with the molecule. This energetic gap is represented by the difference between two energy levels of a molecular vibration [75].

When the electromagnetic radiation interacts with the electrons of the molecules, it induces an electric dipole responsible for the diffusion process of the incident radiation. Depending on the state of the molecules with which it interacts, the photon can be scattered with three different energies. Rayleigh scattering represents the most intense component of the scattered radiation in which there is no energy exchange with the system and the protons have the same energy as the incident radiation. Instead, Raman scattering involves inelastic scattering, characterized by a loss of energy. This process leads from the fundamental vibrational state (hv_0) to the absorption of energy by the molecule and promotes the transition to a higher excited vibrational state. This step is known as *Stokes scattering* and has lower energies when compared to the excitation source (hv_0-hv_m). However, some molecules may already be present in an excited state, for this reason the energy transfer to the diffuse proton jumps to a virtual state (hv_0) and then decays to the ground state (hv_m) but with an energy higher than the incident radiation (hv_0+hv_m); this phenomenon is called *anti-Stokes scattering* [76]. The Stokes and anti-Stokes lines are symmetrical to the Rayleigh signal, but the Stoke lines are considered for diagnostic purposes as their signal is more intense than that of the anti-Stokes lines (Fig. 16).
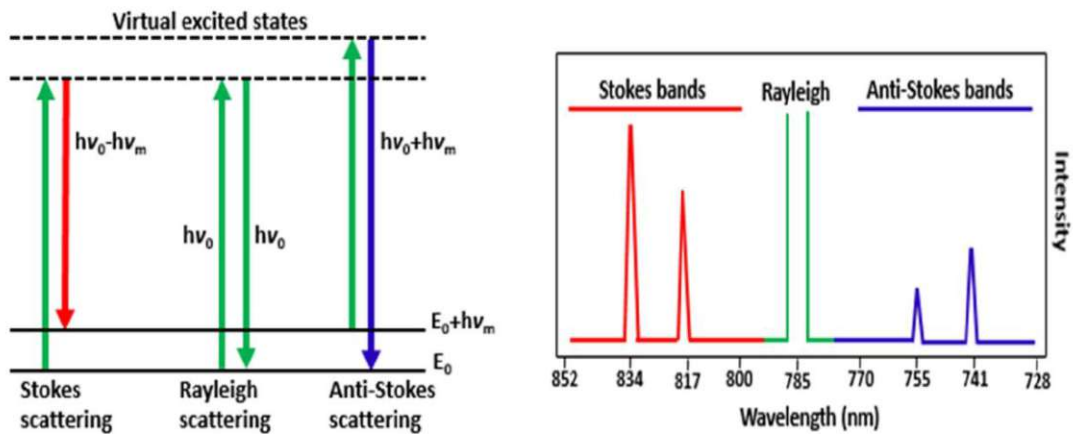
Fig. 16: Representation of Rayleigh and Raman scattering process [77].

Unlike resonant Raman scattering, fluorescence results from the emission of a photon from the lowest vibrational level of an excited electronic state. This occurs after the direct absorption of the incident photon and the relaxation of the molecule from its excited vibrational level of the electronic state to the lower vibrational level of that electronic state. Fluorescence is highly dependent on the wavelength of the source and asymmetries in the shape of the scattering peaks can be detected in the Raman spectra. Since the fluorescence is typically much more intense, it can cover the presence of compounds present in low amounts in the Raman dispersion of a material [78].

The factors that influence the Raman scatter intensities and therefore the appearance of fluorescence is: intensity of the light source (directly proportional), frequency of the source, number of molecules in a vibrational state (directly proportional), and dispersion properties of the sample (specific sample). Therefore, to avoid the contribution of fluorescence, it is necessary to:

- Select an excitation wavelength distant from any electronic transition, e.g. NIR laser;

- Try to get useful information from the anti-Stokes shift;

- Try testing the so-called *photo-bleaching* process. It consists in irradiating the sample with a Raman laser in order to decompose the fluorescent components until the material under examination is reached. However, considering that

even the sample itself can cause fluorescence, it is necessary to close the confocal hole of the Raman microscope to reduce the collection volume and so the fluorescence.

When a material is analyzed by Raman spectroscopy, which is complementary to IR spectroscopy, the energy of the constituent molecules can be divided into "*degrees of freedom*". Therefore, considering that the number of atoms present corresponds to 3N, for a non-linear molecule the degrees of freedom will be calculated as 3N-6, while for a linear molecule 3N-5. These vibrations are called *normal vibration modes* of the molecule and each of them is characterized by its symmetry, intensity, and frequency [79]. Also in this case, the vibrational motions can be characterized as: stretching, bending vibrations, and out-of-plane deformation modes. However, a molecule with a three-dimensional structure will have a variable electron density pattern that covers the entire molecule. Therefore, if one of the two molecules vibrate, the electron cloud will be altered with the change in position of the positive nuclei and this can cause a dipolar moment charge or polarization. In these triatomic molecules, symmetrical elongation causes large polarization charges and therefore strong Raman scattering. Instead, the deformation mode causes a dipole change but little polarization charge and therefore a strong infrared absorption and a weak Raman scattering [74]. The change is described by the polarizability derivative (Eq. 6), which determines the section rules for a Raman-active vibration.

$$\left(\frac{\partial a}{\partial q}\right) \neq 0 \; ; \; I_{Raman} \propto \left(\frac{\partial a}{\partial q}\right)^2$$

(6)

The scattering intensity is proportional to the square of the induced dipole moment and therefore to the square of the polarizability derivative. If a vibration does not change much the polarizability, the value of the derivative will be close to zero and the intensity of the Raman band will be low. For this reason, the vibrations of molecules with a high polar fraction, e.g. the O-H bond, are usually weak.

4.2.1 Raman spectroscopy: Instrument and parameters

A confocal micro-Raman system Alpha RSA+ (WITec, Germany) was employed to measure the samples in combination with an Atomic Force Microscopy (AFM). Measurements were performed using 532 nm excitation radiation with a real output laser power of 42 mW, integration time 0.06 s, and time/line 9 s. The sample surfaces were observed with the Zeiss objective 20x, and the scanned areas (20 x 20 μm^2) were analysed using a camera connected to the microscope. The acquisition of the spectra and their evaluation was performed with the WITec Project 5.1 software. The spectra obtained for the three scanned areas were averaged, baseline corrected, and vector normalized in order to obtain a more reliable chemical mapping of specific Raman bands.

4.3 Atomic Force Microscopy (AFM)

Atomic Force Microscope (AFM) is used for studies on atomic scale dimensions of surfaces of various compounds: thin or thick films of ceramic materials, amorphous materials, glass, synthetic or biological membranes, metals, polymers, semiconductors, etc. AFM was developed in 1986 by Gerd Binnig et al. [80] as a consequent variant of its precursor, the scanning (electron) tunneling microscope whose most significant disadvantages are the requirements of a conducting sample surface as well as relatively stable measurement conditions. While the latter maps the topography of the surface by scanning along with the lateral directions, AFM measures the deflection of a small cantilever with a small tip due to the inter-atomic forces between tip and surface atoms. In force microscopy, the probing tip, the so-called cantilever, is attached to a spring that in response to the force between tip and sample deflects the cantilever. The deflection of the cantilever is detected over the reflection of a laser beam from the backside of the cantilever into an array of photodiodes. It has a resolution of 0.01-1 nm along the x- and y-axes, and 0.01 nm along the z-axis. In this

way, it is possible to study the phenomena and processes of abrasion, adhesion, cleaning, corrosion concerning surfaces in detail [81].

Generally, the piezo stage can move in the vertical (z) or horizontal (x and y) direction and when the cantilever tip (made of Si or Si_3N_4) interacts with the sample molecules it causes a reduction in its resonance frequency. This deflection is detected by a laser which is pointed at the back of the cantilever tip and the reflected laser beam is recorded by a four-quadrant photodiode. The movement of the sample, the variation in the deflection of the beam, its amplitude, and the frequency of oscillation are subsequently converted into an electrical signal. Using the collected signals, the computer is able to generate an image given by scanning the sample surface (Fig. 17) [82].
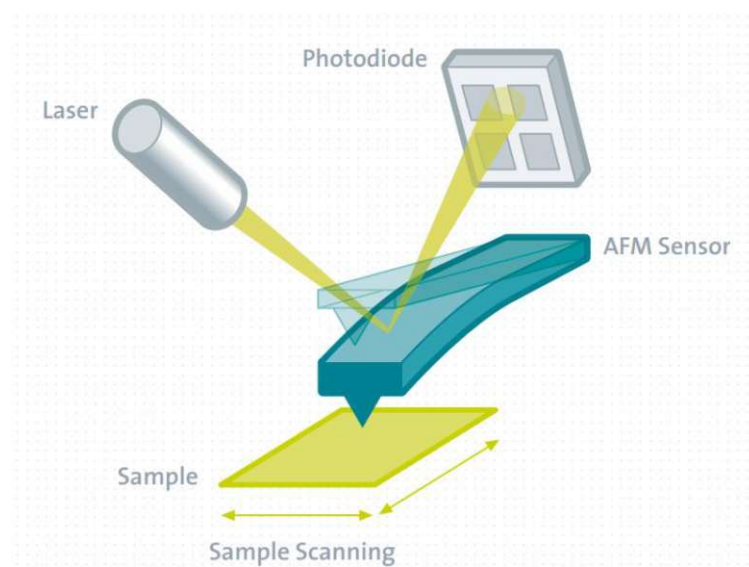

Fig. 17: Working principle of cantilever system.

In addition to high-resolution topographic information, the physical properties of the material such as adhesion, roughness, and stiffness can be studied considering the tip-sample interaction forces. In all scanning modes, the basic principle of topography imaging is the repulsive or attractive interaction between the sample surface atoms and the tip surface. When an atom of the cantilever interacts with a single atom from the surface of the sample, the variation of the repulsive interatomic forces allows to obtain

high resolution images and to obtain information on the physical-mechanical characteristics of the material depending on the distance between the sample surface, the attractive or repulsive cantilever forces (such as Coulomb forces between charges), dipole-dipole interactions, polarization forces, Van der Waals dispersion forces, and capillary forces that affect tip deflection. The change in the distance between the tip and the sample causes a change in the force interaction between the sample and the tip. The acting forces involved during the approach of the tip can be described with the Lennard Jones potential, as shown in Fig. 18. The attractive interaction (Van der Waals forces) dominates in the long range, while in the short range the Pauli-repulsion
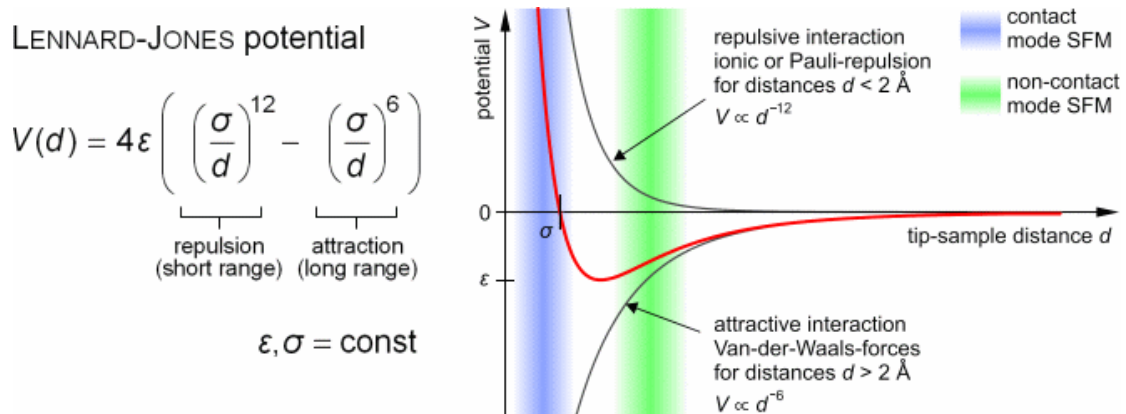
of the electron clouds of the atoms between the sample and the surface causes the flexible cantilever tip to move away [83].

Fig. 18: Forces involved during AFM analysis [84].

Depending on how the tip interacts with the sample surface, the AFM can be used in: (i) attractive or no-contact, i.e. where the tip does not actually touch the surface, (ii) repulsive or contact, and (iii) tapping mode, in the case in which the tip explores the sample in order to have a discontinuous contact determined by a regular succession of oscillatory movements (i.e., continuously passing from the contact condition to no contact). The non-contact AFM mode uses the interatomic attractive force between the tip and the sample to scan and reconstruct the surface under examination (with distances between tip and sample greater than 1 nm). However, the attractive forces alone are too weak to have a correct cantilever deflection and then a reliable sample

image. Therefore, it is necessary that, when the cantilever vibrates near its resonant frequency during the imaging process, a piezoelectric modulator is used which allows to facilitate the acquisition of the topographic characteristics correlating the changes in the phase and amplitude of the cantilever (Van der Waals forces). The most important factor in NC-mode is that the distance between the tip and the surface must be maintained during the measurement, enabling with a feedback loop controlled by the Z-servo. This mode allows to obtain information on the magnetic or chemical force [85].

Instead, in the contact mode, the tip of the cantilever and the surface of the sample are in constant physical contact (the ion repulsion forces prevail), as shown in Fig. 19. A feedback loop maintains the cantilever deflection at a present load force. The resulting force is transmitted directly through the tip and is measured. The feedback response is evaluated to generate the AFM image. This method also allows measuring lateral forces (friction) at the nanometer level. The disadvantage of the AFM contact mode, however, is that the sample surface could be easily damaged (especially with soft materials), the tip could be contaminated with the sample, and the original resolution could be lost. Therefore, the force must be applied gently. For this reason, this mode is preferred for materials with high stiffness mechanical properties which, by means of the short-range force, provide the highest resolution [86]. Finally, in the tapping mode, the cantilever is driven to its resonant frequency by the piezoelectric oscillator, where the interaction with the sample surface dampens the resonant frequency. In this case, the tip is not in constant contact with the sample surface but touches the surface lightly and repeatedly. The amplitude of its oscillation is damped and by means of the amplitude the surface topography is generated. Since the oscillating tip also experiences a phase shift relative to the driving oscillator, this information can also be used to provide suggestions when the surface composition changes.

Non-contact (dynamic) mode

Contact (static) mode
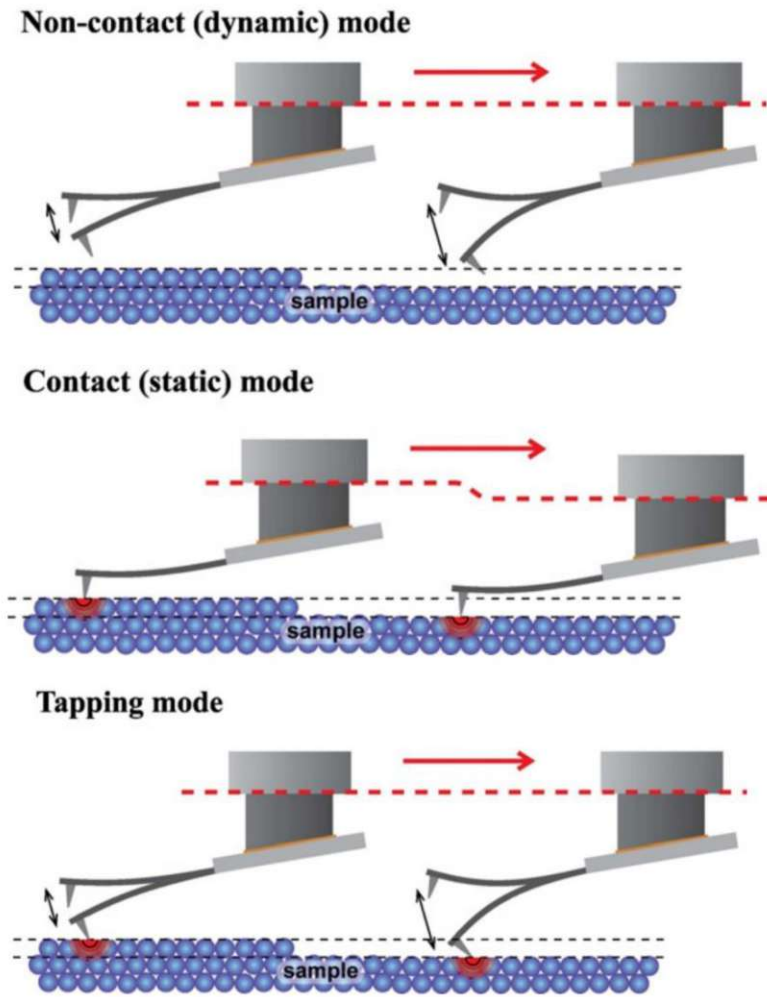

Tapping mode

Fig. 19: AFM operation modes [87].

The variation of the output and cantilever drive signal is used to generate phase images (topography, amplitude error, and phase contrast). The advantage of phase imaging is that the resulting images show very noticeable contrasts of the sample phases, and furthermore, unlike the contact mode, low shear forces of the tip sample are employed during the scanning process [88].

4.3.1 AFM: Instrument and parameters

The topographies related to the surface samples were obtained using an Atomic Force Microscope WITec Alpha RSA+ (WITec, Germany) in tapping mode. The cantilever tip is a WITec arrow reflex coated FM (AC), spring constant k at 2.8 N/m, with a resonance frequency of 75 kHz, and lateral resolution of down to 1 nm and depth resolution of < 0.3 nm. It allows a stereometric analysis obtaining the 3D surface texture of reference and aged samples. All scans were collected over a 50 x 50 μm^2 area (512 lines per image). The surface images of films were evaluated using the software WITec Project FIVE 5.1. The data discussed concern the topographies obtained and the respective roughness values (Sa) compared between the reference and aged samples. For an accurate and reproducible evaluation of the topographic results, three different surface areas of the samples were scanned and the roughness and particle size values were averaged. Statistical data deriving from the evaluation of AFM topographies (average particle size (μ), standard deviation (σ), and correlation coefficient (R)) were obtained using the software Project FIVE 5.1 (WITec, Germany). Specifically, the topographic scans were color line corrected by slope substraction and subsequently the statistical values were obtained.

4.4 Laser-Induced Breakdown spectroscopy (LIBS)

Laser-Induced Breakdown spectroscopy (LIBS) is an atomic emission spectroscopic technique that allows both qualitative and quantitative analyzes. This technique enables the study of the optical spectrum emitted by the plasma, which is generated by the interaction between a high-power laser radiation and a sample that can be solid, gaseous, or liquid [89]. From the interaction between the focused laser pulses and the sample, plasma composed of ionized matter is generated. It can consist of discrete lines, bands or an overlying continuum. These discrete lines that characterize the material have three main characteristics: wavelength, intensity, and shape. These factors depend on the very structure of the emitting atoms (whose different energy

levels determine the wavelength of the line). In addition to the qualitative identification of the elements in the sample, it is possible to make a quantitative evaluation of each element in the sample considering also the line intensities [90].

The environment in which an atom is found strongly determines the emission of intensity and shape of the lines. For low plasma densities, the linear form dominates both for natural broadening (due to the Heisenberg´s principle) and Doppler broadening (due to thermal motion of the emitters). On the other hand, for high plasma densities, the electric fields generated by the fast moving of electrons and the slow one of ions shift atomic energy levels by affecting the atoms in the plasma. This phenomenon causes the broadening of the emission lines and changes their intensity and shape [91].

There are three stages in the plasma life time (Fig. 20). The first is the (a) *ignition* process. This process causes bond breakage and plasma shielding during the laser pulse and varies depending on the type of laser, irradiance and pulse duration (femtoseconds or nanoseconds). Plasma shielding is highly dependent on environmental (surrounding gas or vacuum) and experimental conditions (laser irradiation and wavelength). It allows to reduce the ablation speed so that the radiation does not reach the surface of the sample. The next phase is called (b) *cooling and expansion*. During this phase, the plasma causes the atomic emission and allows the optimization during the LIBS spectral acquisition. After ignition, the plasma will continue to expand and cool and at the same time, the temperature and density of the electrons will change [92].

At the high temperatures during the plasma emission, the ablated material breaks down into excited ionic and atomic species. Only when a small timeframe of plasma expands at supersonic velocities and cools, it is possible to observe the characteristic atomic emission lines of the elements. The last phase of plasma life is generally not interesting for LIBS measurements. In fact, a small amount of ablated mass of material is ablated as particles in the form of condensed vapor that does not emit radiation [93].
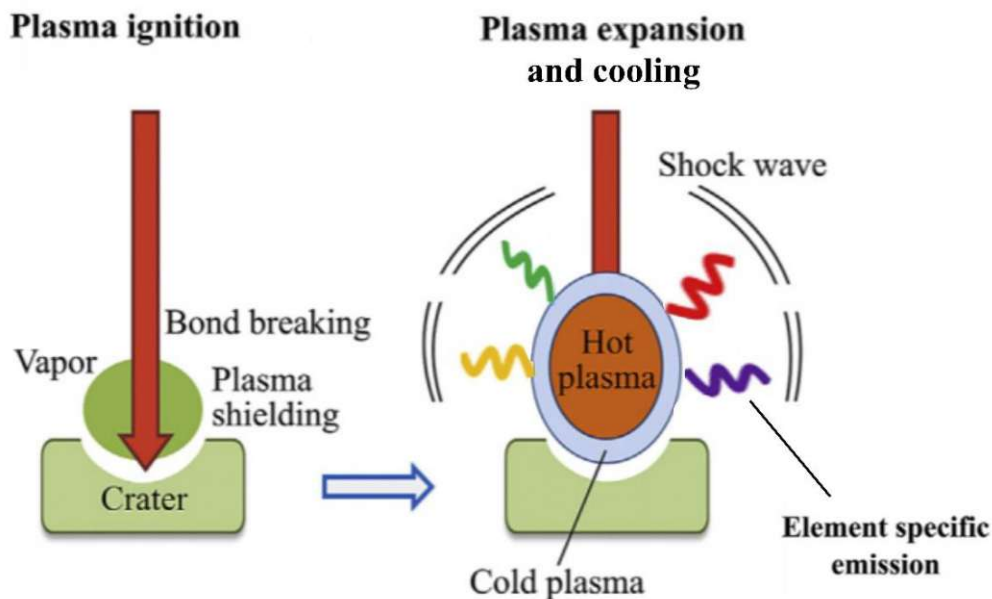
Fig. 20: Plasma lifetime schematics during LIBS process.

4.4.1 LIBS: Instrument and parameters

LIBS analysis was carried out using J200 Tandem LIBS instrumentation (Applied Spectra Inc., Fremont, CA) equipped with a 266-nm frequency quadrupled Nd:YAG laser. For collection and spectroscopic analysis of the radiation emitted by the laser-induced plasma, an optical fibers system connected to a Czerny-Turner spectrometer with six-channel CCD detection was employed. For every laser shot, full spectra over the wavelength range from 185 to 1040 nm were recorded by Axiom 2.0 data acquisition software provided by the manufacturer. All samples were analyzed using 16 parallel line scans with a distance of 100 μm between each line and a length of each line scan of 2 mm. The measurement was carried out in the center of the samples to avoid edge effects. Using a 100-μm laser beam diameter, at a stage scan speed of 1 mm/s, and with a repetition rate of 10 Hz on each line, 320 laser shots were performed per sample. Concerning the acquisition of LIBS spectra for organic binders, they were recorded after proper optimization of the choice of the gas flow used in the measurement chamber. LIBS spectra were recorded in argon atmosphere (flow rate of

1 L min^{-1}). Argon yields the best results as it usually gives higher emission signals for especially C, H, and, O, therefore reducing the noise and improving the classification.

4.5 Multivariate analysis

Chemometrics is a branch of chemistry that studies the application of mathematical or statistical methods to chemical data. Specifically, once the data has been collected with computerized systems, it allows the extraction of the information collected, using methods such as multivariate analysis and statistical analysis. Therefore, through these evaluations it is possible to design or select optimized measurement procedures and experiments and to extrapolate more relevant chemical information by analyzing the chemical data [94].

The chemometric methods applied to analytical techniques are important evaluation systems for the field of cultural heritage as they allow to better understand and study the mechanisms of degradation in order to better preserve the works of art or evaluate the restoration treatments. Conservators and conservation scientists collect large amounts of data during their monitoring so this statistical approach allows them to manage and extract information more accurately to preserve and analyze collections. The effective extraction of large data sets also allows to study the degradation behaviors due to different environmental conditions, interactions between materials, different chemical properties of materials using various microscopic or non-invasive as well as minimum invasive methods.

In the following chapters, the theoretical basis of the multivariate methods chosen for the evaluation of the spectroscopic results under consideration are briefly discussed.

4.5.1 Principal Component Analysis (PCA)

Considering the various case studies in the field of cultural heritage [95,96], the most common technique used for the chemical analytical representation of data is the Principal Component Analysis (PCA). In general, it is the most common technique used for exploratory analysis of complex datasets. This multivariate method allows retaining only the useful information from the investigated data by analyzing the most representative variability sources according to their variance. Indeed, the main aspect of PCA consists in obtaining a new set of variables, named Principal Components (PCs), calculated as linear combinations of the original variables, orthogonal to each other and accounting for the directions of maximum data variance [97]. In this way, multivariate datasets composed of hundreds of variables can be represented in an alternative space defined by few PCs, able to retain only the relevant information related to data structure and to discard noise. PCA decomposes the original data matrix into three matrices: the score matrix accounting for the variance associated with the samples, the loading matrix accounting for the variance associated with the variables and the residual matrix accounting for the variability sources not described by the PCs. Such decomposition allows analyzing common features among clusters of samples easily. Indeed, samples sharing similar spectral features tend to group in the score space, and the simultaneous evaluation of score and loading vectors allows to identify the spectral bands mainly responsible for the observed behaviours.

4.5.2 Analysis-of-Variance-Simultaneous Component Analysis (ASCA)

To evaluate the influence of pigment type, gas and RH% on binder deterioration, the ATR-FTIR spectra of the aged samples prepared with the three different binder types were separately analyzed using ASCA. It can be considered as an extension of the ANalysis Of VAriance (ANOVA) applied to multivariate datasets resulting from a designed experiment [98]. In the same way as ANOVA, the variation of the response data collected from an experimental design can be partitioned into the contributions

determined by the different experimental factors and their interactions. Therefore, in the present study, for each binder type, the variation observed in the ATR-FTIR pre-processed spectra of the aged painting samples (X) can be obtained by adding the contribution of the matrices estimating the effect of the individual experimental factors ($X_{pigment}$, X_{gas}, $X_{RH\%}$), their two-way interactions ($X_{pigment \times gas}$, $Xp_{igment \times RH\%}$, $X_{gas \times RH\%}$) and the residual matrix (E), as shown in Equation 7:

$$X = X_{pigment} + X_{gas} + X_{RH\%} + X_{(pigment \times gas)} + X_{(pigment \times RH\%)} + X_{(gas \times RH\%)} + E$$

(7)

For each factor, the effect estimate matrix contains the averages of the sample responses belonging to the same level. For example, considering gas factor with two levels (i.e. SO_2 and NO_x,), the resulting effect matrix (X_{gas}) has as many rows as the number of samples, and each row corresponding to a sample aged with SO_2 contains the mean spectrum of SO_2 level, obtained by averaging all the spectra of the samples belonging to SO_2 level. In the same way, all the rows of X_{gas} matrix corresponding to samples aged with NO_x contain the average spectrum of NO_x level (Fig. 21). The same procedure is used to calculate the effect estimate matrices of each factor and interaction, but the computation of the interaction matrices is performed after subtraction of the matrices corresponding to the main effects. According to the ASCA method, the effect matrices obtained by ANOVA decomposition are then analyzed using PCA, obtaining a PCA sub-model for each factor and interaction. In this manner, ASCA allows to estimate the magnitude of the influence of the considered experimental factors and to obtain a straightforward interpretation of the variations induced by the different levels of each design factor or interaction. Furthermore, in order to estimate the significance of each experimental factor and interaction, the corresponding p-values were calculated based on a permutation test considering 1000 permutations [99].
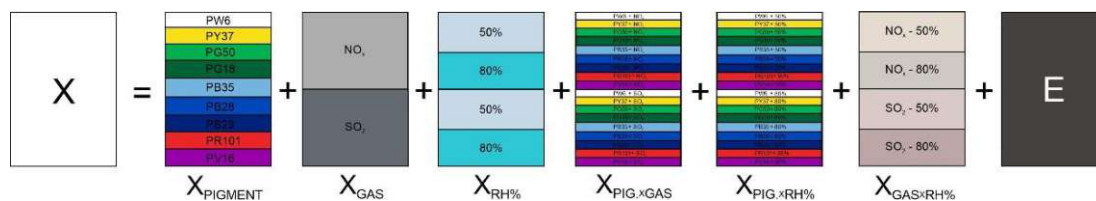
Fig. 21: Representation of variance decomposition obtained with ASCA.

4.5.3 Random Decision Forest (RDF)

Random Decision Forest (RDF) is an advanced algorithm used in the field of machine learning, proposed by Breiman [100]. It is a classifier consisting of a collection of decision trees; each tree-type classifier is trained on a random subset of the data (bootstrap) included in the training set. The multiple classification trees continuously produce training and test sets, maximizing the classes' separation. The predictive power is based on the combination received by the majority vote of each classification tree. The RDF algorithm is a valid classifier because it shows good tolerance for solving problems such as noise and overfitting phenomena. In the following work, RDF was applied to LIBS results as it was already considered as a good technique to identify and classify artworks [101].

The foremost steps of RDF algorithm can be described as follows:

- *Training data*: 27 paint mixtures made of all combinations of pigments and binders were employed as the training data set for the classification model. To correct the shot-to-shot variations, the instrumental drifts, and the defocusing effects caused by surface roughness, all spectra were normalized to the total emission intensity. This dataset was used to build the multivariate classification model. Fig. 22 illustrates the steps from LIBS spectra of the different pigment/binder combinations to the classification results. The results obtained are confusion matrices, i.e., representations of statistical classification accuracy.

- *Cross-validation*: To verify the obtained classification models, cross validation was calculated with a test size of 100 and 10 repetitions for both RDFs. It means that 10 different models are calculated leaving out 100 randomly selected spectra from the training data set. This exclusion method consists in excluding a certain number of spectra from the dataset, then building the new model, and finally checking the ability of the model to correctly classify the excluded spectra. The spectra not included in the model are evaluated by the corresponding model, and true positive (TP) and false positive (FP) rates are calculated. The results obtained are confusion matrices, i.e., representations of statistical classification accuracy.

- *Application*: This approach allows testing the obtained classification with a new set of samples made of the same materials constituting the existing training data set. This application presents some advantages as a low risk of over-fitting and the possibility to check if the training set was correctly developed to describe all the variability of the samples. Through the Imagelab software (Bio-Rad Laboratories, Austria), the One-vs-All (OVA) scheme was performed. The model used a decision boundary at 0.5. By applying this function, it is possible to obtain a class mapping on the surface analyzed [102].
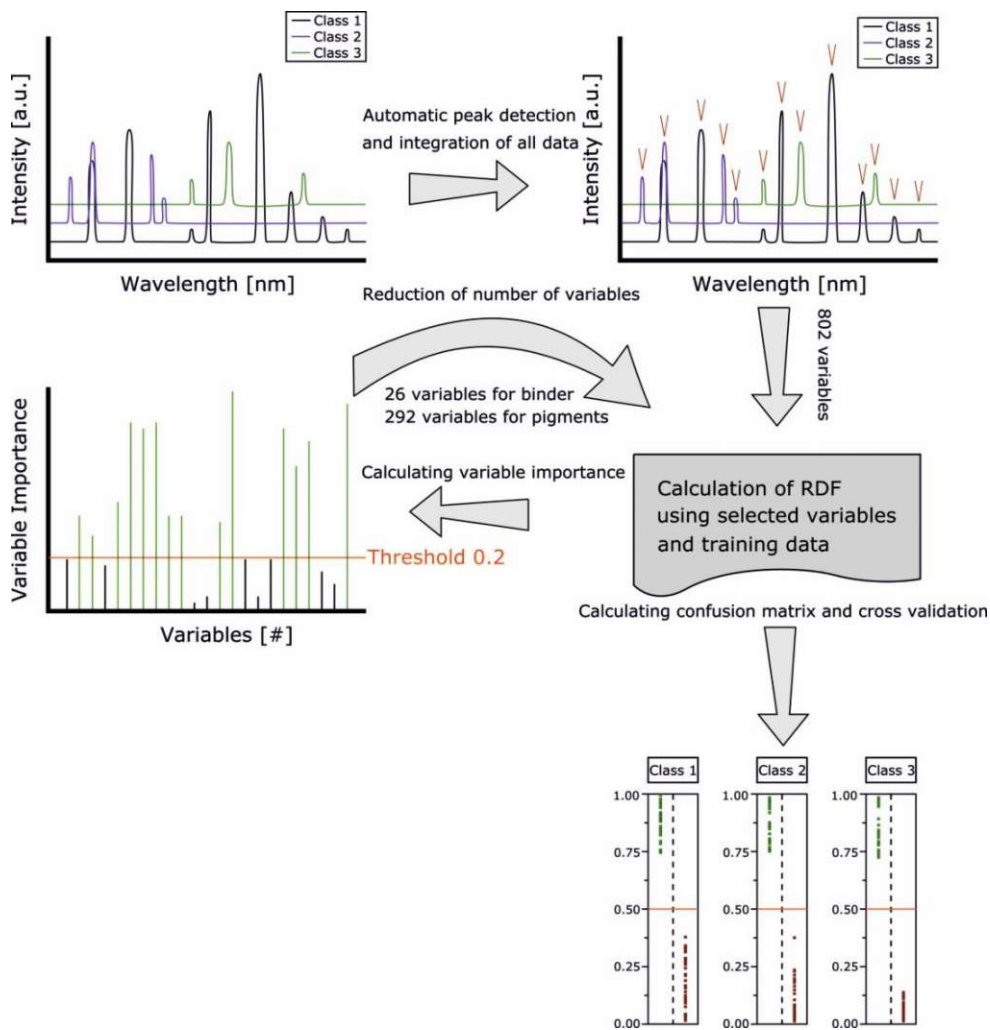
Fig. 22: Schematic procedure of building RDF.

5

SCIENTIFIC PUBLICATIONS

This PhD thesis consists of 6 peer-reviewed publications divided into two main topics. The first represents the final part of a research project carried out a few years ago which focuses on the study of the stability of alkyd paints subjected to accelerated UV-light aging when mixed with different inorganic pigments at different concentrations (**Paper I**). This work mainly carried out chemical investigations of paint surfaces, focusing on the effects that UV-radiation can cause also in the depth-profile of paints and whether the degradation processes can be influenced by the different binders, pigments and pigment/binder ratios (P/BM) in the mixture. To investigate these phenomena, it was decided to employ several advanced analytical methods, combined with multivariate evaluations, first of all to characterize the composition of the paints (**Paper II**) and subsequently evaluate the main factors that lead to a greater deteriorating effect even in-depth (**Paper III, IV**).

The second topic was on the studies of the degradation reactions caused by pollutant gases mixed with different amount of relative humidity (RH). This topic represents the fundamental part of this PhD project. The study is focused on understanding through microscopic, spectroscopic, and multivariate techniques which binder is more subject to degradation caused by pollutant gases, which types of pigment or gas×RH interaction enhance or reduce this process (**Paper V**), and if some restoration practices can prevent or restore the surface damages caused by pollutant gases (**Paper VI**).

5.1 Paper I

As previously discussed, the first publication "*Photodegradation Kinetics of Alkyd Paints: The Influence of Varying Amounts of Inorganic Pigments on the Stability of the Synthetic Binder*" represents the final part of a research project at the Institute of Natural Sciences and Technologies in the Arts (INTK) of the Academy of Fine Arts Vienna. It focused on the chemical identification of modern acrylic [44,103,104] and alkyd paints [101,105,106] and their related photooxidation mechanisms when exposed to UV-light accelerated aging. The following study focused on the photo-oxidation processes occurring mainly in alkyd paints and their stability when mixed with different inorganic pigments (artificial ultramarine blue – PB29, hydrated chromium oxide green – PG18, and cadmium sulfate yellow – PY37) and pigment/binder (P/BM) ratios (1:2, 1:3, and 1:6). The degradation effects were documented by optical 3D microscopy and studied by ATR-FTIR, SEM, and colorimetric analysis.

These investigations revealed that the chemical degradation of the alkyd binder is observed already after 168 h, shown by an intensity decrease of the alkyd resin functional groups over time. This trend is most evident in the mixtures with the blue pigment PB29, followed by PG18 and PY37. As a consequence of the binder's decomposition, the pigments spectral bands increase during light exposure in all paint samples and, in particular, the kinetic evaluation of ΔE^* shows that the PB29 alkyd mixture (P/BM 1:2) undergoes the highest color change, followed by PY37 and PG18. Morphological changes of the paint surfaces are also visible by the employment of 3D microscopy and SEM. Upon aging, the samples' surfaces appear more rigid and opaque, above all in paints with P/BM 1:2. Generally, when the binder content is high, the degradation behavior increases. These results were confirmed by applying Principal Component Analysis (PCA) to the microscopic images of the paint samples, considering the color and texture changes after aging. This approach can be further implemented for quantitative evaluation of aging time for diagnostic purposes.

In conclusion, the paint samples exposed to artificial light aging show degradation processes that vary according to the inorganic pigment and the P/BM ratio employed. The presence of certain pigments can enhance several photo-oxidative effects on the binder; indeed, PB29 causes higher degradation than PY37 and PG18. Additionally, degradation of the binder increases with pigment concentration. With this study, it has been demonstrated that the use of non-invasive analytical techniques, kinetic evaluation, and the combination of analytical data with chemometric methods have high potential in the identification of paint components of complex artworks and in obtaining chemical information to be complemented with historical-artistic knowledge.

5.2 Paper II

After studying the degradation behavior of alkyd paints according to the different pigments and their concentration in the mixture, the PhD thesis focused on the knowledge of how UV-radiation affects the in-depth profile of modern paints (acrylic paints and styrene-acrylics were added as new binders). In the second work entitled "*Multivariate analysis and laser-induced breakdown spectroscopy (LIBS): a new approach for the spatially resolved classification of modern art materials*", Laser-Induced Breakdown spectroscopy (LIBS) was employed to identify modern paints composed of inorganic pigments and organic binders and, in combination with multivariate analysis, distinguish these materials in mixture and employ the method developed for imaging applications on real samples.

For a correct characterization of inorganic and organic materials, after the assignment of each emission signal to the relative element, LIBS spectra were evaluated by principal components analysis (PCA). Through appropriate methodological choices, this statistical method proved to be effective for the discrimination of the different binders and pigments. However, due to the low accuracy of PCA, for the distinction of these materials in mixture, a different method of multivariate classification was considered, i.e., the random decision forest (RDF). Applying this method, it was possible to distinguish each material in mixture choosing a suitable training set subsequently tested by cross-validation. The classification model was tested on an unknown mock-up, made by the same materials previously classified. By the built RDF model, the obtained results were represented as mapping images according to the identified chemical compounds. The application of the model to an unknown sample demonstrated the correct classification of paint mixtures.

All the results demonstrated the high potential of LIBS combined with multivariate methods. In fact, it was not only possible to characterize emission lines for each binder but also to differentiate them and subsequently classify unknown samples. This first approach of data evaluation could possibly extend the classification to other artistic materials (organic binders, inorganic/organic pigments). This information could find future applications in various contexts such as archaeology, biology, industrial chemistry, materials science, and for multiple purposes such as database creation, monitoring during conservation treatments, and the identification of artistic materials and their degradation products.

5.3 Paper III & IV

After the optimization of the experimental and statistical methods for a correct identification of the inorganic and organic materials under examination, LIBS was employed to understand how much UV-radiation affects the in-depth layer of the paints and which are the elements that enhance the interaction between UV-light and paint. The works entitled "*Infrared and Laser-Induced Breakdown Spectroscopy to Characterize UV-Light Degradation of Modern Art Materials*" and "*Combined LA-ICP-MS/LIBS: powerful analytical tools for the investigation of polymer alteration after treatment under corrosive conditions*" compare the results obtained from the IR analysis of the surface paint layers and those of the in-depth layers obtained by LIBS.

Generally, it is observed that the oxidative effect of UV-radiation is greater for alkyd paints than for acrylic ones due to the oily component in the binder which causes photochemical degradation, forming oxidation products. In fact, acrylic paints with pigment/binder (P/BM) 1:2 begin to degrade only after 336 h of aging, while for P/BM 1:6 it was recorded after 672 h. For the alkyd binder, this effect was determined already after 168 h for each P/BM ratio. These results confirm the chemical instability of the alkyd resin exposed to UV-aging. Furthermore, this behavior increases in samples with a high amount of pigment (P/BM 1:2), especially with PB29.

The results obtained from the in-depth LIBS analysis (15 consecutive layers, with an area of 1.9 x 1.0 mm with an average ablation rate of 1 μm per layer) were evaluated by PCA, comparing the data of the unaged and aged samples. Subsequently, their distributions were studied considering the outermost and the inner layers. The results are related to the chemical composition of the unaged and aged paint samples and show different trends. On the other hand, the data obtained from the in-depth layers of the aged samples show chemical profiles similar to those of the unaged surface layers.

In conclusion, by comparing the results obtaining from ATR-FTIR and LIBS, it is possible to identify the alkyd polymer as the binder more subject to photodegradation. When the pigment concentration is high (P/BM 1:2) this process is increased, and the type of pigment determines an increase or decrease of the deteriorating action of UV-radiation. Moreover, due to the chemical-physical properties of the pigment, it will allow the UV-light to interact more deeply into the paint layer, resulting in the loss of the mechanical and aesthetic properties of the paint itself.

These two works represent the latest studies developed during this PhD concerning the investigation of photooxidative processes of modern paints.

5.4 Paper V

This study entitled "*SO₂- and NOₓ- initiated atmospheric degradation of polymeric films: Morphological and chemical changes, influence of relative humidity and inorganic pigments*" is part of the second topic of the PhD thesis and discusses the first results obtained from the evaluation of the influence of pollutant gases on the stability of modern paints. The reactions and chemical changes of modern artistic materials (in this case, acrylic, alkyd, and styrene-acrylic binder mixed with various inorganic pigments) in contact with various polluting atmospheric agents were not studied extensively. In fact, they may vary according to various factors such as the environmental conditions, the product manufacturing process, or the presence of various additives or pigments. In this work, accelerated gas aging was performed on modern paint samples trying to simulate real outdoor environmental conditions. In particular, sulfur dioxide (SO_2) and nitrogen oxide (NO_x) mixed with different relative humidity contents (50% and 80% RH) were used for a total of 168 hours of exposure to the gas.

The morphological observations under the 3D microscope carried out after aging show that the most significant degradation effects are visible for acrylic paints (surface migration of the surfactant) and that, from the evaluation of the depth and roughness profile values, the highest oxidative behavior occurs when the samples are exposed to NO_x. From the qualitative and semi-quantitative ATR-FTIR analysis, the various binders and aging conditions have shown different results. Acrylic paints are more subject to NO_x degradation. Furthermore, semi-quantitative evaluation and chemical mapping showed that paints with PW6, PB29 and PB28 (i.e. titanium white, artificial ultramarine blue, and cobalt blue) favor this deterioration behavior. Alkyd paints show similar degradation levels when exposed to polluting gases. The main degradation reaction is the hydrolysis of the phthalic component in the binder, even if it seems favoured by the interaction with NO_x, while the SO_2 tends to interact more with the drying oil. The pigments that favor these reactions are PW6 and PR101.

Finally, styrene-acrylic paints are more sensitive to the gas-relative humidity interaction, exhibiting two different degradation behaviors. The multivariate methods used (PCA and ASCA) confirmed both the previously obtained results and brought more useful information to understand the different chemical mechanisms between materials and pollutants. Using PCA, it was possible to understand that, in all paints, the functional groups C–H and C=O are the most subject to degradation. The influence of the various pigments on the overall degradation of the binders was confirmed by ASCA. The latter shows that the three binders are subject in different ways to degradation conditions. In fact, the RH has a greater influence on the degradation of acrylic paints than the different gases on alkyd paints, and the gas×RH% combination on styrene-acrylic paints. In general, from all the assessments carried out, NO_x revealed the most significant oxidizing effect on paints. These results are relevant as outdoor artworks are increasingly affected by environmental degradation, due to continuous climate change. Furthermore, understanding the deterioration reactions caused by the interaction with polluting gases is essential to provide appropriate suggestions for their preservation.

5.5 Paper VI

The final part of the PhD thesis focuses on the morphological and chemical-physical changes observed on pure acrylic films after exposure to various pollutant gases. The previous discussed papers investigated the different correlations that polluting gases showed interacting with various modern paints depending on the RH value chosen, type of binder, pigment and their combination. However, in this work entitled "*The Effect of Pollutant Gases on Surfactant Migration in Acrylic Emulsion Films: A Comparative Study and Preliminary Evaluation of Surface Cleaning*", acrylic emulsions have been taken into consideration. Exposed to high humidity and atmospheric polluting gases, their structural and chemical conformation is strongly compromised due to the migration of surfactants. The latter behavior was studied extensively over the years and various cleaning treatments were tested for their effectiveness. However, their choice remains difficult as they easily alter the acrylic component, especially when in contact with aqueous solutions. Therefore, a comparative analytical study was conducted in order to characterize morphologically (by 3D and Atomic Force Microscopy) and chemically (by Raman and Infrared spectroscopy) the reactions and degradation products. Two water-based cleaning treatments were then tested and a preliminary evaluation of their cleaning effectiveness was carried out.

The characterization of the polymeric system was complex, as some molecular structures are very similar to other polymers and some commercial products have different additives. In this specific study, polyethylene oxide (PEO) was identified as the main surfactant in acrylic emulsions. Having hygroscopic properties, once exposed to certain aging conditions, it migrates to the surface in the form of particles which, from observations under the 3D microscope, cause the opacification of the surface acrylic component. Furthermore, depending on the type of pollutant, changes are observed in surface distribution, particle size, and roughness. From the evaluation and comparison of the microscopic (3D and AFM) and chemical (Raman and FTIR

spectroscopy) results, the gaseous pollutant causing the greatest damage to acrylic emulsions, in terms of structural impact, increase in roughness values, extension, and dispersion of surfactant particles is NO_x, followed by $O_3 > SO_2 > H_2S$ and RH 80%. This phenomenon is probably linked to the solubility of gases in humidified environments and the surfactant-gas chemical affinity.

Subsequently, the study focused on the preliminary evaluation of the effectiveness of two cleaning treatments for the removal of surfactants, namely by means of cotton swab rolled and hydrogel system. From AFM topographies and chemical mappings, surfactant removal is most effective with the cotton swab rolled. However, it compromises the structural stability of the acrylic component by causing surface swelling. The hydrogel, on the other hand, does not allow a regular cleaning effect, although it allows the gradual release of water for a more controlled cleaning and limits swelling. Moreover, gel residues are observed after application. The cleaning effects are also influenced by the interaction between acrylic film and pollutants; in fact, the cotton swab rolled test is more effective on samples aged by SO_2 and NO_x, while the hydrogel on those aged by RH80% and H_2S. Both tests seem effective on O_3 aged samples. The results obtained so far show how various physical-chemical interactions are observed, depending on the formulations of acrylic emulsions and the influence of gaseous pollutants.

6

CONCLUSION AND OUTLOOK

This PhD thesis focuses on the study of the stability of modern and contemporary paints when exposed to different atmospheric conditions.

Specifically, the first part concerns the degradation behavior of alkyd paints subjected to accelerated aging by UV-light (**Paper I**). In this work, the paint samples showed different degradation processes depending on the type of inorganic pigment in the mixture and the P/BM ratio used. The presence of pigments can in fact enhance various photo-oxidative effects on the binder and furthermore, the degradation of the binder increases as the concentration of the pigment increases. With this study, it was shown that the use of non-invasive analytical techniques, the kinetic evaluation of their results, and the use of chemometric methods have a high potential in the study of paint components. The obtained results led to further questions concerning the degradation reactions in the inner layers of the paints, if some factors (type of pigment, binder, weight ratio) favor or reduce these degrading behaviors, and how these effects can be prevented or slowed down.

This latter research topic was investigated in subsequent studies (**Paper II, III, IV**) in which the results of advanced (LIBS) and basic (FTIR) techniques were compared and later combined with multivariate evaluation methods to understand which binders are more subject to photodegradation and which pigments or P/BM ratios favour these reactions in the inner layers of the paints. The results demonstrate that the alkyd binder shows the most significant degradation effect (due to the oil component) that increases if the amount of pigment is higher than the binder (P/BM 1:2, mainly for PB29).

This evaluation represents an innovation from the analytical and scientific point of view, as after this first application it allows to obtain excellent results applied to artistic heritage (above all combining statistical methods).

The second part of the thesis focuses on the study of the degradation reactions caused by pollutant gases and relative humidity (RH). The first study carried out (**Paper V**) compared acrylic, alkyd and styrene-acrylic samples aged with sulfur dioxide (SO_2) and nitrogen oxide (NO_x) mixed with different relative humidity contents (50 and 80 RH%). Through the use of analytical and multivariate techniques, it was possible to observe that the binders deteriorating behavior varies according to the type of gas and the RH. In general, NO_x has the most significant oxidizing effect on paints. Specifically, RH has more influence on acrylic paints, different gases on alkyd paints, and the gas×RH combination on styrene-acrylic paints. These results are relevant as outdoor artworks are increasingly affected by environmental degradation. Considering the results previously explained, the prevention methods should be selected according to the type of binder and the environmental conditions of the artworks (internal or external). In order to obtain a broader knowledge, future experiments will be considered, such as the effect of ozone and particulate matter, the synergistic effect of different pollutants, parallel aging tests (accelerated and natural), and investigation of real aged artworks.

If some mechanisms of degradation were clarified with the previous study, others still remained not well known. For example, it was observed that the acrylic paints showed a different level of surface migration of the surfactant according to the different polluting gases. In this final study carried out (**Paper VI**), accelerated aging with polluting gases (O_3, SO_2, H_2S, NO_x) and relative humidity (80%) of the acrylic emulsion was performed. The innovative aspect is the morphological (3D optical and atomic force microscopy) and chemical-physical (Raman and FTIR spectroscopy) evaluation of the degradation products as a function of the different pollutant gas used. Furthermore, a preliminary evaluation of two cleaning methods (swab rolled test and hydrogel system) were tested to study its effectiveness. From the assessments carried out, the gaseous pollutant NO_x favours the migration of the surfactant and damages

the acrylic component the most. As for the results of the cleaning tests, the AFM topographies and chemical mappings confirm a great cleaning effectiveness with swab rolled test which however compromises the structural stability of the acrylic component. On the other hand, the hydrogel allows the gradual release of water but does not allow a regular cleaning effect, leaving residues.

These results could be expanded with further investigations, such as considering real artworks, testing commercial acrylic paints, using different cleaning solvents, setting up new experiments by varying aging conditions, and employing further analytical-diagnostic analyzes (i.e. mechanical, thermal, technical separation methods). Moreover, a future perspective of this study can be the synergistic effect of pollutants and their combination with different relative humidity content, gas concentration, and exposure time. This PhD thesis provides clarifications on some conservative aspects highlighted in the museum environment, related to the degradation processes deriving from environmental variables, and to the effectiveness of cleaning treatments on aged acrylic objects. Furthermore, the diagnostic analysis presented can be used to support the prevention of the degradation of artistic paint materials, develop more sophisticated environmental sensors for monitoring these pollutants (especially in internal museum environments), and, finally, implement knowledge related to the conservation and restoration practices of modern and contemporary artworks.

REFERENCES

[1] Learner TJS, Smithen P, Krueger JW, Schilling MR. Modern Paints Uncovered. The Getty Conservation Institute; 2007.

[2] Chiantore O, Rava A. Conserving Contemporary Art: Issues, Methods, Materials, and Research. 2013.

[3] Jablonski E, Learner T, Hayes J, Golden M. Conservation concerns for acrylic emulsion paints. Stud Conserv 2003;48:3–12. https://doi.org/10.1179/sic.2003.48.supplement-1.3.

[4] Learner TJS. Analysis of Modern Paints. The Getty Conservation Institute; 2005.

[5] Chiantore O, Scalarone D, Learner T. Characterization of artists' acrylic emulsion paints. Int J Polym Anal Charact 2003;8:67–82. https://doi.org/10.1080/10236660304884.

[6] Learner TJS. A review of synthetic binding media in twentieth-century paints. Conservator 2000;24:96–103.

[7] Learner T. The analysis of synthetic resins found in twentieth century. 1995.

[8] Stringari C, Pratt E. The identification and characterization of acrylic emulsion paint media. Sav. Twent. Century Conserv. Mod. Mater., 1993, p. 411–40.

[9] Scalarone D, Lazzari M, Castelvetro V, Chiantore O. Surface monitoring of surfactant phase separation and stability in waterborne acrylic coatings. Chem Mater 2007;19:6107–13. https://doi.org/10.1021/cm0714077.

[10] Evanson KW, Urban MW. Surface and interfacial FTIR spectroscopic studies of latexes. III. The effects of substrate surface tension and elongation on exudation of surfactants. J Appl Polym Sci 1991;42:2309–20. https://doi.org/10.1002/app.1991.070420822.

[11] Ormsby B, Kampasakali E, Learner T. Surfactants and Acrylic Emulsion Paints: Evaluating Changes Induced by Wet Surface Cleaning Treatments. New Insights into Clean. Paint., 2010, p. 159–164.

[12] Fremout W, Verboven M, Saverwyns S. Accelerated tobacco smoke staining on waterborne acrylic paintings caused by exuding surfactants: a study with Py-GC/MS and THM-GC/MS. E-Preservation Sci 2014;11:47–53.

[13] Jansson KD, Zawodny CP, Wampler TP. Determination of polymer additives using analytical pyrolysis. J Anal Appl Pyrolysis 2007;79:353–61. https://doi.org/10.1016/j.jaap.2006.12.009.

[14] Papliaka ZE, Andrikopoulos KS, Varella EA. Study of the stability of a series of synthetic colorants applied with styrene-acrylic copolymer, widely used in contemporary paintings, concerning the effects of accelerated ageing. J Cult Herit 2010;11:381–91. https://doi.org/10.1016/j.culher.2010.02.003.

[15] Germinario G, van der Werf ID, Sabbatini L. Chemical characterisation of spray paints by a multi-analytical (Py/GC–MS, FTIR, μ-Raman) approach. Microchem J

2016;124:929–39. https://doi.org/10.1016/j.microc.2015.04.016.

[16] Melchiorre Di Crescenzo M, Zendri E, Sánchez-Pons M, Fuster-López L, Yusá-Marco DJ. The use of waterborne paints in contemporary murals: Comparing the stability of vinyl, acrylic and styrene-acrylic formulations to outdoor weathering conditions. Polym Degrad Stab 2014;107:285–93. https://doi.org/10.1016/j.polymdegradstab.2013.12.034.

[17] Winnik MA. Latex film formation. Curr Opin Colloid 1997;2:192–9.

[18] Steward PA, Hearn J, Wilkinson MC. An overview of polymer latex film formation and properties. Adv Colloid Interface 2000;86:195–267.

[19] Keddie JL, Meredith P, Jones RAL, Donald AM. Kinetics of film formation with emulsion copolymers. Macromolecules 1995;28:2673–82.

[20] Golden M, Hayes J, Gavett B. Dry Notes on Drying! Understanding how to control the drying process of acrylics. Just Paint Golden Artist Color 1996;3:1–6.

[21] Nicholson J. Film formation by emulsion paints. J Oil Colour Chem Assoc 1989;72:475–7.

[22] Gorkum R, Bouwman E. The oxidative drying of alkyd paint catalysed by metal complexes. Coord Chem Rev 2005;249:1709–28. https://doi.org/https://doi.org/10.1016/j.ccr.2005.02.002.

[23] Soucek MD, Salata RR. Alkyd Resin Synthesis. In: Kobayashi S, Müllen K, editors. Encycl. Polym. Nanomater., Berlin, Heidelberg: Springer Berlin Heidelberg; 2014, p. 1–6. https://doi.org/10.1007/978-3-642-36199-9_278-1.

[24] Morgans WM. Outlines of Paint Technology. Griffin; 1982.

[25] Ploeger R, Scalarone D, Chiantore O. The characterization of commercial artists' alkyd paints. J Cult Herit 2008;9:412–9. https://doi.org/10.1016/j.culher.2008.01.007.

[26] Hubert JC, Venderbosch RAM, Muizebelt WJ, Klaasen RP, Zabel KH. Singlet oxygen drying of alkyd resins and model compounds. J Coatings Technol 1997;69:59–64. https://doi.org/10.1007/BF02696154.

[27] Bartolozzi G, Marchiafava V, Mirabello V, Peruzzini M, Picollo M. Chemical curing in alkyd paints: An evaluation via FT-IR and NMR spectroscopies. Spectrochim Acta - Part A Mol Biomol Spectrosc 2014;118:520–5. https://doi.org/10.1016/j.saa.2013.09.017.

[28] Weissenborn PK, Motiejauskaite A. Emulsification, drying and film formation of alkyd emulsions. Prog Org Coatings 2000;40:253–66. https://doi.org/10.1016/S0300-9440(00)00120-X.

[29] Greimel KJ, Perz V, Koren K, Feola R, Temel A, Sohar C, et al. Banning toxic heavy-metal catalysts from paints: Enzymatic cross-linking of alkyd resins. Green Chem 2013;15:381–8. https://doi.org/10.1039/c2gc36666e.

[30] Lazzari M, Chiantore O. Drying and oxidative degradation of linseed oil. Polym Degrad Stab 1999;65:303–13. https://doi.org/10.1016/S0141-3910(99)00020-8.

[31] Matteini M, Mazzeo R, Moles A. Chemistry for Restoration, Painting and Restoration Materials. Florence: 2016.

[32] Berni A., Mennig M. SH. Doctor blades. Sol-Gel Technol. Glas. Prod. Users, 2004, p. 89–92.

[33] Alebic-Juretic A, Sekulic-Cikovic D. The impact of air pollution on the paintings in storage at the museum of modern and contemporary art, rijeka, croatia. Stud Conserv 2009;54:49–57. https://doi.org/10.1179/sic.2009.54.1.49.

[34] Nazaroff WW, Salmon LG, Cass GR. Concentration and Fate of Airborne Particles in Museums. Environ Sci Technol 1990;24:66–77. https://doi.org/10.1021/es00071a006.

[35] Graeme A, Mathew C. Homogeneous and Heterogeneous Oxidation of Polypropylene. Handb. Polym. Degrad., 2000, p. 4.

[36] https://spectrum.ieee.org/. IEEE Spectrum 2021.

[37] Rabek JF. Polymer photodegradation: mechanisms and experimental methods. 1995.

[38] Feller RL. Accelerated aging: Photochemical and Thermal aspects. 1994.

[39] Kämpf G, Sommer K, Zirngiebl E. Studies in accelerated weathering. Part I. Determination of the activation spectrum of photodegradation in polymers. Prog Org Coatings 1991;19:69–77. https://doi.org/10.1016/0033-0655(91)80011-7.

[40] Learner T, Chiantore O, Scalarone D. Ageing studies on acrylic emulsion paints. Prepr. ICOM Comm. Consrvation 13th Trienn. Meet., Rio de Janeiro: James & James; 2002, p. 911–9.

[41] Scalarone D, Chaintore O, Learner T. Ageing studies of acrylic emulsion paints. Part II. Comparing formulations with poly (EA-co-MMA) and poly (nBA-co-MMA)binders. In: James J&, editor. Prepr. ICOM Comm. Conserv. 14th Trienn. Meet., 2005, p. 350–8.

[42] Whitmore PM, Colaluca VG. The Natural nad Accelerated aging of an acrylic artist´s medium. Stud Conserv 1995;40:51–64.

[43] Chiantore O, Trossarelli L, Lazzari M. Photooxidative degradation of acrylic and methacrylic polymers. Polymer (Guildf) 2000;41:1657–68. https://doi.org/10.1016/S0032-3861(99)00349-3.

[44] Pintus V, Schreiner M. Characterization and identification of acrylic binding media:influence of UV light on the ageing process. Anal Bioanal Chem 2011;399:2961–76.

[45] Ormsby B, Learner T. Artist´s acrylic emulsion paints: materials, meaning and conservation treatment options. Aust Inst Conserv Cult Mater Bull 2014;34:57–65.

[46] Mallégol L, Gardette JL, Lemaire J. Long-term behavior of oil-based varnishes and paints. Photo- and Thermooxidation of cured linseed oil. J Am Oil Chem Soc 2000;70:257–63.

[47] Smith GC. Photochemical degradation of alkyd paints. Pigment Resin Technol 1977;6:4–8.

[48] Christensen PA, Dilks A, Egerton TA, Lawson EJ. Photocatalytic oxidation of alkyd paint films measured by FTIR analysis of UV generated carbon dioxide. J Mater Sci 2002;37:4901–9. https://doi.org/10.7868/S0044513413040144.

[49] Ploeger R, Chiantore O. Characterization and Stability Issues of Artists ' Alkyd Paints. Smithson Contrib to Museum Conserv 2012;3:89–95.

[50] Cakić SM, Ristić IS, Vladislav JM, Stamenković J V., Stojiljković DT. IR-change and colour changes of long-oil air drying alkyd paints as a result of UV irradiation. Prog Org Coatings 2012;73:401–8. https://doi.org/10.1016/j.porgcoat.2010.12.002.

[51] Howells R, Burnstock A. Polymer dispersion artificially aged. Conserv 1985;9.

[52] Kreislova K, Knotkova D, Geiplova H. Atmospheric corrosion of historical industrial structures. 2013. https://doi.org/10.1533/9781782421573.3.311.

[53] Franey JP, Graedel TE. Corrosive effects of mixtures of pollutants. J Air Pollut Control Assoc 1985;35:644–8. https://doi.org/10.1080/00022470.1985.10465940.

[54] Dulog L. The role of sulfur dioxide and nitrogen dioxide on the degradation of polymers. Angew Makromol Chemie 1997;252:1–10. https://doi.org/10.1002/apmc.1997.052520101.

[55] Hamilton R, Kucera V, Tidblad J, Watt J. The Effects of Air Pollution on Cultural Heritage. 2009. https://doi.org/https://doi.org/10.1007/978-0-387-84893-8.

[56] Tidblad J, Kucera V, Ferm M, Kreislova K, Brüggerhoff S, Doytchinov S, et al. Effects of air pollution on materials and cultural heritage: ICP materials celebrates 25 years of research. Int J Corros 2012;2012:2005–6. https://doi.org/10.1155/2012/496321.

[57] Striegel MF, Guin EBB, Hallett K, Sandoval D, Swingle R, Knox K, et al. Air pollution, coatings, and cultural resources. Prog Org Coatings 2003;48:281–8. https://doi.org/10.1016/j.porgcoat.2003.05.001.

[58] De Santis F, Di Palo V, Allegrini I. Determination of some atmospheric pollutants inside a museum: relationship with the concentration outside. Sci Total Environ 1992;127:211–23. https://doi.org/10.1016/0048-9697(92)90504-L.

[59] Camuffo D, Fernicola V, Bertolin C. Basic Environmental Mechanisms Affecting Cultural Heritage. 2010.

[60] Cass GR, Druzik JR, et al. Protection of Works of Art From Atmospheric Ozone. 1989.

[61] Tator KB. Coating deterioration. Prot Org Coatings, ASM Handb 2015;5B.

[62] Šúri M, Huld TA, Dunlop ED, Ossenbrink HA. Potential of solar electricity generation in the European Union member states and candidate countries. Sol Energy 2007;81:1295–305. https://doi.org/10.1016/j.solener.2006.12.007.

[63] D2565 AI-99. Standard Practise for Xenon-Arc Exposure of Plastics Intended for Outdoor Applications. 2008.

[64] https://www.eea.europa.eu/. European Environmental Agency 2020.

[65] Prati S, Sciutto G, Bonacini I, Mazzeo R. New Frontiers in Application of FTIR Microscopy for Characterization of Cultural Heritage Materials. Top Curr Chem 2016;374:1–32. https://doi.org/10.1007/s41061-016-0025-3.

[66] Derrick MR, Stulik D, Landry JM. Infrared Spectroscopy in Conservation Science.

1999.

[67]   Schrader B. Infrared and Raman Spectroscopy: methods and applications. 1995.

[68]   Everall NJ, Chalmers JM, Griffiths PR. Vibrational spectroscopy of polymers: principles and practise. 2007.

[69]   Chalmers JM. Handbook of Vibrational Spectroscopy. Theory and Instrumentation. vol. 1. American Chemical Society; 2002. https://doi.org/10.1021/ja025228w.

[70]   Baker MJ, Trevisan J, Bassan P, Bhargava R, Butler HJ, Dorling KM, et al. Using Fourier transform IR spectroscopy to analyze biological materials. Nat Protoc 2014;9:1771–91. https://doi.org/10.1038/nprot.2014.110.

[71]   Mirabella FM. Practical Spectroscopy Series; Internal reflection spectroscopy: Theory and applications. 1993.

[72]   Robinson JW, Frame EMS, Frame GM. Undergraduate instrumental analysis. Sixth edit. 2005.

[73]   Wiesinger R, Pagnin L, Anghelone M, Moretto LM, Orsega EF, Schreiner M. Pigment and Binder Concentrations in Modern Paint Samples Determined by IR and Raman Spectroscopy. Angew Chemie - Int Ed 2018;57:7401–7. https://doi.org/10.1002/anie.201713413.

[74]   Edwards HGM, Chalmers JM, Hargreaves MD. Infrared and Raman Spectroscopy in Forensic Science. New York: 2011.

[75]   Smith E, Dent G. Modern Raman Spectroscopy, a practical approach. England: 2005.

[76]   Nakamoto K. Infrared and Raman Spectra of Inorganic and Coordination Compounds, Part A. United States: 2009.

[77]   Lohumi S, Kim MS, Qin J, Cho BK. Raman imaging from microscopy to macroscopy: Quality and safety control of biological materials. TrAC - Trends Anal Chem 2017;93:183–98.

[78]   Creagh DC, Bradley DA. Radiation in Art and Archeometry. United States: 2000.

[79]   Hesse M, Meier H, Zeeh B. Metodi spettroscopici in chimica organica. Napoli: 2014.

[80]   Hölscher H, Schwarz UD. Theory of amplitude modulation atomic force microscopy with and without Q-Control. Int J Non Linear Mech 2007;42:608–25.

[81]   Friedbacher G, Bubert H. Surface and Thin Film Analysis, 2. 2011.

[82]   Martin Y. Atomic force microscope–force mapping and profiling on a sub 100-Å scale. J Appl Phys 1987;61:4723–4279.

[83]   Koyun AN. Imaging And Spectroscopic Analysis Of Bitumen With Atomic Force Microscopy And Raman Spectroscopy. 2016.

[84]   Leipzig U. home.uni-leipzig.de 2009.

[85]   Gross L, Mohn F, Moll N, Liljeroth P, Meyer G. The chemical structure of a molecule resolved by atomic force microscopy. Science (80-) 2009;325:1110–4. https://doi.org/10.1126/science.1176210.

[86]   Schmitz I, Al. E. Tapping-Mode AFM in comparison to Contact-Mode AFM as a

Tool for in situ investigations of surface reactions with reference to glass corrosion. Anal Chem 1997;69:1012–8.

[87]   Hrouzek M. Atomic Force Microscopy, modeling, estimation and control. 2008.

[88]   Payton O, Al. E. Feedback-induced instability in tapping mode atomic force microscopy: theory and experiment. Proc R Soc A 2010;467:1801–22.

[89]   Anabitarte F, Cobo A, Lopez-Higuera JM. Laser-Induced Breakdown Spectroscopy: Fundamentals, Applications, and Challenges. ISRN Spectrosc 2012;2012:1–12. https://doi.org/10.5402/2012/285240.

[90]   Miziolek AW, Palleschi V, Schechter I. Laser-Induced Breakdown Spectroscopy (LIBS): Fundamentals and Applications. 2006.

[91]   Musazzi S, Perini U. Laser-Induced Breakdown Spectroscopy. 2014.

[92]   Rusak DA, Castle BC, Smith BW, Winefordner JD. Fundamentals and Applications of Laser-Induced Breakdown Spectroscopy. Crit Rev Anal Chem 1997;27:257–90. https://doi.org/10.1080/10408349708050587.

[93]   Markiewicz-Keszycka M, Cama-Moncunill X, Casado-Gavalda MP, Dixit Y, Cama-Moncunill R, Cullen PJ, et al. Laser-induced breakdown spectroscopy (LIBS) for food analysis: A review. Trends Food Sci Technol 2017;65:80–93. https://doi.org/10.1016/j.tifs.2017.05.005.

[94]   Visco G, Avino P. Employ of multivariate analysis and chemometrics in cultural heritage and environment fields. Environ Sci Pollut Res 2017;24:13863–5. https://doi.org/10.1007/s11356-017-9205-0.

[95]   Sarmiento A, Pérez-Alonso M, Olivares M, Castro K, Martínez-Arkarazo I, Fernández LA, et al. Classification and identification of organic binding media in artworks by means of Fourier transform infrared spectroscopy and principal component analysis. Anal Bioanal Chem 2011;399:3601–11. https://doi.org/10.1007/s00216-011-4677-0.

[96]   Unnikrishnan, V.K. Choudhari KS, Kulkarni SD, Nayak R, Kartha VB, Santhosh C. Analytical predictive capabilities of laser induced breakdown spectroscopy (LIBS) with principal component analysis (PCA) for plastic classification. RSC Adv 2013;3:25872–80.

[97]   Musumarra G, Fichera M. Chemometrics and cultural heritage. Chemom Intell Lab Syst 1998;44:363–72. https://doi.org/10.1016/S0169-7439(98)00069-0.

[98]   Jansen JJ, Hoefsloot HCJ, Van Der Greef J, Timmerman ME, Westerhuis JA, Smilde AK. ASCA: Analysis of multivariate data obtained from an experimental design. J Chemom 2005;19:469–81. https://doi.org/10.1002/cem.952.

[99]   Zwanenburg G, Hoefsloot HCJ, Westerhuis JA, Jansen JJ, Smilde AK. ANOVA–principal component analysis and ANOVA–simultaneous component analysis: A comparison. J Chemom 2011;25:561–7. https://doi.org/10.1002/cem.1400.

[100]   Breiman L. Random forests. Mach Learn 2001;45:5–32.

[101]   Anghelone M, Jembrih-Simbürger D, Schreiner M. Identification of copper phthalocyanine blue polymorphs in unaged and aged paint systems by means of

micro-Raman spectroscopy and Random Forest. Spectrochim Acta - Part A Mol Biomol Spectrosc 2015;149:419–25. https://doi.org/10.1016/j.saa.2015.04.094.

[102] Hufnagl B, Steiner D, Renner E, Loder MGJ, Laforsch C, Lohninger H. A methodology for the fast identification and monitoring of microplastics in environmental samples using random decision forest classifiers. Anal Methods 2019;11:2277–85.

[103] Pintus V, Wei S, Schreiner M. UV ageing studies: evaluation of lightfastness declarations of commercial acrylic paints. Anal Bioanal Chem 2012;402:1567–84.

[104] Pintus V, Wei S, Schreiner M. Synthetic materials used in modern and contemporary art and their UV ageing properties. Proc 4th ALMA Interdiscip Semin 2012.

[105] Anghelone M, Stoytschew V, Jembrih-Simbürger D, Schreiner M. Spectroscopic methods for the identification and photostability study of red synthetic organic pigments in alkyd and acrylic paints. Microchem J 2018;139:155–63.

[106] Anghelone M, Jembrih-Simbürger D, Schreiner M. Influence of phthalocyanine pigments on the photo-degradation of alkyd artists' paints under different conditions of artificial solar radiation. Polym Degrad Stab 2016;134:157–68.

Paper I

Photodegradation Kinetics of Alkyd Paints: The Influence of Varying Amounts of Inorganic Pigments on the Stability of the Synthetic Binder

Laura Pagnin, Rosalba Calvini, Rita Wiesinger, Johannes Weber, Manfred Schreiner

Photodegradation Kinetics of Alkyd Paints: The Influence of Varying Amounts of Inorganic Pigments on the Stability of the Synthetic Binder

Laura Pagnin[1]*, Rosalba Calvini[2], Rita Wiesinger[1], Johannes Weber[3] and Manfred Schreiner[1,4]

[1]Institute of Natural Sciences and Technology in the Arts, Academy of Fine Arts, Vienna, Austria, [2]Department of Life Sciences, University of Modena and Reggio Emilia, Reggio Emilia, Italy, [3]Institute of Conservation Sciences, University of Applied Arts Vienna, Vienna, Austria, [4]Institute of Chemical Technologies and Analytics, Vienna University of Technology, Vienna, Austria

As the effects of climate change pose an increasing risk of damaging outdoor modern and contemporary artworks' aesthetic appearance by affecting their mechanical properties and chemical-physical stability, understanding the degradation processes attacking these objects is becoming more and more essential to their conservation. For this purpose, the kinetics of photo-oxidation processes occurring in alkyd paints and their stability in mixtures with different inorganic pigments were investigated. The aim was to characterize the different degradation reactions over time and study the photodegradation kinetics according to different pigments and pigment/binder ratios. This paper describes the degradation behavior of artificial ultramarine blue, hydrated chromium oxide green, and cadmium sulfate yellow pigments mixed with alkyd resin and aged under simulated sunlight exposure for a total of 1,008 h. The analytical techniques used offer complementary information on the characterization of the samples and their aging. Specifically, 3D Optical Microscopy allowed studying morphological and color changes. These results were supported by Scanning Electron Microscopy and Colorimetry analyses, also focused on studying the physical and granulometric characteristics of the pigments in relation to the binder degradation. Finally, qualitative and quantitative analysis was performed by Attenuated Total Reflection Infrared Spectroscopy. To support the obtained results, Multivariate Analysis of microscopic images was carried out with the aim of studying the degradation effects linked to color and texture changes. The obtained results demonstrate that the degradation processes of alkyd resin are influenced by the presence of the different inorganic pigments used and their concentration in the mixtures. This study should contribute as support to the field of conservation-restoration to find suitable protection strategies for paint surfaces against degradation agents.

Keywords: alkyd resin, photodegradation, inorganic pigments, multivariate analysis, infrared spectroscopy, scanning electron microscopy, colorimetry

INTRODUCTION

With the development of synthetic organic chemistry at the beginning of the 20th century, contemporary artists started to use a significant number of new polymeric materials as paint binders for creating artworks. Consequently, gathering knowledge related to proper preservation techniques for these artworks has become increasingly important on the international level (Chiantore and Rava, 2005). Several polymeric structural changes lead to mechanical properties and chemical stability modifications which eventually result in and degradation of the binder (Rosu and Visakh, 2016). Early studies (Rabek, 1995; Learner, 2008) focused on the characterization of these polymers; later on, attention has been given to the study of chemical and physical factors influencing the light stability of the new binders, especially for artworks exposed to solar radiation (outdoor environment). Additionally, the presence of oxygen was also found to play a major role in polymer stability as it promotes photo-oxidation reactions, such as cross-linking, chain scission, and further oxidation reactions.

Among these polymers, alkyd resins have been widely used in artworks and are the focus of this study. Their first use was documented around the 1940s, and soon they were established as one of the most used materials in modern and contemporary art. They were employed mainly by painters such as Picasso and Pollock, who preferred them to traditional drying oils. During the seventies, they became the prevalent chemical binder in paint artworks (Lake et al., 2004). Chemically, alkyd polymers are composed of oil-modified polyester resins formed from the combination of a polyhydric alcohol (generally glycerol), a polybasic carboxylic acid, and siccative oils or free fatty acids. The oil chain length and weight percent of fatty acids in the alkyd resin molecular structure influence the curing and photodegradation processes (Mallégol et al., 2000a). Photodegradation of alkyd polymers occurs by auto-oxidation of unsaturated bonds of the fatty acid portion forming a cross-linked network.

As a consequence, the newly-formed peroxy and hydroperoxy radicals may react with the alkyd chain leading to further cross-linking and β-scission reactions. Moreover, during auto-oxidation of the oil portion, chemical species such as hydrocarbons, aldehydes, and ketones allow Norrish type I reactions (cleavage or homolysis into free radical intermediates) and chain-scission to take part in the oil degradation. In particular, Norrish type I is the main photodegradation initiation reaction of aromatic polyesters, leading to the formation of free phthalic acid (Lazzari and Chiantore, 1999). Furthermore, hydrogen abstraction (Norrish type II reaction) can take place and products such as ketones, aldehydes, alkene, and carboxylic acids can be formed in the photochemical single state excitation. The abstraction of hydrogen produces alcohols, cyclic structures, carboxylic acids, and vinyl groups. Overall, alkyd resin photo-oxidation results in production of low molecular weight fractions, which either evaporate more easily or remain in the polymeric structure (Lazzari and Chiantore, 1999; Duce et al., 2014). While the several reactions involved in

the long-term photo-oxidation have already been extensively studied in previous projects (Pintus et al., 2015; Anghelone et al., 2016), investigating the effect of pigment interaction to the photo stability of alkyd polymers is also fundamental (Mallégol et al., 2000b). In particular, different studies (Rasti and Scott, 1980; Anghelone et al., 2017) show that inorganic pigments can act as retardants or promoters of light-induced aging reactions. To this respect, pigments can be divided into two categories: 1) photo-absorbers, which reduce the impact of light transmitted into the paint layer, and 2) photo-promotors, which increase the photo-oxidation effect with formation of free radicals. Moreover, characteristics of the pigments such as concentration, refractive index (R.I.), and particle size also play a role in the photodegradation process as they can affect the penetration of radiation into the paint layer (Zubielewicz et al., 2011). This study is focused on three inorganic pigments, namely artificial ultramarine blue, hydrated chromium oxide green, and cadmium yellow. These pigments have been used since 1800 as well as in recent contemporary artworks and are still included in formulations of paint tubes. Because of their widespread use among artists, studying their effects on the overall stability of art objects is of high importance (Bevilacqua et al., 2010), not only to prevent aesthetical damage of artworks but also to lower the risk of their physical degradation.

In this work, the surface chemical changes of alkyd paints exposed to short-time artificial sunlight aging were studied. Paint samples were exposed for 168, 336, 504, 672, 840, and 1,008 h (0–6 weeks) to artificial aging, using spectral and intensity parameters comparable to outdoor solar radiation. Several paint samples were prepared by mixing each inorganic pigment (artificial ultramarine blue, hydrated chromium oxide green, and cadmium yellow) with the synthetic binder. Three different pigment/binder (P/BM) ratios were selected (1:2, 1:3, and 1:6) in order to evaluate how the concentration of pigment influences the binder's degradation. The selection of analytical techniques was based on their reciprocal complementarity, which allows supporting the various obtained results and providing new information on the binder's degradation mechanisms. Specifically, 3D Optical Microscopy, Scanning Electron Microscopy (SEM), and Colorimetry allowed studying the morphological and color changes of the paints.

The binder degradation reactions were investigated by Attenuated Total Reflection Infrared Spectroscopy (ATR-FTIR). Firstly, identification of the functional groups found before and after aging was carried out. Subsequently, quantitative analysis was performed to investigate the binder's photodegradation kinetics, taking into consideration the different pigments and P/BM ratios selected. Finally, microscopic images of the paint samples were analyzed using a multivariate approach based on the extraction and analysis of features related to color and texture properties, using Principal Component Analysis (PCA). PCA is a data exploration technique aimed at extracting useful information from a dataset and displaying data structure in a simple and easy-to-interpret manner. Basically, the original dataset is projected into a lower-

TABLE 1 | List of materials analyzed.

Binder	Chemical composition		Commercial name
Alkyd resin	Polymer oil-modified polyester-resin based on orthophthalic acid and pentaerythritol		Alkyd medium 4 (Lukas®, Germany)
Pigment	**Color index**	**P/BM ratio in weight**	**Chemical composition**
Artificial ultramarine blue	PB29	1:2, 1:3, 1:6	$Na_{6-10}Al_6Si_6O_{24} \cdot S_{2-4}$
Hydrated chromium oxide green	PG18	1:2, 1:3, 1:6	$Cr_2O_3 \cdot 2H_2O$
Cadmium yellow	PY37	1:2, 1:3, 1:6	CdS

dimensional space defined by few Principal Components, which are calculated based on data variance. By analysing PCA outcomes it is possible to identify clusters of objects sharing similar properties or relationships among variables (Musumarra and Fichera, 1998). In this study, PCA was applied to the dataset of image features in order to gain an objective and comprehensive overview of the modifications induced by artificial aging on the morphology of the paint layers.

MATERIALS AND METHODS

Sample Preparation

Different samples were prepared by mixing pure Alkyd Medium 4 (Lukas®, Germany) with inorganic pigments (Kremer Pigmente, Germany), i.e., artificial ultramarine blue (PB29), hydrated chromium oxide green (PG18), and cadmium yellow (PY37). A detailed description of the paint samples is shown in **Table 1**. In total, nine samples were prepared. Different P/BM ratios in weight were prepared, depending on the paint's consistency. After a consultation with a paint manufacturer, the P/BM ratios chosen were confirmed as similar to the commercial formulations. The fresh paints were cast on glass slides with a film thickness of 150 μm. The samples were dried at room conditions (ca. 22°C and 30% relative humidity [RH]) for three weeks before starting the artificial aging in the UV chamber. The samples were analyzed every week (max. 1,008 h exposure).

Artificial Aging

The light aging, which simulates natural sunlight, was carried out in a UVACUBE SOL 2/400F UV chamber, produced by Dr. Hönle GmbH UV-Technology, Germany. The emitting radiation was supplied by a Xenon Arc lamp with the possibility to provide radiations between 295 and ~3,000 nm, similar to outdoor solar conditions. Temperature and RH were separately measured in the chamber using the AQL S500 sensor (Aeroqual Limited, New Zealand).

During artificial aging, the chamber temperature was around 38°C, and the RH varied between 10 and 20%. The radiation intensity was measured by using a UV-Meter Basic (Dr. Hönle, Germany). The Xenon lamp reached an approximate value of 170 W/m². According to the recent data provided by Central Europe, it is possible to assume that the radiation value obtained is similar to natural aging caused by solar radiation (Šúri et al., 2007). The artificial light exposure of alkyd paints was carried out for 1,008 h in total. Considering that there are around 1,000 h of sunshine per year (global approximation), it is possible to

approximate the artificial sun aging of 1,008 h to around one year of natural outdoor sunlight exposure (Šúri et al., 2004). The glass slide was divided into six regions (**Figure 1**) to obtain different aging periods (168–1,008 h) on each paint sample. The regions which were not exposed to artificial light were contact-free covered with a silver-aluminum 100% reflective surface. The reflective cover was moved weekly to obtain the complete 1,008 h aged sample set.

Optical 3-Dimensional Microscope

To monitor the different morphological changes due to artificial light aging, the surface of each colored layer was scanned by the Keyence VHX-6000 microscope (Keyence, Belgium). Three-dimensional optical micrographs and topological images were recorded using a VH-Z100 objective with a zoom lens of 1,000×. For each aging week (from 0 to 1,008 h), surface pictures were acquired. The objective chosen reaches a focus in the range of 100–1,000 μm. The microscope is provided with a LED light source (5,700 K). For the 3D pictures, a magnification of 1,000× was selected, measuring a total area of around 15,376 μm². To obtain the 3D depth profile of the surface, the total depth obtained is 10 μm taking every 2 μm a picture (pitch scans). In total, 63 images were acquired using the optical 3D microscope, corresponding to nine samples (three pigments types × 3 P/BM ratios) aged for seven different times from 0 to 1,008 h.

Multivariate Analysis of Microscopic Images

The data obtained by the microscopic images of the paint samples were subjected to multivariate analysis in order to evaluate the degradation effects caused by artificial UV aging. The main focus is put on the feature of the paint samples and to study the influence of pigment type and concentration on such degradation effects. For this aim, a preliminary data dimensionality reduction step was applied to convert each image of the dataset into a feature vector codifying for the useful information related to color and aspect of the analyzed samples. Generally, a data dimensionality reduction procedure is a mandatory step when several images have to be simultaneously analyzed and compared to each other, to gain a general overview of the whole image dataset structure (Calvini et al., 2016). Different methods have been proposed to extract relevant features from images. The most common approach is based on evaluating the pixel distribution of defined color parameters of each image and using the corresponding frequency distribution curves or statistical
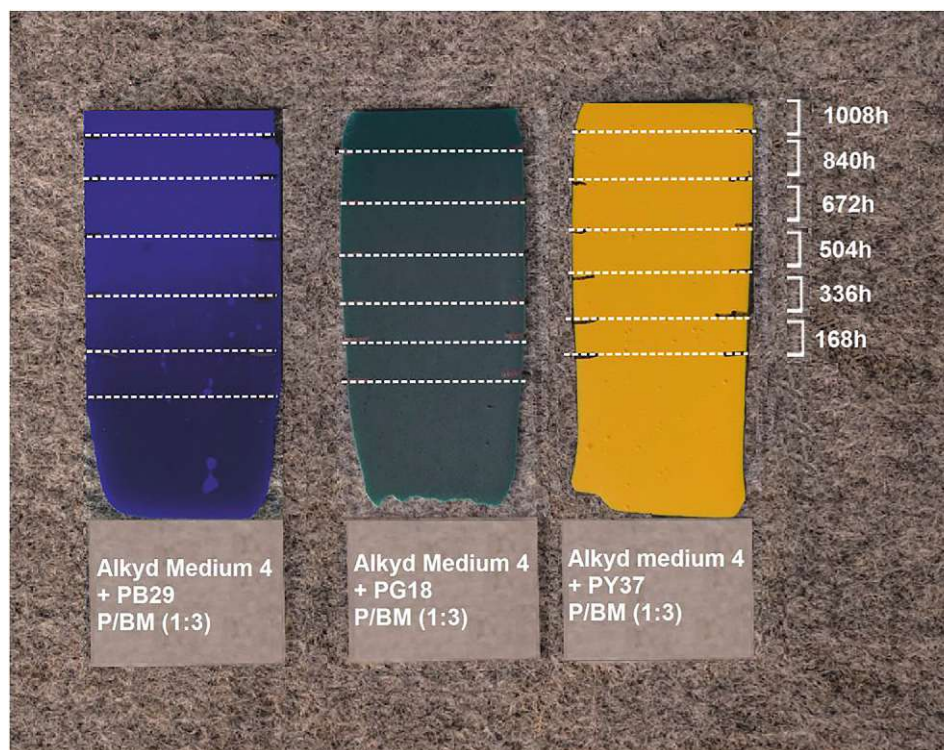
FIGURE 1 | Three paint samples with P/BM ratio 1:3; from left Alkyd Medium 4 + PB29, Alkyd Medium 4 + PG18, Alkyd Medium 4 + PY37. They were exposed to artificial sunlight for 168, 336, 504, 672, 840, and 1,008 h.

parameters calculated from the frequency distribution curves (e.g., mean or standard deviation value) as relevant features (Pereira and Bueno, 2007; Kucheryavski, 2011; Calvini et al., 2020).

Furthermore, in order to fully exploit spatial-related information contained in the images also texture features can be calculated. A widely used image texture analysis approach is the application of Gray Level Co-occurrence Matrices (GLCMs) (Haralick et al., 1973), which records the frequency of occurrence of each possible grey-level pairing of neighboring pixels with a specified spatial arrangement. Given a grey-scale image, four possible orientations of neighboring pixels can be considered to calculate the GLCM: horizontal, right diagonal, vertical, and left diagonal, corresponding to an angle of 0°, 45°, 90°, and 135°, respectively. Then, from each GLCM, it is possible to calculate texture parameters based on first, second, and higher-order statistics and further analyze the obtained texture features using chemometric methods (Malegori et al., 2016; Marschner et al., 2017).

In the present study, a total of 36 features were extracted from each paint sample image. These features include mean, median, and standard deviation and range of red (R), green (G), and blue (B) channels, and of two additional color-related parameters derived from the R, G, and B values: lightness (L), calculated as the sum R, G, and B values, and saturation (S), obtained by converting the RGB color space into the hue-saturation-value

(HSV) color space. These features summarise the color-related properties of the images. Furthermore, texture parameters derived from GLCMs of lightness grey-scale images were extracted. Firstly, each RGB microscopic image was converted into the corresponding grey-scale image of lightness obtained by summing the R, G, and B values of each pixel. Then, GLCMs of each lightness grey-scale image were calculated considering all the possible directions of neighboring pixels (0°, 45°, 90°, and 135°). The calculation of the GLCMs was performed considering a distance of 10 pixels and a resolution of 64 grey-scale levels.

Therefore, four GLCMs were obtained from each original microscopic image. Finally, from each GLCM, the following texture parameters were calculated (Fongaro and Kvaal, 2013):

- *Contrast (Con)*, which measures the intensity variations between one pixel and the neighboring pixel; in a constant image, the value of contrast is equal to zero.
- *Correlation (Corr)*, which measures the relation between one pixel and its neighbors, and this correlation can be direct (positive) or indirect (negative).
- *Energy (En)*, which is calculated as the sum of the square of the GLCM elements; it can range between 0 and 1, and for a constant image, its value is equal to 1.
- *Homogeneity (Hom)*, which measures how close the elements of the GLCM are to the diagonal; it can vary between 0 and 1, and its value is equal to 1 for a diagonal GLCM.

The complete list of the 36 color and texture features extracted from each microscopic image is reported in **Supplementary Table S1**. The feature vectors extracted from all the dataset images were collected into a data matrix with 63 rows, corresponding to the number of acquired images, and 36 columns, corresponding to the number of extracted features. Finally, the matrix of image features was analyzed using PCA using autoscale as a data preprocessing method. The extraction of color and texture features from the images was performed using routines written *ad hoc* in MATLAB language (v. 9.8, The MathWorks, Inc., United States) and based on MATLAB Image Processing Toolbox (v. 11.1). At the same time, PCA models were calculated using the PLS_Toolbox software (v. 8.8.1, Eigenvector Research, Inc., United States) running under the MATLAB environment.

Colorimetric Measurements

To obtain colorimetric values between unaged and aged samples, an SPM50 Gretag-Macbeth (XRite, Switzerland) was used. Measurements were carried out by a D65 light source with the 10° Standard Observer, 45°/0° geometry. The spot size measured is around 1 mm. The system was calibrated with an internal white reference. Five spots were measured per exposure and averaged using Microsoft Excel software (Microsoft®, United States). To determine the color changes between unaged and aged samples, CIELAB coordinates (L*, a*, b*) and ΔE* values were evaluated, according to the Commission Internationale de l'Èclairage 1976 (CIE 1976) (Johnston-Feller, 2001).

Scanning Electron Microscopy

Scanning Electron Microscope (SEM) was employed for investigating the microstructure of paint mixtures, the changes in pigment distribution, and their morphology after aging. Samples were analyzed using a Quanta TM250 FEG Field-Emission Scanning Electron Microscope (Thermo Fisher Scientific, United States), and images were collected under a low vacuum at 20 kV acceleration voltage. Some of the collected images were post-processed using CorelDraw 2018 software, and the pigment particle size was measured using ImageJ v1.52i software.

Attenuated Total Reflection Fourier Transform Infrared Spectroscopy

For the FTIR investigations, a LUMOS FTIR Microscope (Bruker Optics, Germany) in ATR mode with a germanium crystal was employed. The instrument is equipped with a photoconductive cooled MCT detector. Spectra were acquired in a spectral range between 4,000 and 480 cm^{-1}, performing 64 scans at a resolution of 4 cm^{-1}. The resulting spectra were collected and evaluated with the software OPUS® (Bruker Optics, Germany). Five measurement spots were chosen on each unaged and aged paint sample. The spectra were averaged, baseline corrected, and vector normalized. The chemical depth information obtained by the ATR-FTIR measurements, considering the R.I. of the germanium crystal (n_1 = 4.01) and the angle of incidence of the IR beam (θ = 45°), in a spectral region between 4,000 and 480 cm^{-1}, is around 0.65 μm.

RESULTS AND DISCUSSION

Optical 3-Dimensional Microscopy Observations

Figure 2 shows how the morphology of the paint layers of the PB29 alkyd samples changes during the light aging process. The surfaces of the unaged samples show an increasingly glossy appearance with increasing polymer content. The morphology of the pores is also different across P/BM ratios. In fact, as the binder content increases, the pore size tends to widen (especially in the P/BM 1:6 sample). After a total of 1,008 h of light aging, different morphological changes are detectable. In the mixture with P/BM 1:6, it is possible to observe that by increasing the UV exposure time, the pores begin to increase in number and to enlarge until the pigment is more visible on the surface. When the binder content is lower (P/BM 1:2), this phenomenon is already observed after 504 h of UV exposure. After 1,008 h of aging, the pigment grains are more visible on the surface and of sharper morphology; moreover, some discoloration can be observed. This aging effect is more noticeable when the P/BM is high (1:2). In *Principal Component Analysis of Features Extracted From Microscopic Images* and *Colorimetric Measurements*, the color changes will be discussed more in detail through multivariate analysis of the microscopic images and colorimetry.

A similar behavior is also observed in the PG18 alkyd samples (**Supplementary Figure S1**). In the 1:6 mixture, after 1,008 h of aging, the surface is less glossy and more porous. As for the blue sample, also in the green 1:2 mixture, the opacity increases over time, probably as a result of the binder's degradation and pigment accumulation on the surface. However, unlike PB29, the PG18 pigment tends to darken, and this effect is particularly visible in the mixture with a high amount of pigment (P/BM 1:2). This morphological and colorimetric behavior is also observable for the PY37 alkyd sample (**Supplementary Figure S2**). However, differently from the two previous paints, the glossy effect is not evident, the pores are much smaller and after aging, they are no longer well-defined. This effect may be due to the granulometry of the yellow pigment, explained in *Colorimetric Measurements* (SEM results).

Principal Component Analysis of Features Extracted From Microscopic Images
Principal Component Analysis Considering All Samples

For the first evaluation of data structure, PCA of the image features matrix was calculated considering all the samples together, and the corresponding results are reported in **Supplementary Figure S3**. PC1 separates PY37 samples from the other two pigments based on color and texture features like homogeneity, energy, and contrast, which have high PC1 loading coefficients in terms of absolute values. In particular, the images of PY37 have higher *Hom* and *En* values, showing a more homogeneous paint layer and the presence of the binder is less evident.

Furthermore, the PC1 and PC3 score plot show that sample PY37 presents a lower variation due to aging, while PB29 paint
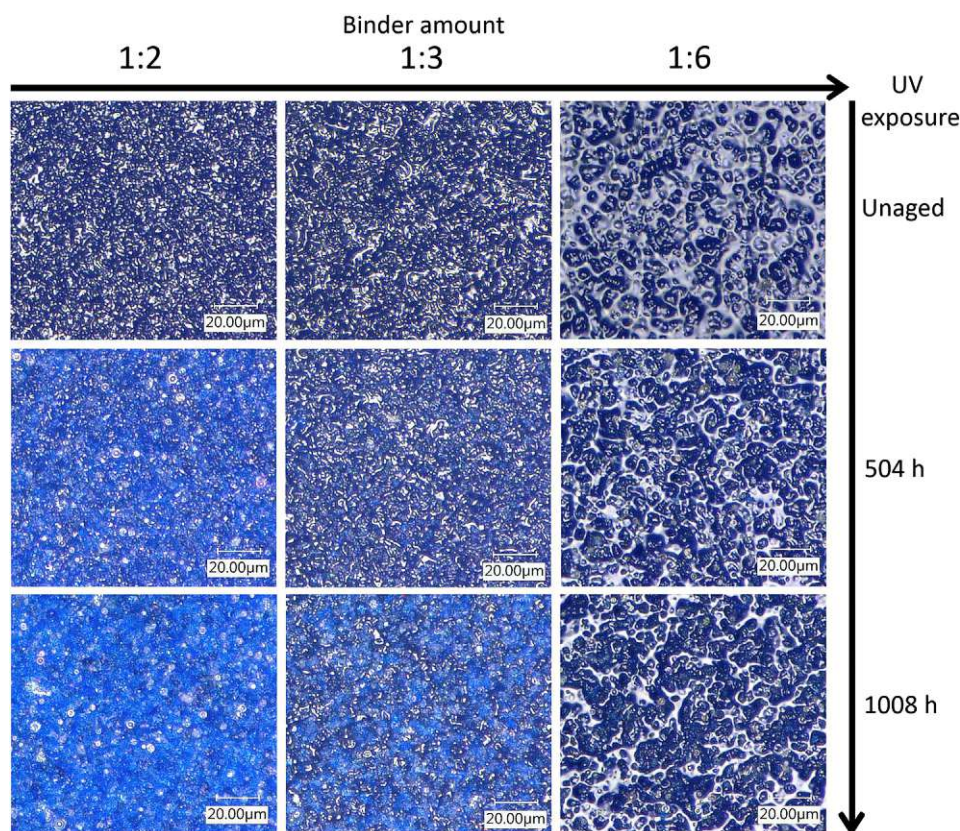
FIGURE 2 | Morphological overview by 3D image (1,000×) of PB29 alkyd samples. From left to right, the samples are displayed according to their different P/BM ratios, whereas the images from top to bottom depict the unaged, 504, and 1,008 h aging.

undergoes higher degradation effects. Similar results are presented in the discussion of the colorimetric measurements (*Colorimetric Measurements*). It has to be noticed that each pigment has a peculiar degradation pattern, and it is difficult to find trends common to all the three pigment types. Besides, it is also possible to observe that there are differences based on the P/BM ratio for each pigment type. Therefore, for a better evaluation of color and texture variations of each pigment due to aging, separate PCA models were calculated for each pigment type.

Principal Component Analysis of PB29 Samples

The PCA model of the samples prepared with PB29 pigment was calculated considering 3 PCs (93.57% of the total variance). The corresponding PC1 and PC2 score and loading plots are reported in **Figures 3A,B**, respectively. The PC1 and PC2 score plot shows that the sample prepared with a P/BM ratio equal to 1:6 presents a lower variation over time due to aging compared to the samples with higher pigment concentrations. In particular, the images of the sample prepared with a P/BM ratio equal to 1:2 have a higher variation in the PC1 and PC2 score plot based on aging time, suggesting that this sample undergoes higher degradation effects. Considering the PC1 and PC2 loading plot, it is possible to observe that the images of the

samples with P/BM ratio equal to 1:6 are characterized by low *Hom* and *En* values, while they have high standard deviation values of R, G, S, and L color parameters. These findings are confirmed by observing the microscopic images of PB29 alkyd samples (**Figure 2**), which show that the surface layer of PB29 sample prepared with a P/BM ratio of 1:6 is very heterogeneous due to the high concentration of the binder. Furthermore, PC1 describes the aging pattern common to the samples with P/BM ratio equal to 1:2 and 1:3. For these two concentrations, the images of the unaged samples have negative PC1 values, while increasing the aging time, the images of the samples move toward positive PC1 values. Considering the PC1 loading vector, the image features with positive PC1 values are mean and median values of G, B, S, and L, and homogeneity texture feature. Therefore, with light aging, the PB29 paints with lower binder concentration tend to lighten, and the paint layer seems more homogeneous as the presence of the binder is less evident.

Principal Component Analysis of PG18 Samples

The PCA model of the samples with PG18 was calculated considering 2 PCs (91.80% of the total variance), and **Figures 3C,D** report the corresponding PC1 and PC2 score and loading plots. In this case as well, the sample with a P/BM equal to 1:6 ratio differs from the samples with higher pigment concentration.
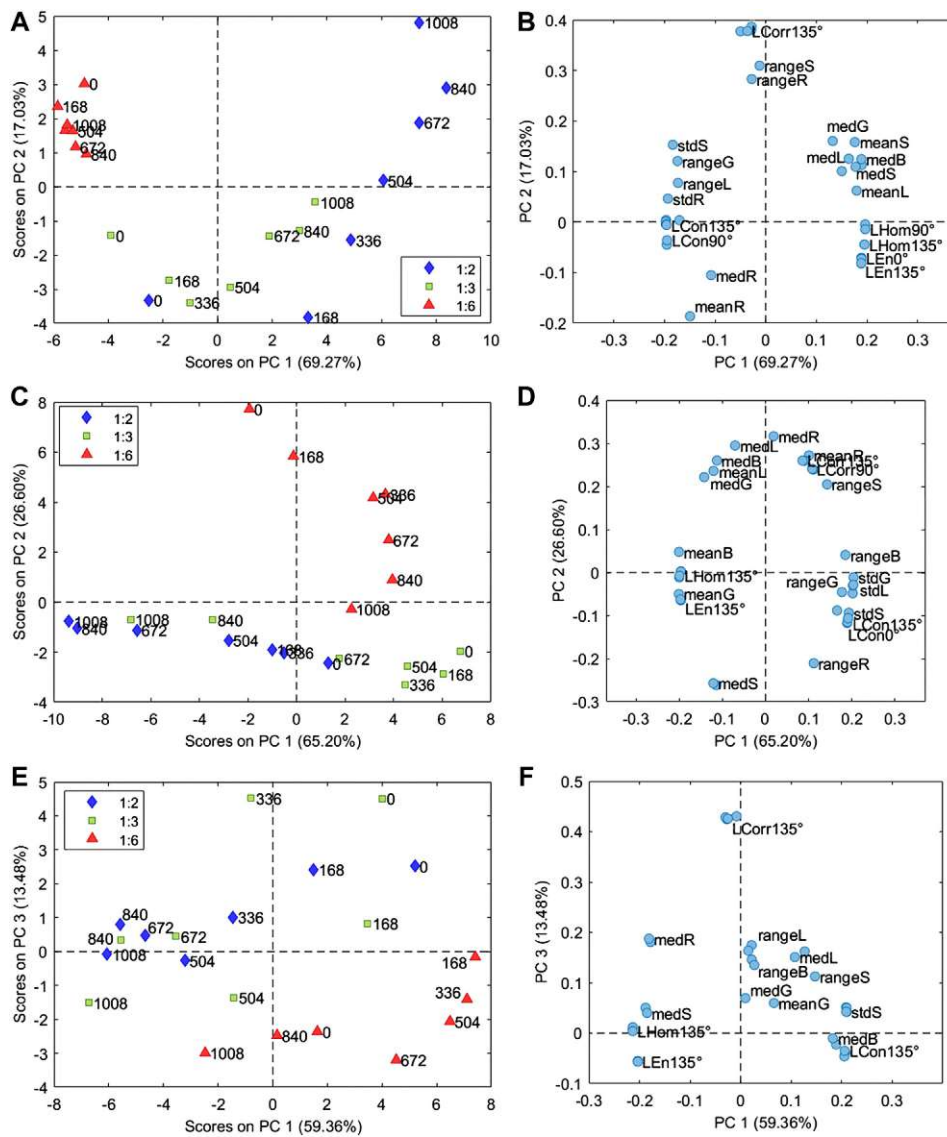
FIGURE 3 | Score and loading plots of the PCA models calculated on the image features matrix (**Supplementary Table S1**) obtained from the microscopic images of samples of alkyd resin mixed with PB29 **(A,B)**, PG18 **(C,D)**, and PY37 **(E,F)**. The samples in the score plot are colored according to the P/BM ratio, while the labels indicate the aging time from 0 to 1,008 h.

Indeed, the variation over time of the 1:6 P/BM ratio sample is mainly described by PC2, while the variation over time of 1:2 and 1:3 P/BM ratio samples is described by PC1. These aging patterns are orthogonal, suggesting that light aging has different effects on the paint layers according to binder concentration. Considering PC1 loadings, it is possible to observe that the images of aged samples with a P/BM ratio of 1:2 and 1:3 exhibit increasing mean and median values of G, B, L, and S parameters while the range and standard deviation of the same color-related parameters tend to decrease. Considering the texture-related parameters, the images of the aged samples have higher *Hom* and *En* values and lower *Con* values. Therefore, during aging, the paint layer of the samples prepared with a lower binder concentration tends to have a more saturated color, and the presence of the binder

becomes less visible. As previously mentioned, the aging behavior of the sample with 1:6 P/BM ratio are mainly described by PC2. Comparing PC2 scores and loadings, it is possible to observe that the images of aged samples show increasing range and standard deviation values of R, G, L, and S parameters and also increasing *Con* values. The mean and median values of R, B, and L tend to decrease.

Principal Component Analysis of PY37 Samples

The PCA model of the samples with PY37 was calculated considering 4 PCs (94.74% of the total variance), and the corresponding PC1 and PC3 score and loading plots are reported in **Figures 3E,F**, respectively. PC1 and PC3 score plot shows that samples prepared with the different P/BM

ratios have a similar variation pattern during aging, conversely to what was observed for the paint layers of PB29 and PG18. Indeed, for PY37, the aged samples tend to move toward negative PC1 score values compared to the corresponding unaged samples. Considering PC1 loadings, it is possible to observe that the images of the aged sample have higher *Hom* and *En* values, higher mean and median values of R and S parameters, and lower mean and median values of L. Therefore, PY37 paint layers tend to darken with aging but, at the same time, they present a more saturated color. This behavior is common for all the considered pigment concentrations. Furthermore, PC3 mainly describes the difference between samples with a 1:6 P/BM ratio and samples with the other two pigment concentrations.

Colorimetric Measurements

In **Supplementary Table S2**, the colorimetric results of unaged and 1,008 h UV-aged alkyd paint samples are shown. The results include the colorimetric changes in the values of the lightness/darkness (L*), red/green (a*), yellow/blue (b*), and the total color change from 0 to 1,008 h exposure (ΔE*). The ΔE* values obtained from each colored paint and P/BM ratio were evaluated and compared. It can be observed in **Figure 4** that the most significant color change is recorded for the PB29 paint with P/BM ratio 1:2. This behavior tends to decrease with the increase of the binder amount. A similar trend is detected for PG18 paints but less significant than for the blue paint. Moreover, a relatively significant difference in the shift of the L*, a*, and b* coordinates between the unaged and aged paint samples is observed, confirming the important role that pigments play on the degradation of this binder when exposed to the light. These findings confirm the results obtained from PCA performed on the color and texture features extracted from the microscopic images

(*Principal Component Analysis of Features Extracted From Microscopic Images*).

Comparing all the colorimetric values of the three inorganic pigments, the PB29 alkyd paint samples have the most significant shift of a* and b* between unaged and aged samples, showing a strong reduction in red and blue, respectively. The decreasing of a* and b* values and the overall increase of the L* parameter might be due to changes in the surface roughness of the paints (Simonot and Elias, 2003). In fact, after aging, the macroscopic properties of the film change, becoming stiffer and more brittle, probably due to the cross-linking of the residual olefinic unsaturation (Hintze-Brüning, 1993). This phenomenon was also previously confirmed by 3D, SEM microscope, and multivariate results. As reported in the literature (Del Federico et al., 2006; Janssens et al., 2016; René de la Rie et al., 2017), artificial ultramarine blue (PB29) has a significant loss of its blue color when mixed with alkyd resin after light irradiation. This effect is probably due to the chromophoric S-anions release after the opening of the sodalite cages of pigment, leading to the discoloration of the pigment itself. However, in the evaluation of the colorimetric variation percentage of the L* value, the PG18 paint also shows relevant results. In fact, the L*, a*, and b* values of the 1:2 and 1:3 mixtures tend to decrease, indicating a less bright paint layer and a color change toward blue. These results are confirmed by the multivariate analysis of the features extracted from microscopic images, indicating higher saturation values with increasing exposure and increasing pigment amount. This trend is not observable for the 1:6 mixture, as the L* and a* values tend to increase. This behavior could be due to the higher organic component in the paint and its interaction with this particular inorganic pigment. Further studies will be necessary in order to understand these
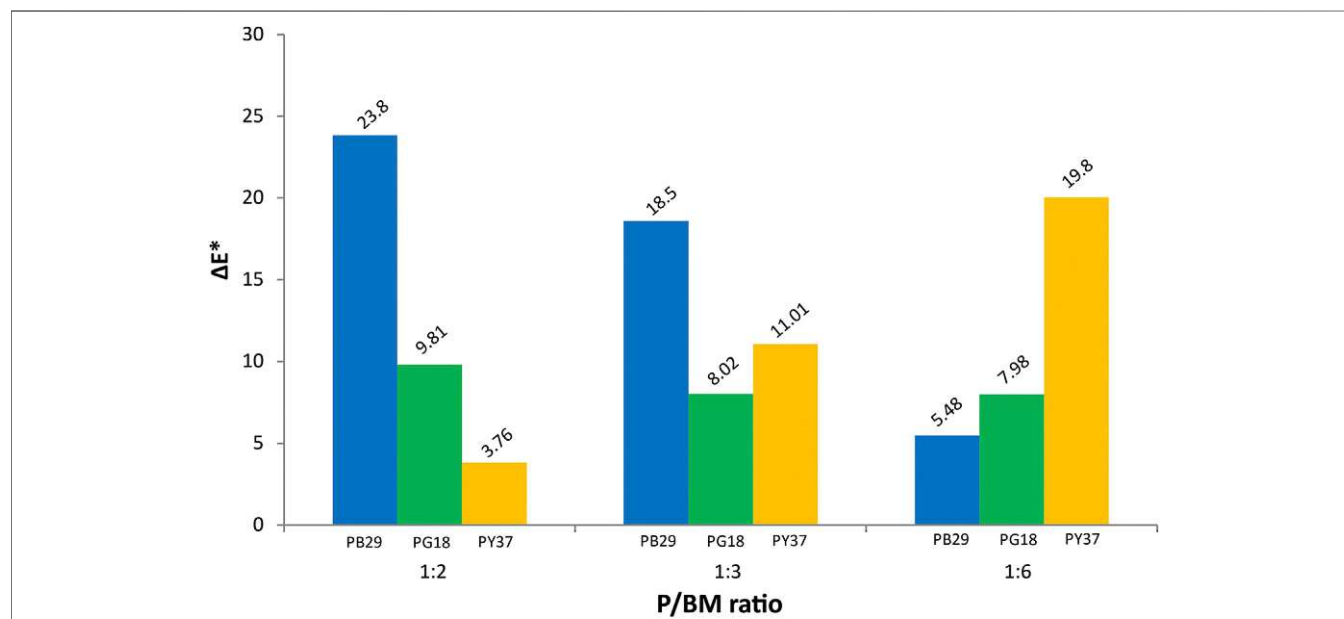
FIGURE 4 | Photodegradation kinetics evaluated by ΔE* changes of alkyd paints over UV exposure.
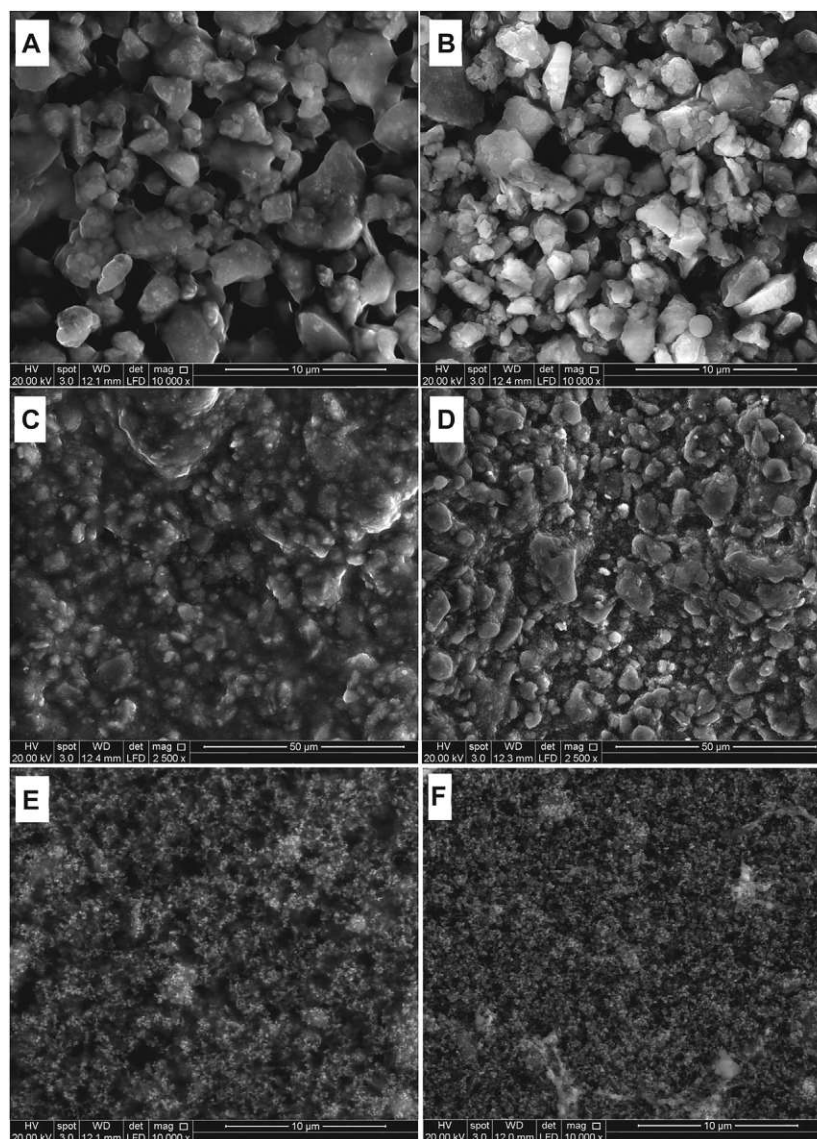
FIGURE 5 | SEM images of alkyd resin mixed with PB29 **(A,B)**, PG18 **(C,D)**, and PY37 **(E,F)**, before aging **(left)** and after 1,008 h aging **(right)**.

effects. As observed in **Figure 4**, the trend of ΔE* for PY37 paints, according to the different P/BM ratio, is different from the two previous paints. Generally, the L* and a* values do not show significant changes, whereas b* shows the greatest change, especially for the 1:6 mixture. As demonstrated by the ATR-FTIR analysis and the chemometric evaluation, PY37 appears to be the pigment that least affects the degradation of the binder. Therefore this different behavior may be due to the colorimetric change of the organic component, more easily detectable in the PY37 paint than the previous two pigments. Further studies will be needed to better understand these effects. Cadmium yellow (PY37) and hydrated chromium oxide green (PG18) are generally considered as lightfast pigments, therefore the origins of their different color changes are not completely clear (Sward, 1972). During aging, some chemical properties of the paints are

deteriorated as the paint film is gradually attacked by oxidizing agents, leading to the breakdown of the polymer molecules into smaller fragments. This phenomenon increases if the pigment concentration is high. During light exposure, the pigment particles placed on the surface will be more subject to photodegradation, leading to the fading or darkening of the color (Turner, 1979). In some cases, the loss of chemical-mechanical properties of the binder mixed with pigment (as for PB29) leads to the highest fragility of the paint on the surface, which becomes almost powdery (chalking).

Scanning Electron Microscopy Results

With SEM analyses it was possible to evaluate the morphological surface changes after artificial light aging considering the different granulometry of the pigments and their amount in

the paint mixtures. Observations of the unaged samples (P/BM 1: 2) showed the different morphological features of the pigments. The particle size range of PB29 is around 1–3 μm in diameter, and their shape and average distribution appear irregular and inhomogeneous (**Figure 5A**). A similar observation is shown for PG18, where, however, the grains have a size range from few nm to 1–2 μm (**Figure 5C**). Finally, PY37 is the pigment with the smallest particle size (few nm) and its grains appear to be distributed in agglomerates, making the surface more homogeneous than the other two pigments (**Figure 5E**).

The particle size distribution and R.I. play an important role in the light beam-material interaction and, therefore, on the degradation of the paints. If a paint film contains a pigment with a high R.I., a high fraction of the incident light tends to be bent or refracted at the surface and therefore less likely to interact with and deteriorate the paint materials (Gueli et al., 2016). Observing the R.I. values of the analyzed pigments (Feller, 1986; Roy, 1993; Vahur et al., 2010), PY37 has the highest R.I. (approx. between 2.35 and 2.48), followed by PG18 (1.62–2.12) and by PB29 (1.5). Therefore, light radiation will have a higher impact on the blue paints, followed by green and yellow paint samples. Moreover, the light scattering imparted by diffraction is further affected by the particle size. The smaller the particle size and the higher R.I. are, the more the light beam has a tendency to be scattered (Baker and Lavelle, 1984; Yousif and Haddad, 2013). As previously reported, the granulometric evaluation of the inorganic pigments carried out by SEM measurements confirmed these considerations (Holland and Gagne, 1970; Kremer Pigmente).

However, it is also necessary to consider the influence of the R.I. of the binding medium, the dispersion level of the pigment (i.e., the degree of aggregation of the pigment particles), the proportion of pigment in the vehicle, called pigment volume concentration (PVC), and the thickness of the paint layer (Merwin, 1917). Furthermore, the R.I. is not a constant value, but changes over time according to other factors including the P/BM ratio and the type of pigment employed. In this study, the granulometry of the pigments played a major role in the binder's degradation. In the unaged samples, the alkyd resin is homogeneously dispersed in the film. After aging (**Figures 5B,D,F**), the chemical transformations cause variations in the surface morphology: the binder is no longer visible and the pigment particles are better defined. This behavior is most evident in PB29 and PG18 samples after 504 h of aging. In PY37 paints, the morphology does not change significantly after exposure to aging.

Attenuated Total Reflection Fourier Transform Infrared Spectroscopy Results

For the determination of the photodegradation effects on alkyd paints, the main ATR-FTIR absorption bands of the binder and inorganic pigments were identified according to **Supplementary Table S3** (Vahur et al., 2009; Coccato et al., 2016). Their characterization was based on the analysis of the unaged samples (P/BM 1:2 mixtures presented as reference example), shown in **Figure 6Aa** (for PB29), **Figure 6Ba** (for PG18), and

Figure 6Ca (for PY37). The unaged spectra of the other mixtures (P/BM 1:3 and 1:6) are not depicted as they show the same absorbance bands but with different intensities, proportional to the binder content. Concerning the alkyd resin, significant contributions of the oil and phthalic components are identified in the polymer. The main absorption bands that identify these two components are related to the C=O stretching vibration at 1,724 cm^{-1}, and the CH$_2$ and CH$_3$ stretching and bending (asymmetric and symmetric) at 2,926, 2,854, 1,465, 1,451, and 1,388 cm^{-1}. Additional phthalic bands can be identified mainly by absorption signals corresponding to C=C stretching aromatic ring at 1,600 and 1,588 cm^{-1}, the C-O-C symmetric stretching at 1,260 and 1,114 cm^{-1}, and the aromatic out-of-plane bending at 741 and 709 cm^{-1} (Ellis et al., 1900; Hayes et al., 2014). By comparing the results of the unaged and 1,008 h light aged samples, significant chemical changes on the surface are detected. The results are evaluated according to the type of pigment used, the P/BM ratios, and the contribution of the inorganic components to the degradation process.

Among the PB29 samples aged for 1,008 h, the intensity of the OH stretching band at 3,244 cm^{-1} is the highest in the sample with a high amount of binder (**Figure 6Ad**). Moreover, the (C-H) CH$_2$ asymmetric and symmetric stretching at 2,926 and 2,854 cm^{-1} disappears. These effects are due to hydrogen abstraction and oxidation of double bonds, respectively (Perrin et al., 2000). A decreasing trend with aging is observed for the carbonyl band at 1,724 cm^{-1}. This band can still be detected after 1,008 h of exposure only in the paint sample with a high amount of binder (P/BM 1:6). Furthermore, in the same sample, the carbonyl band gets broader due to the aging of the oil component in the alkyd binder, which is caused by hydroperoxides and peroxides reactions taking place during photochemical degradation and resulting in oxidation products such as aldehydes, ketones, and carboxylic acids (at 1,735, 1,720, and 1,710 cm^{-1}) (Socrates, 2001). The bands at 1,068 and 984 cm^{-1}, related to the Al,Si-O$_4$ asymmetric stretching, increase with aging time and the pigment amount in the paint mixture (Bruni et al., 1999). As shown in **Figure 6Ab**, additional pigment bands at 691 and 656 cm^{-1}, related to the Al,Si-O$_4$ symmetric stretching, are detected. After the maximum exposure time (1,008 h), the intensity of the small band at 470 cm^{-1} has increased. The signal is identified as the O-Si-O bending vibration (Taylor, 1990). The apparent increase in the characteristic PB29 absorption bands is mainly due to the volatilization of the binder on the superficial level of the paint (Mecklenburg et al., 2013; Keune et al., 2016). This chemical-physical phenomenon is very prominent in the alkyd paints due to the oil component, which is very reactive toward the oxidative elements present in the surrounding environment (such as oxygen, sunlight, and O$_3$), leading to Norrish photo-cleavage reactions and formation of free-radicals, able to make the polymeric films unstable (Berg et al., 1999).

In **Figure 6B**, the ATR-FTIR spectra of alkyd binder in mixture with PG18 in different P/BM ratios (1:2, 1:3, and 1:6) aged for 1,008 h are shown in comparison to the unaged P/BM 1:2 mixture. Overall, all the main absorption bands of the alkyd binder are present (**Supplementary Table S3**), however, after
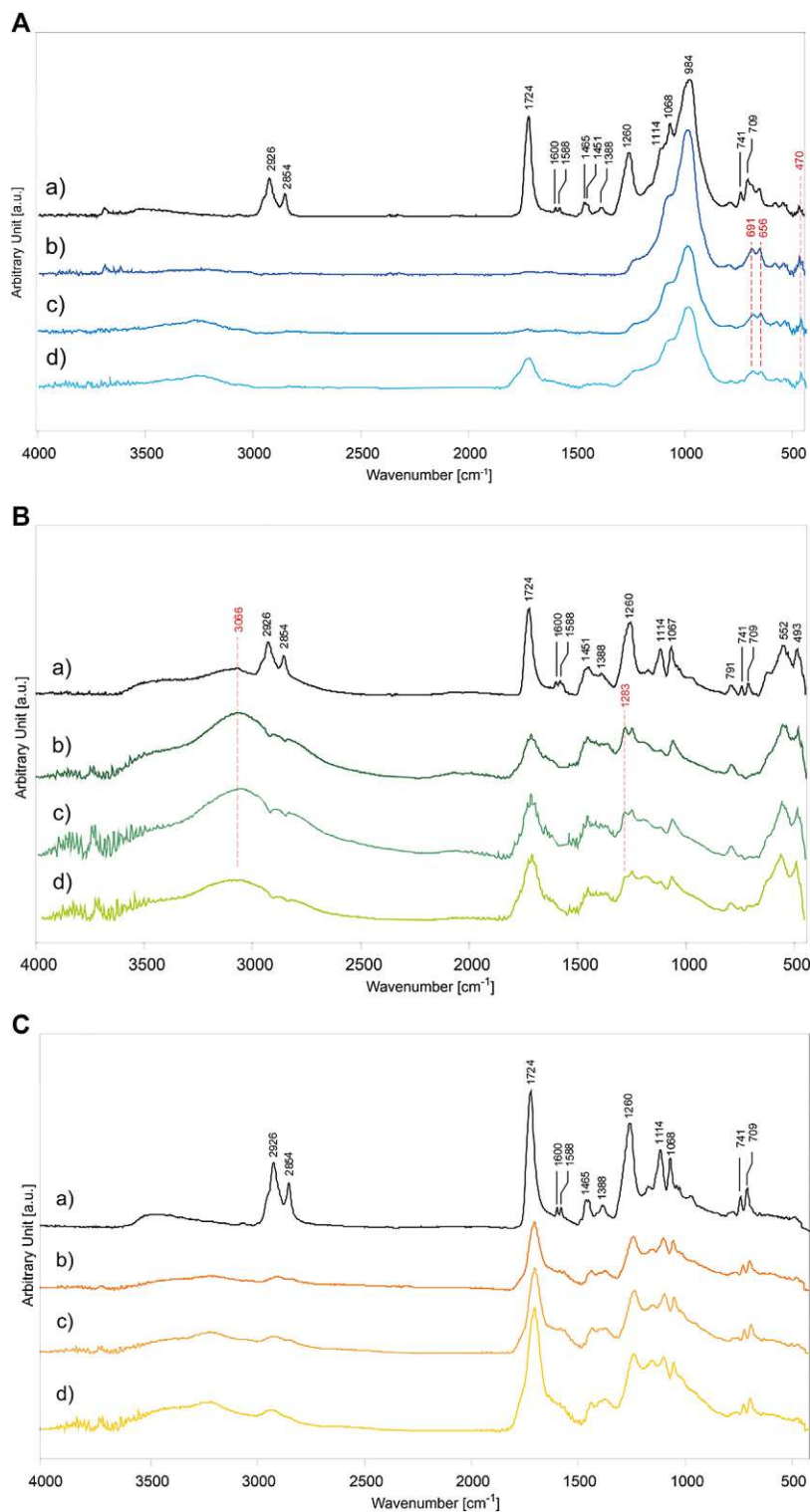
FIGURE 6 | ATR-FTIR spectra of alkyd binder in mixture with inorganic pigments: **(A)** PB29, **(B)** PG18, and **(C)** PY37. The graphs of paint mixtures are, **(a)** unaged P/BM 1:2, and after 1,008 h of UV exposure according to different P/BM ratio: **(b)** 1:2, **(c)** 1:3, and **(d)** 1:6.
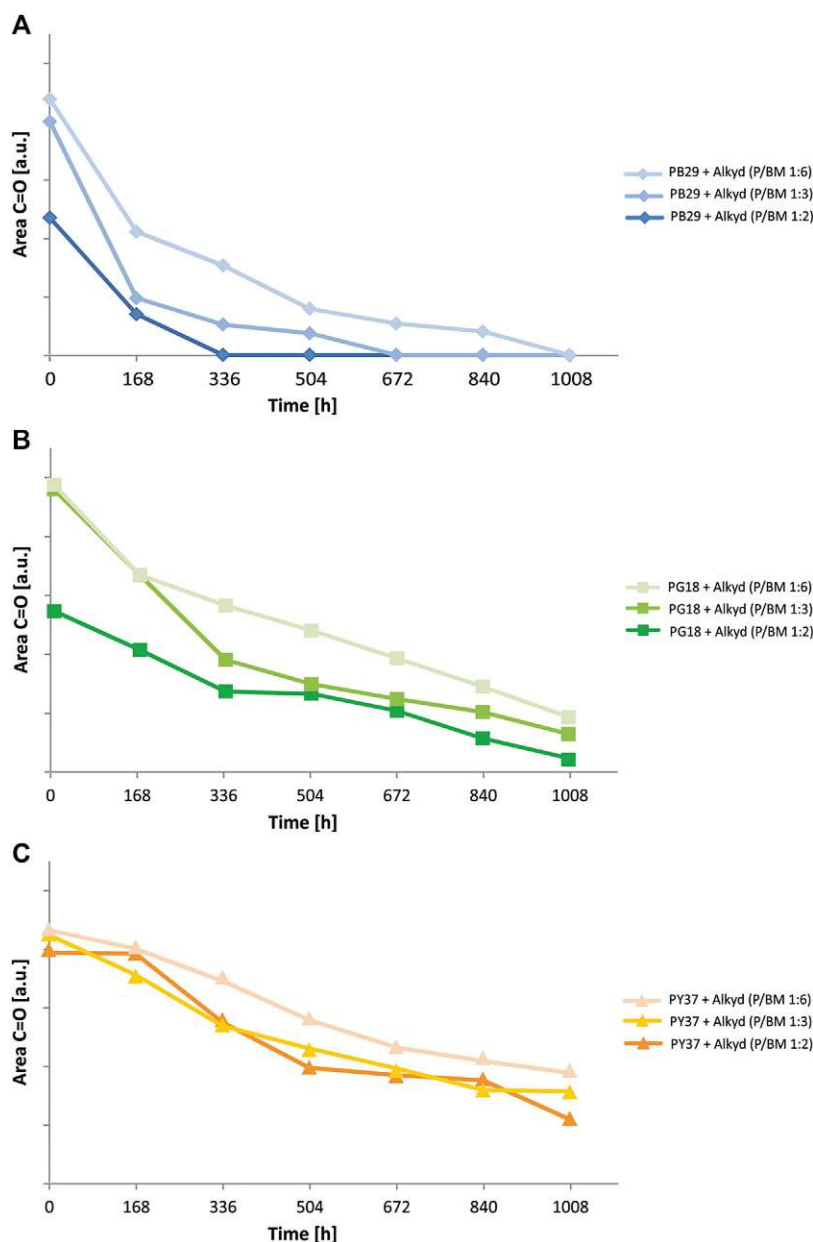
FIGURE 7 | Photodegradation kinetics observed from ATR-FTIR spectra of alkyd paints with **(A)** PB29, **(B)** PG18, and **(C)** PY37, at various P/BM ratios.

light aging, the spectra show a decreasing trend in the intensity of the binder absorption bands, less evident than paints with PB29. In fact, even if the (C-H)CH_2 stretching bands at 2,926 and 2,854 cm^{-1} tend to disappear, the intensity of the C=O band at 1,724 cm^{-1} decreases, the band widens but does not disappear, as seen previously for PB29 mixtures with P/BM 1:2 and 1:3. The decreasing and widening trend of the C=O band may be due to the β-scission and possibly Norrish I reactions of the ester groups in the polyester and oil fractions, leading to the formation of low molecular weight compounds which subsequently volatilize. The formation of the shoulder at about 1,640 cm^{-1} is due to the

formation of C=C functional groups resulting from the photodegradation reaction Norrish type II and bond cleavage of the carbonyl compounds subjected to photolysis (Mallégol et al., 2000b; Cakić et al., 2012). Among the PG18 paint samples, the most intense degradation effect is observed in the mixtures with a high amount of pigment (**Figure 6Bb**). Similarly to the PB29 results, the intensities of the PG18 bands at 552 and 493 cm^{-1} (of the oxide part) increase over time due to the degradation and partial evaporation of the binder degradative by-products. Comparing the spectrum of the unaged sample with the aged ones, the intensity of the OH stretching band at

$3,066\ \text{cm}^{-1}$ increases with the pigment concentration, as opposed to the results obtained in the PB29 mixtures. This is because the same absorption band is also ascribable to the hydrated component of the pigment which, as previously described, increases with aging time. Another absorbance band ascribable to the pigment is registered at $1,283\ \text{cm}^{-1}$. In combination with the band at $1,252\ \text{cm}^{-1}$, its presence can be ascribed to a minor content of chromium borate, a compound used during industrial manufacture of hydrated chromium oxide green pigments (Fitzhugh, 1997; Zambuehl et al., 2009).

In the case of PY37 alkyd paints, the ATR-FTIR spectra present some frequent spectral changes compared with the results obtained for PB29 and PG18 mixtures. The OH stretching band at $3,230\ \text{cm}^{-1}$ tends to increase with aging time, similarly to the PB29 samples, and binder concentration. However, observing the spectrum in **Figure 6Cd** (P/BM 1:6), it is noted that the carbonyl group signal at $1,724\ \text{cm}^{-1}$ decreases, as observed in PG18 mixtures. Furthermore, this band tends to widen in PY37 samples to a higher extent than in the other two (in PB29 mixture even disappears), suggesting that the PY37 tends to limit the UV radiation-paint layer interaction and therefore the degradation of the binder.

Photodegradation Kinetics

To better understand the influence that each inorganic pigment has on the degradation of the alkyd binder, the kinetic behavior of a specific IR-band of the binder was evaluated. It was studied by integrating the carbonyl group C=O band (at $1,724\ \text{cm}^{-1}$, integration range from $1,800$ to $1,640\ \text{cm}^{-1}$) over time. This specific band was selected for several reasons: 1) it shows strong intensity; 2) it is not overlapping with other bands, and 3) it is the most representative band of the binder. In **Figure 7**, the degradation behavior of the different paint mixtures (P/BM 1:2, 1:3, and 1:6) are presented. Generally, the binder's degradation, shown by a decrease of the C=O area values, is observed after 168 h of aging for all three pigment mixtures at P/BM ratios 1:2. In contrast, for those with P/BM ratios 1:6, binder's degradation can be observed approximately after 336 h. However, the kinetic trend changes according to the type of pigment in the mixture. With PB29, the organic binder's degradation is higher than with PG18 and much higher than with PY37. The pigment's contribution to the binder's degradation is important as it can enhance (with PB29 and PG18) or limit (with PY37) the detrimental effects of light irradiation on the degradation process of the binder. At P/BM 1:2, the intensity decrease of the binder's band at $1,724\ \text{cm}^{-1}$ is much faster in the blue paint than in the yellow. On the other hand, by increasing the binder amount (P/BM 1:6), its degradation is reduced in all paint mixtures. For a complete kinetic evaluation, the integration of the characteristic bands of inorganic pigments could have potentially confirmed the presented trend. However, this additional evaluation was difficult to carry out as the spectral signal of PY37 cannot be detected in the Mid-IR range due to the detector cut-off. In further studies, the use of other techniques (such as gravimetric analysis) may support the evaluation of the pigments contribution to the different kinetic degradation trends of alkyd paints.

For a more detailed evaluation of the binder degradation rate, according to the pigment and the P/BM ratio used, the different numerical values obtained by integrating the C=O carbonyl band were compared (**Supplementary Table S4**). The area values of each sample for every week (168 h) of aging were determined (Wiesinger et al., 2018). Subsequently, they were obtained by calculating the difference between the area value of the unaged sample and after 1,008 h of exposure, expressed as $\Delta(\text{C=O}_{\text{unaged/aged}})$. The evaluation showed that there is a direct correlation between light exposure time and degradation. In fact, with high values of $\Delta(\text{C=O}_{\text{unaged/aged}})$, the process of photo-oxidation on the surface is more damaging, with the consequent decrease of the C=O band over time. Moreover, the P/BM ratio also plays a role in the degradation effect. In fact, by observing the $\Delta(\text{C=O}_{\text{unaged/aged}})$ values, it is possible to notice that in the samples with a high amount of binder (P/BM 1:6) the photo-oxidative process is reduced. In contrast, in the samples with a high amount of pigment (P/BM 1:2), these values increase, suggesting a more oxidative effect. This trend also changes according to the pigments used. Comparing the three different paints, this difference is more significant in PB29 paints than in PY37. With the increase of the amount of pigment (1:2), these values tend to decrease for mixtures with PB29 and PG18, while for PY37 the trend is similar to those of mixtures with higher concentration of binder. This numerical difference indicates that with the same amount of pigment, the PB29 further facilitates the interaction of light irradiation with the surface of the paint, causing a more rapid decomposition of the alkyd binder.

CONCLUSION

The chemical surface changes on alkyd paints mixed with inorganic pigments and exposed to short-time artificial light aging were documented by optical 3D microscopy and studied by ATR-FTIR, SEM, and colorimetric analysis. To monitor the degradation behavior of each paint sample, three P/BM ratios were selected: 1:2, 1:3, and 1:6. The paint samples were exposed for 1,008 h in total under conditions comparable to outdoor solar conditions. The main degradation reactions that occur in alkyd paints during light aging are:

- Chemical degradation of the alkyd binder is observed after 168 h, shown by an intensity decrease of the functional groups' IR bands (**Supplementary Table S3**) of the alkyd resin over time. This trend is most evident in the mixtures with the blue pigment PB29, followed by PG18, whereas in those with the yellow pigment PY37, the binder is more stable.
- As a consequence of the binder's decomposition, the pigments' IR absorbance bands show an increase during light exposure in all paint samples.
- The kinetic evaluation of $\Delta E^{\star}$ shows that the PB29 alkyd mixture (P/BM 1:2) undergoes the highest color change, followed by PY37 and PG18.
- Morphological changes of the paint surfaces are visible by 3D microscopy and SEM. Upon aging, the samples' surfaces appear more rigid and opaque, as well as less bright and stiffer in paints

with P/BM 1:2. Generally, when the pigment content is low, the degradation behavior is reduced due to light irradiation.

- Finally, PCA was applied to study the microscopic images of the paint samples, considering the color and texture changes after aging. This application was useful for studying degradation effects, focusing on the objective information related to the modifications induced by artificial UV aging based on the impact of pigments and P/BM ratio. This approach can be further implemented for quantitative evaluation of aging time for diagnostic purposes.

In conclusion, the paint samples exposed to artificial light aging show degradation processes that vary according to the binder, the inorganic pigment, and the P/BM ratio employed. The presence of pigments can enhance several photo-oxidative effects on the binder; indeed, PB29 causes higher degradation than PY37 and PG18. Additionally, degradation of the binder increases with pigment concentration. With this study, it has been demonstrated that the use of non-invasive analytical techniques, kinetic evaluation of their results, and the combination of analytical data with chemometric methods have high potential in the identification of paint components of complex artworks and in obtaining in-depth chemical information to be complemented with historical-artistic knowledge (Rosi et al., 2020).

DATA AVAILABILITY STATEMENT

The original contributions presented in the study are included in the article/**Supplementary Material**, further inquiries can be directed to the corresponding author.

REFERENCES

Anghelone, M., Jembrih-Simbürger, D., Pintus, V., and Schreiner, M. (2017). Photostability and influence of phthalocyanine pigments on the photodegradation of acrylic paints under accelerated solar radiation. *Polym. Degrad. Stabil.* 146, 13–23. doi:10.1016/j.polymdegradstab.2017.09.013

Anghelone, M., Jembrih-Simbürger, D., and Schreiner, M. (2016). Influence of phthalocyanine pigments on the photo-degradation of alkyd artists' paints under different conditions of artificial solar radiation. *Polym. Degrad. Stabil.* 134, 157–168. doi:10.1016/j.polymdegradstab.2016.10.007

Baker, E. T., and Lavelle, J. W. (1984). The effect of particle size on the light attenuation coefficient of natural suspensions. *J. Geophys. Res.* 89, 8197–8203. doi:10.1029/jc089ic05p08197

Berg, J. D. J., Berg, K-J., and Boon, J. J. (1999). "Chemical changes in curing and ageing oil paints," in 12th triennial meeting Lyon, Lyon, France, August 29–September 3, 1999 (ICOM-CC ICOM Committee for Conservation), Vol. 1, 248–253.

Bevilacqua, N., Borgioli, L., and Adrover Gracia, I. (2010). *I pigmenti nell´arte dalla preistoria alla rivoluzione industriale.* Villatora, Italy: Il prato.

Bruni, S., Cariati, F., Casadio, F., and Toniolo, L. (1999). Spectrochemical characterization by micro-FTIR spectroscopy of blue pigments in different polychrome works of art. *Vib. Spectrosc.* 20, 15–25. doi:10.1016/s0924-2031(98)00096-4

Cakić, S. M., Ristić, I. S., Vladislav, J. M., Stamenković, J. V., and Stojiljković, D. T. (2012). IR-change and colour changes of long-oil air drying alkyd paints as a result of UV irradiation. *Prog. Org. Coat.* 73, 401–408. doi:10.1016/j.porgcoat.2010.12.002

Calvini, R., Foca, G., and Ulrici, A. (2016). Data dimensionality reduction and data fusion for fast characterization of green coffee samples using hyperspectral sensors. *Anal. Bioanal. Chem.* 408 (26), 7351–7366. doi:10.1007/s00216-016-9713-7

AUTHOR CONTRIBUTIONS

ACKNOWLEDGMENTS

SUPPLEMENTARY MATERIAL

The Supplementary Material for this article can be found online at: https://www.frontiersin.org/articles/10.3389/fmats.2020.600887/full#supplementary-material.

Calvini, R., Orlandi, G., Foca, G., and Ulrici, A. (2020). Colourgrams GUI: a graphical user-friendly interface for the analysis of large datasets of RGB images. *Chemometr. Intell. Lab. Syst.* 196, 103915. doi:10.1016/j.chemolab.2019.103915

Chiantore, O., and Rava, A. (2005). *Conserving contemporary art: issues, methods, materials, and research.* Los Angeles, CA: Getty Conservation Institute.

Coccato, A., Bersani, D., Coudray, A., Sanyova, J., Moens, L., and Vandenabeele, P. (2016). Raman spectroscopy of green minerals and reaction products with an application in Cultural Heritage research. *J. Raman Spectrosc.* 47, 1429–1443. doi:10.1002/jrs.4956

Del Federico, E., Shöfberger, W., Schelvis, J., Kapetanaki, S., Tyne, L., and Jerschow, A. (2006). Insight into framework destruction in ultramarine pigments. *Inorg. Chem.* 45, 1270–1276. doi:10.1021/ic050903z

Duce, C., Della Porta, V., Tiné, M. R., Spepi, A., Ghezzi, L., Colombini, M. P., et al. (2014). FTIR study of ageing of fast drying oil colour (FDOC) alkyd paint replicas. *Spectrochim. Acta Part A Mol. Biomol. Spectrosc.* 130, 214–221. doi:10.1016/j.saa.2014.03.123

Ellis, G., Claybourn, M., and Richards, S. E. (1900). The application of Fourier Transform Raman spectroscopy to the study of paint system. *Spectrochim. Acta Part A Mol. Biomol. Spectrosc.* 46, 227–241. doi:10.1016/0584-8539(90)80092-D

Feller, R. L. (1986). *Artists' pigments, a handbook of their history and characteristics.* Washington, DC: National Gallery of Art Washington.

Fitzhugh, E. W. (1997). *Artists' pigments, a handbook of their history and characteristics.* Washington, DC: National Gallery of Art Washington.

Fongaro, L., and Kvaal, K. (2013). Surface texture characterization of an Italian pasta by means of univariate and multivariate feature extraction from their texture images. *Food Res. Int.* 51 (2), 693–705. doi:10.1016/j.foodres.2013.01.044

Gueli, A. M., Bonfiglio, G., Pasquale, S., and Troja, S. O. (2016). Effect of particle size on pigments colour. *Color Res. Appl.* 42, 236–243. doi:10.1002/col.22062

Haralick, R. M., Shanmugam, K., and Dinstein, I. H. (1973). Textural features for image classification. *IEEE Trans. Syst., Man, Cybern.* 3 (6), 610–621. doi:10.1109/tsmc.1973.4309314

Hayes, P. A., Vahur, S., and Leito, I. (2014). ATR-FTIR spectroscopy and quantitative multivariate analysis of paints and coating materials. *Spectrochim. Acta Part A Mol. Biomol. Spectrosc.* 133, 207–213. doi:10.1016/j.saa.2014.05.058

Hintze-Brüning, H. (1993). Utilization of vegetable oils in coatings. *Ind. Crops Prod.* 1, 89–99. doi:10.1016/0926-6690(92)90005-G

Holland, A. C., and Gagne, G. (1970). The scattering of polarized light by polydisperse systems of irregular particles. *Appl. Opt.* 9, 1113–1121. doi:10.1364/ao.9.001113

Janssens, K., Van der Snickt, G., Vanmeert, F., Legrand, S., Nuyts, G., Alfeld, M., et al. (2016). Non-invasive and non-destructive examination of artistic pigments, paints, and paintings by means of X-ray methods. *Top. Curr. Chem.* 374, 81. doi:10.1007/s41061-016-0079-2

Johnston-Feller, R. (2001). *Color science in the examination of museum objects: nondestructive procedures.* Los Angeles, CA: The Getty Conservation Institute.

Keune, K., Mass, J., Mehta, A., Church, J., and Meire, F. (2016). Analytical imaging studies of the migration of degraded orpiment, realgar, and emerald green pigments in historic paintings and related conservation issues. *Herit Sci.* 4, 10. doi:10.1186/s40494-016-0078-1

Kremer Pigmente. Catalogue online. Available at: http://www.kremer-pigmente.com (January 20, 2020).

Kucheryavski, S. (2011). Extracting useful information from images. *Chemometr. Intell. Lab. Syst.* 108 (1), 2–12. doi:10.1016/j.chemolab.201va0.12.002

Lake, S., Ordonez, E., and Schilling, M. (2004). A technical investigation of paints used by Jackson Pollock in his drip or poured paintings. *Stud Conser.* 49 (2), 137–141. doi:10.1179/sic.2004.49.s2.030

Lazzari, M., and Chiantore, O. (1999). Drying and oxidative degradation of linseed oil. *Polym. Degrad. Stabil.* 65, 303–313. doi:10.1016/s0141-3910(99)00020-8

Learner, T. (2008). *Modern paints uncovered.* Los Angeles, CA: Getty Conservation Institute.

Malegori, C., Franzetti, L., Guidetti, R., Casiraghi, E., and Rossi, R. (2016). GLCM, an image analysis technique for early detection of biofilm. *J. Food Eng.* 185, 48–55. doi:10.1016/j.jfoodeng.2016.04.001

Mallégol, J., Gardette, J.-L., and Lemaire, J. (2000a). Long-term behavior of oil-based varnishes and paints. Photo- and thermooxidation of cured linseed oil. *J. Am. Oil Chem. Soc.* 77, 257–263. doi:10.1007/s11746-000-0042-4

Mallégol, J., Lemaire, J., and Gardette, J.-L. (2000b). Drier influence on the curing of linseed oil. *Prog. Org. Coating* 39, 107–113. doi:10.1016/s0300-9440(00)00126-0

Marschner, C. B., Kokla, M., Amigo, J. M., Rozanski, E. A., Wiinberg, B., and McEvoy, F. J. (2017). Texture analysis of pulmonary parenchymateous changes related to pulmonary thromboembolism in dogs–a novel approach using quantitative methods. *BMC Vet. Res.* 13 (1), 219. doi:10.1186/s12917-017-1117-1

Mecklenburg, M. F., Tumosa, C. S., and Vicenzi, E. P. (2013). "The influence of pigments and ion migration on the durability of drying oil and alkyd paints," in New insights into the cleaning of paintings: proceedings from the cleaning 2010 international conference, Universidad Politecnica de Valencia and Museum Conservation Institute (Washington, DC: Smithsonian Institution Scholarly Press), 59–67.

Merwin, H. E. (1917). Optical Properties and Theory of Color of Pigments and Paints. *Proc. Amer. Soc. Test. Mater.* XVII, 494–530.

Musumarra, G., and Fichera, M. (1998). Chemometrics and cultural heritage. *Chemometr. Intell. Lab. Syst.* 44, 363–372. doi:10.1016/s0169-7439(98)00069-0

Pagnin, L., Wiesinger, R., and Schreiner, M. (2020). *Photodegradation kinetics of alkyd paints: the influence of varying amounts of inorganic pigments on the stability of the synthetic binder.* Durham, NC: Research Square. . Available at: https://www.researchsquare.com/article/rs-13183/v1 (Accessed June 15, 2020).

Pereira, F. M. V., and Bueno, M. I. M. S. (2007). Image evaluation with chemometric strategies for quality control of paints. *Anal. Chim. Acta.* 588 (2), 184–191. doi:10.1016/j.aca.2007.02.009

Perrin, F. X., Irigoyen, M., Aragon, E., and Vernet, J. L. (2000). Artificial aging of acrylurethane and alkyd paints: a micro-ATR spectroscopic study. *Polym. Degrad. Stabil.* 70, 469–475. doi:10.1016/s0141-3910(00)00143-9

Pintus, V., Wei, S., and Schreiner, M. (2015). Accelerated UV ageing studies of acrylic, alkyd, and polyvinyl acetate paints: influence of inorganic pigments. *Microchem. J.* 124, 949–961. doi:10.1016/j.microc.2015.07.009

Rabek, J. F. (1995). *Polymer photodegradation, mechanisms and experimental methods.* New York, NY: Wiley.

Rasti, F., and Scott, G. (1980). The effects of some common pigments on the photo-oxidation of linseed oil-based paint media. *Stud. Conserv.* 25, 145–156. doi:10.1179/sic.1980.25.4.145

René de la Rie, E., Michelin, A., Ngako, M., Del Federico, E., and Del Grosso, C. (2017). Photo-catalytic degradation of binding media of ultramarine blue containing paint layers: a new perspective on the phenomenon of "ultramarine disease" in paintings. *Polym. Degrad. Stabil.* 144, 43–52. doi:10.1016/j.polymdegradstab.2017.08.002

Rosi, F., Miliani, C., Delaney, J., Dooley, K., Stringari, L., Subelyte, G., et al. (2020). "Chapter I. Jackson pollock's drip paintings: tracing the introduction of alkyds through non-invasive analysis of mid-1940s paintings," in *Science and art.* London, UK: Royal Society of Chemistry, 1–18. doi:10.1039/9781788016384-00001

Rosu, D., and Visakh, P. M. (2016). *Photochemical behaviour of multicomponent polymeric-based materials.* New York, NY: Springer.

Roy, A. (1993). *Artists' pigments, a handbook of their history and characteristics.* Washington, DC: National Gallery of Art Washington.

Simonot, L., and Elias, M. (2003). Color change due to surface state modification. *Color Res. Appl.* 28, 45–49. doi:10.1002/col.10113

Socrates, G. (2001). *Infrared and Raman characteristic group frequencies.* New York, NY: Wiley.

Šúri, M., Huld, T. A., and Dunlop, E. D. (2004). PV-GIS: a web based solar radiation database for the calculation of PV potential in Europe. *Int. J. Sustain. Energy* 24, 55–67. doi:1080/14786450512331329556

Šúri, M., Huld, T. A., Dunlop, E. D., and Ossenbrink, H. A. (2007). Potential of solar electricity generation in the European Union member states and candidate countries. *Sol. Energy.* 81, 1295–1305. doi:10.1016/j.solener.2006.12.007

Sward, G. G. (1972). *Paint testing manual: physical and chemical examination of paints, varnishes, lacquers and colors.* West Conshohocken, PA: ASTM International.

Taylor, W. R. (1990). Application of infrared spectroscopy to studies of silicate glass structure: examples from the melilite glasses and the systems Na_2O-SiO_2 and Na_2O-Al_2O_3-SiO_2. *J. Earth Syst. Sci.* 99, 99–117. doi:10.1007/bf02871899

Turner, G. P. A. (1979). *Introduction to paint chemistry and principle of paint technology.* New York, NY: Chapman and Hall.

Vahur, S., Knuutinen, U., and Leito, I. (2009). ATR-FT-IR spectroscopy in the region of 500-230cm−1 for identification of inorganic red pigments. *Spectrochim. Acta Part A Mol. Biomol. Spectrosc.* 73, 764–771. doi:10.1016/j.saa.2009.03.027

Vahur, S., Teearu, A., and Leito, I. (2010). ATR-FT-IR spectroscopy in the region of 550-230cm−1 for identification of inorganic pigments. *Spectrochim. Acta Part A Mol. Biomol. Spectrosc.* 75, 1061–1072. doi:10.1016/j.saa.2009.12.056

Wiesinger, R., Pagnin, L., Anghelone, M., Moretto, L. M., Orsega, E. F., and Schreiner, M. (2018). Pigment and binder concentrations in modern paint samples determined by IR and Raman spectroscopy. *Angew. Chem. Int. Ed.* 57, 7401–7407. doi:10.1002/anie.201713413

Yousif, E., and Haddad, R. (2013). Photodegradation and photostabilization of polymers, especially polystyrene: review. *SpringerPlus.* 2, 398. doi:10.1186/2193-1801-2-398

Zambuehl, S., Scherrer, N. C., Berger, A., and Eggenberger, U. (2009). Early Viridian pigment composition characterization of a (hydrated) chromium oxide borate pigment. *Stud. Conserv.* 54, 149–159. doi:10.1179/sic.2009.54.3.149

Zubielewicz, M., Kamińska-Tarnawska, E., Ślusarczyk, A., and Langer, E. (2011). Prediction of heat build-up of solar reflecting coatings based on physico-chemical properties of complex inorganic colour pigments (CICPs). *Prog. Org. Coating* 72, 65–72. doi:10.1016/j.porgcoat.2011.02.008

Conflict of Interest: The authors declare that the research was conducted in the absence of any commercial or financial relationships that could be construed as a potential conflict of interest.

Paper II

Multivariate analysis and laser-induced breakdown spectroscopy (LIBS): a new approach for the spatially resolved classification of modern art materials

Laura Pagnin, Lukas Brunnbauer, Rita Wiesinger, Andreas Limbeck, Manfred Schreiner

Multivariate analysis and laser-induced breakdown spectroscopy (LIBS): a new approach for the spatially resolved classification of modern art materials

Laura Pagnin, Lukas Brunnbauer, Rita Wiesinger, Andreas Limbeck & Manfred Schreiner

ONLINE FIRST

Springer

Springer

RESEARCH PAPER

Multivariate analysis and laser-induced breakdown spectroscopy (LIBS): a new approach for the spatially resolved classification of modern art materials

Laura Pagnin[1] · Lukas Brunnbauer[2] · Rita Wiesinger[1] · Andreas Limbeck[2] · Manfred Schreiner[1,2]

Abstract

The ever-increasing speed of exchange of ideas, information, and culture allows contemporary art to be in constant growth, especially concerning the choice of artistic materials. Their characterization is not only crucial for the study of artistic techniques but also for research into the stability of the material and, consequently, the best preservation practices. For this aim, an analytical method should have the advantages of not requiring sample preparation, performing superficial micro-analysis, and obtaining detailed spectral information. For this study, laser-induced breakdown spectroscopy (LIBS) was employed. It was used for the identification of modern paints composed of inorganic pigments and organic binders, such as acrylics, alkyds, and styrene-acrylics. Principal component analysis (PCA) was used to classify the different pure materials, above all, the polymeric binders. To distinguish the paint mixtures, whose LIBS spectral results were more complex due to the pigment/binder interaction, a statistical method recently employed in the cultural heritage field was chosen, namely, random decision forest (RDF). This methodology allows a reduction of the variance of the data, testing of different training data sets by cross-validation, an increase of the predictive power. Furthermore, for the first time, the distribution of different inorganic pigments and organic binder materials in an unknown sample was mapped and correctly classified using the developed RDF. This study represents the first approach for the classification of modern and contemporary materials using LIBS combined with two different multivariate analyses. Subsequent optimization of measurement parameters and data processing will be considered in order to extend its employment to other artistic materials and conservation treatments.

Keywords Organic binders · Inorganic pigments · Laser-induced breakdown spectroscopy · Principal component analysis · Random decision forest

Introduction

In the last 10 years, the applications of laser-induced breakdown spectroscopy (LIBS) have proved to be very promising for the analysis and characterization of many artworks [1].

✉ Laura Pagnin
l.pagnin@akbild.ac.at

[1] Institute of Natural Sciences and Technology in the Arts (INTK), Academy of Fine Arts Vienna, Schillerplatz 3, 1010 Vienna, Austria

[2] Institute of Chemical Technologies and Analytics, Vienna University of Technology, Getreidemarkt 9/164, 1060 Vienna, Austria

Understanding the chemical composition of the materials employed is fundamental for art conservators and archaeologists to obtain information on the origin, the manufacturing techniques, and the history of the objects. Therefore, the choice of proper and efficient analytical methods has become decisive to obtain the most accurate results with the purpose to support the choice of appropriate preservation and restoration concept [2]. To achieve this information, LIBS proved to be a useful alternative to other techniques. In previous studies, the possibility to discriminate different elemental composition of materials by the characteristic atomic emission signals recorded was used to evaluate the distribution of pollutants on stone surfaces [3], the importance of assessing some metal's content in alloys [4], biological samples [5], and the monitoring of cleaning level during restoration [6]. Nowadays, the materials and manifestations of contemporary art are continually growing and changing; for this reason, their identification is

essential. LIBS analysis on pigments was often carried out to help art historians to understand techniques used by the artists in ancient paintings, to provide dating information concerning the manufacturing history of the pigment, and, consequently, to assess the preservation method of a specific work of art [7, 8]. Furthermore, the possibility of evaluating the data through multivariate analysis combined with elementary surface mapping allows optimizing the analysis. Rarely, this analytical technique was considered for the evaluation of conservation methods for modern and contemporary artworks.

The main materials used are inorganic pigments, for their high chemical stability (compared with organic ones), the easy availability, and the relatively low price.

Furthermore, they are mixed with many organic binders, such as acrylics, alkyds, oils, vinyls, or other complex synthetic resins such as nitrocellulose, polyurethane, rubbers, or epoxy resins [9, 10]. In recent times, specific sectors, such as plastic industries, waste disposal, cosmetics, transports, and textiles, require extensive knowledge of these always more innovative materials. For this purpose, the employment of LIBS was revealed efficient for plastic identification [11]. Considering the good results obtained in the previously mentioned studies, the application of this technique for the characterization of contemporary art materials was carried out.

Principles and advantages of LIBS in cultural heritage

Laser-induced breakdown spectroscopy is an atomic emission spectroscopic technique, which first analytic use for elemental analysis of surfaces was published in 1962 by Brech and Cross [12]. Therefore, after its development and improvement, it was employed in a wide variety of qualitative, semi-quantitative, and quantitative analytical applications [13]. In principle, by the plasma, characteristic radiations of the excited atoms in the plume are emitted. For this reason, LIBS can detect all elements, limited only by the power of the laser and the wavelength range of the spectrograph. However, the formation of plasma depends on certain factors, such as the threshold for the optical breakdown, the environment, and the investigated material [14].

According to the fact that ablation and excitation depend heavily on the investigated material, this technique is often coupled with statistical software able to perform multivariate analysis such as cluster and principal component analysis (PCA). By combining LIBS with multivariate statistical data evaluation approaches, often better results compared with univariate evaluation are achieved [15]. This efficient analytical instrumentation led to significant improvements in the field of cultural heritage analysis, also through the numerous advantages of this technique: it allows a very short time of analysis, sample preparation is not required, and it uses a small area of

interaction of the laser pulse with the sample surface [16, 17]. Considering that LIBS is a micro-destructive technique and sampling is necessary, for the analysis of some real artworks, its employment could be limited. However, the possibility to extend the spatial resolution in the micrometer range and perform depth analysis makes it useful for the research of various materials, as polymeric multi-layer systems [18].

In recent years, LIBS imaging applications have shown increasing interest. The possibility of investigating the elementary surface distribution, using lateral resolutions in the low micrometer range, analyzing with rapid measurement times, has made LIBS a very promising technique for the application of imaging on modern art materials. In particular, in this study, imaging was applied not only to inorganic materials but also it was extended to polymeric binders both pure and in paint mixtures [19]. Therefore, the potential of LIBS, confirmed by several studies in the last few years, is continuously growing and can also be employed in the field of contemporary art conservation.

Materials and methods

Sample preparation

Different samples were prepared by mixing pure Plextol® D498 (Kremer Pigmente, Germany), Alkyd Medium 4 (Lukas®, Germany), and Acronal S790 (BASF, Germany) in combination with 9 inorganic pigments (Kremer Pigmente, Germany). A detailed description of the paint materials used can be found in Table 1. The pigment/binder (P/BM) ratio chosen is 1:3. The paint mixtures were cast on glass slides with a wet film thickness of approx. 150 μm. In total, 27 paint samples were prepared, combining each binder with each inorganic pigment.

The samples were dried at ambient conditions (approx. 22 °C and 50% relative humidity) for 1 week. Pure paint materials were also analyzed. The three pure binders were cast on a glass slide and dried as described above. For pure pigment analysis, pellets were prepared by mixing the inorganic pigment (P) with cellulose (C) powder (P/C ratio 1:1) and subsequent pressing with a pressure of approx. 10 bar for 1 min. This preparation is necessary to prevent that colored powder residues, after interaction with the laser, are dispersed in the LIBS chamber (Fig. 1). In total, 12 pure samples (3 binders and 9 pigments) were prepared.

Sample analysis using laser-induced breakdown spectroscopy

LIBS analysis was carried out using J200 Tandem LIBS instrumentation (Applied Spectra Inc., Fremont, CA)

Table 1 List of polymeric binders and inorganic pigments analyzed

Pigment name	Chemical composition	Color index (C.I.) number
Titanium white	TiO_2	PW6
Cadmium yellow	CdS	PY37
Cobalt green	Co_2TiO_4	PG50
Hydrated chromium oxide green	$Cr_2O_3 \cdot 2H_2O$	PG18
Cobalt blue	$CoO \cdot Al_2O_3$	PB28
Cerulean blue	$CoSnO_3$	PB35
Artificial ultramarine blue	$Na_{8-10}Al_6Si_6O_{29}S_{2-4}$	PB29
Iron oxide red	Fe_2O_3	PR101
Manganese violet	$NH_4MnP_2O_7$	PV16
Binder name	**Chemical composition**	**Commercial name**
Acrylic resin	p(nBA/MMA)	Plextol® D498
Alkyd resin	Polymer oil-modified polyester resin based on orthophthalic acid and pentaerythritol	Alkyd Medium 4
Styrene-acrylic emulsion	Styrene acrylate copolymer	Acronal® S790

equipped with a 266-nm frequency quadrupled Nd:YAG laser. For collection and spectroscopic analysis of the radiation emitted by the laser-induced plasma, an optical fiber system connected to a Czerny-Turner spectrometer with six-channel CCD detection was employed. For every laser shot, full spectra over the wavelength range from 185 to 1040 nm were recorded by Axiom 2.0 data acquisition software provided by the manufacturer. All samples were analyzed using 16 parallel line scans with a distance of 100 μm between each line; the length of each line scan is 2 mm; and the measurement was carried out in the center of the samples to avoid edge effects of the sample.

Using a 100-μm laser beam diameter, at a stage scan speed of 1 mm/s, and with a repetition rate of 10 Hz on each line, 320 laser shots were performed per sample. Concerning the acquisition of LIBS spectra for organic binders, they were recorded after proper optimization of the choice of the gas flow used in the measurement chamber. LIBS spectra were recorded in argon atmosphere (flow rate of 1 L min^{-1}). Argon yields the best results as it usually gives higher emission signals for especially C, H, and, O, therefore reducing the noise and improving the classification.

Fig. 1 Set of 9 pure pigment powder pellets analyzed by LIBS

Data treatment

For the statistical analysis, the spectra obtained by LIBS measurements were evaluated using Imagelab 2.97 (Epina GmbH, Austria).

Principal component analysis The use of statistical techniques is increasingly growing and, especially in the field of cultural heritage, the choice of the most representative method is essential. Considering the various case studies [20, 21], the most common technique used for the chemical analytical representation of data is the principal component analysis (PCA). It is a technique for simplifying the data used in the context of multivariate statistics by which the set of original variables is transformed into another group of variables called principal components (PC). The reduction of complexity occurs only by analyzing the most representative main data sets for their variance [22]. The number of principal components chosen for the evaluation tries to obtain the simplest and most explanatory model. In the present assessment, the multivariate analysis was performed on spectra in the range of 185 and 1040 nm. Additional data employed for the analysis of principal components are reported in Table 2.

For a correct PCA evaluation, a certain number of emission lines were selected for pigment and binder spectra. The selection of the most representative lines for both materials is important to obtain an accurate discrimination. Emission signals were selected manually with a special focus on avoiding any spectral interference. In Table 3, the selected 26 emission lines for pigments and 5 emission lines for binders are listed (not interfered by cellulose matrix). Once the emission lines were integrated separately for both pure materials, the PCA was performed. The pre-processing carried out for the PCA is the baseline correction of the integrated emission signals. It was

Table 2 Data information used for principal component analysis

	Pigments	Binders
Number of samples	9	3
Recorded spectra per sample	335	180
Emission signals selected as variables	26	5

performed using the mean value of 5 neighboring pixels of the detector when integrating each emission signal. Moreover, centering and autoscaling (standardization) were performed before calculating the PC model.

Random decision forest Random decision forest (RDF) is an advanced algorithm used in the field of machine learning, proposed by Breiman [23]. It is a classifier consisting of a collection of decision trees; each tree-type classifier is trained on a random subset of the data (bootstrap) included in the training set [24].

The multiple classification trees continuously produce training and test sets, maximizing the classes' separation. The predictive power is based on the combination received by the majority vote of each classification tree [25]. The RDF algorithm is a valid classifier because it shows good tolerance for solving problems such as noise and overfitting phenomena; for this reason, LIBS combined with RDF was already considered a good technique to identify and classify artworks [26].

The foremost steps of RDF algorithm can be described as follows:

– Training data: 27 paint mixtures made of all combinations of pigments and binders (Table 1) were employed as the training data set for the classification model. To correct the shot-to-shot variations, the instrumental drifts, and the defocusing effects caused by surface roughness, all spectra were normalized to the total emission intensity. This dataset was used to build the multivariate classification model. Figure 2 illustrates the steps from LIBS spectra of the different pigment/binder combinations to the

classification results. The results obtained are confusion matrices, i.e., representations of statistical classification accuracy.

– Cross-validation: To verify the obtained classification models, cross-validation was calculated with a test size of 100 and 10 repetitions for both RDFs. It means that 10 different models are calculated leaving out 100 randomly selected spectra from the training data set. This exclusion method consists in excluding a certain number of spectra from the dataset, then building the new model, and finally checking the ability of the model to correctly classify the excluded spectra [27]. The spectra not included in the model are evaluated by the corresponding model, and true-positive (TP) and false-positive (FP) rates are calculated [28]. The results obtained are confusion matrices, i.e., representations of statistical classification accuracy.

– Application: This approach allows testing the obtained classification with a new set of samples made of the same materials constituting the existing training data set. This application presents some advantages as a low risk of overfitting and the possibility to check if the training set was correctly developed to describe all the variability of the samples. Through the Imagelab software, the one-vs-all (OVA) scheme was performed. The model used a decision boundary at 0.5. By applying this function, it is possible to obtain a class mapping on the surface analyzed [29].
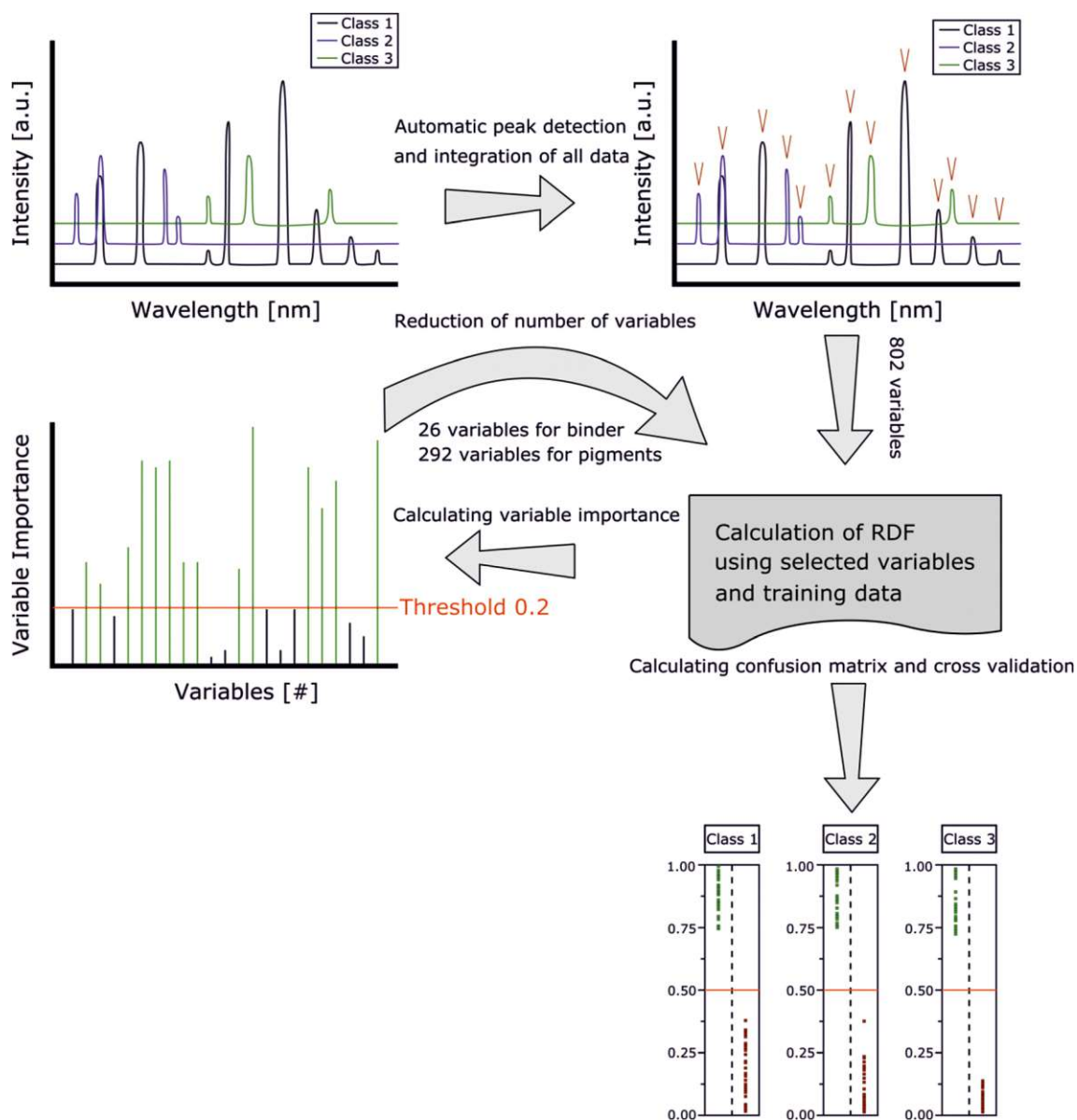
Results and discussion

Selection of emission lines for pure binders and pigments

LIBS measurements were performed on each pure material (Table 1) in order to characterize their elemental composition

Table 3 Emission lines selected for principal component analysis

Pigment elements	Wavelength (nm)	Binder elements	Wavelength (nm)
Ti	394.4; 498.2; 499.1, 499.9	C	192.9; 247.8
Al	390.6; 396.1	C_2 swan	516.5
Na	589; 589.6	H	656.4
Si	288.1	O	777.5
Cd	228.8; 361.1; 508.6		
S	921.4		
Co	238.9; 352.9		
Fe	238.2; 241; 317.5; 407.1		
Cr	326.2; 427.4; 520.6		
O	777.5		
Mn	253.5; 478.3; 482.3		

Author's personal copy

Multivariate analysis and laser-induced breakdown spectroscopy (LIBS): a new approach for the spatially...

Fig. 2 Schematic procedure of building RDF

and obtain reference spectra for statistical evaluation of the paint mixtures. Observing each LIBS spectrum, the characterization of the different elements, constituting the pure materials, is assigned [30–33].

Figure 3 shows for comparison the LIBS spectra of the acrylic, alkyd, and styrene-acrylic binder in the range of 450–660 nm (the range 800–1000 nm of the spectra is not shown because only the argon lines were visible, at 763.5 and 772.5 nm). By comparing the spectra, it is possible to observe that organic materials can be characterized by the principal emission lines of C_2, H, and O.

The Swan band emission (C_2 molecules) is shown in the range 465–590 nm, and it is the main result produced at high laser irradiance due to excitation resulting from electron-ion and ion-ion recombination. The Swan bands arise from

transitions between the different electronic states of the C_2 molecules when intense laser pulses are focused on carbon-containing solids or gases [34, 35].

Thus, for the identification of organic binders, the following emission lines are observed: C_2 molecules at 467.8, 468.5, 469.7, 471.5, 473.7, 512.9, 516.5, 550.2, 554.1, 558.5, and 563.5 nm; oxygen at 777.5 nm; and hydrogen at 656.4 nm [28]. At 485.9 nm, a broad emission band is present; by the application of the Balmer series [36], able to accurately separate spectral peaks in LIBS spectra, the emission band was identified as the beta line of hydrogen (H_β) [37].

The main analytical emission lines of pigments under investigation are shown in the Electronic Supplementary Material (ESM) Table S1.
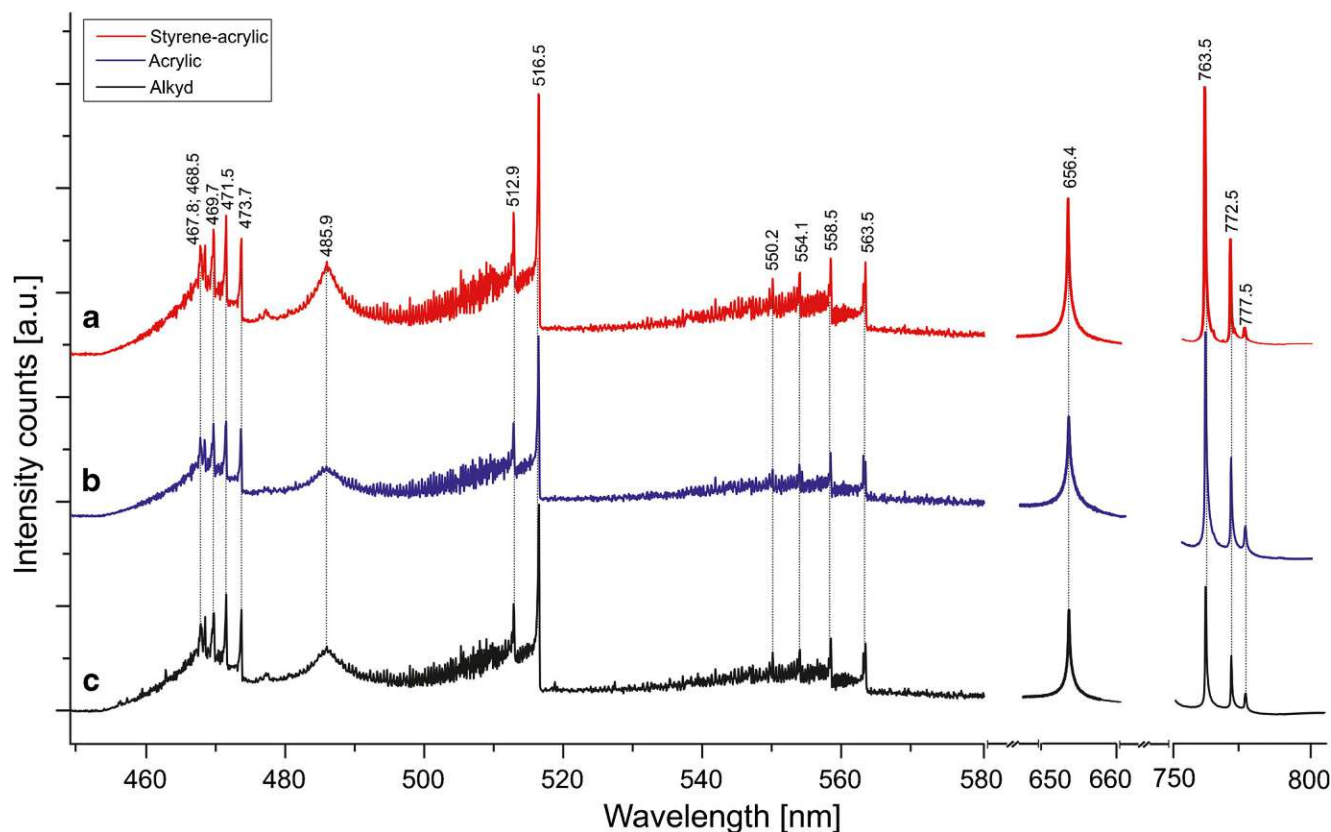
Fig. 3 LIBS spectra of pure (a) styrene-acrylic binder, (b) acrylic, and (c) alkyd

PCA evaluation of pure materials

The score plot in Fig. 4a shows the results obtained for the multivariate analysis of pure binders. Three clusters of data are represented according to the first two principal components PC1 and PC2 that express the 62.9% and 19.8% of the explained variance, respectively (Table 4), for a total spectral variance of 82.7%. The three resulting clusters are well-differentiated within the graph, and the distribution of the points is not particularly extensive. Although the three organic binders generally contain the same elements (C, O, and H), their spectral intensities obtained by LIBS measurements allow to distinguish them separately into three distinct clusters.

For a better understanding of which variables had the most significant contribution to clustering the samples in the score plot, the projection of the variables (loading plot) was added to the evaluation. When a variable has a high projection value on the PC axis, it is considered significant for the distinction of clusters [38]. In the case of organic binders (Fig. 4c), mainly the PC1 was possible to cluster the samples; in fact, the oxygen peak (777.5 nm) had an important negative contribution, whereas the carbon (193.0 and 247.9 nm), C_2 swan (516.5 nm), and hydrogen signals (656.4 nm) show an important positive contribution.

Concerning the evaluation of inorganic pigments (Fig. 4b), the score plot is represented according to the PC2 and

PC3 and can distinguish each pigment individually. Both principal components explain a total variance of 27.7%. In this case, the best clustering was achieved by using lower percentages of explained variances than those used for the binders. The choice of this representation and its validity is confirmed by the study carried out by Jeffers [39]. He states that the relationships between the dependent variable and all components should be considered. In fact, it is always possible that one of the components (even with low variance) may be better correlated to the dependent variable; the present case study exactly explains this concept. Furthermore, the explained multivariate information is considered acceptable and accurate for the discrimination of pure pigments, even not expressing a high percentage value of explained variance. It is due to the choice of manually selecting the main emission lines for each pigment (to minimize also cluster overlap).

In this way, each signal was considered as an important component for the PCA (Table 3), although in some cases, the explained variance had a low value. According to the literature [40], it is not always necessary to employ the first variables, solely based on their size of variance, to consider it a valid principal component regression. Also, in this case, the projection of the variables was evaluated (Fig. 4d) and, comparing it with the pigment score plot obtained (Fig. 4b), each pigment was clustered by the main atomic elements
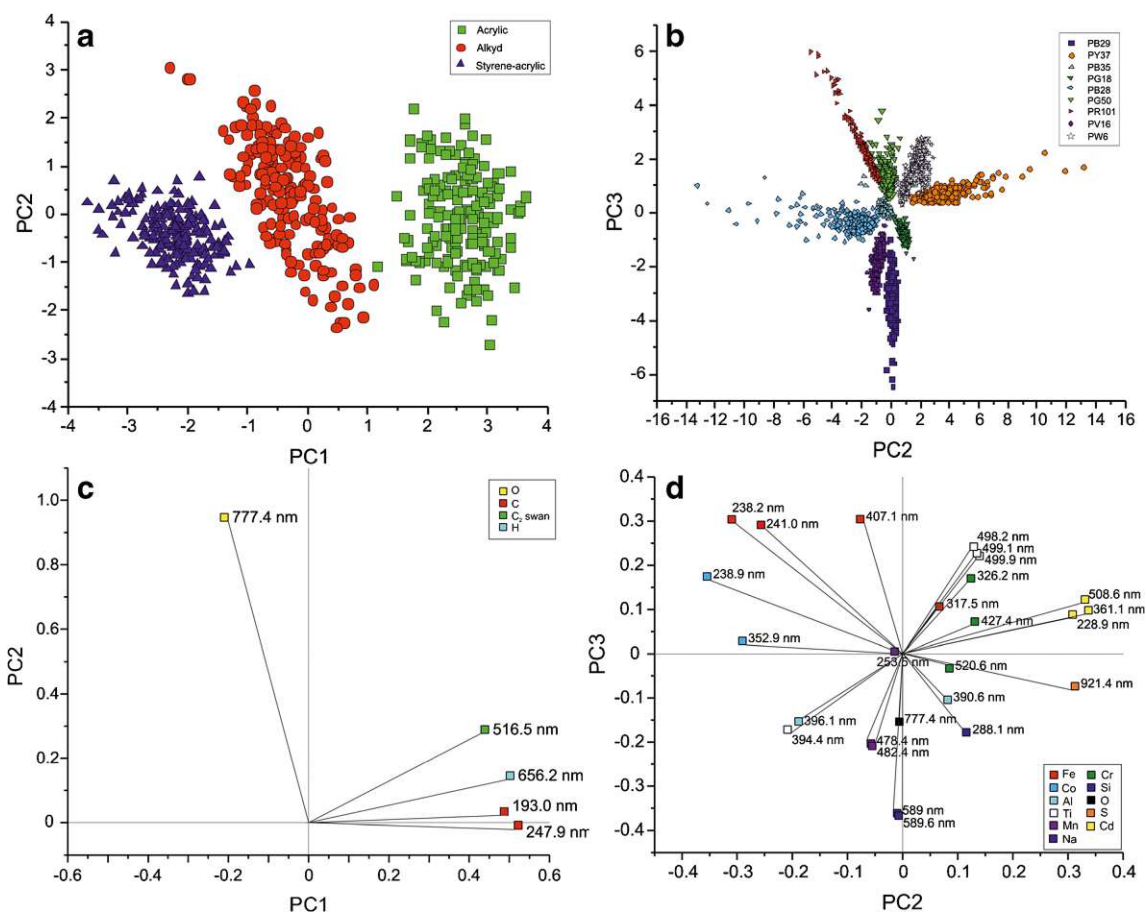
Fig. 4 Score plot of **a** organic binders and **b** inorganic pigments, and corresponding loading plot on **c** PC1 and PC2 for binders and **d** PC2 and PC3 for pigments

constituting each pigment by the negative and positive contribution of PC2 and PC3, respectively.

Therefore, the chosen procedure and the results obtained confirm that the developed statistical model is useful and effective for the statistical identification of pure inorganic and organic materials.

As demonstrated in this section, the developed PCA procedure is able to distinguish each pure material (binders and pigments) in independent clusters and separate them according to their explained information. However, when investigating mixtures of different pigments and binders, PCA is not

able to differentiate between those different samples anymore. The presence of different pigments may change the plasma properties and therefore influence the observed emission intensities of the binder. Additionally, emission signals of pigments might interfere with binder signals, which increase the difficulty of the classification task. Although PCA is a powerful tool to differentiate pure pigments and pure binders, a different classification model has to be employed for the classification of pigment/binder mixtures prevailing in real paint samples.

Table 4 The main components (PCs) resulted from the statistical evaluation and the explained variance values (%). Italicized PCs, used for the PCA of pure binders and pigments, are highlighted

PC binders	Explained variance (%)	PC pigments	Explained variance (%)
1	*62.9*	1	29.78
2	*19.8*	*2*	*15.65*
3	10.23	*3*	*12.09*
4	4.92	4	11.36
5	2.15	5	10.67
		6	7.11
		7	5.64
		8	3.12
		9	1.14

RDF evaluation of paint mixtures

To overcome the difficulties of classification of different pigment/binder mixtures by using PCA, a different classification approach namely random decision forest (RDF) was developed.

In a first step, an algorithm was applied to automatically find and integrate all emission signals in representative LIBS spectra of each pigment/binder combination (Fig. 5).

This resulted in a total number of 1069 integrated emission signals, which were further used as variables to build the RDF. To allow a better classification of paint mixtures, two separate RDFs were calculated: one for the classification of the different pigments and one for the different binders. All recorded LIBS data (total number of 1350 spectra) were used as training data set for the RDF. In a second step, RDFs were calculated using 75 trees with a resampling rate of 0.5. Due to the large number of used variables, computation times were rather long. Therefore, the variable importance was calculated and all variables with a value lower than a certain threshold (0.2) were dismissed resulting in a total number of 265 variables for the pigment classification and 29 variables for the binder classification. By this threshold value, a certain tolerance range is fixed according to the proximity of the predicted value to the target one corresponding to a given class.

In this way, the sample under study is attributed to a specific class [41]. The obtained confusion matrices are shown in Fig. 6 which indicates a satisfying classification result. To verify the obtained classification models, cross-validation was calculated with a test size of 100 and 10 repetitions for both RDFs. This means that 10 different models are calculated leaving out 100 randomly selected spectra from the training data set. The spectra not included in the model are evaluated by the corresponding model and true-positive (TP) and false-positive (FP) rates are calculated. The values considered for the verification of the discriminatory power of the RDF are the sensitivity, expressed as the average of TP and FP rates, and the standard deviation (STD TP and STD FP rates), shown in Table 5. As the resulting values are high TP rates and low FP rates, the cross-validation model is able to accurately classify each mixture. However, the better results were registered for the classification of the different pigments than binders. As the different inorganic pigments present various and different elemental emission lines between each other, they can be more easily classified. The organic binders consist of the same elements, namely, carbon, hydrogen, oxygen, and nitrogen.
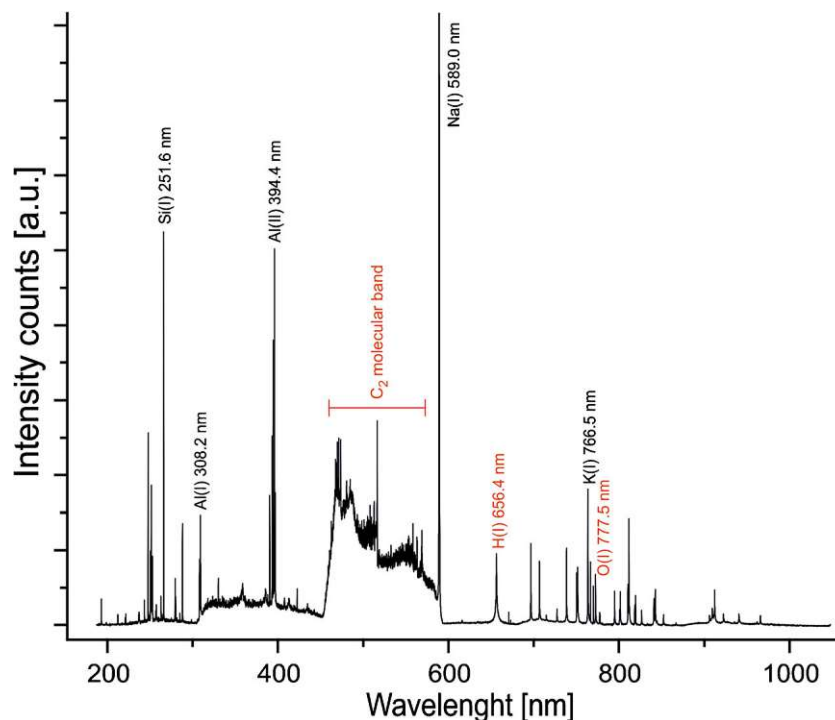
Therefore, there are no prominent features in the LIBS spectra allowing for easy classification of the different binders. Slight variations in the emission intensities of the elements, already mentioned in the PCA results, are used for the distinction and the classification. Another critical issue is the influence that the inorganic pigments on the final emission signals of the binder materials; for this reason, the correct binders' classification is more challenging compared with the pigment ones. Nevertheless, the results obtained for the RDF classification of different pigments and binders investigated are to be considered good and reliable.

Fig. 5 Example of LIBS spectrum integrated for the RDF evaluation. In detail, a combination of alkyd resin with artificial ultramarine blue pigment (PB29). Black labels indicate the main emission lines of the pigment, whereas the red ones of the alkyd binder

Author's personal copy

Multivariate analysis and laser-induced breakdown spectroscopy (LIBS): a new approach for the spatially...

Fig. 6 Confusion matrices of **a** the three different investigated binders and **b** the nine investigated pigments. The scale to the left indicates the ratio of trees that agree on the *positive* classification. The default decision boundary at 0.5 is highlighted in red. The green dots represent the *true/positives*, whereas the gray dots the *true/ negatives*. The cases where the known and the predicted labels differ are marked using a red "x." The numbers in each confusion matrix specify the absolute number of cases for each quadrant
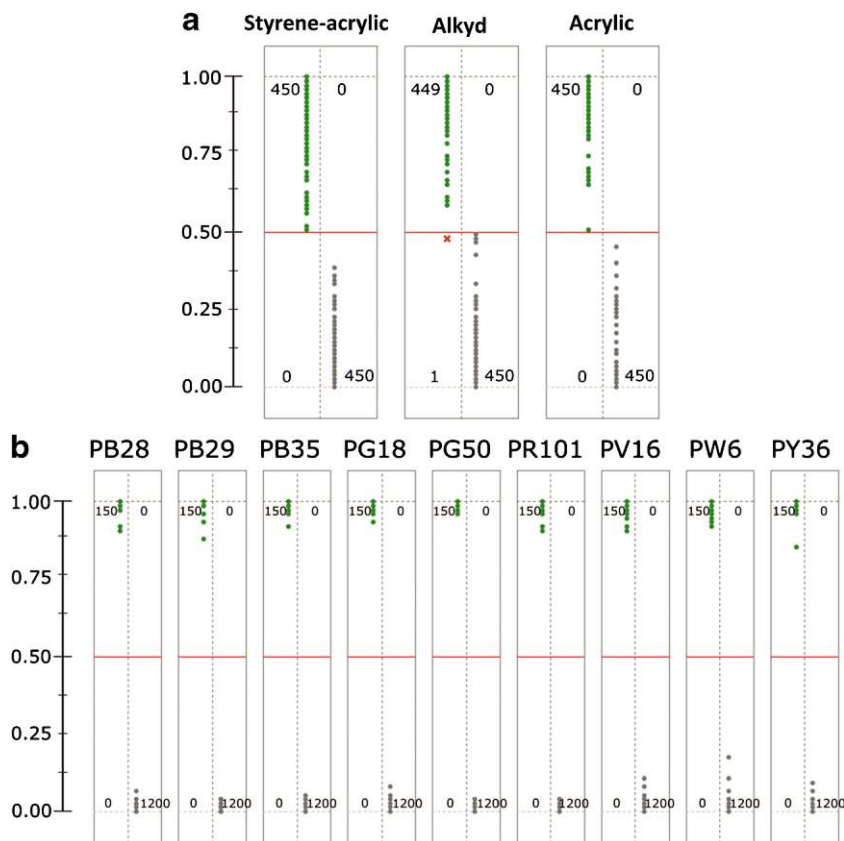
RDF application on unknown paint sample

The final approach is validating the current classification with a new paint sample set, representative of the main materials recently used in modern art, made of the same materials constituting the existing training data set. For this purpose, a striped texture mock-up was prepared with different pigment/binder combinations, which were considered as unknown samples. The application test aimed to identify, using the obtained RDFs, the distribution of each inorganic pigment and organic binder constituting the mock-up. In Fig. 7a and c, a microscope image of the investigated surface is shown. The marked red area was analyzed by LIBS using parallel line scans with the settings previously listed resulting in the ablation of about 1 μm of sample material. The obtained image consists of a total number of 12,800 pixels covering a total area of 16 mm × 8 mm. In contrast to conventional bulk measurements, where usually multiple measurements could be

Table 5 Results of the cross-validation for both RDFs calculated for the pigment and the binder classification

Pigment	Average TP rate	STD TP rate	Average FP rate	STD FP rate
PB28	1	0	0	0
PB29	0.9987	0.0030	0	0
PB35	1	0	0	0
PG18	1	0	0	0
PG50	1	0	0	0
PR101	1	0	0	0
PV16	1	0	0	0
PW6	0.9987	0.0030	0.0005	0.0005
Py37	1	0	0	0
Binder	Average TP rate	STD TP rate	Average FP rate	STD FP rate
Styrene-acrylic	0.9118	0.0013	0.0220	0.0036
Alkyd	0.9532	0.0033	0.0318	0.0023
Acrylic	0.9781	0.0030	0.0179	0.0007

Fig. 7 Microscope image of the test sample divided by **a** different inorganic pigments and **c** organic binders employed. RDF classification mapping of **b** pigments and **d** binders identified
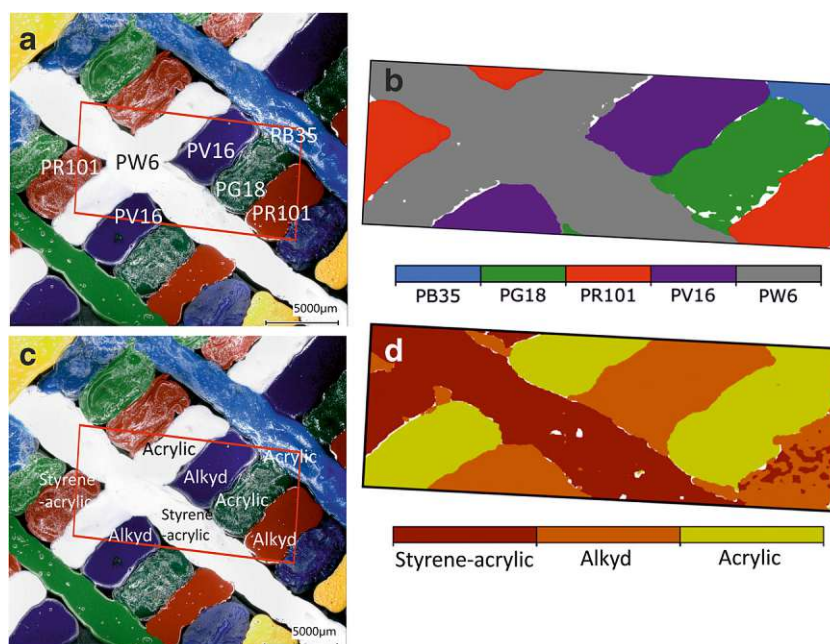
used for classification, for spatially resolved analysis, only one LIBS spectrum is available per pixel. The collected data were classified using the pigment and binder RDF models previously developed. The application results of the different pigments and binders are shown in Fig. 7b and d, respectively. All various pigments and binders were classified correctly, except some pixels displayed in white, and the lateral distribution of each pigment and binder is in very good agreement with the distribution seen in the microscope image of the sample.

Conclusion

In this paper, LIBS was used to identify and characterize different organic binders and inorganic pigments. After the assignment of each emission signal to the relative element, in order to distinguish each material from each other, LIBS spectra were evaluated by principal components analysis (PCA). Through appropriate methodological choices, such as the manual selection of the main variables, this statistical method proved to be effective for the discrimination of the different binders and pigments. However, due to the low accuracy of PCA, for the distinction of these materials in mixture, a different method of multivariate classification was considered, i.e., the random decision forest (RDF). Initially, the set-up of this method was challenging due to the high number of automatic variables selected for the creation of the training set. However, by neglecting variables that did not contribute to the classification results using a threshold for the variable importance, and testing its accuracy, it was possible to choose a suitable training set subsequently tested by cross-validation. From the verification of the sensitivity and standard deviation

values, the built RDF classification method was revealed to be good and reliable. However, it should be considered that the accuracy of cross-validation is generally more optimistic than true test accuracy; therefore, to improve the prediction on the test set, a minimal data pre-processing on categorical variables is necessary. Finally, the classification model was tested on an unknown mock-up, made by the same previously classified materials. A section of the paint surface was analyzed by LIBS, the obtained spectra classified by the built RDF model, and finally the obtained results were represented as mapping images according to the identified chemical compounds.

The application of the model to an unknown sample demonstrated the correct classification of paint mixtures. Compared with existing literature, the proposed procedure presents significant improvements. Instead of bulk classification already published, we present laterally resolved classification of modern art materials. The possibility of creating elemental mappings is important not only for the subsequent applications of this statistical method but also for the multiple purposes that it can reach in the field of cultural heritage. All the results presented demonstrate the high potential of this analytical technique and the possibility to employ extended data processing by different multivariate statistics. The most remarkable result concerns the identification and classification of organic materials. As a matter of fact, it was not only possible to characterize emission lines for each binder but also to differentiate them and subsequently classify unknown samples. This first approach of data evaluation could possibly extend the classification to other organic binders used in the artistic field.

Furthermore, an implementation of this application can be the characterization of organic pigments mixed with polymeric binders. In this case, identification problems could arise due

to similar chemical compositions. However, considering that LIBS is also able to provide molecular information, such as CN violet and C_2 Swan bands, this investigation could represent a future approach to research for the identification of organic art materials. Consideration of simultaneous Raman analysis, as already published for bulk samples, could further improve the quality of the classification model. However, it is necessary to consider that LIBS is a micro-destructive technique. Therefore, especially for unique artworks of high historic value, its use could be problematic. The application of the classification method (RDF) tested in this study could be significant for the resolution and simplification of data obtained by other analytical techniques. This information could find future applications in various contexts such as archaeology, biology, industrial chemistry, materials science, and for multiple purposes such as database creation, monitoring during conservation treatments, and the identification of artistic materials and their degradation products.

Compliance with ethical standards

Conflict of interest The authors declare that they have no conflict of interest.

References

1. Giakoumaki A, Melessanaki K, Anglos D. Laser-induced breakdown spectroscopy (LIBS) in archaeological science - applications and prospects. Anal Bio Chem. 2007;387:749–60.

2. Melessanaki K, Mateo M, Ferrence SC, Betancourt PP, Anglos D. The application of LIBS for the analysis of archaeological ceramic and metal artifacts. Appl Surf Sci. 2002;197-198:156–63.

3. Maravelaki-Kalaitzaki PN. Innovative techniques for the characterization of encrustation on Pentelic marble from the Parthenon, chapter in "Cultural heritage conservation and environmental impact assessment by non-destructive testing and micro-analysis". 2005;135–148.

4. Corsi M, Crisoforetti G, Palleschi V, Salvetti A, Tognoni E. A fast and accurate method for the determination of precious alloys caratage by laser induced plasma spectroscopy. Eur Phys J. 2001;13:373–7.

5. Grolmusová Z., Mináriková L., Rakovský J., Čermák P., Veis P., Elementar LIBS. Analysis of biological samples. Proc of Contr Papers, 2009;Part III:189–192.

6. Colao F, Fantoni R, Lazic V, Morone A, Santagata A, Giardini A. LIBS used as a diagnostic tool during the laser cleaning of ancient marble from Mediterranean areas. Appl Phys A Mater Sci Process. 2004;79(2):213–9.

7. Roy A. Artists' pigments, vol. 2. Washington DC: National Gallery of Art; 1993.

8. Fitzhugh E. Artists' pigments, vol. 3. Washington DC: National Gallery of Art; 1997.

9. Learner T. Analysis of modern paints. The Getty Conservation Institute, 2004.

10. Learner T. Modern paints uncovered. The Getty Conservation Institute, 2008.

11. Sattmann R, Monch I, Krause H, Noll R, Couris S, Hatziapostolou A, et al. Laser-induced breakdown spectroscopy for polymer identification. Appl. Spectr. 1998;52(3):456–61.

12. Brech F, Cross L. Optical microemission stimulated by a ruby laser. Appl Spectr. 1962;16:59.

13. Anabitarte F, Cobo A. Lopez-Higuera J.M., Laser-induced breakdown spectroscopy: fundamentals, applications, and challenge, ISRN Spectroscopy, 2012.

14. Musazzi S, Perini U. Laser-induced breakdown spectroscopy, theory and applications. Opt Sci. 2014.

15. Bonta M, Limbeck A. Metal analysis in polymers using tandem LA-ICP-MS/LIBS: eliminating matrix effects using multivariate calibration. J Anal At Spectrom. 2018;33:1631–7.

16. Rai S, Rai AK. Characterization of organic materials by LIBS for exploration of correlation between molecular and elemental LIBS signals. AIP Adv. 2011;042103.

17. Borgia I, Burgio LMF, Corso M, Fantoni R, Palleschi V, Salvetti A, et al. Self-calibrated quantitative elemental analysis by laser-induced plasma spectroscopy: application to pigment analysis. J Cult Herit. 2000;1:S281–6.

18. Gornushkin IB, Smith BW, Nasajpour H, Winefordner JD. Identification of solid materials by correlation analysis using a microscopic laser-induced plasma spectrometer. Anal Chem. 1999;71(22):5157–64.

19. Jolivet L, Leprince M, Moncayo S, Sorbier L, Lienemann C-P, Motto-Ros V. Review of the recent advances and applications of LIBS-based imaging. Spectr Acta Part B: Atom Spectr. 2019;151: 41–53.

20. Sarmiento A, Pérez-Alonso M, Olivares M, Castro K, Martínez-Arkarazo I, Fernández LA, et al. Classification and identification of organic binding media in artworks by means of Fourier transform infrared spectroscopy and principal component analysis. Anal Bioanal Chem. 2011;399:3601–11.

21. Unnikrishnan VK, Choudhari KS, Kulkarni SD, Nayak R, Kartha VB, Santhosh C. Analytical predictive capabilities of laser induced breakdown spectroscopy (LIBS) with principal component analysis (PCA) for plastic classification. RSC Adv. 2013;3:25872–80.

22. Musumarra G, Fichera M. Chemometrics and cultural heritage. Chem Intel Lab Syst. 1998;44:363–72.

23. Breiman L. Random forests. Mach Learn. 2001;45(1):5–32.

24. Anghelone M, Jembrih-Simbürger D, Schreiner M. Identification of copper phthalocyanine blue polymorphs in unaged and aged paint systems by means of micro-Raman spectroscopy and random forest. Spectr Acta Part A: Mol Biomol Spectr. 2015;149:419–25.

25. Sheng L, Zhang T, Niu G, Wang K, Tang H, Duan Y, et al. Classification of iron ores by laser-induced breakdown spectroscopy (LIBS) combined with random forest (RF). J Anal At Spectrom. 2015;30:453–8.

26. Qi J, Zhang T, Tang H, Li H. Rapid classification of archaeological ceramics via laser-induced breakdown spectroscopy coupled with random forest. Spectr Acta Part B: Atom Spectr. 2018;149:288–93.

27. Tropsha A, Gramatica P, Gombar VK. The importance of being earnest: validation is the absolute essential for successful application and interpretation of QSPR models. QSAR Comb Sci. 2003;22:69–77.

28. Grégoire S, Boudinet M, Pelascini F, Surma F, Detalle V, Holl Y. Laser-induced breakdown spectroscopy for polymer identification. Anal Bionanal Chem. 2011;400:3331–40.

29. Hufnagl B, Steiner D, Renner E, Loder MGJ, Laforsch C, Lohninger H. A methodology for the fast identification and monitoring of microplastics in environmental samples using random decision forest classifiers. Anal Methods. 2019;11:2277–85.

30. Miziolek AW, Palleschi V, Schechter I. Laser induced breakdown spectroscopy: Cambridge University; 2006.

31. Kroonen J, Vader D. Line interference in emission spectrographic analysis: Elsevier; 1963.
32. AtomTrace website.
33. Osticioli I, Mendes NFC, Nevin A, Gil Francisco PSC, Becucci M, Castellucci E. Analysis of natural and artificial ultramarine blue pigments using laser induced breakdown and pulsed Raman spectroscopy, statistical analysis and light microscopy. Spectr Acta Part A. 2009;73:525–31.
34. Harilal SS, Bindhu CV, Nampoori VPN, Vallabhan CPG. Influence of ambient gas on the temperature and density of laser produced carbon plasma. Appl Phys Lett. 1998;72:167.
35. Harilal SS, Issac RC, Bindhu CV, Nampoori VPN, Vallabhan CPG. Optical emission studies of C2 species in laser-produced plasma from carbon. J Phys D Appl Phys. 1997;30:1703–9.
36. Parigger CG, Plemmons DH, Oks E. Balmer series H measurements in a laser-induced hydrogen plasma. Appl Opt. 2003;42:5992.
37. Gautam G, Parigger CG, Surmick DM, El Sherbini AM. Laser plasma diagnostics and self-absorption measurements of the Hβ Balmer series line. J Quant Spectr Rad Trans. 2016;170:189–93.
38. Daher C, Bellot-Gurlet L, Le Hô A, Paris C, Regert M. Advanced discriminating criteria for natural organic substances of Cultural Heritage interest: spectral decomposition and multivariate analyses of FT-Raman and FT-IR signatures. Talanta. 2013;115:540–7.
39. Jeffers JNR. Two case studies in the application of principal component analysis. J R Stat Soc Series C (Appl Stat). 1967;16:225–36.
40. Jolliffe IT. A note on the use of principal components in regression. J R Stat Soc, Ser C (Appl Stat). 1982;31:300–3.
41. El Haddad J, Canioni L, Bousquet B. Good practices in LIBS analysis: review and advices. Spectr Acta Part B: Atom Spectr. 2014;101:171–82.

Publisher's note Springer Nature remains neutral with regard to jurisdictional claims in published maps and institutional affiliations.

Paper III

Infrared and Laser-Induced Breakdown Spectroscopy to Characterize UV-Light Degradation of Modern Art Materials

Laura Pagnin, Lukas Brunnbauer, Rita Wiesinger, Andreas Limbeck, Manfred Schreiner

Infrared and Laser-Induced Breakdown Spectroscopy to Characterize UV-light Degradation of Modern Art Materials

5 authors, including:

Laura Pagnin
Akademie der Bildenden Künste Wien
19 PUBLICATIONS 15 CITATIONS

SEE PROFILE

Rita Wiesinger
Akademie der Bildenden Künste Wien
75 PUBLICATIONS 535 CITATIONS

SEE PROFILE

Andreas Limbeck
TU Wien
160 PUBLICATIONS 3,649 CITATIONS

SEE PROFILE

Manfred Schreiner
Akademie der Bildenden Künste Wien
337 PUBLICATIONS 3,877 CITATIONS

SEE PROFILE

Some of the authors of this publication are also working on these related projects:

MnemoART View project

Coating Protection of Metal Objects in Cultural Heritage View project

INFRARED AND LASER-INDUCED BREAKDOWN SPECTROSCOPY TO CHARACTERIZE UV-LIGHT DEGRADATION OF MODERN ART MATERIALS

L. PAGNIN[1], L. BRUNNBAUER[2], R. WIESINGER[1], A. LIMBECK[2], M. SCHREINER[1, 2]

[1]*Institute of Science and Technology in Art, Academy of Fine Arts Vienna,*

Schillerplatz 3, 1010, Vienna, Austria;

l.pagnin@akbild.ac.at; r.wiesinger@akbild.ac.at; m.schreiner@akbild.ac.at

[2] *Institute of Chemical Technologies and Analytics TU Wien,*

Getreidemarkt 9/164, 1060, Vienna, Austria;

lukas.brunnbauer@tuwien.ac.at; andreas.limbeck@tuwien.ac.at

Introduction

Since the last century, research concerning modern and contemporary artworks is steadily growing, above all the knowledge of materials, such as synthetic polymeric binders and inorganic pigments.

The characterization of their degradation processes is of considerable scientific interest and great importance for the preservation of such cultural artworks [1].

In fact, the increasing environmental pollution led to further studies of the stability and chemical reactions taking place on these paint mixtures exposed to the outdoor condition. The main cause is the photodegradation provoked by the interaction between UV-light and the surface paint layer. Generally, the main degradation effects on the superficial paint layer are of mechanical (chalking and cracking), physical (fading), and chemical (breaking of the bonds constituting the organic material) origin and therefore, the stability and durability of artistic objects are compromised over time. In previous studies [2, 3], the applicability of different analytical techniques for the study of degradation processes and the chemical stability of acrylic and alkyd binders was described.

In the present paper, the focus was on the chemical surface changes on modern paints exposed to short-time UV-light artificial aging and the influence of various pigments. In fact, different inorganic pigments, such as artificial ultramarine blue (PB29), hydrated chromium oxide green (PG18), and cadmium yellow (PY37) mixed with synthetic binders (acrylic emulsion or alkyd resin) were exposed for 1, 2, 3, 4, 5, and 6 weeks (0-1008 h) to artificial UV-light, using spectral and intensity parameters comparable to outdoor solar radiation. Three different pigment/binder (P/BM) ratios were chosen: 1:2, 1:3, and 1:6. Subsequently, the unaged and aged paint samples were analyzed using Attenuated Total Reflection Infrared Spectroscopy (ATR-FTIR) and colorimetric measurements. The main aim was to understand which functional groups are more subject to deterioration UV exposure by band

integration, expand the knowledge on the different influence of inorganic pigments in these oxidative reactions, and evaluate the role of selected inorganic pigments at different concentrations (P/BM ratio) in the photodegradation of binders by kinetic study.

Moreover, Laser-Induced Breakdown Spectroscopy (LIBS) was applied for analytical characterization of the aged samples. This technique offers the possibility to obtain elemental information and enables the measurement of depth profiles. Besides, analysis of broadband LIBS spectra could be used for the classification of different polymer types. Thus, specific regions in the LIBS spectrum were used to characterize changes in the paint mixtures. Depth analysis of degradation changes in the polymer network was analyzed and evaluated by multivariate statistics.

Experimental methods

- *Artificial aging.* A UVACUBE SOL 2/400F UV chamber (GmbH UV-Technology, Germany) was used for the UV aging. The UV source provided radiation in a wavelength range between 295 and approx. 3000 nm with an approximate intensity value of 170 W/m^2, similar to outdoor conditions. The temperature was around 38 °C, and the relative humidity varied between 10 and 20 % (RH). The artificial UV exposure of acrylic and alkyd paints was carried out for a maximum of 1008 h.

- *ATR-FTIR Spectroscopy.* A LUMOS FTIR Microscope (Bruker Optics, Germany) in ATR mode with a germanium crystal was employed. The spectral range acquired was between 4000 and 480 cm^{-1}, performing 64 scans at 4 cm^{-1} resolution. Five measurement spots were chosen on each sample, acquired on unaged and aged paint samples. The spectra were averaged and baseline corrected. The chemical depth information obtained by the ATR-FTIR measurements was around 0.65 μm.

- *Colorimetric analysis.* An SPM50 Gretag-Macbeth (XRite, Switzerland) was available and reflection spectra in the visible range (380-730 nm) were observed. By using a D65 illuminant with the 10° Standard Observer, 45°/0° geometry. Five spots were measured with a measuring spot size of around 1 mm. The color changes between unaged and aged samples were evaluated according to the CIELAB coordinates values (L*, a*, b*, and ΔE*).

- *Laser-Inducted Breakdown Spectroscopy.* A J200 Tandem LA/LIBS instrumentation (Applied Spectra Inc., Fremont, CA), equipped with a 266 nm frequency quadrupled Nd:YAG laser was used for LIBS experiments. For each laser shot, full spectra over the wavelength range from 190 to 1040 nm were recorded. The parameters used are laser output energy of 12.5 mJ, with a gate delay of 0.2 μsec, and a spot size of 100 μm.

Results and Discussion

In Figure 1, the comparison between the ATR-FTIR spectra of alkyd paint (P/BM 1:2) mixed with pigment PB29 and aged after 0, 504, and 1008 h is shown. Significant chemical changes on the surface are observed. Over time, all the functional groups of the binder decrease such as the (C-H)CH$_2$

asymmetric and symmetric stretching at 2926 and 2854 cm^{-1} and the C=O band at 1724 cm^{-1}, due to the photochemical degradation of the oil component in the binder, forming oxidation products.

On the other hand, the spectral signal of PB29 in the mixture (at 1068 and 977 cm^{-1}), related to the Al,Si-O$_4$ asymmetric stretching, increases over aging time and its amount in the paint (P/BM).

This chemical-physical phenomenon is more prominent in the alkyd paints than in the acrylic ones due to the oil component. The photodegradation kinetics using the intensity of the C=O band of acrylic and alkyd paints could be studied by ATR-FTIR [4]. The degradation of acrylic paints with P/BM 1:2 was observed already after 336 h of aging, whereas for P/BM 1:6 it was registered after 672 h. For alkyd binder, this effect was determined already after 168 h for every P/BM ratio. These results confirm the chemical instability of alkyd resin exposed to UV aging. However, this phenomenon not only depends on the different binder used but also on the pigment and the P/BM ratio [5]. The binder degradation increases in the samples with a high amount of pigment (P/BM 1:2), above all with pigment PB29 in both mixtures.
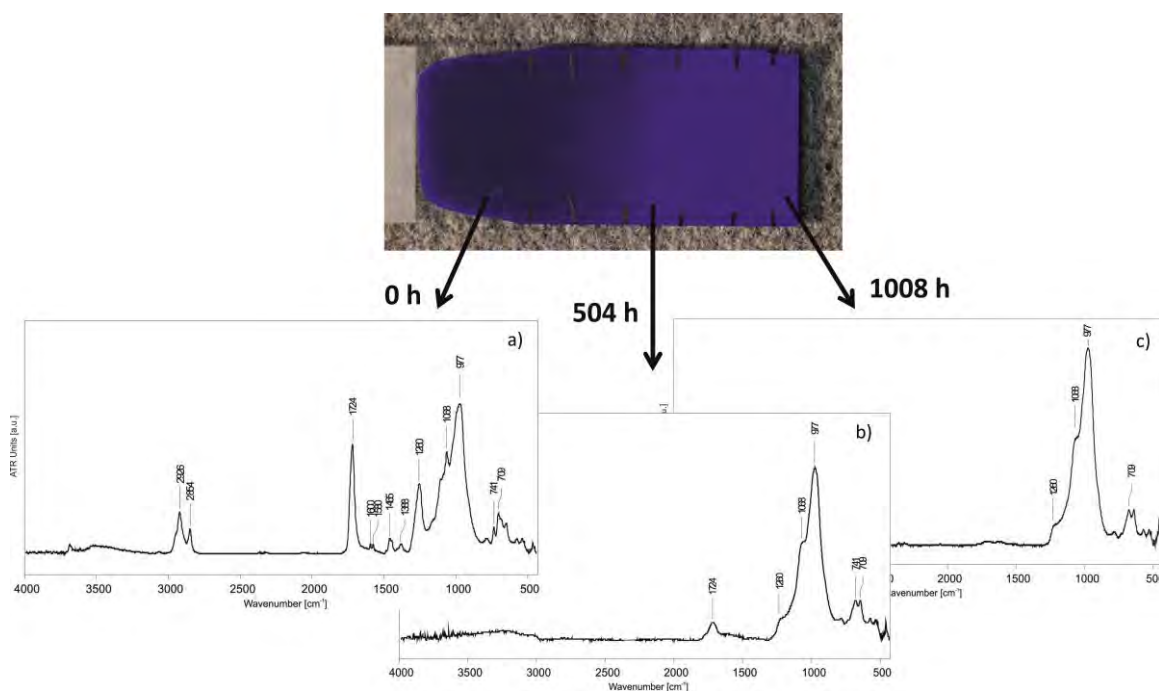
Figure 1 Image of alkyd + PB29 paint (P/BM 1:2) UV aged for a total of 1008 h with the respective ATR-FTIR spectra at a) 0 h, b) 504 h, and c) 1008 h of UV exposure.

In addition to ATR-FTIR, colorimetric measurements were performed. During the UV exposure, the L* values for alkyd paints mixed with PB29 and PY37 increase, whereas for PG18, they decrease. Generally, the color change increases with the content of the pigment in the mixture. For acrylic paints, the L* values show no significant change.

LIBS measurements were initially performed to determine the elemental composition of the inorganic and organic materials in the samples. Measuring the unaged PB29 + alkyd binder sample, the distinction between pigment and binder by their different atomic emission lines was carried out.

In order to investigate the chemical variations occurred on UV aged paint surfaces, statistical analysis was performed applying Principal Component Analysis (PCA), taking into account the different LIBS emission lines previously selected. This analysis was performed by comparing the results obtained at the superficial surfaces, before and after UV-aging, and the results obtained from depth analysis.

The depth profile was recorded by measuring 15 consecutive layers, each covering an area of 1.9 x 1.0 mm. Every single layer was ablated with 190 laser shots, resulting in a mean ablation rate of 1 μm per layer. Observing and comparing the score plots obtained from the 1008 h aged and unaged samples and from the superficial layer (#1) and the deepest one (#15), a significant difference is noticed (Fig. 2).
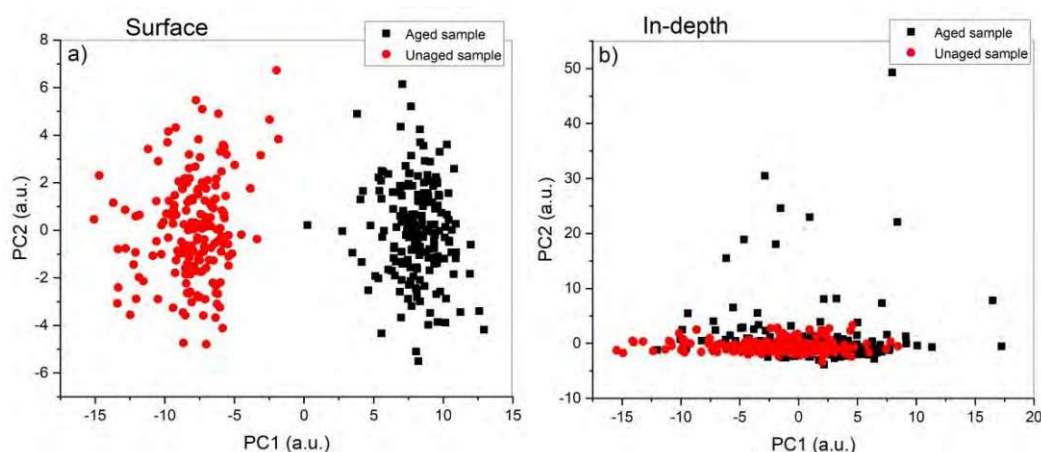
Figure 2: Comparison between different score plots of selected layers: a) surface level (layer #1) evaluation of unaged sample (black) and UV aged sample (red); b) depth level (layer #15) evaluation of unaged sample (black) and UV aged sample (red).

The distribution of data in the analysis of the principal components (PC) shows that at the surface level, by comparing the unaged and aged sample, the chemical composition of the two paint samples is completely different. Probably, it is due to the degradation of the main functional groups of the binder. The chemical composition of the bulk (depth profile analysis 15) does not present significant changes (Fig. 2b). In conclusion, by photodegradation kinetics evaluation observed by ATR-FTIR and colorimetric analysis, alkyd binder presents the most significant degradation effect. It increases if the pigment amount is higher than the binder (P/BM 1:2), and predominantly for PB29. LIBS is a useful technique to investigate modern art materials and, by PCA, it is possible to discriminate inorganic and organic materials in the mixture and the different levels of superficial degradation.

REFERENCES

[1] O. Chiantore, A. Rava, Conserving Contemporary art: issues, methods, materials, and research, Getty Publications, 2007.
[2] V. Pintus, S. Wei, M. Schreiner, Micr. Jour., 124 (2015) 949-961.
[3] M. Anghelone, D. Jembrih-Simbürger, M. Schreiner, Polym. Degrad. Stabil., 134 (2016) 157-168.
[4] R. Wiesinger and L. Pagnin, M. Anghelone, L. M. Moretto, E. F. Orsega, M. Schreiner, Angew. Chem. Int. Ed., 57 (2018), 7401–7407.
[5] K. Janssens, F. Vanmeert, S. Legrand, G. Nuyts, M. Alfeld, L. Monico, W. Anaf, W. De Nolf, M. Vermeulen, J. Verbeeck, K. De Wael, Top Curr. Chem. (Z), (2016) 374:81.

Paper IV

Combined LA-ICP-MS/LIBS: powerful analytical tools for the investigation of polymer alteration after treatment under corrosive conditions

Lukas Brunnbauer, Maximilian Mayr, Silvia Larisegger, Michael Nelhiebel, Laura Pagnin, Rita Wiesinger, Manfred Schreiner, Andreas Limbeck

SCIENTIFIC REPORTS
natureresearch

Check for updates

OPEN

Combined LA-ICP-MS/LIBS: powerful analytical tools for the investigation of polymer alteration after treatment under corrosive conditions

Lukas Brunnbauer[1✉], Maximilian Mayr[1], Silvia Larisegger[2], Michael Nelhiebel[2], Laura Pagnin[3], Rita Wiesinger[3], Manfred Schreiner[1,3] & Andreas Limbeck[1✉]

Polymers are used in a variety of different areas, including applications in food packaging, automotive and the semiconductor industry. Information about degradation of these materials during application, but also uptake of pollutants from the surrounding environment is therefore of great interest. Conventional techniques used for polymer characterization such as FT-IR or Raman spectroscopy, but also thermo-analytical techniques offer insights into degradation processes but lack the possibility to detect uptake of inorganic species. Moreover, these techniques do not allow the measurement of depth profiles, thus information about degradation or pollutant uptake with sample depth is not accessible. In this work, we propose LA-ICP-MS and LIBS as powerful analytical tools for polymer characterization, overcoming the limitations of conventional analytical techniques used for polymer analysis. Applicability of the developed procedures is demonstrated by the analysis of artificially weathered polyimides and modern art materials, indicating that the degradation of the polymer but also the uptake of corrosive gases is not limited to the sample surface. Finally, a tandem LA-ICP-MS/LIBS approach is employed, which combines the advantages of both laser-based procedures, enabling the simultaneous analysis of polymer degradation and cadmium uptake of polystyrene after exposure to UV radiation and treatment with artificial sea water.

Synthetic polymers and plastics are among the most commonly used materials in our modern world[1]. They are mainly employed as packaging materials for consumer goods such as food and cosmetics and also bottles and boxes, but also frequently applied for construction materials[2]. Polymers are also used as passivation or encapsulation materials in the semiconductor industry[3,4] or, in combination with pigments, as paints in the fields of art and cultural heritage[5,6]. In general, the applied synthetic polymers are composed of an organic-carbon-chain polymer and different additives that give the materials the intended chemical and physical properties. Commonly applied additives include plasticizers, antioxidants, antistatic agents, lubricants, flame retardants or inorganic pigments.

During application, polymers are often exposed to harmful environmental conditions, causing changes in their chemical composition. In this context, the negative influences of sunlight but also contact with ambient gases and environmental liquids have to be mentioned. Whereas UV light and oxidative gases are known to promote degradation[7–9], corrosive gases or metals dissolved in rain, snow and river or sea-water are susceptible for uptake into the polymer network, resulting in increased concentrations of inorganic constituents in aged materials. All of these possible interactions contribute to unwanted changes in the polymer composition, which finally lead to altered material properties (e.g. bleaching of colors, reduced thermal stability, increased brittleness, etc.). A comprehensive characterization of aged polymers is therefore necessary not only to control if the polymers still fulfill the requirements for further application (e.g. in the semiconductor industry[10–14]), but also

[1]Institute of Chemical Technologies and Analytics, TU Wien, Getreidemarkt 9/164-IAC, 1060 Vienna, Austria. [2]KAI Kompetenzzentrum Automobil- und Industrieelektronik GmbH, Technologiepark Villach Europastraße 8, 9524 Villach, Austria. [3]Institute of Science and Technology in Art, Academy of Fine Arts Vienna, Schillerplatz 3, 1010 Vienna, Austria. ✉email: lukas.brunnbauer@tuwien.ac.at; andreas.limbeck@tuwien.ac.at

to achieve desired material properties (e.g. resistance to weathering is important in the field of cultural heritage research[15–17]).

At the end of their life-cycle, polymers often end up in the environment, for example in the form of microplastics which pose a significant threat to various ecosystems[18]. Accordingly, the composition and metal contents of the degraded polymers should be monitored, to better estimate the adverse health effects of microplastics in the environment[19–21].

Due to their wide range of properties and applications, the composition of synthetic polymers is rather versatile. Polymer analysis is therefore a great challenge to analytical chemistry. The most commonly used analytical techniques for characterization and analysis of polymers are FT-IR and Raman spectroscopy. Besides being able to identify and classify different polymers, these techniques are also employed to investigate polymer degradation[22–25]. Furthermore, Py-GC–MS[26] and MALDI-ToF–MS[27] are also commonly applied for polymer analysis, providing information about the molecular composition of the investigated polymer sample. Thermogravimetric analysis (TGA) and differential thermal analysis (DTA) are frequently used techniques giving bulk information about thermo-oxidative polymer degradation[22,28,29]. However, information about the metal contents prevailing in the polymer samples is not accessible with these techniques. For this purpose, polymers are first converted into a solution and subsequently analyzed using liquid analysis techniques such as inductively coupled plasma-optical emission spectroscopy (ICP-OES) or inductively coupled plasma-mass spectrometry (ICP-MS)[30,31]. However, the applied digestion methods are always accompanied by the risk of contamination or elemental loss and the complete procedure of analysis is often time-consuming. Nowadays, elemental analysis of polymers is carried out using solid sampling techniques such as electrothermal vaporization [[32,33]] or laser ablation[34,35] in combination with ICP-OES or ICP-MS detection to overcome the limitations of wet chemical analysis. With these techniques, accurate and highly sensitive trace elemental measurements are possible. However, they do not offer information about polymer degradation. Summing up, with the analytical procedures reported so far it is not possible to study polymer degradation and inorganic species with one single measurement.

In this work, we present an analytical technique that permits the simultaneous detection of polymer degradation as well as changes in the elemental composition. The developed procedure is based on the concurrent sample analysis using laser induced breakdown spectroscopy (LIBS) and laser ablation-inductively coupled plasma-mass spectrometry (LA-ICP-MS). In this so-called tandem LA-ICP-MS/LIBS approach a focused laser beam is fired on the sample surface. With LIBS, the radiation emitted by the formed plasma plume is detected. Thereby information about the major components of polymers, namely carbon, oxygen, hydrogen and nitrogen but also molecular sample information in the form of the C_2 swan band and the CN violet band is collected[36]. Together with different statistical methods, the acquired LIBS data can be used for compound identification. Broadband LIBS spectra have, for example, already been used for the classification of different polymer types[37,38]. The aerosol generated in the ablation process is measured with LA-ICP-MS and provides data about the inorganic sample constituents[39]. Attributes making LA-ICP-MS attractive for the analysis of trace elements in solid samples are the high sensitivity, reaching LODs in the range of $\mu g \cdot g^{-1}$ to $ng \cdot g^{-1}$, the large dynamic working range and the capability for multi-elemental analysis[40,41]. The combination of these laser based analytical techniques allows overcoming the above stated limitations of state-of-the-art polymer characterization techniques. Furthermore, the proposed procedure does not only allow the analysis of surface near sample regions, the ability to measure depth profiles provides also information about the distribution within the sample. The advantages of this tandem LA-ICP-MS/LIBS setup are demonstrated by the analysis of polymer samples from the fields of the semiconductor industry, cultural heritage science and environmental research. Derived findings are discussed in detail in the context of this work.

Experimental

Instrumentation and sample analysis. LA-ICP-MS measurements were carried out using an ESI NWR213 (Fremont, CA) laser ablation system operating at a wavelength of 213 nm coupled to an iCAP Qc ICP-MS system (ThermoFisher Scientific, Bremen, Germany) using PTFE tubing. The samples were ablated under a constant stream of helium (0.65 L/min). Argon was used as a make-up gas (1 L/min) before introducing the aerosol to the ICP-MS. Tuning of the instrument was carried out daily for maximum ^{115}In signal using a NIST612 glass standard (National Institute of Standards and Technology, Gaithersburg, MD). Data was collected using Qtegra 2.10 provided by the manufacturer of the instrument.

LIBS experiments were carried out using a commercially available LIBS J200 system (Applied Spectra, Inc., Fremont, CA). A frequency quadrupled Nd:YAG laser operating at a wavelength of 266 nm with a 5 ns pulse duration was used for ablation and excitation. Emitted radiation after each laser pulse was collected using two different collection optics connected to optical fibers: one collection optic optimized for UV-light (188–300 nm) and a second collection optic for the remaining part of the spectrum (300–1.048 nm). The collected light was analyzed using a Czerny-Turner spectrometer with 6 channels covering a total wavelength range from 188 to 1.048 nm. LIBS data was recorded using Axiom 2.0 software provided by the manufacturer of the instrument.

Tandem LA-ICP-MS/LIBS measurements were carried out by directly coupling the ablation chamber of the LIBS J200 system to the ICP-MS using PTFE tubing with a 3 mm inner diameter and a length of 1.2 m. He (0.6 L/min) was used as a carrier gas which was mixed with Ar (0.6 L/min) using a t-piece placed directly after the ablation chamber. This setup allows the simultaneous acquisition of LIBS, as well as ICP-MS data, increasing the total information obtained from each measurement.

For analysis using LA-ICP-MS, LIBS or Tandem LA-ICP-MS/LIBS the polymer samples of interest were fixed on high purity silicon wafers (Infineon Austria AG, Villach, Austria). The applied measurement parameters are described in detail in the respective results sections.

Crater depths obtained in depth profile measurements as well as coating thicknesses were determined using a profilometer (DektakXT, Bruker, Massachusetts, USA).

Reagents. 30% (v/v) H_2O_2 (p.a.) supplied by Merck (Darmstadt, Germany) was used for aging experiments of polystyrene samples. Artificial seawater (prepared as described by Kester et al.[43]) spiked with 10 ppb of Cd (ICP-multi elemental solution VIII in diluted HNO_3 obtained from Sigma–Aldrich, Buchs, Switzerland) was used for exposure of polystyrene samples. Metal-free water (resistivity 18.2 MΩ cm^{-1}) dispensed from a Barnstead EASYPURE II water system (ThermoFisher Scientific, Marietta) was used for sample rinsing and dilutions. H_2S (100 ppm), SO_2 (100 ppm) and synthetic air (5.0) used for weathering experiments was supplied by Messer, Austria. O_3 was produced using an ozonisator (Airmaster OMX 500, Topchem GmbH, Germany) with O_2 (5.0) supplied by Messer, Austria.

Weathering equipment. Accelerated stress tests were performed to cause degradation of the polymers as well as uptake of sulfur within the investigated samples. Therefore, samples were exposed to synthetic air in combination with corrosive gases (SO_2, H_2S and O_3) or UV light in two separate chambers. For weathering experiments with corrosive gases, a chamber (Bel-Art, SP Scienceware) with gas in- and outlets with a total volume of 30 cm^3 was used. To generate the desired concentration of corrosive gases, synthetic air is humidified using double-distilled water and mixed with the different gases. The chamber is continuously flushed with the gas mixture with a gas flowrate of 100 L/h. A detailed description of the weathering chamber is given by Wiesinger et al.[42]. For simulating artificial sunlight, an UVACUBE chamber (Dr Hönle GmbH, Germany) equipped with a xenon arc lamp with 170 W/m^2 was used.

Note that the detailed weathering procedure for each example of application (i.e. polyimide samples, paint samples and polystyrene samples) is described in the respective result and discussion sections.

Sample preparation. To demonstrate the broad application range of laser ablation techniques, three different polymer samples are investigated within this work.

Paint samples relevant in the field of cultural heritage science were prepared by casting a gravimetric 1:3 mixture of an inorganic pigment (manganese violet ($NH_4MnP_2O_7$, Kremer Pigmente, Germany) and an organic polymeric binder (Alkyd, Lukas Farben, Germany) on a glass slide. A total wet thickness of 150 μm was achieved. After preparation, the samples were dried for one week under ambient conditions, resulting in a final thickness of 100 μm. Note that these samples are referred to as paint samples from now on.

Standard polyimide samples (6 μm thickness) were provided by Infineon Technologies (Infineon Austria AG, Villach, Austria). Samples were cut into 10×10 mm^2 pieces. Note that these samples are referred to as polyimide samples from now on.

Polystyrene (PS) films with a thickness of 20 μm were obtained from Goodfellow Inc. (Hamburg, Germany). Samples were manually cut into 10×10 mm^2 pieces using ceramic scissors. Note that these samples are referred to as polystyrene samples from now on.

Results and discussion

For a complete characterization of aged polymers, information about the progress of polymer degradation but also about the absorption of pollutants from the environment is required. As reported in several studies, LIBS is a promising tool for the detection of degradation[44,45], whereas for the second task LA-ICP-MS has been applied[34,35]. However, in all of these works only bulk analyses have been performed. Within this study, polymer degradation and uptake of inorganic species will be analyzed as a function of the sample depth for the first time. In a first step the ability of LIBS and LA-ICP-MS to measure depth profiles has been exploited. Finally, the two analytical techniques were combined in a tandem LA-ICP-MS/LIBS approach.

Depth profiling of polymer degradation and oxidation using LIBS.
In this section, a LIBS method is developed that allows detection of polymer degradation as well as oxidation of the sample. The developed method is applied to perform depth profile investigations of aged paint samples.

As LIBS has already been used for (spatially resolved) polymer classification[36,46,47], it is a promising tool for the dectection of polymer degradation. LIBS inherently enables analysis of oxygen and should therefore also be able to detect oxidation of polymers. Additionally, other polymer specific LIBS signals may change due to degradation and aging of the sample, enabling measurement of polymer degradation.

Figure 1 shows a representative LIBS spectrum of the investigated unaged paint sample consisting of an inorganic pigment (manganese violet) and a polymeric binder (alkyd). Emission signals of both materials are found and marked in the representative LIBS spectrum.

In a preliminary set of experiments laser energy and gate delay were optimized for a high signal-to-noise ratio in the regions of interest of the LIBS spectrum. Emission signals of polymers observed in LIBS spectra usually consist of the atomic emission lines of the main components carbon, hydrogen, oxygen and nitrogen, where short gate delays yield higher signal-to-noise ratios. In addition, molecular emission signals (e.g. C_2 swan band) are observed, which are reported to appear sooner in the plasma and consequently require a short gate delay too[48]. Table 1 shows the optimized LIBS parameters.

LIBS measurements were carried out using patterns of 10 parallel line scans with a distance of 100 μm between each line and a total length of 2 mm each, resulting in 21 shots per line and 210 recorded spectra per pattern. For data evaluation, obtained LIBS spectra of each layer of each sample were averaged and the standard deviation was calculated. LIBS signals of interest were integrated and background correction was performed using the mean value of 5 neighboring pixels of the detector when integrating each emission signal.
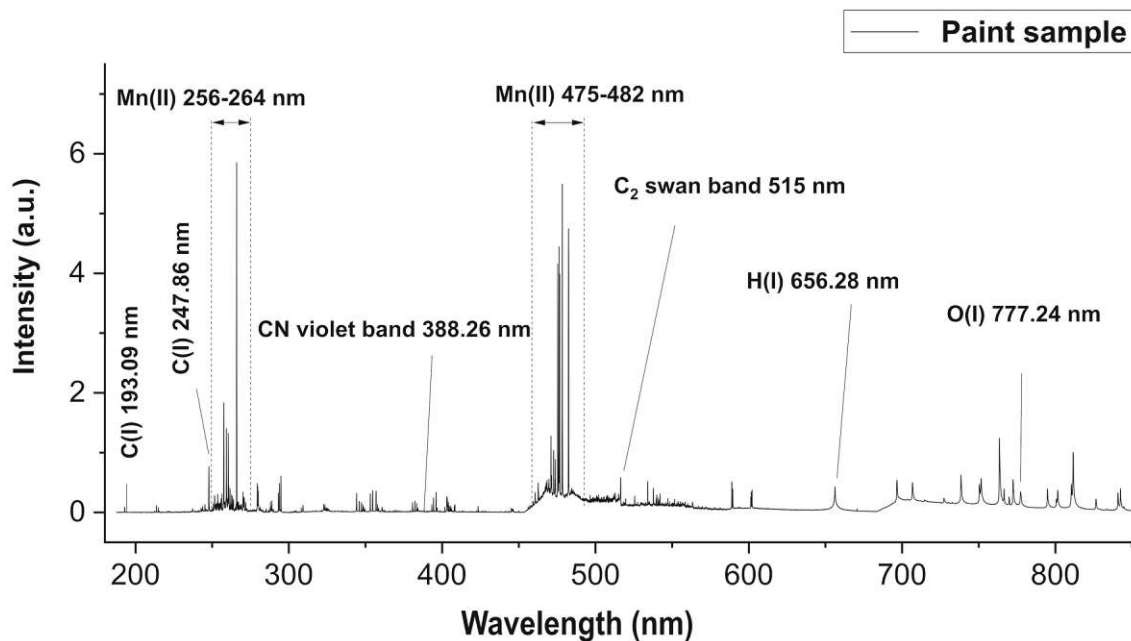
Figure 1. Representative LIBS spectrum of the investigated paint samples. Aside from polymer specific emission signals, signals from the inorganic pigment (manganese violet) are observed.

Laser system (Applied Spectra J200)	
Laser fluence (J/cm^2)	29.03
Laser spotsize (μm)	100
Laser repetition rate (Hz)	10
Laser beam geometry	Circular
Stage scan-speed (mm/s)	1
Atmosphere	Argon
Laser wavelength (nm)	266
Spectrometer system (Czerny-Turner)	
Detection channels	6
Gate delay (μs)	0.3
Gate width (ms)	1.05
Covered wavelength range (nm)	188–1048

Table 1. LIBS measurement parameters for paint samples.

Weathering parameters were especially focused on conditions conventionally used in the field of heritage science[49–51]. Paint samples with a thickness of 100 μm were weathered under two different conditions: To determine the degradation of polymers, one set of paint samples was exposed to UV radiation for 1 up to 6 weeks. To investigate the oxidation of polymers a second set of paint samples was weathered with a gas mixture containing 10 ppm O_3 (20 mg/m^3) and 10 ppm SO_2 (26 mg/m^3) and 80% relative humidity in synthetic air for 72 h.

Paint samples exposed to UV radiation for 1 up to 6 weeks were used to evaluate the applicability of LIBS to detect polymer degradation. The surface of these samples was analyzed using FT-IR spectroscopy (LUMOS, MCT detector, BRUKER Optik GmbH, Germany) and in accordance to literature[51–53] the main characteristic polymer absorbance bands (C–H stretch at 2930 cm^{-1}, C=O stretch at 1730 cm^{-1}, and C-O stretch at 1100 cm^{-1}) were used to evaluate polymer degradation over aging time. Figure 2 shows the sum of the characteristic polymer FT-IR signal over the aging time of 6 weeks. A significant decrease of the FT-IR signal is observed for increased aging time. The same samples were also analyzed using the developed LIBS procedure. For data interpretation the C_2 swan band intensity, derived via accumulation of the 210 recorded spectra per sample pattern, is plotted against the aging time (Fig. 2). As the trend of obtained LIBS results is in good agreement with the trend of FT-IR measurements, it is confirmed that LIBS can be used to detect polymer degradation.

In a next step, depth profiles of paint samples exposed to a mixture of 50 ppm O_3 (38 mg/m^3) and SO_2 (131 mg/m^3) for 72 h are analyzed using LIBS. For depth profile measurements the applied multiple line patterns were repeated 12 times at the same position, resulting in a total depth of 95 μm and a thickness of approximately 6.7 μm per layer. Using the C_2 swan band, it is now possible to investigate the propagation of the degradation into the sample. Depth profile measurements comparing the aged sample to an unaged sample are shown in
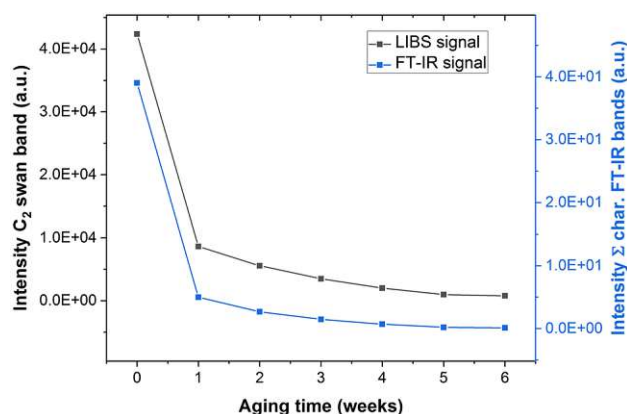
Figure 2. Trend of polymer degradation on the sample surface of paint samples aged for 1 up to 6 weeks detected with FT-IR (sum of C-H stretch at 2930 cm^{-1}, C=O stretch at 1730 cm^{-1}, and C–O stretch at 1100 cm^{-1}) and detected using the C_2 swan band from LIBS measurements.
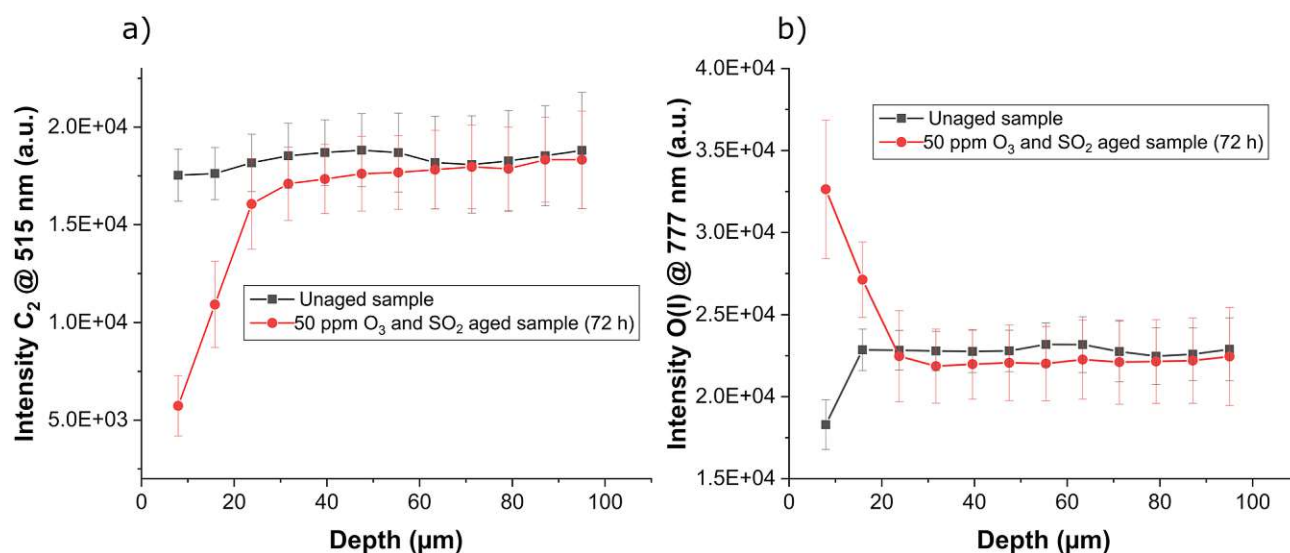
Figure 3. Depth profile measurement comparing a sample exposed to a mixture of 50 ppm O_3 and 50 ppm SO_2 for 72 h to an unaged sample: (**a**) Changes in the C_2 swan band are used to detect polymer degradation and (**b**) O emission signal indicates oxidation of the investigated paint sample. Average signals and standard deviations are calculated from 210 LIBS spectra recorded per layer.

Fig. 3a. Similar as observed for the sample aged with UV light, sample treatment with ozone results in decreased signal intensities for the C_2 swan band in the degraded sample region. Depth profiles reveal that degradation of the sample did not only occur on the sample surface, even for the second layer-corresponding to a depth of approximately 15 µm—significant differences compared to the reference samples was observed. In layer 3 the average intensity of the C_2 swan band seems still to be lower for the weathered sample, but this difference disappeared with increasing sample depths. However, weathering in the presence of ozone results not only in sample degradation, there is also the possibility of substantial sample oxidation. Thus, exposure to oxidizing gases should result in increased oxygen contents for the weathered samples. This is also confirmed using LIBS depth profiling. In Fig. 3b the findings for the oxygen emission intensities of aged and unaged reference samples are presented. Compared to the unaged sample a significant increase in the oxygen content was detected in the first two layers (approximately 15 µm) of the aged sample. This outcome is in good agreement with the findings of the C_2 swan band, indicating that the applied corrosive gases penetrated the first 20 µm of the investigated modern art material. Therefore, LIBS offers not only the possibility to analyse polymer degradation in depth but can also be employed to detect an increase of oxygen caused by oxidation within the sample. These results confirm that LIBS offers many benefits when it comes to analysis of polymer degradation.

Depth profiling of uptake of sulfur species in polymers using LA-ICP-MS. LA-ICP-MS is an analytical technique commonly reported in the literature for elemental depth profiling experiments[54,55] but has, to

LA system (NWR 213)	
Laser fluence (J/cm^2)	1.08
Laser spotsize (µm)	200
Laser repetition rate (Hz)	20
Laser beam geometry	Circular
Stage scan-speed (mm/s)	1
Atmosphere	He
Laser wavelength (nm)	213
ICP-MS (Thermo iCAP Q)	
Aux. gas flow (L/min)	0.8
Cool gas flow (L/min)	13
Dwell time per isotope (ms)	10
RF power (W)	1550
Cones	Ni
Measured isotopes	$^{13}C^+$, $^{29}Si^+$, $^{34}S^+$

Table 2. LA-ICP-MS measurement parameters for polyimide samples.

our knowledge, never been employed to investigate the uptake of corrosive species in polymers. In this section, we present LA-ICP-MS as a powerful analytical tool to investigate sulfur uptake within polyimides after weathering experiments. Investigations were focused on the impact of sulfur-dioxide and hydrogen-sulfide as these gases are more prominent in corrosion studies in semiconductor devices[56–58]. In a first set of experiments polyimide samples were exposed to 50 ppm H_2S (70 mg/m^3) with 80% relative humidity in synthetic air for 192 h. The second weathering experiment was conducted using 50 ppm SO_2 (131 mg/m^3) with 80% relative humidity in synthetic air for 192 h.

The uptake of these corrosive gases was measured using LA-ICP-MS. Measurement parameters were optimized carefully in preliminary experiments for maximum depth resolution while maintaining a high sensitivity for sulfur (Table 2). As the main isotopes of sulfur and silicon ^{32}S and ^{28}Si are interfered by $^{16}O^{16}O$ and $^{14}N^{14}N$ respectively, elements which are both present in the investigated sample, the less abundant isotopes ^{34}S and ^{29}Si were selected for ICP-MS anaylsis.

Depth profiles of the weathered polyimide samples were carried out by measuring subsequent line scans with a total length of 6 mm repeatedly on the same position for 14 times. Considering a mean ablation rate of around 420 nm per measured line this results in full penetration of the 6 µm tick polyimide film after the last line (indicated by an increase of $^{29}Si^+$ signal). Obtained transient signals were averaged and used for further data evaluation. Averaged $^{34}S^+$ signals were normalized to $^{13}C^+$ to compensate for instrumental drifts during the measurement. Even though this approach is discussed controversially for quantitative measurements in the field of elemental bio-imaging[59], we believe that it can be used for the correction of instrumental drifts in this work. Especially when considering that the investigated polymer represents a rather homogeneous composition compared to biological tissue samples consisting of various carbonaceous species. Average signals and standard deviations are calculated from three consecutive measurements on the same sample. Depth profiles of sulfur uptake of the investigated polyimide samples exposed to H_2S, SO_2 and an unaged reference sample are shown in Fig. 4.

Between the polyimide sample exposed to H_2S and the unaged reference sample, no significant differences in the $^{34}S^+/^{13}C^+$ signal ratios were found, whereas weathering the sample with SO_2 results in a significant uptake of sulfur. Moreover, it was shown that the uptake is enhanced for surface near regions, and decreases with sample depth. Nevertheless, the substantial sulfur signal measured in the polyimide film near the silicon indicates a complete penetration of the polymer by the gas and thus insufficient protection of the underlying material. Obtained results demonstrate the high potential of LA-ICP-MS for the investigation of uptake of inorganic species in polymers.

Tandem LA-ICP-MS/LIBS analysis: combining depth profiling of oxidation and trace metal uptake. Results presented in the previous sections demonstrate that LA-ICP-MS/LIBS offer many advantages in terms of polymer analysis compared to conventional analytical techniques, in particular because the spatially resolved analysis of polymer degradation and uptake of contaminants is possible. As both techniques enable investigations with unique features (e.g. high sensitivity for inorganic species, capability to detect degradation and increase of oxygen), combining both techniques in a tandem LA-ICP-MS/LIBS setup should enable a more complete characterization of polymeric samples.

Development of a tandem LA-ICP-MS/LIBS approach, where polymer specific LIBS signals as well as signals from inorganic species are acquired simultaneously, is presented in the following section. Therefore, polystyrene films which served as a synthetic substitute for microplastics were aged using UV radiation and H_2O_2. Afterwards the films were exposed to cadmium dissolved in artificial sea water. A tandem LA-ICP-MS/LIBS system was employed to simultaneously investigate the polymer oxidation caused by UV and H_2O_2 aging as well as the uptake of cadmium.

For tandem LA-ICP-MS/LIBS measurements, laser parameters have to be optimized taking into account the higher laser fluence typically used for LIBS measurements. Therefore, the laser energy was optimized in
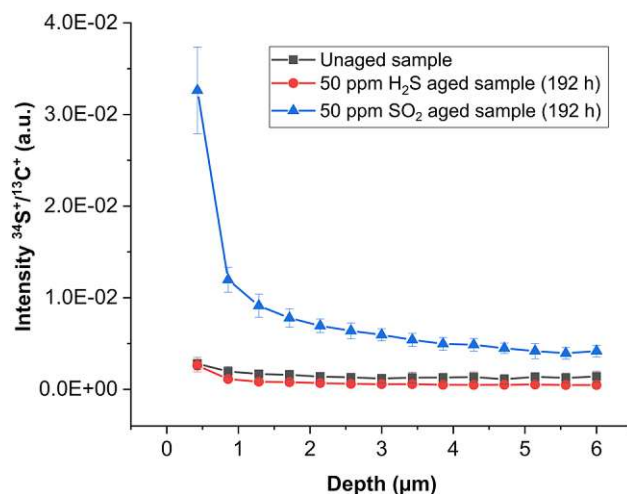
Figure 4. LA-ICP-MS depth profiles of the investigated polyimide sample showing different sulfur uptake depending on the gas used for weathering. Average signals and standard deviations are calculated from three consecutive measurements on the same sample.

LIBS system (J200)	
Laser fluence (J/cm^2)	8.91
Laser spotsize (µm)	100
Laser repetition rate (Hz)	10
Laser beam geometry	circular
Stage scan-speed (mm/s)	1
Atmosphere	He
Laser wavelength (nm)	266
Detection channels	6
Gate delay (µs)	0.3
Gate width (ms)	1.05
Covered wavelength range (nm)	188–1048
ICP-MS (Thermo iCAP Q)	
Aux. gas flow (L/min)	0.8
Cool gas flow (L/min)	13
Dwell time per isotope (ms)	10
RF power (W)	1550
Cones	Ni
Measured isotopes	$^{13}C^+$, $^{114}Cd^+$

Table 3. Tandem LA-ICP-MS/LIBS measurement parameters for polystyrene.

preliminary experiments to obtain good depth resolution while maintaining adequate LIBS signal intensity. Tandem LA-ICP-MS/LIBS measurement parameters are shown in Table 3. Depth profiles were recorded by subsequent ablation of line scans with a total length of 2 mm. Penetration of the 20 µm thick samples was achieved after 6 ablated line scans resulting in a depth resolution of 3.3 µm.

One side of the polystyrene films was aged for 4 weeks by the combined exposure to UV radiation and 30% (v/v) H_2O_2 H_2O_2 was repeatedly reapplied to the sample surface to avoid complete evaporation of the liquid. Subsequently, aged samples and unaged blank samples were submerged and exposed from both sides to artificial seawater spiked with 10 ppb of Cd After an exposure time of 24 h, samples were separated from the solution and rinsed with metal-free water to remove remaining droplets of artificial sea water. After a drying step with synthetic air the samples were measured using the developed Tandem LA-ICP-MS/LIBS procedure.

Depth profiles from simultaneous analysis of Cd using ICP-MS and oxygen using LIBS are shown in Fig. 5. Compared to the unaged sample ICP-MS depth profiles reveal an increase of Cd at the aged side of the polystyrene film as well as a Cd diffusion gradient into the bulk of the aged polystyrene film. The unaged sample, which was not exposed to H_2O_2/UV radiation, shows only a small uptake of Cd. The unaged side of the aged sample shows the same uptake of Cd as the unaged sample. LIBS results reveal oxidation not only at the surface of the
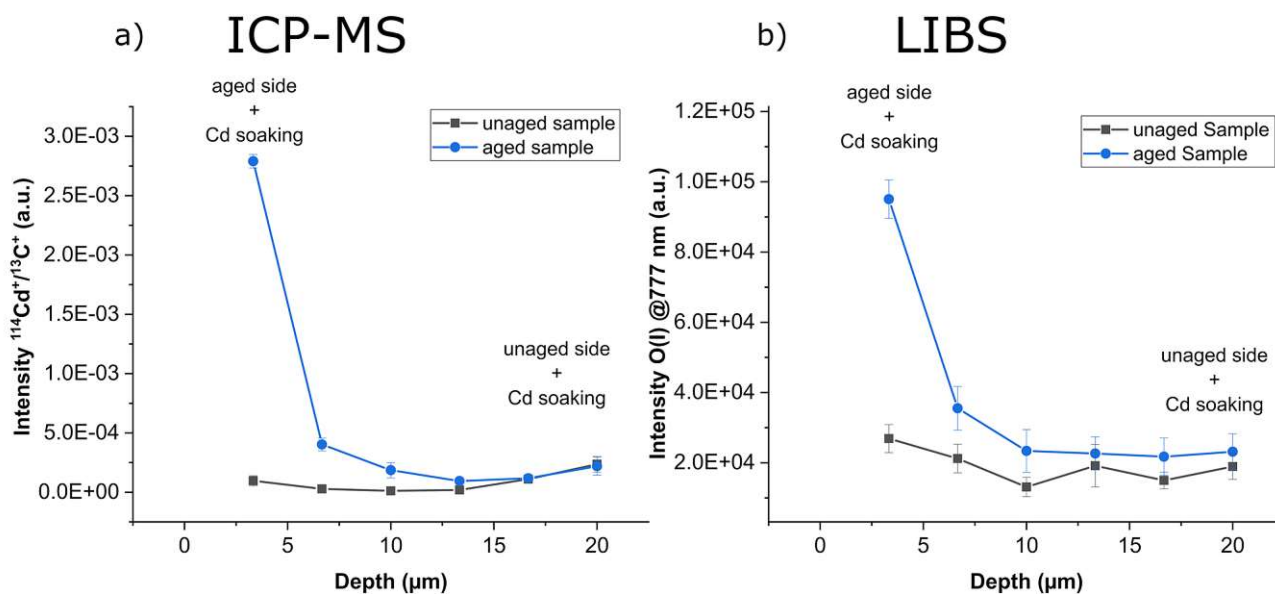
Figure 5. Depth profiles of an aged and an unaged polystyrene sample analyzed using a tandem LA-ICP-MS/LIBS setup: (**a**) shows the obtained depth profile of [114]Cd detected with ICP-MS and (**b**) shows uptake of O detected with LIBS indicating oxidation of the sample.

aged side of the aged sample but also 5 µm into depth. The opposite side does not show a significant increase of oxygen signal.

Summing up, the proposed tandem approach delivers the desired benefits in the characterization of degraded polymers. Nevertheless, it should be mentioned that laser systems that are usually employed for LIBS analysis are typically operated with higher laser fluence and longer wavelength (266 nm in this work). Compared to LA-ICP-MS, where a laser system operating at a wavelength of 213 nm was used this leads to more material being ablated with each laser shot, resulting in a decrease of the obtained depth resolution.

Conclusion

In this work, laser based analytical techniques, namely LA-ICP-MS and LIBS were employed to investigate their applicability to study the behavior of various polymeric samples exposed to corrosive and degrading conditions. In contrast to techniques traditionally used for polymer characterization, LA-ICP-MS and LIBS offer trace element analysis as well as depth profiling. Additionally, LIBS inherently enables the detection of oxygen which can be used to detect oxidation of polymeric samples and also offers polymer specific signals which can be used to detect polymer degradation. These advantages were applied to 3 different examples covering a wide range of polymer applications demonstrating the beneficial information these laser-based techniques have to offer. Depth profiling of sulfur uptake in high-performance polyimides was investigated using LA-ICP-MS. Degradation of polymeric pigment binder mixtures from the field of cultural heritage science was analyzed using LIBS.

Besides conventional LA-ICP-MS and LIBS depth profiling, a tandem approach is also evaluated where signals of both techniques are acquired simultaneously. The obtained results from the tandem LA-ICP-MS/LIBS analysis show that the employment of such a measurement setup is beneficial to study the behavior of polymers under corrosive and degrading conditions. The measured uptake of the toxic trace metal Cd could be directly correlated with the information obtained for degradation and oxidation of the polymer sample.

Although the qualitative findings obtained in this feasibility study offer new and valuable information, future work will be focused on the collection of quantitative data to further improve existing knowledge about polymer degradation. Moreover, ongoing research will be devoted to enhancing the depth resolution of LIBS and tandem LA-ICP-MS/LIBS measurements, which is a precondition for the investigation of thin polymer films.

Data availability

The datasets generated during and/or analyzed during the current study are available from the corresponding author on reasonable request.

References

1. *Plastics Europe. Plastics - the facts 2019*. https://www.plasticseurope.org/application/files/9715/7129/9584/FINAL_web_version_Plastics_the_facts2019_14102019.pdf (2019).
2. Akovali, G. *Polymers in Construction* (Rapra Technology Limited, Column House, 2005).
3. Hayakawa, A., Murata, Y., Nakanishi, Y. & Tohriiwa, N. Epoxy resin composition for semiconductor encapsulation. (1998).

4. Kinjo, N., Ogata, M., Nishi, K., Kaneda, A. & Dušek, K. Epoxy Molding Compounds as Encapsulation Materials for Microelectronic Devices. in *Speciality Polymers/Polymer Physics* (eds. Godovsky, Yu. K. et al.) 1–48 (Springer Berlin Heidelberg, 1989).

5. Institute, G. C. *Modern Paints Uncovered: Proceedings from the Modern Paints Uncovered Symposium* (Getty Publications, Los Angeles, 2007).

6. Lodge, R. G. A history of synthetic painting media with special reference to commercial materials. *Preprints of Papers Presented at the Sixteenth Annual Meeting of the AIC. New Orleans,* 118–127 (1988).

7. Göpferich, A. Mechanisms of polymer degradation and erosion. *Biomaterials* **17**, 103–114 (1996).

8. Grassie, N. & Scott, G. *Polymer Degradation and Stabilisation* (CUP Archive, Cambridge, 1988).

9. Hamid, S. H. *Handbook of Polymer Degradation* (CRC Press, Boca Raton, 2000).

10. Jacobsen, J. B., Krog, J. P., Rimestad, L., Riis, A. & Holm, A. H. Climate-protective packaging: using basic physics to solve climatic challenges for electronics in demanding applications. *IEEE Ind. Electron. Mag.* **8**, 51–59 (2014).

11. Ambat, R., Jensen, S. G. & Møller, P. H. Corrosion reliability of electronic systems. *ECS Trans.* https://doi.org/10.1149/1.2900650 (2008).

12. Valdez Salas, B. *et al.* Copper corrosion by atmospheric pollutants in the electronics industry. *ISRN Corros.* **2013**, 1–7 (2013).

13. Minzari, D., Jellesen, M. S., Møller, P. & Ambat, R. Morphological study of silver corrosion in highly aggressive sulfur environments. *Eng. Fail. Anal.* **18**, 2126–2136 (2011).

14. Schueller, R. Creep Corrosion on lead-free printed circuit boards in high sulfur environments. in *SMTA International Conference* 643–654 (2007).

15. Mass, J. *et al.* SR-FTIR imaging of the altered cadmium sulfide yellow paints in Henri Matisse's Le Bonheur de vivre (1905–6)—examination of visually distinct degradation regions. *Analyst* **138**, 6032–6043 (2013).

16. Manfredi, M., Barberis, E. & Marengo, E. Prediction and classification of the degradation state of plastic materials used in modern and contemporary art. *Appl. Phys. A* **123**, 35 (2016).

17. Izzo, F. C., van den Berg, K. J., van Keulen, H. & Ferriani, B. Zendri E (2014) Modern oil paints—formulations, organic additives and degradation: some case studies. In *Issues in Contemporary Oil Paint* (eds van den Berg, K. J. *et al.*) 75–104 (Springer, Berlin, 2014). https://doi.org/10.1007/978-3-319-10100-2_5.

18. Cole, M., Lindeque, P., Halsband, C. & Galloway, T. S. Microplastics as contaminants in the marine environment: a review. *Mar. Pollut. Bull.* **62**, 2588–2597 (2011).

19. Turner, A. & Holmes, L. A. Adsorption of trace metals by microplastic pellets in fresh water. *Environ. Chem.* **12**, 600–610 (2015).

20. Holmes, L. A., Turner, A. & Thompson, R. C. Adsorption of trace metals to plastic resin pellets in the marine environment. *Environ. Pollut.* **160**, 42–48 (2012).

21. Ashton, K., Holmes, L. & Turner, A. Association of metals with plastic production pellets in the marine environment. *Mar. Pollut. Bull.* **60**, 2050–2055 (2010).

22. Wilkie, C. A. TGA/FTIR: an extremely useful technique for studying polymer degradation. *Polym. Degrad. Stab.* **66**, 301–306 (1999).

23. Trchová, M., Šeděnková, I., Tobolková, E. & Stejskal, J. FTIR spectroscopic and conductivity study of the thermal degradation of polyaniline films. *Polym. Degrad. Stab.* **86**, 179–185 (2004).

24. Bhargava, R., Wang, S.-Q. & Koenig, J. L. FTIR Microspectroscopy of PolymericSystems. In *Liquid Chromatography/FTIR Microspectroscopy/MicrowaveAssisted Synthesis 137–191* (ed. Kausch, H.) (Springer, Berlin, 2013). https://doi.org/10.1007/b11052.

25. Lenz, R., Enders, K., Stedmon, C. A., Mackenzie, D. M. A. & Nielsen, T. G. A critical assessment of visual identification of marine microplastic using Raman spectroscopy for analysis improvement. *Mar. Pollut. Bull.* **100**, 82–91 (2015).

26. Li, L. *MALDI Mass Spectrometry for Synthetic Polymer Analysis* (Wiley, Hoboken, 2009).

27. Rial-Otero, R., Galesio, M., Capelo, J.-L. & Simal-Gándara, J. A Review of synthetic polymer characterization by Pyrolysis–GC–MS. *Chromatographia* **70**, 339–348 (2009).

28. Liu, X. & Yu, W. Evaluating the thermal stability of high performance fibers by TGA. *J. Appl. Polym. Sci.* **99**, 937–944 (2006).

29. Celina, M. C. Review of polymer oxidation and its relationship with materials performance and lifetime prediction. *Polym. Degrad. Stab.* **98**, 2419–2429 (2013).

30. Pereira, J. S. F. *et al.* Evaluation of sample preparation methods for polymer digestion and trace elements determination by ICPMS and ICPOES. *J. Anal. At. Spectrom.* **26**, 1849–1857 (2011).

31. Flores, E. M. M., Muller, E. I., Duarte, F. A., Grinberg, P. & Sturgeon, R. E. Determination of Trace Elements in Fluoropolymers after Microwave-Induced Combustion. *Anal. Chem.* **85**, 374–380 (2013).

32. Resano, M., Aramendía, M., Devos, W. & Vanhaecke, F. Direct multi-element analysis of a fluorocarbon polymer via solid sampling-electrothermal vaporization-inductively coupled plasma mass spectrometry. *J. Anal. At. Spectrom.* **21**, 891–898 (2006).

33. Börno, F., Richter, S., Deiting, D., Jakubowski, N. & Panne, U. Direct multi-element analysis of plastic materials via solid sampling electrothermal vaporization inductively coupled plasma optical emission spectroscopy. *J. Anal. At. Spectrom.* **30**, 1064–1071 (2015).

34. Villaseñor, Á, Boccongelli, M. & Luis Todolí, J. Quantitative elemental analysis of polymers through laser ablation—inductively coupled plasma by using a dried droplet calibration approach. *DDCA. J. Anal. At. Spectrom.* **33**, 1173–1183 (2018).

35. Voss, M. *et al.* A new approach to calibration and determination of selected trace elements in food contact polymers by LA-ICP-MS. *Talanta* **170**, 488–495 (2017).

36. Liu, K. *et al.* A review of laser-induced breakdown spectroscopy for plastic analysis. *TrAC Trends Anal. Chem.* **110**, 327–334 (2019).

37. Banaee, M. & Tavassoli, S. H. Discrimination of polymers by laser induced breakdown spectroscopy together with the DFA method. *Polym. Test.* **31**, 759–764 (2012).

38. Unnikrishnan, K. *et al.* Analytical predictive capabilities of Laser Induced breakdown spectroscopy (LIBS) with principal component analysis (PCA) for plastic classification. *RSC Adv.* **3**, 25872–25880 (2013).

39. Bonta, M. & Limbeck, A. Metal analysis in polymers using tandem LA-ICP-MS/LIBS: eliminating matrix effects using multivariate calibration. *J. Anal. At. Spectrom.* **33**, 1631–1637 (2018).

40. Koch, J. & Günther, D. Review of the state-of-the-art of laser ablation inductively coupled plasma mass spectrometry. *Appl. Spectrosc.* **65**, 155–162 (2011).

41. Limbeck, A. *et al.* Recent advances in quantitative LA-ICP-MS analysis: challenges and solutions in the life sciences and environmental chemistry. *Anal. Bioanal. Chem.* **407**, 6593–6617 (2015).

42. Wiesinger, R., Schreiner, M. & Kleber, Ch. Investigations of the interactions of CO2, O3 and UV light with silver surfaces by in situ IRRAS/QCM and ex situ TOF-SIMS. *Appl. Surf. Sci.* **256**, 2735–2741 (2010).

43. Kester, D. R., Duedall, I. W., Connors, D. N. & Pytkowicz, R. M. Preparation of Artificial Seawater1. *Limnol. Oceanogr.* **12**, 176–179 (1967).

44. Farhadian, A. H. *et al.* A novel approach for investigation of chemical aging in composite propellants through laser-induced breakdown spectroscopy (LIBS). *J. Therm. Anal. Calorim.* **124**, 279–286 (2016).

45. Liang, D. *et al.* Degradation of polyacrylate in the outdoor agricultural soil measured by FTIR-PAS and LIBS. *Polymers* **10**, 1296 (2018).

46. Anzano, J. M., Bello-Gálvez, C. & Lasheras, R. J. Identification of Polymers by Means of LIBS. In *Laser-Induced Breakdown Spectroscopy: Theory and Applications 421–438* (eds Musazzi, S. & Perini, U.) (Springer, Berlin, 2014). https://doi.org/10.1007/978-3-642-45085-3_15.

47. Brunnbauer, L., Larisegger, S., Lohninger, H., Nelhiebel, M. & Limbeck, A. Spatially resolved polymer classification using laser induced breakdown spectroscopy (LIBS) and multivariate statistics. *Talanta* https://doi.org/10.1016/j.talanta.2019.120572 (2019).
48. Grégoire, S. *et al.* Laser-induced breakdown spectroscopy for polymer identification. *Anal. Bioanal. Chem.* **400**, 3331–3340 (2011).
49. López-Aparicio, S. *et al.* Measurement of organic and inorganic pollutants in microclimate frames for paintings. *E-Preserv. Sci.* **7**, 59–70 (2010).
50. Blades, N., Oreszczyn, T., Cassar, M. & Bordass, W. *Guidelines on pollution control in museum buildings* (Museums Association, London, 2000).
51. Pintus, V., Wei, S. & Schreiner, M. Accelerated UV ageing studies of acrylic, alkyd, and polyvinyl acetate paints: Influence of inorganic pigments. *Microchem. J.* **124**, 949–961 (2016).
52. Anghelone, M., Jembrih-Simbürger, D. & Schreiner, M. Influence of phthalocyanine pigments on the photo-degradation of alkyd artists' paints under different conditions of artificial solar radiation. *Polym. Degrad. Stab.* **134**, 157–168 (2016).
53. Wiesinger, R. *et al.* Pigment and binder concentrations in modern paint samples determined by ir and raman spectroscopy. *Angew. Chem. Int. Ed.* **57**, 7401–7407 (2018).
54. Panighello, S., Van Elteren, J. T., Orsega, E. F. & Moretto, L. M. Laser ablation-ICP-MS depth profiling to study ancient glass surface degradation. *Anal. Bioanal. Chem.* **407**, 3377–3391 (2015).
55. Fehrenbacher, J. S., Spero, H. J., Russell, A. D., Vetter, L. & Eggins, S. Optimizing LA-ICP-MS analytical procedures for elemental depth profiling of foraminifera shells. *Chem. Geol.* **407–408**, 2–9 (2015).
56. Lopez, G., Valdez, B. & Schorr, M. Chapter13: H2S Pollution and Its Effect on Corrosion of Electronic Components. In *Air Quality: New Perspective* (eds Badilla, G. L. *et al.*) (BOD—Books on Demand, Norderstedt, 2012).
57. SungSoon C. & ByungJin M. Corrosive tendency of Ag plated lead frame applied to white LED. in *18th IEEE International Symposium on the Physical and Failure Analysis of Integrated Circuits (IPFA)* 1–3 (2011). https://doi.org/10.1109/IPFA.2011.5992736.
58. Jellesen, M. S., Verdingovas, V., Conseil, H., Piotrowska, K. & Ambat, R. Corrosion in electronics: Overview of failures and countermeasures. In *Proceedings EuroCorr 2014* (2014).
59. Frick, A. & Günther, D. Fundamental studies on the ablation behaviour of carbon in LA-ICP-MS with respect to the suitability as internal standard. *J. Anal. At. Spectrom.* **27**, 1294–1303 (2012).

Acknowledgements

Author contributions

L.B., S.L., M.N. and A.L. conceived the presented study. R.W. performed weathering experiments with UV radiation, SO_2, H_2S and O_3. L.B. carried out LIBS and tandem LA-ICP-MS/LIBS measurements and did the corresponding data evaluation. M.M performed LA-ICP-MS measurements and carried out the corresponding data evaluation. L.P. prepared paint samples and did the FT-IR measurements. A.L., S.L., R.W. and M.S. were involved and supervised the work. L.B. wrote the manuscript in consultation with M.M., S.L., M.N., L.P., R.W., M.S. and A.L.

Competing interests

The authors declare no competing interests.

Additional information

Correspondence and requests for materials should be addressed to L.B. or A.L.

Reprints and permissions information is available at www.nature.com/reprints.

Publisher's note Springer Nature remains neutral with regard to jurisdictional claims in published maps and institutional affiliations.

Paper V

SO₂- and NOₓ- initiated atmospheric degradation of polymeric films: Morphological and chemical changes, influence of relative humidity and inorganic pigments

Laura Pagnin, Rosalba Calvini, Rita Wiesinger, Manfred Schreiner

SO$_2$- and NO$_x$- initiated atmospheric degradation of polymeric films: Morphological and chemical changes, influence of relative humidity and inorganic pigments

Laura Pagnin [a,*], Rosalba Calvini [b], Rita Wiesinger [a], Manfred Schreiner [a,c]

[a] *Academy of Fine Arts Vienna, Institute of Science and Technology in Art, Schillerplatz 3, 1010 Vienna, Austria*
[b] *University of Modena and Reggio Emilia, Department of Life Sciences, Via Amendola 2, 42122 Reggio Emilia, Italy*
[c] *Technische Universität Wien, Institute of Chemical Technologies and Analytics, Getreidemarkt 9/164, 1060 Vienna, Austria*

ABSTRACT

The influence of polluting gases on the stability of polymeric films has not been studied extensively. In fact, the chemical interactions of such materials in contact with the ambient atmosphere depend on different factors such as the environmental conditions, the manufacturing process of the product, the presence of additives or various pigments. In this study, accelerated artificial gas ageing was carried out. The experiments were performed in a gas chamber exposing the samples to sulphur dioxide (SO$_2$) and nitrogen oxide (NO$_x$) with a concentration of 15 ppm. The relative humidity (RH) content chosen was 50% and 80% for a total of 168 h of gas exposure. The paint samples under investigation were composed of three different binding media (acrylic, alkyd, and styrene-acrylic) with various inorganic pigments. The morphological changes on the sample surface due to the different impact of the pollutant gases were investigated using a 3D microscope. Moreover, qualitative and semi-quantitative analyses were performed by Fourier-Transform Infrared (ATR-FTIR) spectroscopy, focusing on the degradation reactions and surface mapping evaluation. In order to fully exploit the chemical information on these materials contained in the ATR-FTIR spectra, multivariate analysis was carried out. In particular, Principal Component Analysis (PCA) enabled verifying the main spectral differences between the unaged and aged samples. Moreover, Analysis-of-Variance-Simultaneous Component Analysis (ASCA) was carried out to understand the influence of gas type, relative humidity, and inorganic pigment type on the deterioration process of the binders.

1. Introduction

The knowledge of degradation processes of modern materials, linked to the chemical changes due to the pollutants in the ambient atmosphere, is still of current interest. The outdoor art materials are the most at risk, as the monitoring of environmental parameters, such as humidity, pollutants, or temperature, are not easily controlled and vary according to the different seasonal climatic changes [1]. The atmospheric degradation affects the stability of these materials, and it occurs mainly due to the interaction of the atmospheric constituents including humidity. In fact, water settles in a thin layer on these materials and, acting as a solvent, attracts the pollutants present in the air both gaseous and particulate matter [2]. The main gaseous air pollutants include sulphur dioxide (SO$_2$), nitrogen oxides (NO$_x$), ozone (O$_3$), and particulate matter (PM). The latter two were not considered in this study,

however, they also significantly affect artworks. Ozone, being present at high levels in urban areas, is one of the most oxidising pollutants found in nature. Its effect on artwork, combined with sunlight, oxygen, and other pollutants, was tested on different art materials such as watercolours [3], metals, stones, and polymeric binders [4], showing different interactions and physical–chemical reactions depending on the material. A similar deteriorating influence was also evaluated for atmospheric particulate matter [5]. However, being composed of a mixture of solid and liquid particles suspended in the air, and having particles that vary in size and composition, its deteriorating effect changes depending on the art material [6].

SO$_2$ and NO$_x$, as reported in the literature [7], have different characteristics: SO$_2$ is released from the combustion of fossil fuels and the metal refining process, resulting in one of the most important polluting gases present in the atmosphere, whereas, NO$_x$ is produced from both

natural and anthropogenic sources, but also the combustion processes. Generally, in the air, it contributes to the formation of other air pollutants and, combined with SO_2, forms the so-called acid rain. Although the concentration of these gases in the air has slowly been decreasing over the last decades, their oxidizing effects affected the early 20th century and older artworks. Studies on different artworks such as stone materials [8] and metals [9] exposed to outdoor environmental agents confirm the presence of sulphates and nitrates on the surfaces. They caused multiple degradation effects as morphological deformations and dry corrosive deposits that, once in contact with water (as rain or high humidity) can dissolve penetrating into the material and causing aesthetic and mechanical damages. While many studies focus on the influence of those gases on traditional art materials [10], the knowledge of the interaction of modern synthetic polymers with those gases is still rudimentary. Some artificial gas ageing studies were already carried out by testing materials similar to those under investigation, but including a stone or metal ground [11–14]. However, the experimental setup presented in this study combined with innovative chemometric methods represents an interesting analytical approach for the evaluation of the chemical behaviour that each polymeric binder develops when exposed to different gaseous pollutants. Moreover, their investigation can be of support for the storage and display practices of artworks in museum environments. Their concentration levels require continuous monitoring to allow an adequate prevention action of more sensitive artistic objects [15].

In this study, the impact of SO_2 and NO_x on the degradation behaviour of modern synthetic polymers was investigated. Alkyd resins, acrylics, and styrene-acrylic emulsions, represent the principal organic binding media used in modern and contemporary art, mainly used in the 20th century but also recently applied in the field of conservation-restoration. Alkyd resins became the modern substitutes of traditional oil painting due to their low-costs, fast-drying, the possibility to employ it with a great variety of pigments, and its excellent optical properties [16]. However, acrylic emulsions became the most common and versatile polymer. Initially, it was used in industry as a plastic material for structural applications. Subsequently, it was possible to develop a more flexible and transparent polymer due to the possibility to add two or more acrylic monomers within the same polymer chain. Its stability, excellent mechanical properties, and rapid drying have made it attractive for artists too. The application and use of these two binders expanded into various other sectors such as coatings for furniture and architectural, product finishes, or for special coatings in the automotive sector. Furthermore, their chemical-physical properties make them suitable for the protection of various materials such as metals, wood, or other plastics from corrosive agents [17].

During the last years of technological development, monomers were added to the acrylic emulsions in order to lower the production costs and to improve its chemical-physical performances, creating new synthetic binders such as styrene-acrylic emulsions. In recent years, this synthetic polymer was widely applied in the coating industry as well as in the artistic field, especially for spray paints and contemporary murals [18]. To study the different influence that gas pollutants have on the degradation of polymers, an accelerated gas ageing study was performed, using synthetic air containing sulphur dioxide (SO_2) and nitrogen oxide (NO_x) combined with different relative humidity (RH%) contents for a total exposure period of 168 h. The samples under investigation were paint mixtures of three different binding media (acrylic, alkyd, and styrene-acrylic) in mixture with nine inorganic pigments. These pigments were chosen because still present in formulations of paint tubes, and their employment is documented also in previous centuries. Therefore, being present both in recent contemporary artworks and in modern ones (since 1800), it is important to study their effects for the long-term stability of artworks [19–22]. The study focused on the application of 3D microscope and ATR-FTIR analysis to investigate degradation products according to the different gas and RH employed. This investigation allowed understanding which binder is more prone to

degradation due to gas exposure and which inorganic pigment increases or decreases this effect.

Multivariate statistical analysis of spectroscopic data is becoming an established tool in the field of cultural heritage studies thanks to the ability of these methods to extract the useful information from the analysed data and to find patterns in the spectral response related to the phenomena under investigation [23–26]. In the conservation of cultural heritage, the combination of spectroscopic techniques and chemometrics allows to monitor in a non-destructive manner the deterioration processes of the analysed samples and to gain a comprehensive evaluation of the modifications occurring during degradation [27,28]. This information can be further exploited for age estimation of artworks or to select the proper pigments to be used to artwork restoration [29,30].

For these reasons, in this study multivariate data analysis of the FTIR spectra based on Principal Component Analysis (PCA) and Analysis-of-Variance-Simultaneous Component Analysis (ASCA) were performed to support the chemical information obtained from the FTIR mapping and enabled verifying spectral differences between unaged and aged samples, as well as evaluating the influence of pollutant gases, relative humidity, and inorganic pigments. Having a general overview of the chemical-physical reactions occurring during the surface degradation of materials, it is essential to develop and apply new strategies that can monitor and prevent future deterioration processes.

2. Materials and methods

2.1. Sample preparation

Different samples were prepared by mixing pure acrylic emulsion Plextol® D498 (Kremer Pigmente, Germany), Alkyd Medium 4 (Lukas®, Germany), and styrene-acrylic binder Acronal S790 (BASF, Germany) in combination with 9 inorganic pigments (Kremer Pigmente, Germany). The pigment/binder (P/BM) ratio chosen was 1:3 in weight according to commercial formulations, which guarantee a homogenous mixture with optimum consistency and colourfulness. After mixing them with a ceramic mortar, the fresh paints were cast on glass slides with a film thickness of 150 μm using the so-called Doctor-Blade procedure [31]. The samples were dried at ambient conditions (approx. 22 °C and 30% RH) for three weeks. Mock-ups with pure binders were also prepared (150 paint samples in total). The paint materials investigated are listed in Table 1.

Table 1
List of materials analysed.

Pigments	Chemical composition	Colour Index (C.I.) number
Titanium white	TiO_2	PW6
Cadmium yellow	CdS	PY37
Cobalt green	Co_2TiO_4	PG50
Hydrated chromium oxide green	$Cr_2O_3 \cdot 2H_2O$	PG18
Cobalt blue	$CoO \cdot Al_2O_3$	PB28
Cerulean blue	$CoSnO_3$	PB35
Artificial ultramarine blue	$Na_{8-10}Al_6Si_6O_{29}S_{2-4}$	PB29
Iron oxide red	Fe_2O_3	PR101
Manganese violet	$NH_4MnP_2O_7$	PV16
Binders	**Chemical composition**	**Commercial Name**
Acrylic emulsion (Alk)	p(nBA/MMA)	Plextol® D498
Alkyd resin (Acr)	Polymer oil-modified polyester-resin	Alkyd Medium 4
Styrene-acrylic emulsion (Sty)	Styrene acrylate copolymer	Acronal® S790

2.2. Weathering experiments

The weathering system used for the atmospheric exposure experiments consists of two parts: the system for mixing synthetic air with corrosive gases [32], and the weathering chamber for gas exposure. To generate the desired concentration of corrosive gases, synthetic air 5.0 (Messer, Austria) is humidified using double-distilled water and mixed with the selected gas. The chamber is continuously flushed with the gas mixture with a gas flow rate of 100 L/h. The chamber (Bel-Art™SP Scienceware™) is made of a co-polyester glass (Purastar®) including gas in- and outlets with a total volume of 30 cm^3. The samples were aged for 168 h. The relative humidity (RH) content chosen was 50 and 80%, whereas the gas concentration selected was 15 ppm both for SO_2 and NO_x. The gas concentration was monitored daily during the artificial ageing using a specific gas sensor for SO_2 and NO_x detection (Aeroqual Limited, New Zealand, model AQL S200). During the ageing experiments, the value could vary by ± 1–0.5 ppm. The values of the gas concentrations were selected in order to reproduce an artificial outdoor ageing. In fact, according to European Environmental Agency for the air quality monitoring, the annual mean concentration of SO_2 in the atmosphere is between 5 and 20 ppb, whereas of NO_x is between 10 and 45 ppb [33]. Converting the experimental gas concentration used in the experiment, the corresponding yearly value is 288 ppb. Therefore, from the annual experimental concentration value and those monitored as average mean in the atmosphere, the exposure time resulting from the artificial accelerated ageing carried out is equal to a value between 10 and 15 years. The RH% values were chosen according to the yearly outdoor weathering changes and to reproduce extreme situations in case of inappropriate museum preventions.

It has to be highlighted that the degradation reactions occurring during natural aging may differ from the degradation process induced by accelerated aging, as reported in several studies [13,34]. However, studies based on accelerated aging represent a necessary step in the preliminary evaluation of degradation processes occurring on artwork materials due to specific pollutants. Indeed, accelerated aging studies allow to monitor the degradation process under controlled conditions and in relatively short times compared to long-term natural degradation.

2.3. Optical 3D Microscope

Each sample was scanned by using the Keyence VHX-6000 microscope (Keyence, Japan). Three-dimensional morphological images were recorded using a VH-Z100 objective (magnification of 1000x). The microscope is equipped with a LED light source (5700 K). To obtain a complete and accurate evaluation of the superficial changes, two different lighting angles were selected. First, the full light ring was used for observations in the dark field and subsequently, the mix light beam (full ring and full coaxial) to emphasize height differences as scratches. To obtain the roughness depth profile of the surface, the total depth obtained is of 10 μm taking a picture every 2 μm (pitch scans).

2.4. Attenuated total reflection fourier transform infrared spectroscopy (ATR-FTIR)

For the ATR-FTIR investigations, a LUMOS FTIR Microscope (Bruker Optics, Germany) in ATR mode with a germanium crystal was employed. The instrument is equipped with a photoconductive cooled MCT detector. Five measuring spots for each sample were acquired in a spectral range between 4000 and 480 cm^{-1} performing 64 scans at a resolution of 4 cm^{-1}. The resulting spectra were collected and evaluated by the software OPUS® (Bruker Optics, Germany). Subsequently, the spectra were averaged, baseline corrected and vector normalized. From the treated spectra, the semi-quantification of selected bands was carried out. As shown in a previous study [35], the chosen integrated bands are the most characteristic of each material and show a significant change in the relative intensity depending on different weathering. In

Table S1, the integrated bands divided according to the paint mixtures are listed. For the chemical mapping, the total mapped area had a dimension of 1.0 × 1.5 mm^2; six measuring spots along the x-axis (optical aperture approx. 0.2 mm) and six spots along the y-axis (optical aperture approx. 0.1 mm) have been collected for a total of 36 spots. Each chemical mapping experiment was carried out in three different areas of the samples.

2.5. Chemometrics methods

In the present study, the ATR-FTIR spectra of the paint samples were evaluated by a multivariate statistical approach in order to study the influence of the different experimental conditions on binder degradation [36,37]. Firstly, PCA was applied to gain a preliminary overview of the main differences between unaged and aged samples. Then, ASCA was used in order to systematically assess the effect of pigment type and weathering conditions on the aged samples [38,39]. Both PCA and ASCA were applied to the ATR-FTIR spectra taking into account only the range between 3030 cm^{-1} and 1500 cm^{-1}. This specific spectral range was selected as it only includes the absorption bands ascribable to the considered binders, excluding the spectral regions related to the pigments. The ATR-FTIR spectra were averaged, baseline corrected, and normalized. Before calculating PCA and ASCA models, the spectra were pre-processed using Savitzky-Golay smoothing [40] and mean centering. In the present study, PCA was performed using Chemometric Agile Tool (CAT) software [41] running under R environment (v. 3.1.0). ASCA models were calculated using PLS_Toolbox software (v. 8.5, Eigenvector Research Inc., USA) running under MATLAB environment (R2017b, The MathWorks, USA). Further details about the considered multivariate methods can be found in Supporting Information.

3. Results and discussion

3.1. Optical 3D microscopy

The 3D pictures of each paint sample show the morphological changes and the degradation products appearing after the artificial gas ageing. On pure samples of alkyd and styrene-acrylic binder, no visible morphological changes on the surfaces can be observed, whereas on the pure acrylic sample degradation phenomena are visible after SO_2 and NO_x ageing at 50% RH. Increasing the relative humidity value to 80%, they completely cover the entire polymeric surface making it opaquer. However, a morphological difference between the corrosion products is observed. In fact, depending on the type of gas used, these products deriving from ageing have a different shape (Fig. S1). After NO_x exposure, they are large, broad (radial), surrounded by other smaller ones. On the contrary, after SO_2 exposure, they have a more uniform and compact shape, of a smaller size compared to NO_x ageing. The roughness evaluation obtained from the 3D depth profile confirms that on the sample aged with SO_2, they reach a size between 10 and 15 μm, while after NO_x ageing, the larger ones reach a diameter of 100 μm and the smaller ones between 20 and 30 μm. This behaviour is due to the different interaction that the binder shows according to the type of pollutant gas. However, further analyses are needed to obtain a complete knowledge of this behaviour. The degradation products can be attributed to the surfactant (possibly polyethylene oxide, see chapter ATR-FTIR results) present in the acrylic binder. In fact, having a hygroscopic nature, it tends to migrate to the surface when exposed to high relative humidity values. To confirm its presence, a solubility test was performed [42].

The swab-rolling cleaning test was carried out using distilled water and applied on the surface for a total of 10 s. The surfactant present on the surface of the sample aged with SO_2 were removed, and the surface morphological condition appeared similar to the original one (Fig. 1a). However, those present on the sample aged with NO_x (Fig. 1b) were not completely removed by the action of water. This behaviour is confirmed
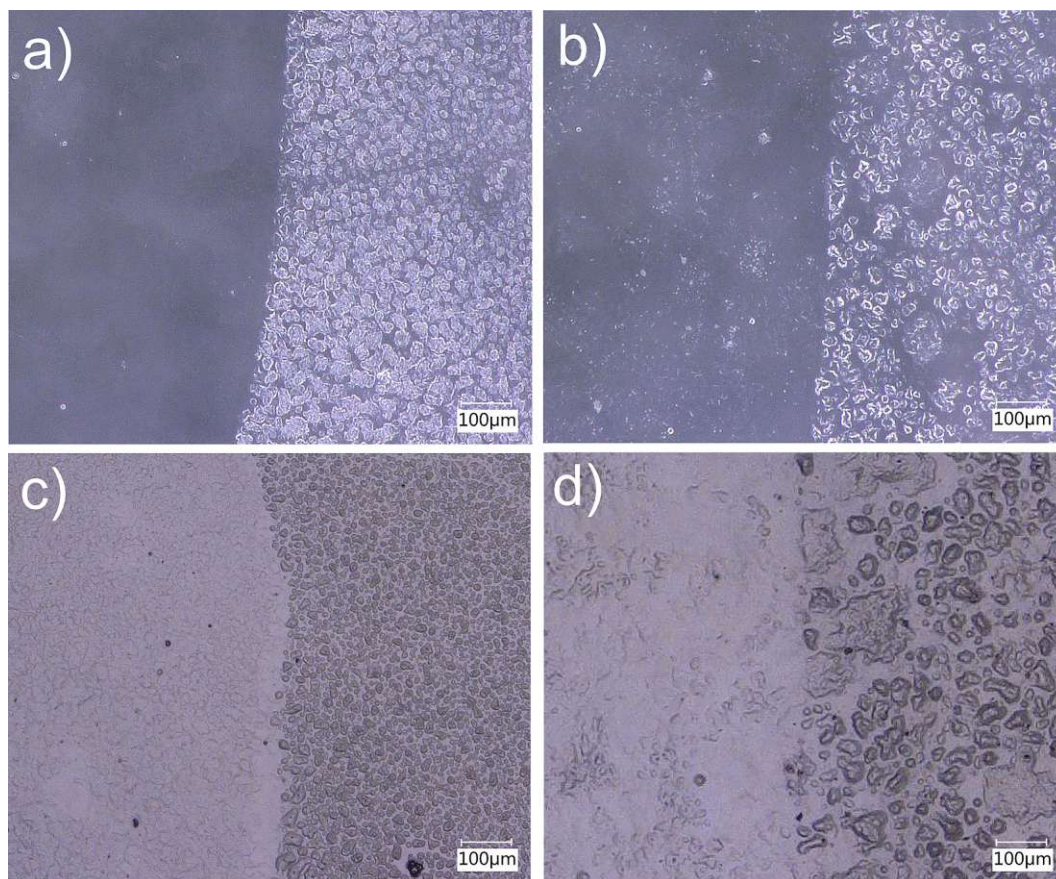
Fig. 1. Overview of the cleaning test results on degraded pure acrylic samples. The images a) and c) show the acrylic surface aged with SO₂ before and after cleaning, whereas, the images b) and d) depict the acrylic surface aged with NOₓ. For the top images, the full ring lighting was used, for the bottom images; the mixed lighting was applied.

by observations using the mix light beam (Fig. 1c-d). Furthermore, from the observation of their roughness vertical profiles (Fig. S2a.1-b.1), NO_x ageing had the strongest oxidative effects since the difference between the clean and the aged area is higher than that of SO_2 ageing. In support of this evaluation, a comparison between their horizontal profiles was performed (Fig. S2a.2-b.2). By overlapping the roughness profiles (Table 2), it is observed that the cleaning action had a better result on the surface aged with SO_2 compared to NO_x. In fact, in the latter, the surfactant is still present in some parts (blue areas), probably since the depth of the surfactant particles migrated on the surface of the polymer is more significant and then hard to remove (red areas). Another factor that influences the different degradation effects is the presence of different inorganic pigments in the mixture. In Fig. S3, it can be observed how the degradation effect caused by NO_x exposure is favoured for pigments as PW6, showing evident superficial variations. For pigments such as PB28 and PB29, these effects can only be observed after SO_2 ageing. The same behaviour is observed for alkyd paints (Fig. S4). In this case, the surfaces show the presence of micro-pores after gas ageing (the sizes vary according to the pigment in the mixture) which tend to be more numerous after SO_2 ageing. Finally, styrene-acrylic paints depict the presence of small surface cracks after

the exposure to both pollutant gases. In this case, the two different gases cause similar morphological changes and even the various inorganic pigments used do not show a different superficial degradation effect.

3.2. ATR-FTIR results

The main functional bands of each paint sample were identified by the use of ATR-FTIR analysis and listed in Table S2. Concerning the acrylic emulsion, ATR-FTIR analysis provided characteristic signals of nBA/MMA copolymer, as identified primarily by the C—H bond stretching vibrations (2956–2876 cm^{-1}), the C=O stretching (1726 cm^{-1}) and the additional bands of the C—O—C and C—O stretching (1236, 1160, 1146 cm^{-1}). Furthermore, PEO (polyethylene ox-ide) surfactant bands are present at 2895, 1343, and 1115 cm^{-1} [35,43]. Observing Fig. 2a–d, it is possible to notice that, in all the acrylic samples aged both with NO_x and SO_2, the intensity of the functional groups increases. It is related to the increase of humidity levels (50–80 RH %) which allow the polymeric structure to gradually open. This behaviour is favoured by the absorption of water by hygroscopic materials inside the paint (in this case the non-ionic surfactant PEO), which can exist in isolated pockets inside the films or can be diffused in the polymer [44]. Consequently, also the spectral signals of the surfactant increase and are higher with increasing the RH content. As reported in the literature [45], the hygroscopicity and solubility of this surfactant promote the migra-tion to the air-film interface. Its accumulation at the interface may affect the mechanical strength of acrylic paints, such as the adhesion of the film to the support, its permeability, surface gloss, and exposure to dirt [46]. However, depending on the type of gas used, the amount of the surfactant on the surface is different. In fact, by exposure of the samples

Table 2
Morphological values acquired after 3D depth profile evaluation.

	RH %	Gas	Size PEO migrated on the surface after gas ageing	3D depth profile before cleaning	3D depth profile after cleaning
Acrylic film	80	SO₂	10–15 μm	9.38 μm	5.88 μm
	80	NOₓ	20–30 μm	10.58 μm	8.84 μm
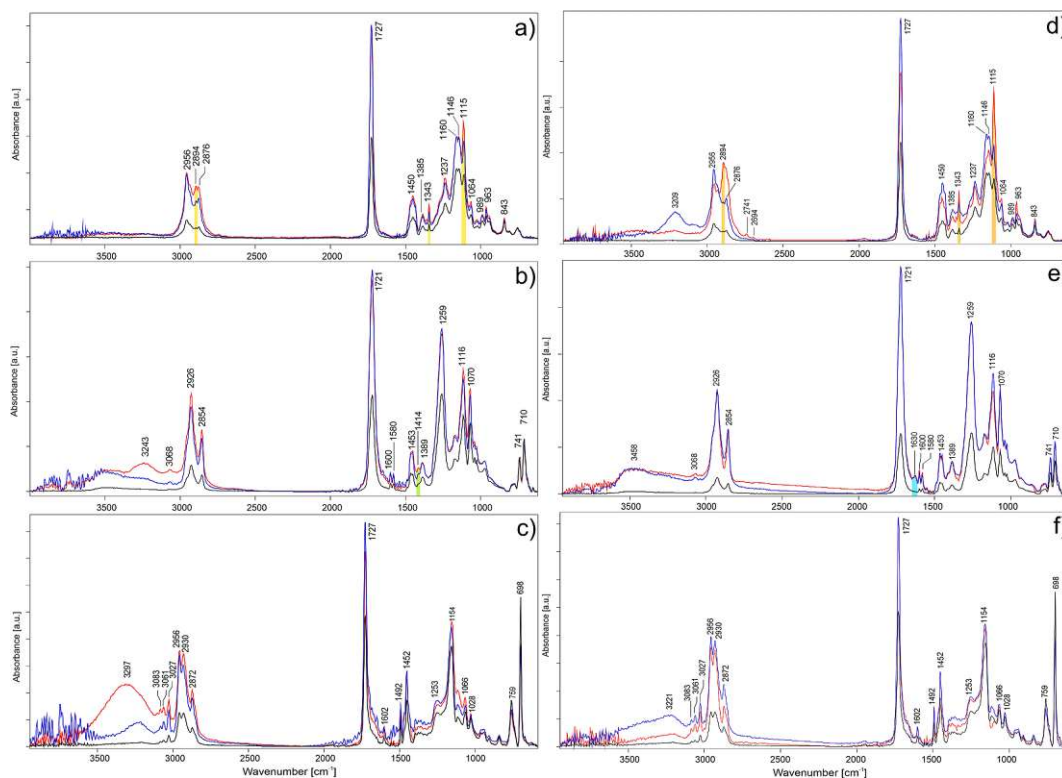
Fig. 2. ATR-FTIR spectra comparison of pure binders: a) and d) acrylic emulsion; b) and e) alkyd resin; c) and f) styrene-acrylic binder. The samples on the left were aged with SO$_2$, and on the right with NO$_x$. In each graph, the unaged (black), the 50% RH (blue), and the 80% RH (red) aged samples are showed.

to NO$_x$, the absorbance signals of PEO increase more than those aged with SO$_2$. This behaviour is due to the properties of both the binder and the gas. NO$_x$ is more reactive as an oxidative agent than SO$_2$ [47], and its radicals can abstract the hydrogen atoms from the less strong C—H bonds or interact with the C=C bonds of the macromolecules, initiating the degradation of free radical polymers at room temperature [48]. It may be related to the formation of the bands at 2741–2694 cm^{-1} associated with the overtone of the aldehyde bond. This behaviour, combined with the possibility of the surfactant to form hydrophilic moieties with water, facilitates the migration of PEO to the surface and the hydrolyzation of the binder. The ATR-FTIR analysis per-formed on alkyd paints allows the identification of the most characteristic bands, as shown in Table S2 [49]. The strong band at 1721 cm^{-1} is due to the C=O stretching vibration, common to both oil and phthalate component, whereas the C—O—C stretching (1259 and 1116 cm^{-1}) and the aromatic in-plane and out-of-plane bending (1600–1580, 1070, and 740–710 cm^{-1}) are typical for phthalate structures. Relative to the oil portion, the CH$_2$ and CH$_3$ symmetric and asymmetric stretching and bending are assigned [26]. As shown in Fig. 2b–e, also in this case, the intensity of the bands of the alkyd binder tends to increase with the increase of relative humidity, for both gas ageing. This spectral behaviour indicates a hydrolytic degradation of the binder, attributed to the sensitivity to water of *ortho*-phthalate esters in acidic conditions. It is confirmed by the relative decrease in the phthalate group (741–710 cm^{-1}) and by the broadening of the carbonyl band C=O, due to the formation of new oxidized products during the artificial ageing cycles. Therefore, for alkyd paint, the hydrolysis of the phthalate fractions is the main degradation process which also leads to the loss of physical properties of the top layer [50]. Furthermore, two degradation products are observed because of gaseous ageing. From SO$_2$ exposure, a small band at 1414 cm^{-1} is shown, indicating the formation of the SO-CH$_3$ bond. According to Simendinger and Balk [51], SO$_2$ interacts mainly with the drying oil leading to the formation of cross bonds of sulphate esters between the drying oil molecules. This phenomenon is also stimulated by the

propensity of fatty acids to be more reactive with SO$_2$, leading to oxidation reactions. Contrary to these results, a small band at 1630 cm^{-1} is observed for NO$_x$, related to the formation of the -O-NO$_2$ bond [52]. As previously mentioned for the acrylic binder, the high relative humidity leads to hydrolytic degradation which, interacting with the gas, forms this bond with the binder. This band is more visible in alkyd paints because favoured by the high reactivity of fatty acids to interact with the gas. Finally, in Fig. 2c-f, the main functional groups of the styrene-acrylic polymer can be identified. Related to the acrylate part, the C—H bond stretching vibrations (2956–2930–2872 cm^{-1}), the C=O stretching (1721 cm^{-1}), and the additional bands of the C—C and C—O stretching (1154–1128–1066 cm^{-1}) are observed, whereas the bands of the C—H stretching (3083–3061–3027 cm^{-1}), the C=C stretching (1601 cm^{-1}), the C—C vibration (1493–1454 cm^{-1}), and the C—H bending (759–698 cm^{-1}) are related to the aromatic ring of phenyl group [53]. As shown for the previous two binders, the strong hydrolytic degradation increases the intensity of most spectral signals. The presence of new —OH groups within the molecular structure of the binder yields to the decrease of the spectral signal at 759–689 cm^{-1} of the phenyl group (aromatic C—H out of plane bending). This intensity signal decreases with the increase of relative humidity. Furthermore, a shoulder around 1670 cm^{-1} is formed. This band is assigned to the carbonyl group C=O of the formed carboxylic acids. These carboxylic groups are the result of a splitting of the lateral groups due to their oxidative decomposition. The broadening of the main carbonyl absorption at 1726 cm^{-1} may also be due to the formation of ketone and aldehyde groups which act more rapidly than the degradation of the ester groups [53]. Lastly, it is possible to observe that styrene-acrylic and acrylic samples, exposed to NO$_x$, show an increase of the —OH band (around 3220 cm^{-1}) at RH values of 50%, which however tends to decrease at higher RH (80%). It is due to the impact of humidity on the catalytic conversion of NO$_2$ on both paints. Their interaction increases with the decrease in relative humidity from 80% to 50%. It may be due to the fact that, as humidity increases, more water vapour is adsorbed

onto the surface, increasing competition for adsorption sites. Furthermore, the effect of humidity on the conversion of a pollutant also depends on its concentration. In fact, the competition for the adsorption sites between NO_2 and water vapour is already sufficient with a small amount of humidity for the generation of OH radicals. Therefore, the catalytic activity of NO_2 decreases [54].

3.3. ATR-FTIR mapping and semi-quantification of functional groups

ATR-FTIR chemical mapping is increasingly used to investigate cultural heritage materials. In fact, it was already employed as a valuable technique for analysing the distribution of pigments, additives, and binders. In recent studies, it was also applied to investigate degradation products formed on paint surfaces [55]. During this study, mapping was mainly necessary to investigate the distribution of specific degradation products on the different paint mixtures caused by the influence of each inorganic pigment. For the mapping of acrylic paints, the spectral signal of the surfactant (2895 cm^{-1}) was considered as its intensity changes with the different pigment in the mixture. In Fig. 3, the spectra of the acrylic paint samples exposed to SO_2 (Fig. 3a) and NO_x (Fig. 3b) at 80% RH are shown. Integrating the area of the selected band, and observing its distribution on the surface of the samples, it is possible to conclude that the mixture with PW6 facilitates the migration of the surfactant on the surface followed by PB29 and PB28 (exposed to SO_2), and pure binder and PB35 (exposed to NO_x). As reported in literature [56], titanium dioxide (PW6) has a strong catalytic effect and, in this case, when the water molecule comes into contact with the surface, its O atom strongly interacts with the Ti atoms present in the paint layer. In this way, H atoms trap electrons from Ti atoms and become negative. The water molecule is then adsorbed and the surfactant is more prone to migrate to the surface. The surfactant behaviour has been further investigated by semi-quantitative evaluation. It was performed on unaged, 50% and 80% RH aged samples for both corrosive gases, integrating not only the surfactant band area at 2895 cm^{-1} but also those at 1343 and 1115 cm^{-1} (Table S2). From the integration values of the three set of samples, the differences between the unaged and 50% RH aged, and between 50% and 80% RH aged were calculated (Table S3).

In Fig. S5, it is possible to confirm that the acrylic mixture with PW6 causes the most significant migration of surfactant on the surface. Furthermore, NO_x appears to have a more oxidizing effect than SO_2, confirming the previous results discussed. The mapping of the alkyd paint samples was performed by integrating the C=O carbonyl band at 1721 cm^{-1} and the C–H bond at 2926–2854 cm^{-1}. Furthermore, the degradation product bands at 1414 cm^{-1} and 1630 cm^{-1} were also considered.

In all paint mixtures, exposed to SO_2 and NO_x the distribution of these bands on the surface show already a sharp increase, after the first ageing cycle at 50% RH. Subsequently, increasing the relative humidity, this trend is only slightly increased. Generally, all paint mixtures show this behaviour. However, those with PR101 and PW6 are more prone to hydrolytic degradation (Fig. S6).

This trend is confirmed by the semi-quantitative evaluation (Fig. S5c, d) of the bands mentioned above. The degradation effects on alkyd paints are similar for both gases, as they are chemically more prone to interact with the drying oil present in the binder, influencing the oxidation process [57]. Finally, the mapping of styrene-acrylic paints was investigated by integrating the C–H bands at 2961 cm^{-1}, the C=O carbonyl band at 1725 cm^{-1}, and the OH band at 3248 cm^{-1}. The evaluation of this latter band, through chemical mapping and semi-quantification confirms the decreasing catalytic effect of NO_x with increasing of relative humidity. In Fig. S5e, f, this behaviour is particularly evident in comparison to SO_2 ageing. Therefore, the evaluation of the degradation processes of styrene-acrylic paints is the most complex, since the catalytic activity of NO_x is already activated at RH of 50%. In contrast, the deterioration action of SO_2 grows exponentially with increasing of relative humidity.

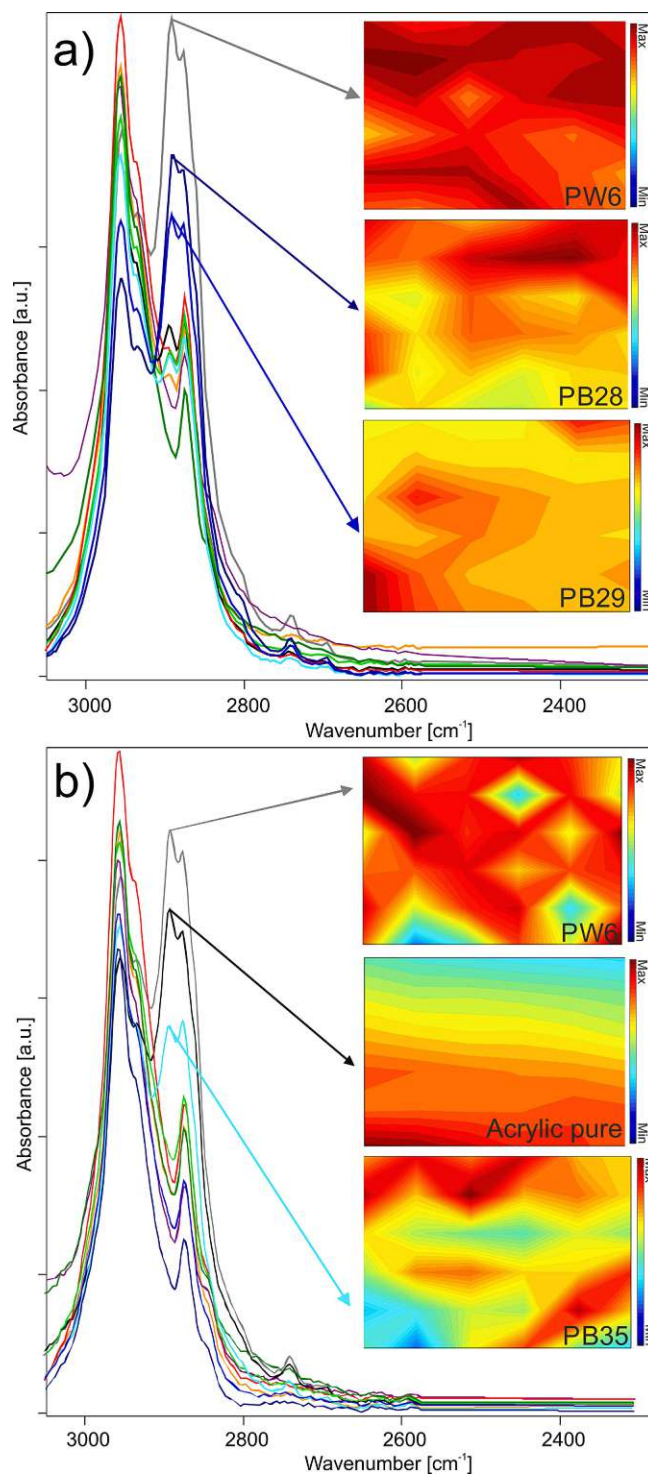**Fig. 3.** ATR-FTIR chemical mapping of the surfactant distribution, after a) SO_2 and b) NO_x exposure of acrylic paint mixtures with PW6 (grey), PY37 (orange), PG50 (light green), PG18 (dark green), PB35 (cyan), PB28 (blue), PB29 (dark blue), PR101 (red), PV16 (purple), and pure binder (black).

3.4. Principal component analysis results

The score plots in Fig. 4 show the results obtained from the multivariate exploratory analysis on the paint mixtures, divided according to binder type and gas exposure. Fig. 4a reports the PC1 and PC2 score plot obtained from the spectra of the acrylic mixtures aged with SO_2. PC1 and PC2 retain 78.2% and 15.5% of explained variance, respectively, with a
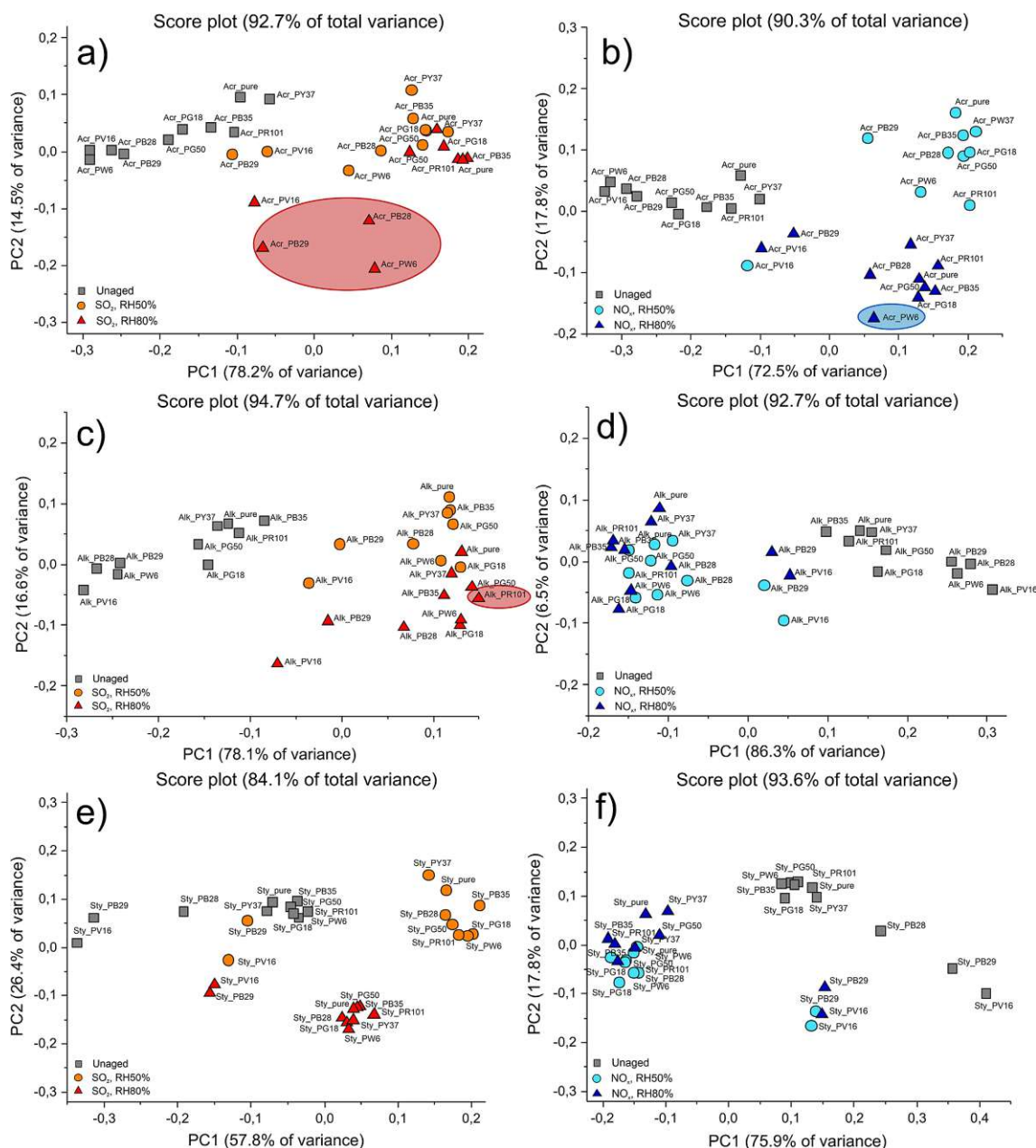
Fig. 4. PC1 and PC2 score plots of acrylic samples aged with a) SO_2 (50, 80% RH), b) NO_x (50, 80% RH); alkyd samples aged with c) SO_2 (50, 80% RH), d) NO_x (50, 80% RH); and styrene-acrylic samples aged with e) SO_2 (50, 80% RH), f) NO_x (50, 80% RH).

total of 92.7% of data variance. The cluster of unaged samples is well-differentiated from the others mainly along PC1. From the evaluation of the corresponding PC1 loading vector (Fig. S7a), this behaviour is related to the carbonyl band C=O (at 1727 cm^{-1}); therefore, this separation is given by the effect of hydrolytic degradation. Considering the aged samples, it is not possible to clearly separate the samples according to RH% values, even if the samples aged at RH% values equal to 80% tend to have higher PC1 score values than the samples aged with 50% of relative humidity. Interestingly, PC2 describes the ageing behaviour of the three mixtures prepared with PB28, PB29 and PW6 pigments and aged at 80% of relative humidity, which have negative score values along PC2. In this case, one of the more relevant spectral regions observed on the PC2 loading vector is represented by the aliphatic C—H band at 2894 cm^{-1}, assigned to the surfactant signal. This behaviour shows that the three paint mixtures appear more subject to the effects of SO_2 at high humidity, causing the greatest migration of the surfactant on

the surface. The PC1 and PC2 score plot obtained from the analysis of the acrylic samples aged with NO_x is reported in Fig. 4b, PC1 and PC2 account for 72.5% and 17.8% of explained variance, respectively. Also in this case, PC1 allows separating unaged and aged samples, while PC2 allows differentiating the aged samples according to the RH% values. Considering the PC2 loading vector reported in Fig. S7b, the surfactant band at 2894 cm^{-1} has a strong influence in the separation of the set of samples aged at RH 80%. The paint mixture with PW6 pigment again shows a more deteriorating effect. Therefore, the exposure of NO_x gas results more oxidizing for acrylic paints compared to SO_2, especially at RH 80%. The PCA score plots obtained from the analysis of the alkyd mixtures aged with SO_2 and NO_x are reported in Fig. 4c and d, respectively. For both evaluations, the clusters of data are represented according to the first two principal components PC1 and PC2. Concerning SO_2 ageing, the main distinction between unaged and aged samples is described by PC1, accounting for 78.1% of data variance. The

observation of the corresponding PC1 loading vector (Fig. S7c) shows that this separation is mainly ascribable to the C=O carbonyl band at 1721 cm^{-1} and the C–H bond at 2926–2854 cm^{-1}. Furthermore, PC2 separates quite well the samples subjected to different humidity levels.

This separation is mainly ascribable to the spectral region at 2926–2854 cm^{-1} (C–H bond) influenced by the presence of water in the molecular structure. This trend allows understanding that the high humidity facilitates the hydrolysis of the bonds of the phthalate group of the binder. The consequent broadening of the band C=O (PC1) defines the mixture with PR101 as the most subject to degradation effect. Also considering NO$_x$ ageing, PC1 allows separating unaged and aged samples and the relevant spectral bands responsible for this separation are the same as those observed for SO$_2$ ageing (C=O and C–H bond). However, in this case, it is not possible to easily differentiate the aged samples according to the different relative humidity values. Lastly, Fig. 4e-f show the PC1 and PC2 score plots obtained from the analysis of the styrene-acrylic mixtures, representing the 84.1% of explained variance for SO$_2$ aged samples, and 93.6% of explained variance for NO$_x$ aged samples.

Concerning SO$_2$ ageing, the main distinction between unaged and aged samples is given by PC1 and this behavior is mainly ascribable to

C=O carbonyl band at 1727 cm^{-1} (Loadings in Fig. S7e, f). Furthermore, PC2 allows separating the samples aged with SO$_2$ + RH80% from the other clusters; indeed, these samples show negative values of PC2 scores. Observing the corresponding PC2 score vector (Fig. 4e), the spectral region related to the C–H bond (2926–2854 cm^{-1}) has a higher relevance in defining PC2 direction. It means that, by increasing the relative humidity, the OH groups present in the artificial atmosphere are more able to have an oxidizing effect on the phenyl groups of the binder. Finally, also for NO$_x$ ageing, the main distinction between unaged and aged is given by PC1 (Fig. 4f), whose direction is mainly influenced by the spectral regions related to C=O (1727 cm^{-1}) and C–H (2926–2854 cm^{-1}) bonds (Fig. S7f). Considering the RH% values, in this case, it is not possible to observe a clear separation between samples aged with different relative humidity levels, however, the samples processed with an RH% equal to 50% tend to be more distant from the corresponding unaged samples in the PC1 and PC2 score plot. For both gaseous exposures, both for alkyd and styrene-acrylic paints, the mixtures with PB29 and PV16 show a similar trend. They are always placed between the unaged and aged clusters, independently of the relative humidity value selected. This behaviour may be due to a lower degrading effect of corrosive agents on these two paints, leading to a lower spectral signal
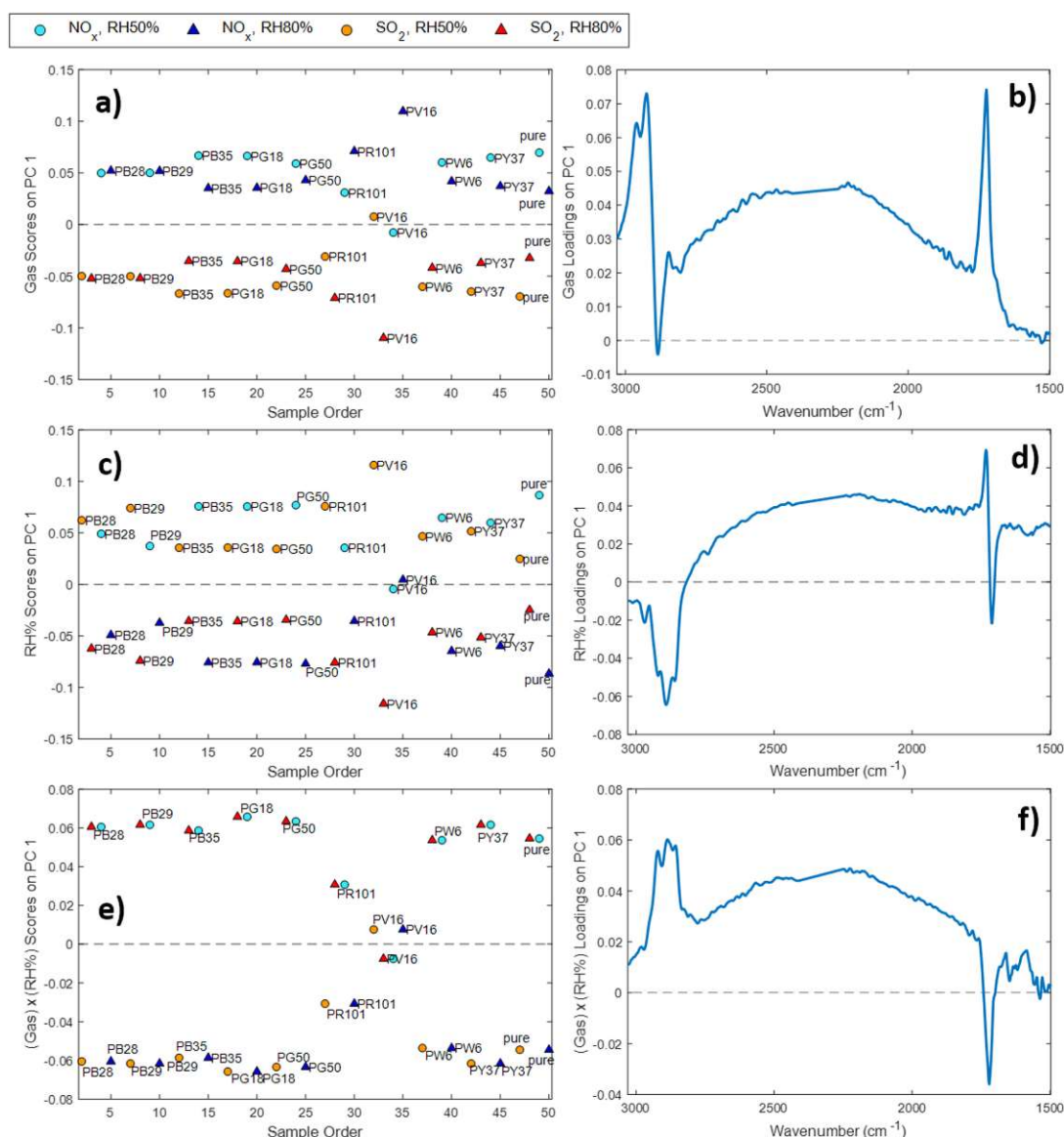

Fig. 5. ASCA results of acrylic paint samples; score and loading plots of the a-b) gas, c-d) RH%, and e-f) gas × RH% sub-models.

compared to the other paint mixtures.

3.5. ASCA results

Table S4 reports the results obtained by applying ASCA to the aged samples separated according to binder type in order to systematically evaluate the influence of individual experimental factors (pigment, gas, RH%) and their interactions (pigment × gas, pigment × RH%, gas × RH%) on the degradation process of the different paint mixtures. Generally, for all the three datasets pigment type is the factor showing the highest effect on the spectral response, accounting for more than 50% of data variance, while its interaction with gas or RH% is not significant. The investigation of the PCA sub-models related to pigment factor allowed to observe that such effect is due to the peculiar behaviour of the mixtures containing PV16 and PB29 pigments for all the three binder types, which have a lower degradation and, as a consequence, spectra with lower intensity (as previously outlined). The ASCA results obtained on the samples of acrylic paints show that RH% factor (12.88%) has a higher influence on the spectral response compared to gas factor (10.81%) or gas × RH% interaction (10.51%). Considering the score and loading plots of gas sub-model (Fig. 5a-b), the exposure to NO_x causes the greatest intensity increase of the bands at 1727 cm^{-1} (C=O bond) and 2895 cm^{-1} (PEO surfactant), and therefore a higher degradation of the sample. As far as the RH% effect is concerned, the influence of high levels of relative humidity (Fig. 5c, d) mainly affects the surfactant band at 2956–2876 cm^{-1} (C–H bond). From the evaluation of the gas × RH% interaction (Fig. 5e, f), it is possible to observe that the exposure of the paint samples to NO_x at RH 80% mainly causes the intensity increase of the band at 1721 cm^{-1}, while the exposure to SO_2 at RH 80% has a great influence on the surfactant band at 2895 cm^{-1}. Therefore, the degradation of acrylic paints is mainly caused by the exposure of NO_x to 80% RH, causing the migration of the surfactant on the surface. These results confirm the previous considerations. Regarding the ASCA results for alkyd paint samples (Table S4), gas factor (15.42%) has the stronger influence on the spectral response, followed by gas × RH% interaction (11.50%) and RH% factor (7.40%).

Compared to the results obtained with acrylic mixtures, for alkyd paint samples the effect of gas type in the degradation process is more evident. Indeed, in this case, gas factor accounts for a higher percentage of explained variance and the score plot of gas sub-model shows a clear separation between the samples aged with the two gases (Fig. S8a). Considering the loading vector of gas sub-model (Fig. S8b), it is possible to observe that NOx degradation determines a higher increase of the spectral bands related to C=O (1721 cm^{-1}) and C–H bonds (2956–2876 cm^{-1}). Besides, the spectra of the sample aged with NOx have a peculiar band at about 1630 cm-1, which can be ascribable to the -O-NO$_2$ degradation product. For alkyd paints, RH% factor has a lower effect compared to gas × RH% interaction, therefore the degradation of the aged samples (ascribable only to the different humidity levels) is less marked than the degradation due to the combination of gas and RH%. Considering the results of gas × RH% sub-model (Fig. S8e, f), the samples aged with NOx and RH% equal to 80% are characterized by a higher increase in the C=O band at 1721 cm^{-1}, while the spectral region centred at about 2880 cm^{-1} is mainly influenced by SO_2 ageing with RH% values equal to 80%. Considering the ASCA results reported in Table S4, for styrene-acrylic paint samples the degradation process is more influenced by gas × RH% interaction (16.45%) than gas (13.11%) and RH% (9.02%) factors taken individually. Therefore, the degradation process of these paints depends on the specific combination between gas type and RH% level. Similarly, to what observed for the other binders, NO$_x$ generally determines a higher increase of the two characteristic bands at 1727 cm^{-1} and 2956–2930 cm^{-1} (Fig. S9a, b). Furthermore, the score plot of gas sub-model shows a quite marked separation between the samples according to gas type, as previously observed for alkyd paints. Considering gas × RH% sub-model (Fig. S9e, f), the different combinations of the two factors have a different deteriorating

effect. In fact, the peak centred at 1740 cm^{-1} has a higher intensity for the samples aged with NO$_x$ and RH% equal to 80% and for the samples aged with SO_2 and RH% equal to 50%. Conversely, the degradation process observable in the spectral region centred at 2915–2880 cm^{-1} is more influenced by the exposure to SO_2 and RH% equal to 80% or to NO$_x$ and RH% equal to 50%. Summarizing the ASCA results related the effect of the gas, RH%, and their two-way interaction on the mixtures prepared with the three binder types, it is possible to observe that the exposure to NO$_x$ generally has a more degrading effect on the paint samples. In particular, alkyd mixtures are more subjected to the influence of the gas type. The effect of the different levels of RH% is mainly observable in the spectral region at 2915–2880 cm^{-1}, and the ageing process of acrylic paints is slightly more influenced by relative humidity. Furthermore, ASCA results also showed that the interaction between gas and RH% plays an important role in the degradation of the samples, in particular for styrene-acrylic mixtures.

4. Conclusion

During this study, an accelerated gas ageing on modern paint samples was performed trying to simulate real outdoor environmental conditions. In particular, sulphur dioxide (SO_2) and nitrogen oxide (NO$_x$) were used and mixed with different relative humidity content (50% and 80% RH) for a total of 168 h gas exposure. The paint samples are mixtures of three different binding media (acrylic, alkyd, and styrene-acrylic) with various inorganic pigments. After ageing, the samples were analyzed by various analytical techniques whose results are listed as follows: morphological observations by 3D microscope seemed to show the most significant degradation effects on acrylic paints with the consequent surface migration of the surfactant. The different morphological changes deriving from the exposure of the two gases were studied by analyzing the depth and roughness profile showing a higher oxidative behaviour with NO$_x$. From the qualitative and semi-quantitative ATR-FTIR analysis, the various binders and ageing conditions showed different results: the acrylic paints are more subjected to NO$_x$ degradation (surfactant migration). Moreover, the semi-quantitative evaluation and chemical mapping showed that paints with PW6, PB29, and PB28 favour this deteriorating behaviour. Alkyd paints show similar degradation levels when exposed to pollutant gases. The main degradation reaction is the hydrolysis of the phthalic component in the binder, although it seems favoured by the interaction with NO$_x$, while SO_2 tends to interact more with the drying oil. The pigments that favour these reactions are PW6 and PR101. Finally, styrene-acrylic paints are more sensitive to the interaction gas-relative humidity, showing two different degradation behaviours. The multivariate methods used (PCA and ASCA) confirmed both the results previously obtained and brought more information useful for understanding the different chemical mechanisms between materials and polluting agents. By PCA, it was possible to understand that, in all paints, the functional groups C–H and C=O are the most subject to degradation. Furthermore, it confirmed that this effect is enhanced with certain pigments. The influence that different pigments have on the overall degradation of the binders was confirmed by ASCA. In addition, ASCA results show that the three binders are differently subject to degradation conditions. In fact, RH% has more influence on acrylic paints, than different gases on alkyd paints, and the gas × RH% combination on styrene-acrylic paints. Generally, from all the assessments performed, NO$_x$ revealed the most significant oxidizing effect on the paints. These results are relevant as the outdoor artworks are more and more affected by environmental degradation, due to the continuous climatic changes. Understanding their deterioration reactions caused by the interaction with pollutant gases, it is essential to provide appropriate suggestions for their preservation. Considering that samples show different degradation behaviours depending on the chosen degrading agent, prevention methods should be selected according to the type of binder and the environment (indoor or outdoor) in which the artwork is

exposed or stored [58,59]. In order to obtain extensive and more detailed knowledge about artificial gas aging, future experiments will be considered. As mentioned in the introduction, the effect of ozone and particulate matter also significantly influences the stability of artworks. Therefore, their chemical-physical evaluation and correlation with the pollutants presented in this study remain a subject for future study. Another consideration for future study is the cross evaluation of pollutants and parallel aging tests (accelerated and natural). These two additional approaches will provide additional information about the stability of polymer films and the oxidising effect that each gas has with different art materials.

CRediT authorship contribution statement

Laura Pagnin: Conceptualization, Investigation, Writing - original draft, Methodology. **Rosalba Calvini:** Software, Validation. **Rita Wiesinger:** Supervision, Conceptualization. **Manfred Schreiner:** Supervision, Writing - review & editing.

Declaration of Competing Interest

The authors declare that they have no known competing financial interests or personal relationships that could have appeared to influence the work reported in this paper.

Availability of data and materials

Additional data about 3D images, FTIR results, and multivariate analysis are available upon request.

Appendix A. Supplementary data

Supplementary data to this article can be found online at https://doi.org/10.1016/j.microc.2021.106087.

References

[1] Hamilton R, Kucera V, Tidblad J, Watt J. The Effects of Air Pollution on Cultural Heritage. 2009.
[2] 2. Phipps PBP, Rice DW. The Role of Water in Atmospheric Corrosion. In: Corrosion Chemistry. 1979:235–61.
[3] Cass GR, Druzik JR, et al. Protection of Works of Art From Atmospheric Ozone. The Getty Conservation Institute, 1989.
[4] F.C. Izzo, E. Balliana, F. Pinton, E. Zendri, A preliminary study of the composition of commercial oil, acrylic and vinyl paints and their behaviour after accelerated ageing conditions, Conserv. Sci. Cult. Herit. 14 (1) (2014) 353–369.
[5] Health effects of air Pollution with Particulate Matter, Ozone and Nitrogen Dioxide. World Heal Organ. 2003;EUR/03/504:95–113.
[6] J. Grau-Bové, B. Budič, I.K. Cigič, D. Thickett, S. Signorello, M. Strlič, The effect of particulate matter on paper degradation, Herit. Sci. 4 (1) (2016) 4–11.
[7] J. Tidblad, V. Kucera, M. Ferm, K. Kreislova, S. Brüggerhoff, S. Doytchinov, et al., Effects of air pollution on materials and cultural heritage: ICP materials celebrates 25 years of research, Int. J. Corros. 2012 (2012) 2005–2006.
[8] G. Ranalli, M. Matteini, I. Tosini, E. Zanardini, C. Sorlini, Bioremediation of cultural heritage: removal of sulphates, nitrates and organic substances, Of Microbes Art. 2000 (2000) 231–245.
[9] J. Aramendia, L. Gómez-Nubla, K. Castro, J.M. Madariaga, Spectroscopic speciation and thermodynamic modeling to explain the degradation of weathering steel surfaces in SO2 rich urban atmospheres, Microchem. J. 115 (2014) 138–145.
[10] M.P. Colombini, F. Modugno, R. Fuoco, A. Tognazzi, A GC-MS study on the deterioration of lipidic paint binders, Microchem. J. 73 (1–2) (2002) 175–185.
[11] W. Funke, H. Haagen, Influence of sulfur dioxide on organic coatings, ACS Symp. Ser. 309–15 (1983).
[12] L. Dulog, The role of sulfur dioxide and nitrogen dioxide on the degradation of polymers, Angew. Makromol Chem. 252 (1997) 1–10.
[13] V. Gomes, A. Dionísio, Pozo-Antonio J. Santiago, The influence of the SO2 ageing on the graffiti cleaning effectiveness with chemical procedures on a granite substrate, Sci. Total Environ. 625 (2018) 233–245.
[14] Camuffo D, Fernicola V, Bertolin C. Basic Environmental Mechanisms Affecting Cultural Heritage, 2010.
[15] F. De Santis, V. Di Palo, I. Allegrini, Determination of some atmospheric pollutants inside a museum: relationship with the concentration outside, Sci. Total Environ. 127 (3) (1992) 211–223.
[16] Learner TJS. Analysis of Modern Paints. The Getty Conservation Institute; 2005.
[17] NIIR Board of Consultants & Engineers. Modern Technology of Synthetic Resins & Their Applications. Asia Pacific Business Press Inc. 2018.
[18] Learner TJS, Smithen P, Krueger JW, Schilling MR. Modern Paints Uncovered. The Getty Conservation Institute; 2007.
[19] L. Feller Artists' Pigments A Handbook of Their History and Characteristics. 1986.
[20] A. Roy Artists' Pigments A Handbook of Their History and Characteristics. 1993.
[21] Fitzhugh EW. Artists' Pigments. A Handbook of Their History and Characteristics. 1997.
[22] B. Berrie Artists' Pigments A Handbook of Their History and Characteristics. 2007.
[23] G. Musumarra, M. Fichera, Chemometrics and cultural heritage, Chemometr. Intell. Labor. Syst. 44 (1–2) (1998) 363–372.
[24] G. Capobianco, M.P. Bracciale, D. Sali, F. Sbardella, P. Belloni, G. Bonifazi, M. C. Guidi, et al., Chemometrics approach to FT-IR hyperspectral imaging analysis of degradation products in artwork cross-section, Microchem. J. 132 (2017) 69–76.
[25] G. Abdel-Maksoud, M. Ibrahim, Y.M. Issa, M. Magdy, Investigation of painting technique of coptic icon by integrated analytical methods: imaging, spectroscopic and chemometric methods, J. Archaeol. Sci. Rep. 29 (2020).
[26] L. Pagnin, R. Calvini, R. Wiesinger, J. Weber, M. Schreiner, Photodegradation kinetics of alkyd paints: the influence of varying amounts of inorganic pigments on the stability of the synthetic binder, Front. Mater. 7 (2020) 1–15.
[27] E. Marengo, M.C. Liparota, E. Robotti, M. Bobba, Monitoring of paintings under exposure to UV light by ATR-FT-IR spectroscopy and multivariate control charts, Vibrat. Spectrosc. 40 (2) (2006) 225–234.
[28] G. Bonifazi, G. Capobianco, C. Pelosi, S. Serranti, Hyperspectral imaging as powerful technique for investigating the stability of painting samples, J. Imag. 5 (1) (2019) 8.
[29] C. Pelosi, G. Capobianco, G. Agresti, G. Bonifazi, F. Morresi, S. Rossi, S. Serranti, et al., A methodological approach to study the stability of selected watercolours for painting reintegration, through reflectance spectrophotometry, Fourier transform infrared spectroscopy and hyperspectral imaging, Spectrochim. Acta A Mol. Biomol. Spectrosc. 198 (2018) 92–106.
[30] L. Ortiz-Herrero, I. Cardaba, S. Setien, L. Bartolomé, M.L. Alonso, M.I. Maguregui, OPLS multivariate regression of FTIR-ATR spectra of acrylic paints for age estimation in contemporary artworks, Talanta 205 (2019).
[31] Berni A, Mennig M, Schmidt H. Doctor Blade. Sol-Gel Technologies for Glass Producers and Users. 2004:89–92.
[32] R. Wiesinger, M. Schreiner, C. Kleber, Investigations of the interactions of CO2, O3 and UV light with silver surfaces by in situ IRRAS/QCM and ex situ TOF-SIMS, Appl. Surf. Sci. 256 (9) (2010) 2735–2741.
[33] 33. Available from https://www.eea.europa.eu/.
[34] P.M. Carmona-Quiroga, R.M.J. Jacobs, S. Martínez-Ramírez, H.A. Viles, Durability of anti-graffiti coatings on stone: natural vs accelerated weathering, PLoS ONE 12 (2) (2017) 1–18.
[35] R. Wiesinger, L. Pagnin, M. Anghelone, L.M. Moretto, E.F. Orsega, M. Schreiner, Pigment and binder concentrations in modern paint samples determined by IR and raman spectroscopy, Angew. Chem. Int. Ed. 57 (25) (2018) 7401–7407.
[36] A. Sarmiento, M. Pérez-Alonso, M. Olivares, K. Castro, I. Martínez-Arkarazo, L. A. Fernández, et al., Classification and identification of organic binding media in artworks by means of Fourier transform infrared spectroscopy and principal component analysis, Anal. Bioanal. Chem. 399 (10) (2011) 3601–3611.
[37] L. Pagnin, L. Brunnbauer, R. Wiesinger, A. Limbeck, M. Schreiner, Multivariate analysis and laser-induced breakdown spectroscopy (LIBS): a new approach for the spatially resolved classification of modern art materials, Anal. Bioanal Chem. 412 (2020) 3187–3198.
[38] J.J. Jansen, H.C.J. Hoefsloot, J. Van Der Greef, M.E. Timmerman, J.A. Westerhuis, A.K. Smilde, ASCA: analysis of multivariate data obtained from an experimental design, J. Chemom. 19 (9) (2005) 469–481.
[39] G. Zwanenburg, H.C.J. Hoefsloot, J.A. Westerhuis, J.J. Jansen, A.K. Smilde, ANOVA–principal component analysis and ANOVA–simultaneous component analysis: a comparison, J. Chemom. 25 (10) (2011) 561–567.
[40] A. Savitzky, M.J.E. Golay, Smoothing and differentiation of data by simplified least squares procedures, Anal Chem. 36 (8) (1964) 1639–1643.
[41] 41. Leardi R, Melzo C, Polotti G. Chemometric agile software (CAT). Gruppo di chemiometria; Available from: http://gruppochemiometria.it/index.php/software.
[42] S. Digney-Peer, A. Bumstock, T. Leamer, H. Khanjian, F. Hoogland, J. Boon, The migration of surfactants in acrylic emulsion paint films, Stud. Conserv. 49 (2) (2004) 202–207.

[43] M. Anghelone, V. Stoytschew, D. Jembrih-Simbürger, M. Schreiner, Spectroscopic methods for the identification and photostability study of red synthetic organic pigments in alkyd and acrylic paints, Microchem. J. 139 (2018) 155–163.

[44] B. Ormsby, G. Foster, T. Learner, S. Ritchie, M. Schilling, Improved controlled relative humidity dynamic mechanical analysis of artists' acrylic emulsion paints: Part II. General properties and accelerated ageing, J. Therm. Anal. Calorim. 90 (2) (2007) 503–508.

[45] B. Ormsby, T. Learner, M. Schilling, J. Druzik, H. Khanjian, G. Foster, et al., The effects of surface cleaning on acrylic emulsion paintings: a preliminary investigation, Tate Pap. 6 (2006) 1–14.

[46] E. Jablonski, T. Learner, J. Hayes, M. Golden, Conservation concerns for acrylic emulsion paints, Stud Conserv. 48 (1) (2003) 3–12.

[47] J.N.B. Bell, M. Treshow, Air Pollution and Plant Life, Wiley, 2002.

[48] E. Davydov, I. Gaponova, G. Pariiskii, T. Pokholok, R. Academy, Reactivity of polymers on exposure to nitrogen oxide, Chem. Chem. Technol. 4 (4) (2010).

[49] M. Anghelone, D. Jembrih-Simbürger, M. Schreiner, Influence of phthalocyanine pigments on the photo-degradation of alkyd artists' paints under different conditions of artificial solar radiation, Polym. Degrad Stab. 134 (2016) 157–168.

[50] F.X. Perrin, M. Irigoyen, E. Aragon, J.L. Vernet, Evaluation of accelerated weathering tests for three paint systems: a comparative study of their aging behaviour, Polym. Degrad. Stab. 72 (1) (2001) 115–124.

[51] W.H. Simendinger, C.M. Balik, Chemical reactions of sulfur dioxide and oxygen with unsaturated drying oils and an alkyd paint, J. Coatings Technol. 66 (837) (1994) 39–45.

[52] Socrates G. Infrared and Raman characteristic group frequencies. Tables and charts. Journal of Raman Spectroscopy. 2001.

[53] Z.E. Papliaka, K.S. Andrikopoulos, E.A. Varella, Study of the stability of a series of synthetic colorants applied with styrene-acrylic copolymer, widely used in contemporary paintings, concerning the effects of accelerated ageing, J. Cult. Herit. 11 (4) (2010) 381–391.

[54] T. Maggos, J.G. Bartzis, P. Leva, D. Kotzias, Application of photocatalytic technology for NOx removal, Appl. Phys. A Mater. Sci. Process. 89 (1) (2007) 81–84.

[55] E.J. Henderson, K. Helwig, S. Read, S.M. Rosendahl, Infrared chemical mapping of degradation products in cross-sections from paintings and painted objects, Herit. Sci. 7 (1) (2019).

[56] E. Rangel, G. Ruiz-Chavarria, L.F. Magana, Water molecule adsorption on a titanium-graphene system with high metal coverage, Carbon N. Y. 47 (2) (2009) 531–533.

[57] Spence JW, Haynie FH. Paint Technology and Air Pollution: A Survey and Economic Assessment. 1972.

[58] Pollution Prevention in the Paints and Coatings Industry. Agency USEP. 1996.

[59] C.M. Grzywacz, Monitoring for gaseous pollutants in museum environments, Tools Conserv. (2006) 1–76.

Paper VI

The Effect of Pollutant Gases on Surfactant Migration in Acrylic Emulsion Films: A Comparative Study and Preliminary Evaluation of Surface Cleaning

Laura Pagnin, Rita Wiesinger, Ayse Nur Koyun, Manfred Schreiner

Article

The Effect of Pollutant Gases on Surfactant Migration in Acrylic Emulsion Films: A Comparative Study and Preliminary Evaluation of Surface Cleaning

Laura Pagnin [1,*], Rita Wiesinger [1], Ayse Nur Koyun [2] and Manfred Schreiner [1,3]

1   Academy of Fine Arts Vienna, Institute of Science and Technology in Art, Schillerplatz 3, 1010 Vienna, Austria; r.wiesinger@akbild.ac.at (R.W.); m.schreiner@akbild.ac.at (M.S.)
2   Institute of Materials Chemistry, Technische Universität Wien, Getreidemarkt 9/165, 1060 Vienna, Austria; ayse.koyun@tuwien.ac.at
3   Institute of Chemical Technologies and Analytics, Technische Universität Wien, Getreidemarkt 9/164, 1060 Vienna, Austria
*   Correspondence: l.pagnin@akbild.ac.at

Abstract: From their first employment in the 1950s, acrylic emulsions have remained widely used as art material today. Although under certain deteriorating conditions they are very stable, if exposed to high humidity and atmospheric pollutant gases, their structural and chemical conformation is strongly affected. Dealing with the resulting surfactant migration, various cleaning treatments were considered over the years. However, their choice remains difficult as they easily alter the acrylic component, especially if in contact with aqueous solutions. The present study focuses on investigating the stability of acrylic emulsion films exposed to accelerated aging by various pollutant gases. Firstly, a comparative analytical study was carried out in order to morphologically (by 3D optical and Atomic Force Microscopy) and chemically (by Raman and Infrared spectroscopy) characterize the reactions and degradation products. Subsequently, two water-based cleaning treatments were tested, and a preliminary evaluation of their cleaning effectiveness was performed. The results show that the reaction of atmospheric gas pollutants with water molecules in moisture leads to acidic reaction products that attack the acrylic matrix and favor the migration of the surfactant to the surface. The effectiveness of cleaning treatments depends on the aging conditions applied, which further lead to different surface morphological changes.

1. Introduction

The first water-based acrylic emulsion paint used as an art material was produced in 1954 [1], presenting innovative features such as fast drying time, dilution with water, and flexibility [2]. Since the 1980s, the main chemical composition of acrylic emulsion paints was poly butyl acrylate/methyl methacrylate (p(nBA/MMA)), although there are also variants of contemporary commercial products such as polyethyl acrylate/methyl methacrylate (pEA/MMA). Its easy availability, low cost, and versatility have made acrylic emulsion extremely popular, and indeed, nowadays, contemporary art collections mainly include artworks composed of this binding medium [3]. The drying process of acrylic emulsion paints occurs through a process known as polymeric coalescence. Once the paint has been applied, the acrylic polymer molecules are assembled in droplets suspended in the aqueous phase. During the drying phase, the droplets begin to become closer to each other as water evaporates, eventually forming a continuous film. The degree of coalescence of the polymer can vary depending on the ambient conditions during drying, the glass transition temperature (Tg) of the paint film, the elasticity, the viscosity, and the presence of additives

in the mixture that can affect the film porosity [4]. Therefore, the physical properties of dried acrylic emulsion paint can vary according to the distribution and concentration of these components in the mixture, which influences the film formation process.

Specifically, additives allow higher polymer stability in the aqueous phase, the cohesion of the film, and pH stability. Being non-volatile, they also allow a better mixing or thickening of the paint components by remaining within the paint film after coalescence and curing. Therefore, their presence can affect paint aging stability and subsequent preservation treatments such as cleaning [5]. Thus, their identification in painted artworks is important for predicting possible aging behaviors and their reactivity towards the products used during the restoration practices. Several studies [6–8] have confirmed that polyethylene oxide (PEO) is the most used additive in acrylic emulsions. Being a non-ionic surfactant, it acts as a wetting, dispersing, and emulsifying agent in paint production. Furthermore, it can stabilize the polymer in aqueous dispersions under different environmental conditions, even in the presence of various pigments. However, it can migrate to the air-film interface [9], resulting in more sensitivity to light exposure. Its accumulation at the interfaces can affect the paint films in terms of mechanical resistance, adhesion to the substrates, permeability, surface gloss, and promoting dirt attraction [10].

The migratory behavior of the surfactant derives firstly from the chemical properties of the material, being hygroscopic, and secondly from the environment in which it is exposed. The high percentages of atmospheric water monitored in the outdoor exhibition spaces can favor and increase the surfactant affinity with water. Therefore, hygrometric controls will be necessary in order to monitor this physical-chemical behavior, both for artworks exhibited in outdoor or indoor environments. From a recent study [11], the surfactant migration, particle size, and its distribution were investigated in relation to the exposure of the acrylic films to pollutant gaseous agents commonly present in the ambient atmosphere (SO_2 and NO_x). According to the pollutant gas used for accelerated aging, the structural conformation of the particles and their accumulation on the surface changes. For this reason, a part of this study will focus on the morphological and chemical investigation of the different effects that gases cause on polymeric films. The degradation processes of modern art materials, related to the corrosive effect of atmospheric gaseous pollutants, is still a topic of current interest. The stability of outdoor acrylic artworks, such as contemporary murals, paintings on metal, frescoes, and polychrome sculptures, is very unstable as environmental conditions, such as humidity, pollutants, and temperature, are not easily monitored and vary seasonally [12]. Therefore, the results obtained from this investigation could support the conservation and exhibition practices of artworks, also in museum environments. The diagnostic analyses for evaluating their chemical behavior and the continuous environmental monitoring will allow an adequate preventive action of the most sensitive artistic objects [13].

As previously mentioned, the surfactant chemical properties favor its surface migration; however, being also soluble in water may be removed by green water-based cleaning methods. The choice of a correct and effective method for cleaning painted surfaces is essential in order to remove degradation deposits and, at the same time, maintain the aesthetic and physical mechanical integrity of the original materials [14]. In the case of acrylic paints, these factors are still being studied. Recent studies [15–17] have shown that this material is particularly susceptible to organic solvents and mechanical actions; therefore, further strategies and materials for its cleaning were considered and tested. Water and aqueous solutions have proved to be the most effective systems considering that the effect of pH and conductivity are variables that should not be underestimated for the overall evaluation of the cleaning action. However, this system has some disadvantages in terms of application; in fact, the water directly applied to the surface could cause swelling of the polymeric film with consequent structural and chemical fragility [18,19]. Therefore, the method of applying aqueous solutions is also a widely studied issue. In addition to the evaluation of direct application on surfaces, the use of hydrogels was also widely considered. As a thickening agent that acts as a viscous container for the aqueous

solutions it is soaked in, and it can gradually release the water on the deteriorated film with minimum pressure and mechanical action. However, even in this case, some problems were encountered, such as the irregular cleaning effect on the films and the presence of gel residues after application [20]. However, it is important to consider that other variables can also limit the cleaning effect of acrylic works. One of these is the particulate matter (PM), which is a risk for painted surfaces both because its deteriorating effect changes according to the art material (being composed of a mixture of solid and liquid particles suspended in the air), and because its accumulation on surfaces can alter the morphology of the material and compromise the cleaning operations favoring surface abrasion [21]. Another factor that can affect both degradation processes and cleaning practices is the growth of microorganisms—including algae, fungi, bacteria and even lichen—on painted surfaces [22]. In indoor environments, their expansion is influenced by heating, air conditioning, humidifiers/dehumidifiers, and human activities which, however, are more controlled factors than in an outdoor environment. In fact, higher water availability and light exposure might favor the growth of microorganisms depending on the climate of the environment and the exposition of the painted surfaces. Furthermore, additional elements can stimulate (presence of NO_2 in the urban atmosphere, availability of carbon sources in dust and dirt) or inhibit (metals present in the pigments, SO_2 from the atmosphere) their expansion on painted surfaces. These factors can make the assessment of degradation processes and subsequent cleaning practices more challenging to monitor and evaluate [23]. The experiments in this study are based on the effect of non-biological factors, and the study of biodeterioration will be a next step in order to achieve a more comprehensive understanding about aging of paint coatings in the environment.

The aims of this study focused on two main objectives: the first is to understand the degradation behaviors observed for pure acrylic films when exposed to various gaseous pollutants. The detected degradation products will be investigated firstly by microscopic and topographic observations. Subsequently, the results will be implemented by the chemical information obtained from the qualitative and semi-quantitative spectroscopic analyses. The focus is to identify the most harmful pollutant gas for acrylic paints and understand which factors increase or mitigate the deteriorating effect. The second objective is to perform a preliminary evaluation of two cleaning systems commonly used in restoration practices. They, having a different impact on acrylic surfaces, will have different cleaning effects, even according to the different pollutants used for accelerated aging. This evaluation represents a precursor study to subsequent innovative cleaning methods for acrylic paints that can be tested and compared to the results introduced here. The diagnostic analysis presented can be used to: support the prevention of the degradation of acrylic materials, develop more sophisticated environmental sensors for monitoring these pollutants (especially in indoor museum environments), and, finally, implement the knowledge related to conservation and restoration practices of acrylic artwork.

2. Experimental

2.1. Sample Preparation

Several mock-ups were prepared using a pure acrylic emulsion Plextol® D498 (Kremer Pigmente, Aichstetten, Germany). The fresh films were cast on glass slides with a wet film thickness of 150 μm using the so-called doctor-blade procedure [24]. The samples were dried at ambient conditions (approx. 22 °C and RH 30%) for three weeks.

2.2. Weathering Experiments

The artificial gas aging was carried out in a chamber (Bel-Art™SP Scienceware™) made of a co-polyester glass (Purastar®), including gas in- and outlets with a total volume of 30 cm³. The desired concentration of corrosive gas is generated by humidifying synthetic air 5.0 (Messer, Gumpoldskirchen, Austria) using double-distilled water and subsequently mixing it with the selected gas. The chamber was continuously flushed with the gas mixture with a gas flow rate of 100 L/h. The relative humidity (RH) content chosen is 80% for a

total exposure time of 168 h. The gas concentration values were selected according to the annual report released by the European Environmental Agency for air quality monitoring (see Table 1) in order to reproduce a long-term gas aging [25]. The samples were aged with gaseous pollutants representing the main and most harmful corrosive gases at the atmospheric level, namely hydrogen sulfide (H_2S), sulfur dioxide (SO_2), nitrogen oxide (NO_x), and ozone (O_3). In order to better understand the effects of aging on the polymeric films, a set of samples was aged only at RH 80%.

Table 1. Gas selected for the artificial accelerated aging and corresponding concentrations chosen.

Gas Pollutant	Concentration (ppm)	Relative Humidity (RH%)
H_2S	0.25	80
SO_2	15	80
NO_x	15	80
O_3	2500	80

2.3. Cleaning Methods

In this study, cleaning tests were performed on pure acrylic samples once artificially aged. Considering the previously mentioned studies, two cleaning systems were chosen, allowing cross-checking and evaluation of results by selected techniques.

The first test was by cotton swab rolled, a common cleaning method still used for the conservation of acrylic artworks [26]. Cleaning tests were performed using commercial cotton swabs made from pure pharmaceutical cotton. The cotton swabs were immersed in slightly acidic distilled water (pH around 5–6.5) with a conductivity of around 2–4 µS/cm (pH meter *LAQUAtwin pH33*® and conductivity meter *EC33*®, Horiba, respectively). The monitoring of pH and conductivity values is important as they are fundamental parameters for a correct surface cleaning action. The acrylic binders have acidic components in commercial products, thus, chemically susceptible to ionization/dissociation reactions already at pH 6. Therefore, an acceptable pH value is around 5–6 [27]. The cotton swab was used on the surface by applying controlled pressure for an application time of 3 min.

The second cleaning test was performed using a hydrogel system called Nanorestore Gel® Dry [28]. It is a water-based chemical gel developed by the Research Center for Colloids and Nanosciences (CSGI). Specifically, it is composed of poly(2-hydroxyethyl-methacrylate) p(HEMA)/poly (vinylpyrrolidone) (PVP), a hydrophilic polymeric film with high water retention properties and mechanical strength, designed for cleaning highly water-sensitive painting surfaces [29,30]. Its characteristics allow a cleaning action limited to the gel–paint interface. The aqueous solution/solvent is gradually released on the surface, reducing the impact and possible damage to the polymeric film given by the water. Using distilled water to carry out the cleaning test, the specific hydrogel chosen was Nanorestore Gel®—Medium Water Retention (MWR), as it is suitable for polymeric surfaces and the removal of water-soluble residues. As indicated by the product technical data sheet [31], it was immersed in distilled water for 12 h. Once the absorption phase was completed, the excess water was removed by placing each side of the hydrogel on absorbent paper for 1–2 s. Subsequently, it was placed on the aged acrylic surface and left to act for 3 min. For both tests, the distilled water used and the time of application was the same allowing a more accurate evaluation of the resulting data. Tests were conducted on all aged samples.

2.4. Optical 3D Microscopy

A Keyence VHX-6000 microscope (Keyence, Osaka, Japan) was employed to scan each sample surface. Three-dimensional morphological images were recorded using a VH-Z100 objective (1000×), obtaining a depth profile of 10 µm (pitch scans every 2 µm). The microscope is equipped with a LED light source (5700 K). The lighting selected was partial coaxial for observations in a partial dark field to emphasize height differences. The pictures acquired were processed by using the free version ImageJ software [32]. This program

is usually applied to determine selected areas with a particular shape or a specific color range. This study used this method to obtain histograms representing the distribution and average size of the surfactant particles according to the different gas exposures. Through different image processing steps, the results were obtained as follows. Firstly, the image was converted into an 8-bit grayscale image. In this way, 256 intensity graduations (shade of grey, 0 black, and 256 white) were obtained and were assigned to each pixel. Subsequently, all pixels were separated with intensity graduation in a specific range according to the "thresholding grayscale" function. These pixels formed a unique subset of the image. Finally, the grayscale image was converted into a binary image by defining a grayscale cut-off point. Grayscale values below the cut-off become black (surfactant particles), and those above this value become white (background). The area value for each surfactant particle was obtained from this image processing, and subsequently, the from diameter value useful for the particle size distribution histograms (by using Origin software).

2.5. Atomic Force Microscopy (AFM) Combined with Raman Spectroscopy

Images were obtained using an Atomic Force Microscope WITec Alpha RSA+ (WITec, Ulm, Germany) in tapping mode. The cantilever tip is a WITec arrow reflex-coated FM (AC), spring constant k at 2.8 N/m, with a resonance frequency of 75 kHz, and lateral resolution of down to 1 nm and depth resolution of <0.3 nm. It allows a stereometric analysis obtaining the 3D surface texture of reference and aged acrylic samples. All scans were collected over a 50×50 μm^2 area (512 lines per image). The surface images of films were evaluated using the software WITec Project FIVE 5.1. The data discussed concern the topographies obtained and the respective roughness values (Sa) compared between the reference and aged samples. For an accurate and reproducible evaluation of the topographic results, three different surface areas of the samples were scanned and the surfactant roughness and particle size values were averaged. Statistical data deriving from the evaluation of AFM topographies (average particle size (μ), standard deviation (σ), and correlation coefficient (R)) were obtained using the software Project FIVE 5.1 (WITec, Germany). Specifically, the topographic scans were color line corrected by slope substraction and subsequently the statistical values were obtained in the "image histogram and statistics" section. Atomic force microscopy (AFM) was combined with Raman spectroscopy, using a confocal micro-Raman system (WITec Alpha RSA+). Measurements were performed using 532 nm excitation radiation with a real output laser power of 42 mW, integration time 0.06 s, and time/line 9 s. The sample surfaces were observed with the Zeiss objective $20\times$, and the scanned areas (20×20 μm^2) were analysed using a camera connected to the microscope. The acquisition of the spectra and their evaluation was performed with the WITec Project 5.1 software. The spectra obtained for the three scanned areas were averaged, baseline corrected, and vector normalized in order to obtain a more reliable chemical mapping of specific Raman bands.

2.6. Attenuated Total Reflection Fourier Transform Infrared Spectroscopy (ATR-FTIR)

A LUMOS Microscope (Bruker Optics, Ettlingen, Germany) with a germanium crystal was employed for the ATR-FTIR investigations. The instrument is equipped with a photoconductive cooled MCT detector. On each sample, five measuring spots were acquired in the spectral range between 4000 and 480 cm^{-1} performing 64 scans at a resolution of 4 cm^{-1}. The resulting spectra were collected and evaluated by the software OPUS® 8.0 (Bruker Optics, Germany). For the qualitative and semi-quantitative analysis, the spectra were averaged, baseline corrected, and vector normalized. Subsequently, the main absorbance bands of the surfactant were integrated. As shown in a previous study [33], selecting specific bands for the semi-quantitative evaluation will allow more reliable data to be obtained, in order to better investigate the chemical changes after aging. In Table S1, the specific surfactant absorbance bands integrated for the semi-quantitative evaluation are listed. For the chemical mapping, the total mapped area had a dimension of 1.0×1.5 mm^2; six measuring spots along the *x*-axis (optical aperture approx. 0.2 mm) and six spots along

the *y*-axis (optical aperture approx. 0.1 mm) were collected for a total of 36 spots. Each chemical mapping experiment was carried out in three different areas of the samples.

3. Results and Discussion
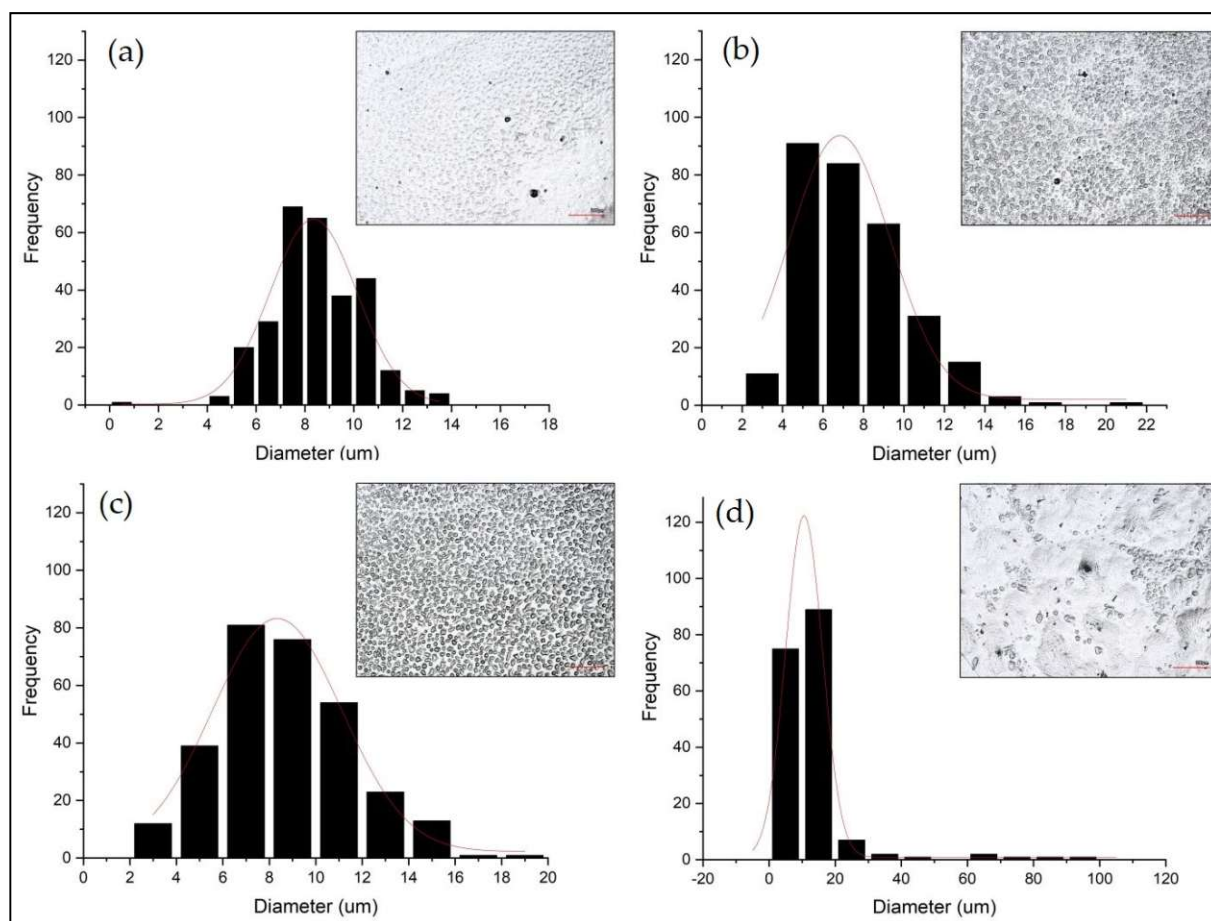
3.1. Three-Dimensional Optical Microscopy

3.1.1. After Aging

The observations using 3D optical microscopy allowed the morphological changes observed on the surface of the acrylic samples after gas aging to be evaluated. From a first investigation, with all four pollutant gases, it is possible to observe a homogeneous opacification of the surfaces. Furthermore, even with a magnification of $200\times$, the presence of some surface particles is noted. However, depending on the gas used for accelerated aging, a different feature is observed. With H_2S, SO_2, and O_3, they have a relatively uniform rounded shape and are well grouped together. On the other hand, with NO_x, they are less homogeneous, and their size varies. The acrylic sample aged exclusively with RH 80% shows some morphological changes related to the acrylic matrix; these particles are not so evident for a reliable 3D microscopic investigation. For a more detailed understanding of their different superficial migration levels, the evaluation of the particle size distribution and their average size was performed. In the present study, the particle size distribution was represented by histograms resulting from the diameter average of the particles and their frequency on the surface (Figure 1). For all four samples, the particle size distribution trend is described as a Gaussian function. The results, summarized in Table 2, are expressed as correlation coefficient (R), average particle size (μ), and standard deviation (σ).

From Figure 1, different distributions and sizes of the particle are observed. In general, after aging with H_2S and SO_2, they appear more cohesive. Their average particle size does not vary significantly, resulting in a well-distributed cluster over the entire surface. In addition, their migration after aging with O_3 presents a distribution similar to the previous ones; however, the particles are less similar and homogeneous in size. Finally, the most evident morphological changes are observed after aging with NO_x (Figure 1d). The average particle size value is very high, indicating that the particles are unevenly distributed and at different sizes on the surface. From these preliminary results, it is already possible to observe the different impacts of the pollutant gases on the polymeric film. Through subsequent AFM results, it will be possible to investigate their identification and effects in more detail.

Table 2. Parameters derived from the particle size histogram corresponding to Gaussian equations.

Samples	Weathering Conditions	Average Particle Size (μ)	Standard Deviation (σ)	Correlation Coefficient (R)
Acrylic emulsion films	H_2S + RH80%	8.35 μm	±2.09 μm	0.92
	SO_2 + RH80%	6.84 μm	±2.93 μm	0.91
	O_3 + RH80%	8.38 μm	±3.28 μm	0.98
	NO_x + RH80%	10.56 μm	±6.5 μm	0.99

Figure 1. Histograms and Gaussian functions resulting from 3D image processing (top right image in each graph): samples aged at RH 80% with (**a**) H_2S, (**b**) SO_2, (**c**) O_3, and (**d**) NO_x.

3.1.2. After Cleaning

As reported in the literature [34,35], one of the main causes of deterioration in contemporary artworks is the surface dirt and the accumulation of pollutants. In the specific case of acrylic binders, the pollutant agents employed for accelerated aging cause the migration of the surfactant, favoring the capture of dust and causing mechanical-physical damages of the polymeric layer. For this reason, as introduced in the chapter "Experimental", two cleaning practices were tested, in an attempt to evaluate the preliminary results by comparing their effectiveness on aged surfaces. The observations using 3D optical microscopy show how the two methods have a different cleaning impact depending on the type of gaseous pollutant used. In Figure S1, the acrylic films aged with RH 80% and H_2S have a surface free of surfactant particles after the application of the gel.

The samples aged with SO_2 and NO_x show the same effect, if cleaned with cotton swab rolled, and finally, for the samples aged with O_3 the cleaning action is the same with both practices. However, it is evident that the two cleaning methods have different cleaning agent release on the surface. Therefore, the water action causes mechanical-physical damages to the acrylic matrix (swelling). The AFM-Raman spectroscopy results will extend this behavior.

3.2. AFM Combined with Raman Spectroscopy

3.2.1. After Aging

Acrylic surfaces exposed to accelerated gas aging were analyzed by AFM combined with Raman spectroscopy. Figure 2 shows the comparison between the topographies of the

unaged sample (Figure 2a) and those of the samples aged with the single pollutants. As already observed, the high relative humidity used (RH 80%) caused the particle migration to the surface; however, the exposure to the various gaseous pollutants may determine a variable morphology and distribution of the amorphous particles. From the observation of the topographies and the evaluation of the roughness values (Sa) in Table 3, it is evident that all aging exposures result in a morphological change of the surface. However, it is observed that, with the same exposure time and relative humidity amount mixed with the gas, the degradation effects change. In fact, all pollutant gases favor the superficial migration of the particles based on their concentration, corrosive power, and solubility in humidified air [36]. Exposing the sample only to humidity, the morphological change mainly involves the acrylic component of the binder, resulting in swelling [37]. The different polymer/aging condition affinity is also verified by the different migration behaviors on the surface. In fact, they present a larger particle size when exposed to H_2S and NO_x and more inhomogeneous distribution when exposed to O_3 and NO_x. Probably, this behavior is due to the easier dissolubility of NO_x in humidified water mixed in the weathering chamber and the chemical affinity between surfactant and NO_x [38].
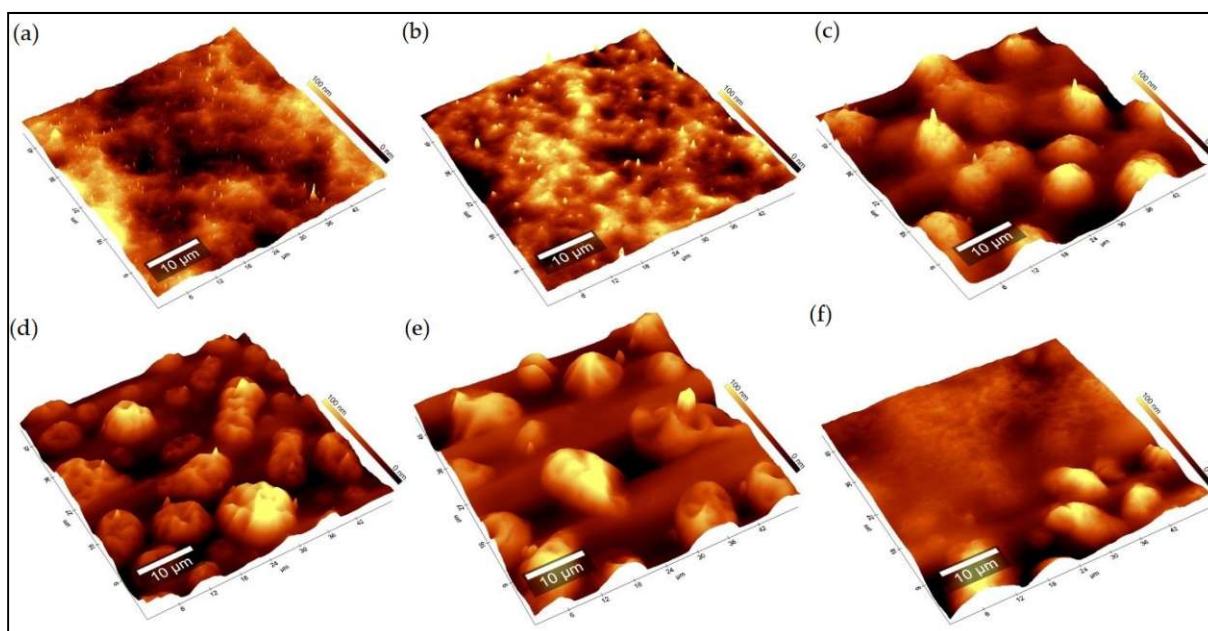

Figure 2. AFM topography images of acrylic films: (**a**) unaged; (**b**) RH 80%; (**c**) H_2S; (**d**) SO_2; (**e**) O_3; (**f**) NO_x aged.

Table 3. AFM roughness values for acrylic films.

Samples	Weathering Conditions	Sa [nm]	Average Particle Size [µm]
	Unaged	76.3	-
	RH80%, 168 h	95.2	-
Pure acrylic film	H_2S, RH80%, 168 h	207.5	8.74 ± 1.24
	SO_2, RH80%, 168 h	231.6	5.44 ± 2.1
	O_3, RH80%, 168 h	333.5	7.84 ± 4.5
	NO_x, RH80%, 168 h	407.8	10.8 ± 6.7

By combining AFM images with Raman chemical mappings (Figure 3), it was possible to identify the polymeric binder as methyl methacrylate and butyl acrylate compound (PMMA-nBA) by the presence of the main bands at 813 and 847 cm^{-1} of C-H rocking, 1300 cm^{-1} of C-H twisting/rocking, 1456 cm^{-1} of the C-H bending, 1738 cm^{-1} of the C=O stretching, and 2877, 2935, and 2950 cm^{-1} of the C-H stretching [39]. Furthermore, the band at 2924 cm^{-1} was identified as a surfactant signal, i.e., polyethylene oxide (PEO) [40].

After normalization of the spectra obtained from the scanned sections, the band area of the surfactant was integrated, and the chemical mapping for each aged sample was acquired. As shown with the AFM topographies, the impact of the pollutant gases on the surfaces favors the migration of the surfactant, which, depending on the gas exposure, assumes different conformations and distributions. The worst degrading effect is observed for the samples aged with NO_x and O_3, subsequently decreasing with SO_2, H_2S, and finally RH 80%.
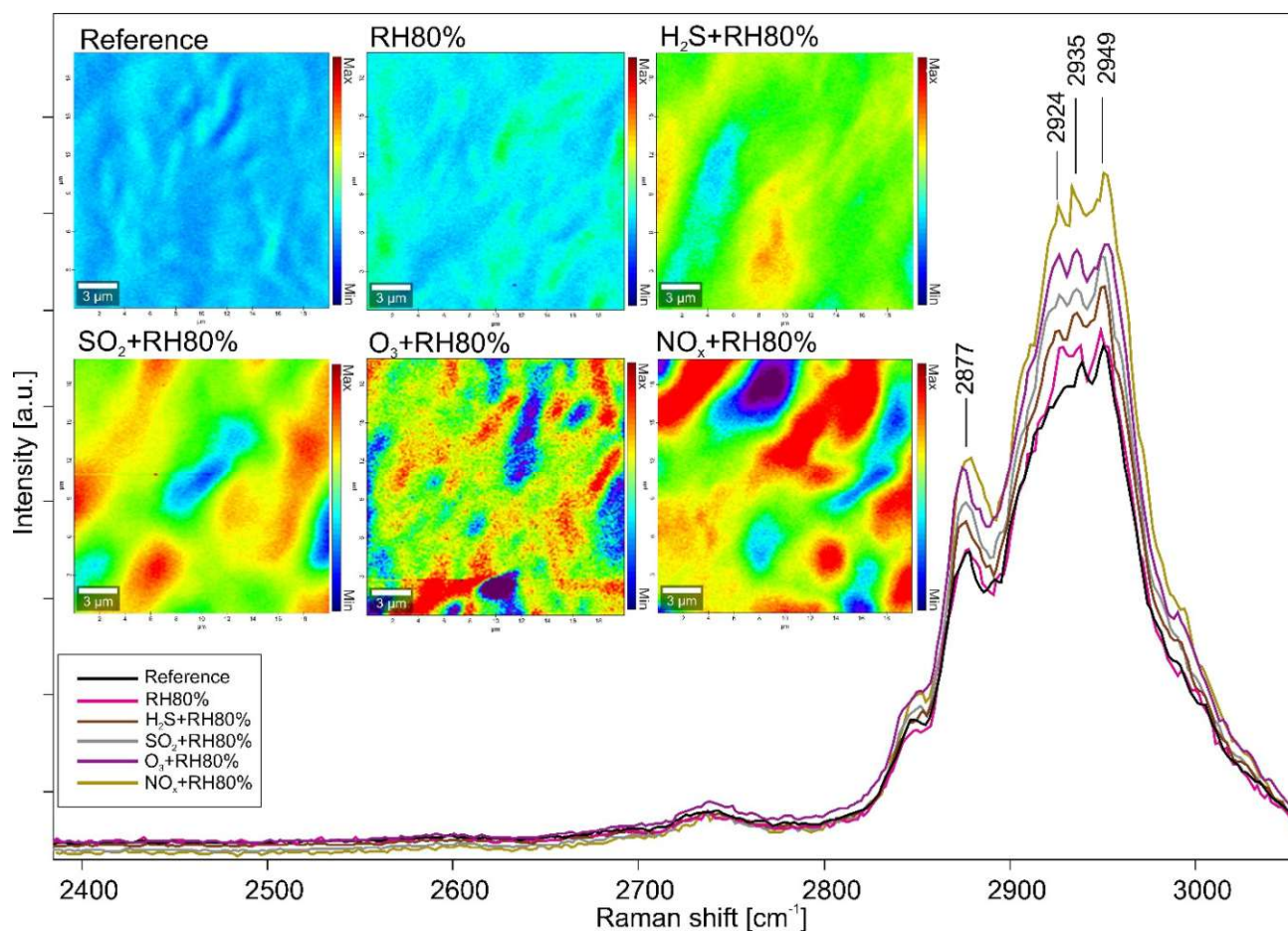
Figure 3. Raman chemical mapping of the PEO band at 2924 cm^{-1} for all investigated acrylic samples.

3.2.2. After Cleaning

The same data processing and morphological-chemical investigation were carried out to evaluate the cleaning method's efficacy under examination [41]. Figure 4 and Table 4 compare the topographies and related roughness values (Sa) between the aged and cleaned samples using a cotton swab rolled and hydrogel test. In detail, the most effective cleaning method would result from the swab rolled test, obtaining Sa values very similar to those of the unaged acrylic surface. Using the hydrogel, these values remain high; however, if compared to the aged sample, they are lower. Furthermore, samples aged with NO_x appear to be less subject to cleaning, while the Sa value of the RH 80% aged sample slightly increases, probably due to the action of water that favored the swelling process. For samples cleaned with the swab rolled, the trend slightly changes. NO_x is still the pollutant causing the worst degradation effect; whereas, the surface exposed to O_3, once cleaned, shows morphological changes comparable to those of unaged samples. On the other hand, observing the Raman chemical mappings, a superficial morphological improvement does not always correspond to a total removal of the surfactant particles on the surface. Integrating the PEO band (2924 cm^{-1}), according to the different pollutant exposure, the

effectiveness of the cleaning method changes. In samples aged with RH 80% and H₂S, the surfactant particles easily dissolve when treated with the gel; those aged with SO₂ and NO$_x$ when treated with swab rolled, while those aged with O₃ show a similar cleaning effect with both methods.
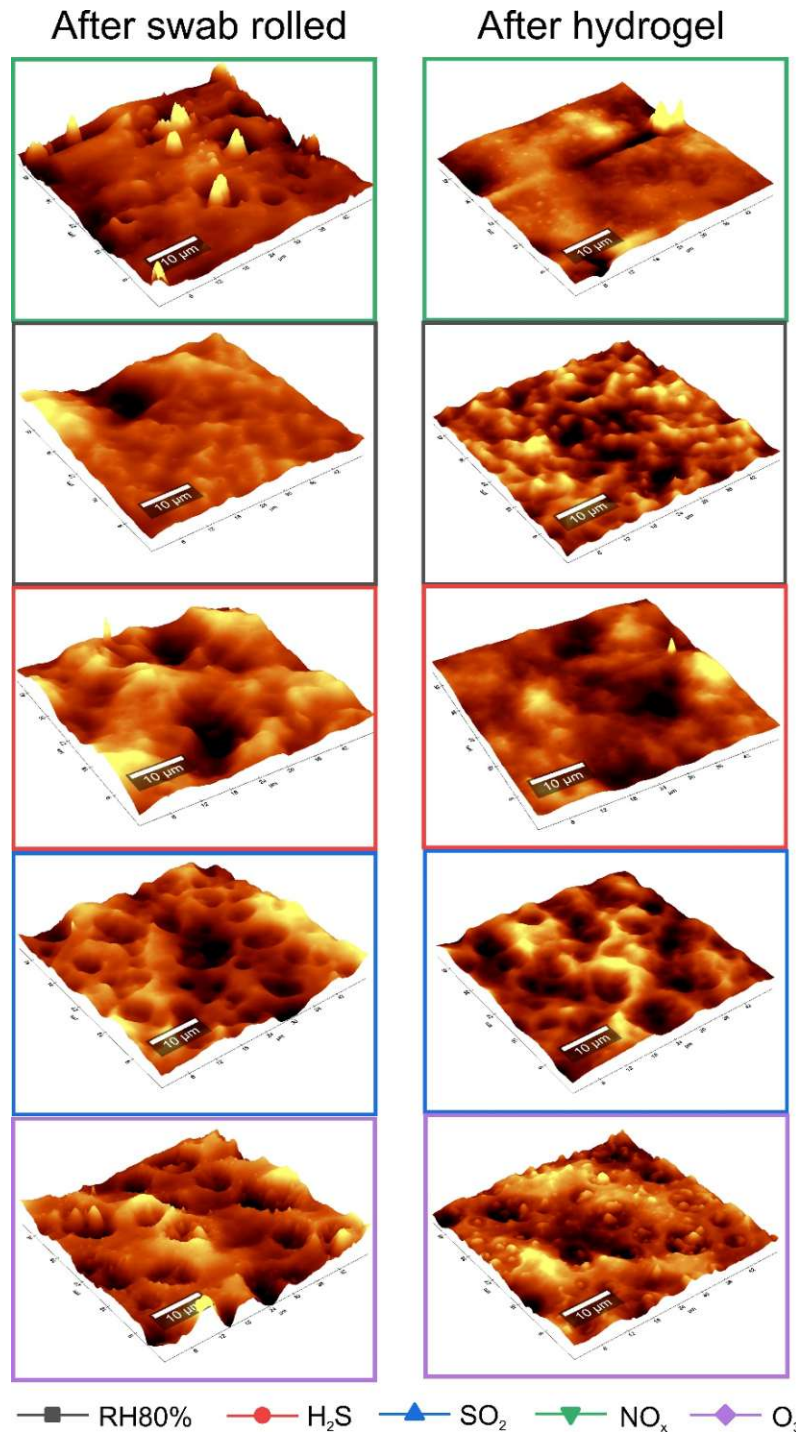

Figure 4. AFM topographies after gas aging and cleaning with swab rolled and hydrogel test.

Table 4. AFM roughness values (Sa) obtained after gas aging and after cleaning treatments.

Weathering Conditions	Sa [nm]		
	After Aging	After Swab Rolled	After Hydrogel
RH 80%	95.1	85.2	123.5
H_2S + RH 80%	207.4	75.9	145.7
SO_2 + RH 80%	231.6	75	136
O_3 + RH 80%	333.4	62.5	146.6
NO_x + RH 80%	407.8	174.1	385.7

As previously mentioned for the 3D Optical Microscopy results, it was possible to determine with Raman chemical mappings that the action of the water had an impact on the acrylic matrix. In fact, with both cleaning methods, the release of the water on the surface led to the deformation of the polymeric film; moreover, despite the removal of the surfactant particles, they left cavities on the surface layer of the acrylic binder. These cavities could allow the accumulation of dirt, and favor the penetration of subsequent pollutants (UV radiation, pollutant gas, humidity, temperature), leading to further degradation processes [36].

3.3. ATR-FTIR Spectroscopy

3.3.1. After Aging

The main functional bands of acrylic samples were identified using ATR-FTIR analysis and listed in Table S2. The specific co-polymer identified is nBA/MMA through the following spectral IR signals: the stretching vibrations of the C-H bond (at 2956–2876 cm^{-1}), the C=O stretching (at 1726 cm^{-1}), and the bands of the C-O-C and C-O stretching (at 1236, 1160, 1146 cm^{-1}) in the fingerprint region [33]. Furthermore, the three absorbance bands at 2895, 1343, and 1115 cm^{-1} were characterized as spectral signals of the surfactant PEO (polyethylene oxide) [42,43], confirming the previous Raman characterization. To understand the different degradation processes of the acrylic binder, FTIR chemical mapping was performed. It was used to investigate the various surface distributions of the surfactant according to the different pollutants and compared the results with Raman ones. The surfactant spectral signal (2895 cm^{-1}) was integrated for the mapping of the acrylic emulsions, and its distribution on the scanned area was evaluated. This absorbance band was integrated to better compare the chemical mapping performed with Raman spectroscopy in which the same functional group was integrated. In Figure 5, it is observed that the inhomogeneous surfactant distribution on the surface is mainly favored by NO_x, followed by O_3, SO_2, H_2S, and finally RH 80%, confirming the previous Raman results. They also lead to the understanding that surfactant particles differ not only morphologically but also by molecular analysis. In fact, the intensity of the integrated absorbance band appears to be higher for the samples aged with NO_x and O_3, confirming that the surfactant particles are more widespread and thicker under these aging conditions (as observed with the AFM evaluation of roughness).

To support this evaluation, semi-quantitative analysis was performed by integrating the three spectral bands of the surfactant (2895, 1343, 1115 cm^{-1}) and comparing the values obtained from the unaged and aged samples. In Figure S2 and Table S3, the degradation trends and the respective plotted values are presented. From this evaluation, it is possible to understand that the deteriorating effect is more significant with NO_x than with other pollutant gases. It seems that the band at 1115 cm^{-1} is more affected, contrary to the other two bands; however, the corrosive trend (NO_x > O_3 > SO_2 > H_2S > RH80%) is always observed. Additionally, the integration of the band at 1726 cm^{-1} of the carbonyl group (acrylic component) and the calculation of the difference between these values and those of the band at 1115 cm^{-1} were performed. It is observed that the increase of the IR signal of the surfactant is directly proportional to the decrease of the carbonyl band, indicating that

the pollutants not only favor the migration of the surfactant but also oxidize the functional groups of the polymeric matrix.
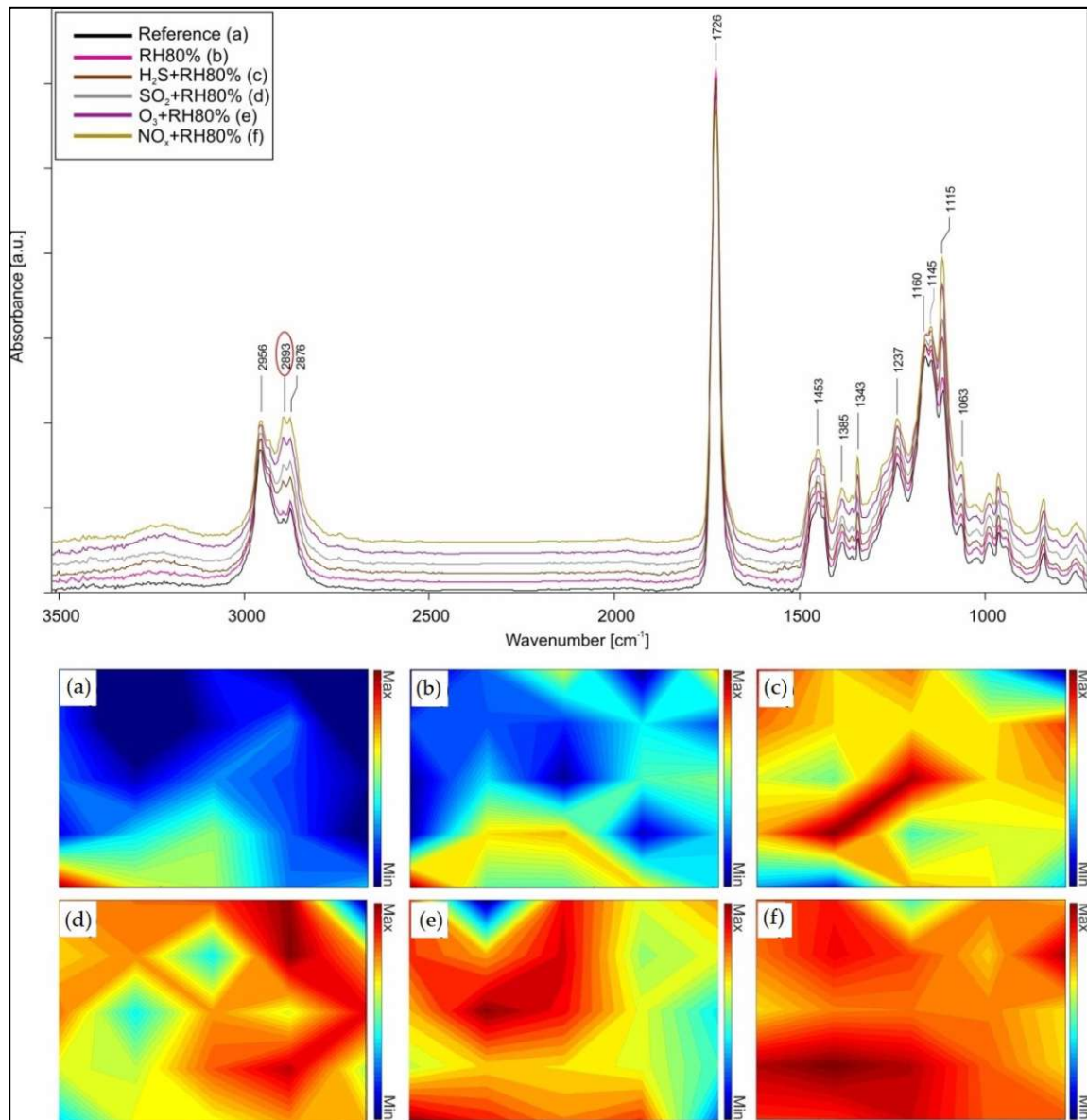
Figure 5. ATR-FTIR spectra and chemical mapping of the surfactant absorbance band integration at 2895 cm^{-1}: (**a**) before aging and after (**b**) RH 80%, (**c**) H$_2$S + RH 80%, (**d**) SO$_2$ + RH 80%, (**e**) O$_3$ + RH 80%, and (**f**) NO$_x$ + RH 80%.

These degradation mechanisms can be explained by considering the solubility kinetics of the various pollutant gases used. As underlined by the results presented, NO$_x$ and O$_3$ are the most impacting corrosive agents on the stability of the acrylic emulsions, although they have two different physical-chemical behaviors in an aqueous environment. The solubility of NO$_x$ is the least understood, as it has numerous species and reactions involved in the reactive process [44]. In this study, the gaseous mixture used mainly includes two nitrogen oxides, namely NO and NO$_2$. According to the literature [38,45], NO (nitric oxide) hardly dissolves in water, while NO$_2$ (nitrogen dioxide) reacts immediately with water upon dissolution resulting in HNO$_3$ (nitric acid). It leads to a stronger corrosive kinetics than the other pollutant gases causing bond breaking of the acrylic matrix by oxidation and the promotion of surfactant migration to the surface. Furthermore, as shown by previous studies [46], NO$_x$ has a greater affinity with organic compounds that, summed

to the capability to dissociate in an aqueous environment easily, promotes hydrolysis reactions. It leads to an increasing level of degradation of acrylic films, also depending on the relative humidity value in the environment. On the contrary, when O_3 is in an aqueous environment (or at high humidity values), it leads to the formation of radical species [47]. These radicals are strong oxidizing agents attacking unsaturated linkages of the acrylic emulsions. Furthermore, the presence of water causes hydrolysis reactions attacking the sensitive groups present in the polymer. Specifically, PBMA is not one of the most stable conformations of acrylic emulsion and, if exposed to deteriorating agents, it undergoes a rapid and extensive fragmentation, leading to an overall loss of structural and molecular properties [48].

3.3.2. After Cleaning

An ATR-FTIR evaluation was also performed after the subsequent cleaning treatments of the acrylic emulsions. It was important to understand the cleaning level of the two chosen methods (swab rolled and hydrogel test) both at a qualitative and semi-quantitative level. As shown in Figure 6, both cleaning procedures reduce the intensity some spectral signals characterized as surfactant bands. In particular, the signal at 1115 cm^{-1} verifies the impact of the different releases of water on the surface, according to the chosen degradation conditions. In fact, supporting these results with the FTIR chemical mappings carried out on larger areas (Figure S3 and Table S4), it is evident how the surface particles of surfactant are reduced. In particular, the use of the swab rolled test favors the cleaning of acrylic surfaces aged by SO_2 and NO_x, whereas the hydrogel test is more effective on those aged by RH 80% and H_2S. Both cleaning methods on O_3 aged samples are equally suitable.
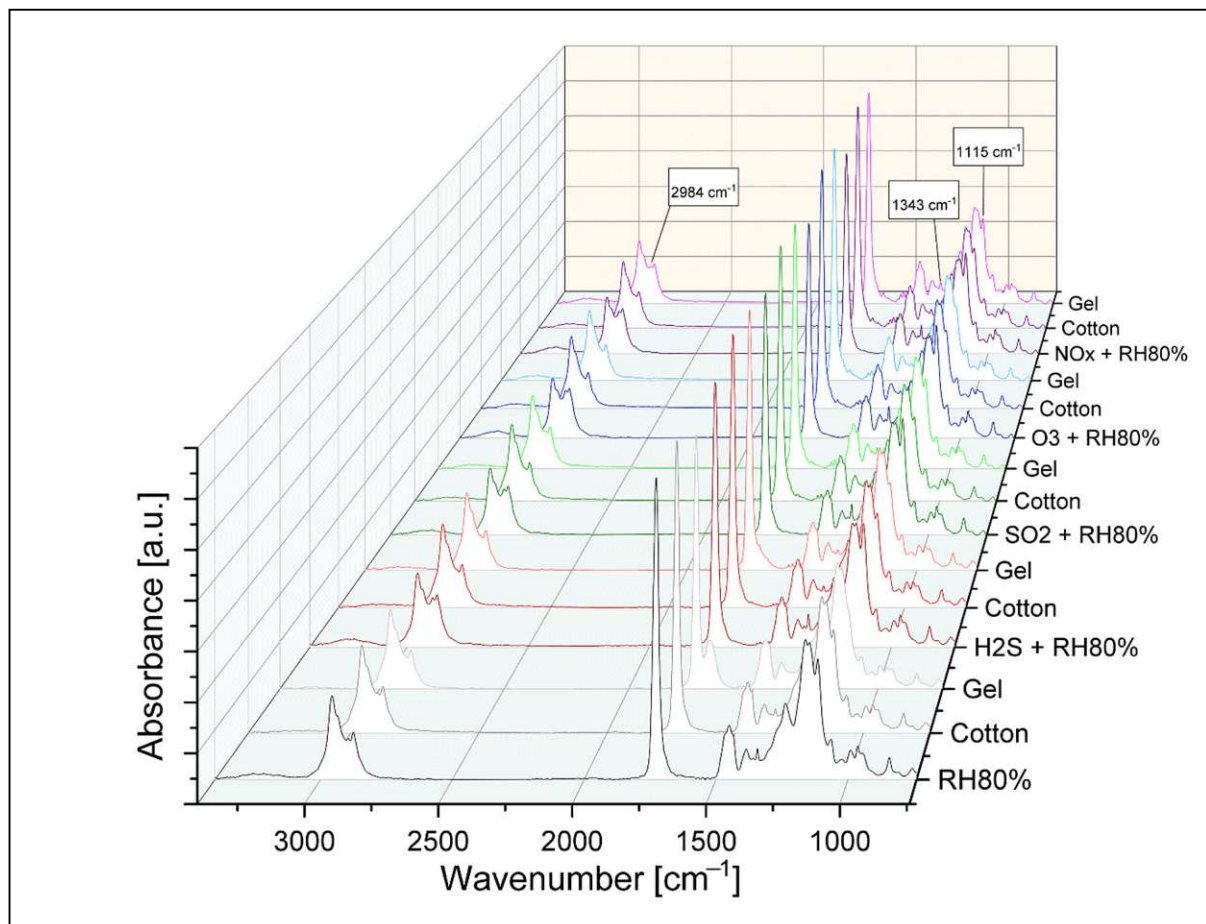

Figure 6. Comparison between ATR-FTIR spectra of aged samples and their surfaces after cotton swab rolling and gel test.

However, as mentioned in the literature [49,50], the aqueous treatments always cause physical-mechanical damage on acrylic emulsions. The two methods proposed have advantages as well as disadvantages. Although the swab rolled is the most effective, as it allows roughness values similar to the initial ones to be reached, it causes more significant surface swelling effects. In fact, the water release on the surface is not easily controlled, and the direct contact intensified by mechanical action causes damages to the acrylic matrix, making the film structurally and chemically weaker and prone to the attack of subsequent pollutants (dust, dirt, light radiation, humidity, air pollutants).

On the other hand, the hydrogel can modulate the aqueous impact on the acrylic surface (less swelling), but the cleaning action seems to be more effective on surfaces subject to high humidity values or on aged samples with less aggressive pollutant gases. This issue may be solved by increasing the time of gel application on the acrylic emulsions, while continuing to monitor possible structural changes. Finally, in some regions of samples, an ATR-FTIR band at 1680 cm^{-1} was observed after the application of the gel. It was identified as gel residue (Figure 6) [51].

4. Conclusions

In this study, accelerated aging by pollutant gases and relative humidity of acrylic emulsion films was performed. The innovative aspect of this evaluation is the use of microscopic analyses not focusing only on the surface morphological observations but applying statistical evaluations to understand the particle size, distribution, and roughness of the degradation products according to the different pollutant gas employed. In addition to being compared with each other, the results will be implemented using non-invasive spectroscopic techniques that explain the chemical-physical nature of the degradation processes focused on the acrylic film surfaces. Another new aspect of this study is the comparative investigation between the results obtained after accelerated aging and those after cleaning. In detail, in the first part, the results focus on the characterization of acrylic emulsions and degradation products resulting from gaseous aging. The identification of this polymeric system is complex, as some molecular structures are very similar, and some formulations include the presence of different additives. In this specific study, polyethylene oxide (PEO) was identified as the main additive in the acrylic emulsions. As it has hygroscopic properties, once it is exposed to certain aging conditions, it migrates to the surface in the form of particles which, from observations to the 3D microscope, cause the opacification of the superficial acrylic component. This behavior can influence the mechanical resistance, the adhesion, the permeability, and the attraction of dirt on the acrylic emulsion surfaces. Furthermore, depending on the type of pollutant, different changes concerning the superficial distribution, particle size, and roughness are observed. From the evaluation and comparison of the microscopic (3D and atomic force microscopy) and chemical (Raman and FTIR spectroscopy) results, the gaseous pollutant that causes the greatest damage to acrylic emulsions, in terms of structural impact, increases of roughness values, and extends the dispersion of surfactant particles is NO$_x$, followed by O$_3$, SO$_2$, H$_2$S, and RH 80%. Probably, this phenomenon is related to the solubility of gases in humidified environment and the chemical surfactant–gas affinity.

Subsequently, the study focused on the preliminary evaluation of the effectiveness of some cleaning treatments used for the surfactant removal. The choice of the most appropriate cleaning method for acrylic emulsions is a topic still discussed today because, depending on the treatment used, it can damage the structural and chemical integrity of the acrylic matrix. For this reason, two cleaning procedures were considered: the first using cotton swab rolled and the second using a hydrogel system. From the assessments performed, both treatments have advantages and disadvantages. From the AFM topographies and chemical mappings, surfactant removal is more effective with cotton swab rolled; however, it compromises the structural stability of the acrylic component by causing surface swelling. On the other hand, although the hydrogel allows the gradual release of water for a more controlled cleaning and limits swelling, it does not allow a regular cleaning effect and gel

residues are observed after application. The cleaning effects are also influenced by the interaction between acrylic film and pollutant; in fact, the cotton swab rolled test is more effective on samples aged by SO_2 and NO_x, whereas the hydrogel on those aged by RH80% and H_2S.

The results obtained so far show how various physical-chemical interactions are observed, depending on the formulations of the acrylic emulsions and the influence of the gaseous pollutant agents. The results obtained from the mock-up tests could then be confirmed and expanded with further investigations (on real cases, commercial acrylic paints, use of different solvents for cleaning, additional accelerated aging conditions) and analytical-diagnostic analysis (mechanical, thermal, separation techniques). The study of the deteriorating behaviors deriving from the gaseous exposure of acrylic paints, mixed with different inorganic and organic pigments, could be a further research topic as they can promote or reduce the consequent degradation reactions [52,53]. In addition to the use of different solvents for cleaning acrylic surfaces, a further implementation of the study can be to test new cleaning products and monitor their effectiveness on the surfaces [54].

To extend the knowledge about artificial gas aging, future experiments will be considered. As mentioned in the introduction, the effect of different pollutant gases and particulate matter also significantly influences the stability of artworks. Therefore, a future study can be the cross evaluation of pollutants. The combination of two or more pollutants and their synergy with different relative humidity values, gas concentration, and exposure time, will provide additional information about their chemical stability and the oxidizing effect. Furthermore, this study provides further clarifications regarding some conservative aspects highlighted in the museum environment [55], related to the degradation processes deriving from environmental variables, and the effectiveness of cleaning treatments on aged acrylic objects.

References

1. Jablonski, E.; Learner, T.; Hayes, J.; Golden, M. Conservation concerns for acrylic emulsion paints. *Stud. Conserv.* **2003**, *48*, 3–12. [CrossRef]
2. Learner, T. A review of synthetic binding media in twentieth-century paints. *Conservator* **2000**, *24*, 96–103. [CrossRef]
3. Learner, T.J.S.; Smithen, P.; Krueger, J.W.; Schilling, M.R. *Modern Paints Uncovered*; The Getty Conservation Institute: Los Angeles, CA, USA, 2007.
4. Ormsby, B.; Learner, T. The effects of wet surface cleaning treatments on acrylic emulsion artists' paints—A review of recent scientific research. *Stud. Conserv.* **2010**, *55*, 29–41. [CrossRef]
5. Crook, J.; Learner, T. *The Impact of Modern Paints*; Tate Gallery: London, UK, 2000.
6. Agarwal, N.; Farris, R.J. Water absorption by acrylic-based latex blend films and its effect on their properties. *J. Appl. Polym. Sci.* **1999**, *72*, 1407–1419. [CrossRef]
7. Owen, L.; Ploeger, R.; Murray, A. The effects of water exposure on surface characteristics of acrylic emulsion paints. *J. Can. Assoc. Conserv.* **2004**, *29*, 8–25.
8. Ploeger, R.; Murray, A.; Hesp, S.; Scalarone, D. Morphological changes and rates of leaching of water-soluble material from artists' acrylic paint films during aqueous immersions. *Mod. Paint. Uncovered Proc. Mod. Paint. Uncovered Symp.* **2007**, 201–207.
9. Digney-Peer, S.; Burnstock, A.; Learner, T.; Khanjian, H.; Hoogland, F.; Boon, J. The Migration of Surfactants in Acrylic Emulsion Paint Films. *Stud. Conserv.* **2004**, *49*, 202–207. [CrossRef]
10. Chiantore, O.; Scalarone, D.; Learner, T. Characterization of Artists' Acrylic Emulsion Paints. *Int. J. Polym. Anal. Charact.* **2003**, *8*, 67–82. [CrossRef]
11. Pagnin, L.; Calvini, R.; Wiesinger, R.; Schreiner, M. SO_{2-} and NO_{x-} initiated atmospheric degradation of polymeric films: Morphological and chemical changes, influence of relative humidity and inorganic pigments. *Microchem. J.* **2021**, *164*, 106087. [CrossRef]
12. Hamilton, R.; Kucera, V.; Tidblad, J.; Watt, J. *The Effects of Air Pollution on Cultural Heritage*; Springer: London, UK, 2009. [CrossRef]
13. De Santis, F.; Di Palo, V.; Allegrini, I. Determination of some atmospheric pollutants inside a museum: Relationship with the concentration outside. *Sci. Total Environ.* **1992**, *127*, 211–223. [CrossRef]
14. Fardi, T.; Pintus, V.; Kampasakali, E.; Pavlidou, E.; Papaspyropoulos, K.G.; Schreiner, M.; Kyriacou, G.; Kampasakali, E. A novel methodological approach for the assessment of surface cleaning of acrylic emulsion paints. *Microchem. J.* **2018**, *141*, 25–39. [CrossRef]
15. Ormsby, B.; Kampasakali, E.; Learner, T. Surfactants and Acrylic Emulsion Paints: Evaluating Changes Induced by Wet Surface Cleaning Treatments. In *New Insights into the Cleaning of Paintings (Proceedings from the Cleaning 2010 International Conference, Universidad Politécnica de Valencia and Museum Conservation Institute)*; The Smithsonian Institution: Washington, DC, USA, 2010; pp. 159–164.
16. Ormsby, B.; Barker, R.; Hellen, R.; Smithen, P. Cleaning Acrylic Emulsion Paintings: Case Study Treatments, Evaluation and Reflections. In *What's Changing: Theories and Practices in the Restoration of Contemporary Art*; Castello di Rivoli Museo D'Arte: Turin, Italy, 2012.
17. Ziraldo, I.; Watts, K.; Luk, A.; Lagalante, A.F.; Wolbers, R.C. The influence of temperature and humidity on swelling and surfactant migration in acrylic emulsion paint films. *Stud. Conserv.* **2016**, *61*, 209–221. [CrossRef]
18. Ormsby, B.; Learner, T.; Foster, G.; Druzik, J.; Schilling, M. Wet–cleaning Acrylic Emulsion Paint Films: An Evaluation of Physical, Chemical and Optical Changes. In *Modern Paints Uncovered*; Institute GC: Los Angeles, CA, USA, 2007; pp. 187–198.
19. Scalarone, D.; Lazzari, M.; Castelvetro, V.; Chiantore, O. Surface Monitoring of Surfactant Phase Separation and Stability in Waterborne Acrylic Coatings. *Chem. Mater.* **2007**, *19*, 6107–6113. [CrossRef]
20. Riedo, C.; Rollo, G.; Chiantore, O.; Scalarone, D. Detection and Identification of Possible Gel Residues on the Surface of Paintings after Cleaning Treatments. *Heritage* **2021**, *4*, 304–315. [CrossRef]
21. Grau-Bové, J.; Budič, B.; Cigić, I.K.; Thickett, D.; Signorello, S.; Strlič, M. The effect of particulate matter on paper degradation. *Herit. Sci.* **2016**, *4*, 79. [CrossRef]
22. Gaylarde, C.; Morton, L.; Loh, K.; Shirakawa, M. Biodeterioration of external architectural paint films—A review. *Int. Biodeterior. Biodegrad.* **2011**, *65*, 1189–1198. [CrossRef]
23. Shirakawa, M.A.; Tavares, R.G.; Gaylarde, C.; Taqueda, M.E.S.; Loh, K.; John, V.M. Climate as the most important factor determining anti-fungal biocide performance in paint films. *Sci. Total Environ.* **2010**, *408*, 5878–5886. [CrossRef] [PubMed]
24. Berni, A.; Mennig, M.S.H. Doctor blades. In *Sol-Gel Technologies for Glass Producers and Users*; Springer: Boston, MA, USA, 2004; pp. 89–92.
25. European Environment Agency. Available online: http://www.eea.europa.eu/ (accessed on 16 December 2020).
26. Ormsby, B.; Kampasakali, E.; Miliani, C.; Learner, T. An FTIR-Based Exploration of the Effects of Wet Cleaning Treatments on Artists. *E-Preserv. Sci.* **2009**, *405*, 186–195.
27. Cremonesi, P. *L'ambiente Acquoso per il Trattamento di Manufatti Artistici*; il Prato, Collana I Talenti: Verona, Italy, 2019.
28. Baglioni, P.; Carretti, E.; Chelazzi, D. Nanomaterials in art conservation. *Nat. Nanotechnol.* **2015**, *10*, 287–290. [CrossRef]
29. Domingues, J.A.L.; Bonelli, N.; Giorgi, R.; Fratini, E.; Gorel, F.; Baglioni, P. Innovative Hydrogels Based on Semi-Interpenetrating p(HEMA)/PVP Networks for the Cleaning of Water-Sensitive Cultural Heritage Artifacts. *Langmuir* **2013**, *29*, 2746–2755. [CrossRef]

30. Eriksson, H.; Wedberg, I.; Nesson, J.; Bronmark-Thourlund, M. The use of nanorestore gels in the conservation of lime-based wall-paintings. In *Gels Conserv. Art*; Archetype Publications Ltd.: London, UK, 2017; pp. 270–273.

31. CSGI. *Nanorestore Gel® Medium Water Retention—MWR*; CSGI: Florence, Italy, 2015.

32. ImageJ Software. 2020. Available online: https://imagej.nih.gov/ij/ (accessed on 16 December 2020).

33. Wiesinger, R.; Pagnin, L.; Anghelone, M.; Moretto, L.M.; Orsega, E.F.; Schreiner, M. Pigment and Binder Concentrations in Modern Paint Samples Determined by IR and Raman Spectroscopy. *Angew. Chem. Int. Ed.* **2018**, *57*, 7401–7407. [CrossRef] [PubMed]

34. Perry, R. Problems of dirt accumulation and its removal from unvarnished paintings: A practical review. In *Dirt Pict. Separated*; UKIC: London, UK, 1990; pp. 3–6.

35. Giordano, A.; Barresi, G.; Rotolo, V.; Schiavone, S.; Palla, F. The Conservation of Contemporary Paintings: From Dry Cleaning to Microemulsions. *Nanotechnol. Nanomater. Diagn. Conserv. Restor. Cult. Herit.* **2019**, 277–298. [CrossRef]

36. Moncmanová, A. Environmental Deterioration of Materials. In *Environmental Deterioration of Materials*; Press, W., Ed.; Southampton: Boston, MA, USA, 2007; pp. 1–25.

37. Kientz, E.; Dobler, F.; Holl, Y. Desorption of the surfactant from the particle surface during latex film formation. *Polym. Int.* **1994**, *34*, 125–134. [CrossRef]

38. Tan, S.P.; Piri, M. Modeling the Solubility of Nitrogen Dioxide in Water Using Perturbed-Chain Statistical Associating Fluid Theory. *Ind. Eng. Chem. Res.* **2013**, *52*, 16032–16043. [CrossRef]

39. Anghelone, M.; Jembrih-Simbürger, D.; Schreiner, M. Identification of copper phthalocyanine blue polymorphs in unaged and aged paint systems by means of micro-Raman spectroscopy and Random Forest. *Spectrochim. Acta Part A Mol. Biomol. Spectrosc.* **2015**, *149*, 419–425. [CrossRef]

40. Elashmawi, I.; Gaabour, L.H. Raman, morphology and electrical behavior of nanocomposites based on PEO/PVDF with multi-walled carbon nanotubes. *Results Phys.* **2015**, *5*, 105–110. [CrossRef]

41. Kampasakali, E.; Ormsby, B.; Cosentino, A.; Miliani, C.; Learner, T. A Preliminary Evaluation of the Surfaces of Acrylic Emulsion Paint Films and the Effects of Wet-Cleaning Treatment by Atomic Force Microscopy (AFM). *Stud. Conserv.* **2011**, *56*, 216–230. [CrossRef]

42. Learner, T.J.S. *Analysis of Modern Paints*; The Getty Conservation Institute: Los Angeles, CA, USA, 2005.

43. Anghelone, M.; Stoytschew, V.; Jembrih-Simbürger, D.; Schreiner, M. Spectroscopic methods for the identification and photostability study of red synthetic organic pigments in alkyd and acrylic paints. *Microchem. J.* **2018**, *139*, 155–163. [CrossRef]

44. Burdick, C.L.; Freed, E.S. The Equilibrium between Nitric Oxide, Nitrogen Peroxide and Aqueous Solution of Nitric Acid. *J. Am. Chem. Soc.* **1921**, *43*, 518–530. [CrossRef]

45. Schwartz, S.E.; White, W.H. Solubility Equilibria of the Nitrogen Oxides and Oxyacids in Dilute Aqueous Solution. In *Advances in Environmental Science and Engineering*; Gordon and Breach Science: New York, NY, USA, 1981; pp. 1–45.

46. Xiao, G.; Huang, A.; Su, H.; Tan, T. The activity of acrylic-silicon/nano-TiO$_2$ films for the visible-light degradation of formaldehyde and NO2. *Build. Environ.* **2013**, *65*, 215–221. [CrossRef]

47. Peleg, M. The chemistry of ozone in the treatment of water. *Water Res.* **1976**, *10*, 361–365. [CrossRef]

48. Chiantore, O.; Trossarelli, L.; Lazzari, M. Photooxidative degradation of acrylic and methacrylic polymers. *Polymer* **2000**, *41*, 1657–1668. [CrossRef]

49. Murray, A.; de Berenfeld, C.C.; Chang, S.S.; Jablonski, E.; Klein, T.; Riggs, M.C.; Robertson, E.C.; Tse, W.A. The Condition and Cleaning of Acrylic Emulsion Paintings. *MRS Proc.* **2002**, *712*, 83–90. [CrossRef]

50. Ormsby, B.; Learner, T.; Schilling, M.; Druzik, J.; Khanjian, H.; Foster, G.; Sloan, M. The effects of surface cleaning on acrylic emulsion paintings: A preliminary investigation. *Tate Pap.* **2006**, *6*, 1–14.

51. Stulik, D.; Miller, D.; Khanjian, H.; Khandekar, N.; Wolbers, R.; Carlson, J.; Petersen, W.C. *Solvent Gels for the Cleaning of Works of Art: The Residue Question*; The Getty Conservation Institute: Los Angeles, CA, USA, 2004; Volume 1.

52. Mohamed, M.; Ahmed, N.; Mohamed, W.; Mabrouk, M. Novel water-based coatings of acrylic-polyurethane reinforced with mixed metal pigment for oil and gas pipelines protection. *Prog. Org. Coat.* **2020**, *149*, 105941. [CrossRef]

53. Mahi, O.; Khaldi, K.; Belardja, M.S.; Belmokhtar, A.; Benyoucef, A. Development of a New Hybrid Adsorbent from Opuntia Ficus Indica NaOH-Activated with PANI-Reinforced and Its Potential Use in Orange-G Dye Removal. *J. Inorg. Organomet. Polym.* **2021**, *31*, 2095–2104. [CrossRef]

54. Yang, J.; Lee, S.; Choi, I.; Shin, J.; Han, W.-H.; Hong, M.-H.; Kang, H.-C.; Kim, Y.-W. Effect of fatty acid-based anionic surfactants on the emulsion properties of self-emulsifying poly(ethylene-co-acrylic acid) waxes. *J. Ind. Eng. Chem.* **2019**, *71*, 393–401. [CrossRef]

55. Canosa, E.; Norrehed, S. *Strategies for Pollutant Monitoring in Museum Environments*; Riksantikvarieämbetet: Stockholm, Sweden, 2019. [CrossRef]

Curriculum Vitae

Laura Pagnin, MSc.

Personal Information

Address	Leibnizgasse 62/23, 1100 Vienna (Austria)
Telephone	+39 3470861103
E-mail	l.pagnin@akbild.ac.at laura.pagnin93@gmail.com
Nationality	Italian
Date of birth	06.07.1993
Links	https://www.akbild.ac.at/portal_akbild_cardbox/D051395837E585E7
	https://at.linkedin.com/in/laura-pagnin-19b81a110
	https://www.researchgate.net/profile/Laura_Pagnin

Work experiences

Dates	March 2018 – present
Employer	Institute for Science and Technology in Art, Academy of Fine Arts Vienna, (Austria)
Position	**Lecturer**
Main activities	Lectures held: - General Chemistry I & II - Practical Examination I - Microchemical Evidences - Technique Examination II - Microscopic Methods - Material science investigations I & II - seminar

Dates	December 2017 – present
Employer	Institute for Science and Technology in Art, Academy of Fine Arts Vienna, (Austria)
Position	**Scientific Technician**
Main activities	- Basic chemical investigations and support to scientific projects; - Preparing detailed reports and reviews on research results; - Analysis of artworks as such or fragments in cross-sections.

Dates	September 2017 – November 2017
Employer	Ca' Foscari University of Venice, (Italy)
Position	**Academic Tutor**
Main activities	Lecture held: - Analytical Chemistry laboratory

Dates	February 2017 – May 2017
Employer	Institute for Science and Technology in Art, Academy of Fine Arts Vienna, (Austria)
Position	**Junior conservation scientist**
Main activities	Scientific support by non-invasive analysis of commercial paints artificially aged by different types of museum lighting.

Dates	March 2015 – June 2015
Employer	Superintendence for the historical artistic heritage of Venice, (Italy)
Position	**Research assistant**
Main activities	Photographic documentation and evaluation reports of samples belonging to Venetian painters of the late 15th and mid-16th centuries.

Education

Dates	September 2018 – present
Qualification title	***Ph.D. in Natural Science, Technical Chemistry*** Technical University of Vienna (TU Wien), Austria
Thesis title	Influence of atmospheric aging on the stability of painting art materials: Study of degradation behaviour when exposed to UV-light, corrosive gases, and humidity

Dates	2015 – 2017
Qualification title	***M.Sc. in Chemical Sciences for Cultural Heritage*** Ca' Foscari University of Venice, Italy
Thesis title	Characterization and quantification of modern painting materials by IR and Raman spectroscopies

Dates	2012 – 2015
Qualification title	***B.Sc. in Technologies for Conservation and Restoration*** Ca' Foscari University of Venice, Italy
Thesis title	Study of the materials and painting techniques of four paintings by the Master of the Madonna del parto (late 14th and early 15th century)

Additional training

- VII Scuola Nazionale di Chimica dell'Ambiente e dei Beni Culturali; L'interazione tra ambiente e superficie per la salvaguardia del patrimonio culturale, University of Venice (30th November - 3rd December 2020);
- Plastics in Peril Focus on Conservation of Polymeric Materials in Cultural Heritage, University of Cambridge (16th - 19th November 2020);
- Applied Chemometrics for Cultural Heritage Winter school, University of Bologna (10th - 13th February 2020);
- Combining NIR Spectroscopy and Chemometrics Winter school, Società Italiana di Spettroscopia NIR (SIS NIR) (14th - 18th January 2019).

Personal skills and expertise

Technical skills	Optical microscope; 3D Microscope; FTIR Spectroscopy; Raman Spectroscopy; Spectrophotometry; Colorimetry; X-ray Radiography; Scanning Electron Microscopy (SEM); X-ray Fluorescence (XRF); Laser Induced Breakdown Spectroscopy (LIBS); Hyperspectral Imaging; Atomic Force Microscopy (AFM); Multivariate Analysis.
IT skills	Microsoft Office: (Word, Excel, PowerPoint); Adobe Reader; OriginPro8; PaintShopPro7; Plot Digitizer; Opus8; CorelDRAWX4; Omnic; ImageJ; FORS Database; Specim IQ Studio; Chemometric Agile Tool (CAT) software running under R environment.
Languages	Italian (Mother Tongue), English (C1), Spanish (B2), French (A2), German (A2).
Membership	Heritage Science Austria group (2018 – present); Online database of pigment collection from the 19th and 20th centuries; Research project "Coating Protection of Metal Objects in Cultural Heritage" (Jan 2017 - Oct 2019).
Award	Erasmus Plus Internship (Feb. 2017), Ca' Foscari University of Venice, Italy
Bibliometrics	*ResearchGate* – 7 papers; RG Score 15.35; h-index 4; 27 citations; *Scopus* – 6 papers; h-index 3; 21 citations; https://orcid.org/0000-0003-0197-7828

Recent **scientific publications** in international journals:

- L. Pagnin, R. Wiesinger, A. Koyun, M. Schreiner; The Effect of Pollutant Gases on Surfactant Migration in Acrylic Emulsion Films: A Comparative Study and Preliminary Evaluation of Surface Cleaning. Polymers. **2021**, 13(12):1941.
- L. Pagnin, R. Calvini, R. Wiesinger, M. Schreiner; SO2- and NOx- initiated atmospheric degradation of polymeric films: Morphological and chemical changes, influence of relative humidity and inorganic pigments. Microchemical Journal. **2021**, 164(1):106087.
- L. Pagnin, R. Calvini, R. Wiesinger, J. Weber, M. Schreiner; Photodegradation Kinetics of Alkyd Paints: The Influence of Varying Amounts of Inorganic Pigments on the Stability of the Synthetic Binder. Frontiers in Materials. **2020**, 7:600887.
- L. Brunnbauer, M. Mayr, S. Larisegger, M. Nelhiebel, L. Pagnin, R. Wiesinger, M. Schreiner, A. Limbeck; Combined LA-ICP-MS/LIBS: powerful analytical tools for the investigation of polymer alteration after treatment under corrosive conditions. Scientific Reports. **2020**, 10:12513.
- L. Pagnin, L. Brunnbauer, R. Wiesinger, A. Limbeck, M. Schreiner; Multivariate analysis and laser-induced breakdown spectroscopy (LIBS): a new approach for the spatially resolved classification of modern art materials, Analytical and Bioanalytical Chemistry. **2020**, 412:3187–3198. Selected for the cover page of the journal.
- L. Pagnin, L. Brunnbauer, R. Wiesinger, A. Limbeck, M. Schreiner; Infrared and Laser-Induced Breakdown Spectroscopy to Characterize UV-light Degradation of Modern Art Materials, METALLA Sonderheft 9. **2019**:137-140.
- R. Wiesinger, L. Pagnin, S. Wei, M. Schreiner; Nano-Coatings to Protect Metal Art Objects from Atmospheric Corrosion, METALLA Sonderheft 9. **2019**:234-237.

- R. Wiesinger and L. Pagnin, M. Anghelone, L. M. Moretto, E. F. Orsega, M. Schreiner; Pigment and Binder Concentrations in Modern Paint Samples Determined by IR and Raman Spectroscopy, Angewandte Chemie. **2018**, 57:7401-7407.

Oral presentation and **posters**:

- L. Pagnin, A. Koyun, R. Wiesinger, K. Sterflinger, M. Schreiner; Surfactant migration in acrylic emulsions: Study of Changes Induced by Pollutant Gases and Preliminary Surface Cleaning Evaluation, 2nd Heritage Science Day, University of Applied Arts Vienna (Austria), 17th Sept **2021**;
- L. Pagnin, R. Wiesinger, M. Schreiner; How environmental pollution affects modern paints: The influence of UV-light, sulfur dioxide, and RH, 14th International Conference on Indoor Air Quality in Heritage and Historic Environments, University of Antwerp, Antwerp (Belgium), 12th – 16th Oct **2020**;
- L. Pagnin, R. Wiesinger, A. Limbeck, M. Schreiner; Infrared and Laser-Induced Breakdown Spectroscopy to Characterize UV-light Degradation of Modern Art Materials, Jahrestagung Archäometrie und Denkmalpflege 2019, Academy of Fine Arts of Vienna, Vienna (Austria), 11th – 14th Sept **2019**;
- R. Wiesinger, L. Pagnin, S. Wei, M. Schreiner; Nano-Coatings to Protect Metal Art Objects from Atmospheric Corrosion, Jahrestagung Archäometrie und Denkmalpflege 2019, Academy of Fine Arts of Vienna, Vienna (Austria), 11th – 14th Sept **2019**.
- A. Limbeck, L. Brunnbauer, M. Mayr, L. Pagnin, R. Wiesinger, M. Schreiner; Degradation of Modern Art Materials: comprehensive examination by the combined use of LIBS and LA-ICP-MS, 15th International Conference on Laser Ablation (COLA 2019), Maui-Hawaii (USA), 8th – 13th September **2019**;
- L. Pagnin, L. Brunnbauer, R. Wiesinger, A. Limbeck, M. Schreiner; Multispectral Investigations as tool to characterize UV-light Degradation of Modern Art Materials, Conference on Solid State Analysis, Vienna (Austria), 1st – 3rd July **2019**;
- L. Pagnin, L. Brunnbauer, R. Wiesinger, A. Limbeck, M. Schreiner; Multispectral Investigations for Characterizing UV-light Degradation of Modern Art Materials, The Plastics Heritage Congress 2019, Young Hipom Professionals (Yhip 2019), Lisbon (Portugal), 27th – 28th May **2019**;
- L. Pagnin, R. Wiesinger, M. Schreiner; Influence of inorganic pigments on photo-oxidation processes of acrylic and alkyd paints exposed to short-time UV-light artificial aging, Technart 2019, Bruges (Belgium), 7th – 10th May **2019**;
- L. Brunnbauer, L. Pagnin, M. Schreiner, A. Limbeck; Investigation of Polymer Degradation of Modern Art Materials Using LIBS and Multivariate Statistics, Anakon 2019, University of Münster (Germany), 25th – 28th Mar **2019**;
- L. Brunnbauer, L. Pagnin, M. Schreiner, A. Limbeck; Depth Profiling of UV-light Degradation of Modern Art Materials Using LIBS, European Winter Conference on Plasma Spectrochemistry, Pau (France), 3rd - 9th Feb **2019**;
- L. Pagnin, R. Wiesinger, M. Anghelone, L. M. Moretto, E. F. Orsega, M. Schreiner; The Potential of IR and Raman Spectroscopy to Determine Pigment and Binder Concentration in Modern Paint Samples, Infrared and Raman Users Group (Irug 13) Conference, Sydney (Australia), 5th – 7th Dec **2018**.
- D. Jembrih-Simbürger, B. Frühmann, A. Schäning, M. Anghelone, L. Pagnin, M. Schreiner; A pigment collection from the 19th and 20th centuries: Compilation to a database with comprehensive material information and spectral data, Conference: Quo vadis, cultural heritage preservation, Litomyšl (Czech Republic), 8th – 9th Nov **2018**.
- L. Pagnin, R. Wiesinger, M. Anghelone, L. M. Moretto, E. F. Orsega, M. Schreiner; Characterization and Quantification of Modern Painting Materials by IR and Raman Spectroscopies, Seminar at University of Science and Technology, Beijing (China), 14th Sept **2018**.